APPENDIX G:
179B(a) Demonstration

Contents

Figures

Tables

1. Conceptual Model

1.1 Objective of Demonstration

Under Section 179B of the Clean Air Act (CAA), air agencies have the authority to develop and submit to the U.S. Environmental Protection Agency (EPA) a demonstration that shows (1) its State Implementation Plan (SIP) would be adequate to attain and maintain the National Ambient Air Quality Standards (NAAQS) in a nonattainment area (NAA) or (2) that the NAA would have attained the NAAQS – *but for* emissions emanating from outside the United States (i.e., international transport). The EPA has the authority to assess a 179B demonstration and provide regulatory relief from otherwise applicable planning and emission control requirements provided the demonstration is to the EPA's satisfaction. There are two pathways to demonstrate that international transport impacted an air agency's ability to attain or maintain the ozone NAAQS. The air agency may demonstrate that its SIP *would be* sufficient to attain the NAAQS by its future attainment date but for international transport; the forward-looking nature of this analysis deems it a "prospective" analysis, as described in section 179B(a). Conversely, the air agency may demonstrate that its SIP *would have been* sufficient to attain the NAAQS by a past attainment date but for international transport; this demonstration is a retrospective analysis on past air quality and is described in section 179B(b).

Effective as of January 21, 2025, the Las Vegas Valley, delineated by hydrographic area 212 (HA 212), in Clark County, Nevada, was designated as serious nonattainment for the 2015 8-hr ozone NAAQS (89 FR 103657). As a result of this classification, the Clark County Department of Air Quality (DAQ) is required to submit a revised attainment plan that addresses the planning requirements for serious nonattainment areas under CAA Section 182(c). The attainment date for HA 212 under the serious area requirement is August 3, 2027. The purpose of the current document is to demonstrate 8-hr ozone NAAQS attainment in HA 212 under Section 179B(a) (i.e., a prospective analysis).

Demonstrations from air agencies whose states do not share an international border may require a more rigorous technical analysis compared with states who share an international border. Therefore, this document will demonstrate attainment under Section 179B(a) prospectively, using (1) ambient observation analysis, including back-trajectory, dispersion, and synoptic analysis, (2) emissions analysis, and (3) photochemical modeling analysis.

1.2 Rule-Based Groundwork for Submission

A Section 179B(a) demonstration is submitted as part of a SIP under the CAA to show that a NAA would attain and maintain the NAAQS but for emissions from outside the United States. To submit a valid 179B(a) demonstration, the air agency must follow several procedural and technical steps. First,

an air agency may submit a 179B(a) demonstration only if the NAA is at a moderate classification or higher (i.e., serious, severe, or extreme). Furthermore, the submitting air agency must determine whether the NAA will likely attain the standard based on existing or potential new domestic emission reductions, including the implementation of required controls, as outlined in the SIP. If existing or potential domestic emission reductions are not sufficient to achieve attainment, the air agency may develop and submit a 179B(a) demonstration. Upon meeting these criteria, the air agency should notify its EPA regional office to discuss the concept, scope, implications, and timing of the 179B(a) demonstration. Upon completion of the 179B(a) demonstration, the air agency should submit it no later than when it submits all other parts of the attainment SIP for EPA review. Once submitted, EPA evaluates whether the demonstration provides satisfactory evidence that but for international transport of emissions, NAAQS attainment would be achievable. The 179B(a) demonstration must include a conceptual model to provide context of international transport as it relates to nonattainment and summaries of analyses performed that provide evidence of international transport. The "weight-of-evidence" approach combines multiple lines of analysis to demonstrate international transport of emissions into the NAA. The types of analysis vary depending on the broader context of the NAA, such as geographical considerations, but generally include an ambient observation analysis, emissions analysis, and modeling analysis.

In the lead-up to the submission of this 179B(a) demonstration, Clark County has fulfilled these obligations by meeting with EPA Region 9 to discuss the concept, scope, implications, and timing of this demonstration. Additionally, this demonstration is also being submitted with the SIP for EPA review. The contents of this demonstration are in line with the "weight-of-evidence" approach to qualify and quantify international contribution in the NAA via ambient air quality and meteorological observations, emissions analyses, dispersion modeling, and photochemical modeling.

In this demonstration, we first include a conceptual model to summarize the results from all "weight-of-evidence" approaches used to demonstrate international transport. All details for each approach are included in the subsequent chapters to fully expand and justify the techniques and results.

1.3 HA 212 Description

HA 212 is centrally located within Clark County, Nevada, and contains the City of Las Vegas, as well as other urban centers. The following sections detail the environmental characteristics of HA 212 within the context of ozone air quality.

1.3.1 Topography, Climatology, and Ozone Formation

Clark County is located in the southern portion of Nevada and borders California and Arizona. Clark County includes the City of Las Vegas, one of the fastest growing metropolitan areas in the United States, with a population of approximately 2.2 million people (U.S. Census Bureau, 2010). Las Vegas is located in a 1,600 km^2 desert valley basin at 500 to 900 m above sea level (Langford et al., 2015). It is

surrounded by the Spring Mountains to the west (~3,000 m elevation) and the Sheep Mountain Range to the north (~2,500 m elevation). Three mountain ranges comprise the southern end of the valley. The valley floor slopes downward from west to east, which influences surface wind, temperature, precipitation, and runoff patterns. The Cajon Pass and I-15 corridor to the east is an important atmospheric transport pathway from the Los Angeles Basin into HA 212 (Langford et al., 2015) (Figure 1). Figure 1 shows HAs, including HA 212, the greater Las Vegas urban area, and major transportation routes overlaid onto surface elevation.

HA 212's climatology features abundant sunshine and hot summertime temperatures (average summer-month high temperatures of 34-40°C). Because of the mountain barriers to moisture inflow, the region experiences dry conditions year-round (~107 mm annual precipitation, 22% of which occurs during the summer monsoon season in July through September). The urban heat island effect in Las Vegas during summer leads to large temperature gradients within the valley, with generally cooler temperatures on the eastern side. During the summer season, monsoon moisture brings high humidity and thunderstorms to the region, typically in July and August (National Weather Service Forecast Office, 2020). Winds in the Las Vegas basin tend to be out of the southwest during spring and summer (Los Angeles is upwind), while winds in the fall and winter tend to be out of the northwest, with air transported between the neighboring mountain ranges and along the valley. The bounding mountain ranges direct basin-wide wind flows while inducing upslope/downslope circulations during weak flow conditions. The altitudes of these ranges are roughly equivalent to the summer daily boundary layer depth, leading to the trapping of pollutants within the basin during stagnant conditions.

From May through September, ozone concentrations are influenced by the photochemical oxidation of local precursor emissions comprising nitrogen oxides (NO_x) and volatile organic compounds (VOCs), regional and intercontinental transport into the region, and by exceptional events such as wildfires and stratospheric intrusions (Langford et al., 2015; Clark County Department of Air Quality, 2019). Local ozone production is maximized during hot, stagnant conditions when strong regional high pressure suppresses boundary layer depth and reduces basin ventilation. Transport from upwind source regions, particularly the Los Angeles Basin, occurs during southwesterly winds, while southerly transport from Mexico dominates later in the season due to the summer monsoon (Langford et al., 2015; Zhang et al., 2020).

Local precursor emissions in Clark County include NO_x and VOCs from mobile and stationary sources, NO_x from natural-gas power generation, and VOCs from consumer products and biogenic sources (vegetation). According to the 2026 NA emission inventory study, local anthropogenic sources emit 61.62 tons of NO_x per day and 91.27 tons of VOCs per day during a typical ozone season weekday (Table 1) (Ramboll Americas Engineering Solutions and Eastern Research Group, 2026). On-road mobile sources comprise 26.6% of total NO_x emissions while total mobile emissions comprise 57.3% of total NO_x emissions during the ozone season. Nonpoint (area) sources contribute 51.6% of total VOC emissions. Biogenic emissions are not reported here as their estimates range by several orders

of magnitude depending on which biogenic emission model is employed (as detailed in Section 8.4.10 of Ramboll Americas Engineering Solutions and Eastern Research Group (2026)).

Table 1. 2026 HA 212 anthropogenic emissions (tons/day) for a typical summer weekday.

Source Category	2026 NO_x	2026 VOCs
Point source	3.25	1.89
Nonpoint source	6.53	47.09
On-road mobile	16.41	15.79
Nonroad mobile	18.91	23.72
Airports (commercial & federal)	15.90	2.75
Locomotives	0.62	0.03
Total	**61.62**	**91.27**

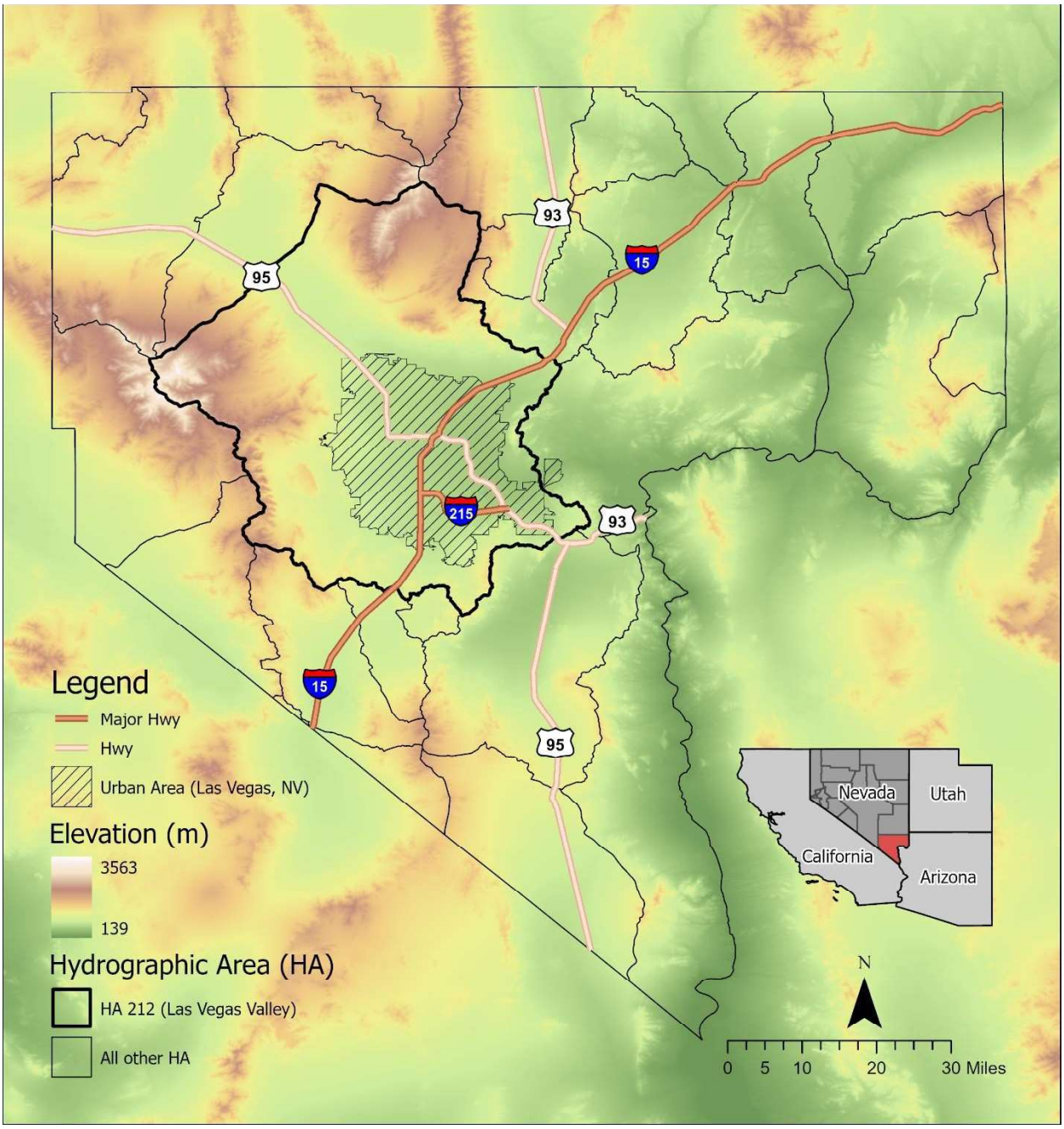

Figure 1. HAs, the greater Las Vegas urban area, and major transportation routes imposed onto surface elevation of the Clark County, Nevada area. The red-shaded area in the inset map indicates Clark County, Nevada.

1.3.2 Monitoring Sites

The Clark County DAQ operates 15 ambient ozone monitoring sites as of 2025. Table 2 lists active ozone monitoring sites along with their data collection temporal range, monitoring objective, and whether the site is within HA 212. 40 Code of Federal Regulations (CFR) Part 58 (including

Appendices A–E) defines the requirements for the ambient air quality monitoring programs mandated by the CAA. Under these rules, every state must establish a monitoring network for criteria air pollutants that meets location and operation specifications. Monitors used to satisfy these requirements are called State and Local Air Monitoring Stations (SLAMS). DAQ operates multiple SLAMS in its network that are designed to monitor ozone concentrations. DAQ's ambient air monitoring network meets the monitoring requirements for criteria pollutants pursuant to Title 40, Part 58, of the CFR, Appendix D. Data are quality-assured in accordance with 40 CFR 58 and submitted to the EPA's Air Quality System (AQS).

The spatial distribution of monitoring sites characterizes the regional air quality in Las Vegas, as well as air quality upwind and downwind of the urban valley region (**Figure 2**). The Jean monitoring site along the I-15 corridor is generally upwind, such that it captures atmospheric transport into the region from the southwest and is typically not impacted by local sources from the greater Las Vegas urban area.

The Spring Mountain Youth Camp site (EPA AQS Site ID 320037771) is operated as a nonregulatory Special-Purpose Monitor (SPM) monitoring site, as described in the annual network plan (Clark County Department of Environment and Sustainability, 2025). This monitor is not used for NAAQS concentration monitoring but provides data on stratospheric ozone intrusions and pollutant mixing heights and assists with model validation.

CAA Section 182(c)(1) requires areas classified as Serious, Severe, or Extreme for ozone to establish Photochemical Assessment Monitoring Station (PAMS) sites, which provide enhanced monitoring of ozone, NO_x, VOCs, and meteorological parameters. The Jerome Mack site includes both the National Core (NCore) and PAMS programs. The monitoring site meets PAMS site requirements, including those in Appendix D Sections 5(b)(1) through 5(b)(13). DAQ formally adopted the approved PAMS Quality Assurance Project Plan (QAPP), follows their approved Criteria Pollutant/NCore QAPP, and adheres to the PAMS Technical Assistance Document (Wang et al., 2023a; Fransioli, 2021; Wang et al., 2023b) to ensure high-quality data.

Table 2. Ozone monitoring sites in Clark County, Nevada, which monitored ozone from 2015-2025.

Site Code	Site Name	Address	City	Ozone Data Year Range	Monitoring Objective	Within HA 212 (Y/N)
320030025	Apex[a]	Apex Valley in Section 7, T18S, R64E, Government Lot Sixteen (16)	Not in a city	2023-2025	NAAQS	N
320030602	Garrett Jr. High	1200 Ave G.	Boulder City	2021-2025	NAAQS	N
320030298	Green Valley	298 Arroyo Grande	Henderson	2015-2025	NAAQS	Y
320037772	Indian Springs[a]	668 Gretta Ln.	Indian Springs	2015-2024	NAAQS	N
320031019	Jean	1965 State Hwy 161	Jean	2015-2025	NAAQS	N
320030540	Jerome Mack-NCore	4250 Karen Ave.	Sunrise Manor	2015-2025	NAAQS	Y
320030075	Joe Neal	6651 W. Azure Ave.	Las Vegas	2015-2025	NAAQS	Y
320030299	Liberty High School	3700 Liberty Heights Ave.	Henderson	2021-2025	NAAQS	Y
320030044	Mountains Edge Park	8101 West Mountains Edge Parkway	Enterprise	2020-2025	NAAQS	Y
320030073	Palo Verde	333 Pavilion Center Dr.	Las Vegas	2015-2025	NAAQS	Y
320030043	Paul Meyer	4525 New Forest Dr.	Spring Valley	2015-2025	NAAQS	Y
320037771	SM Youth Camp[b]	Ries Rd, Spring Mountain Youth Camp	Mount Charleston	2015-2025	Research	Y
320030024	Virgin Valley High School	820 Valley View Dr.	Mesquite	2021-2025	NAAQS	N
320032003	Walnut Community Center	3075 N Walnut Rd	North Las Vegas	2021-2025	NAAQS	Y
320030071	Walter Johnson	7701 Ducharme Ave.	Las Vegas	2015-2025	NAAQS	Y

[a]Seasonally operated as a SLAMS site.
[b]Seasonally operated as an SPM site.

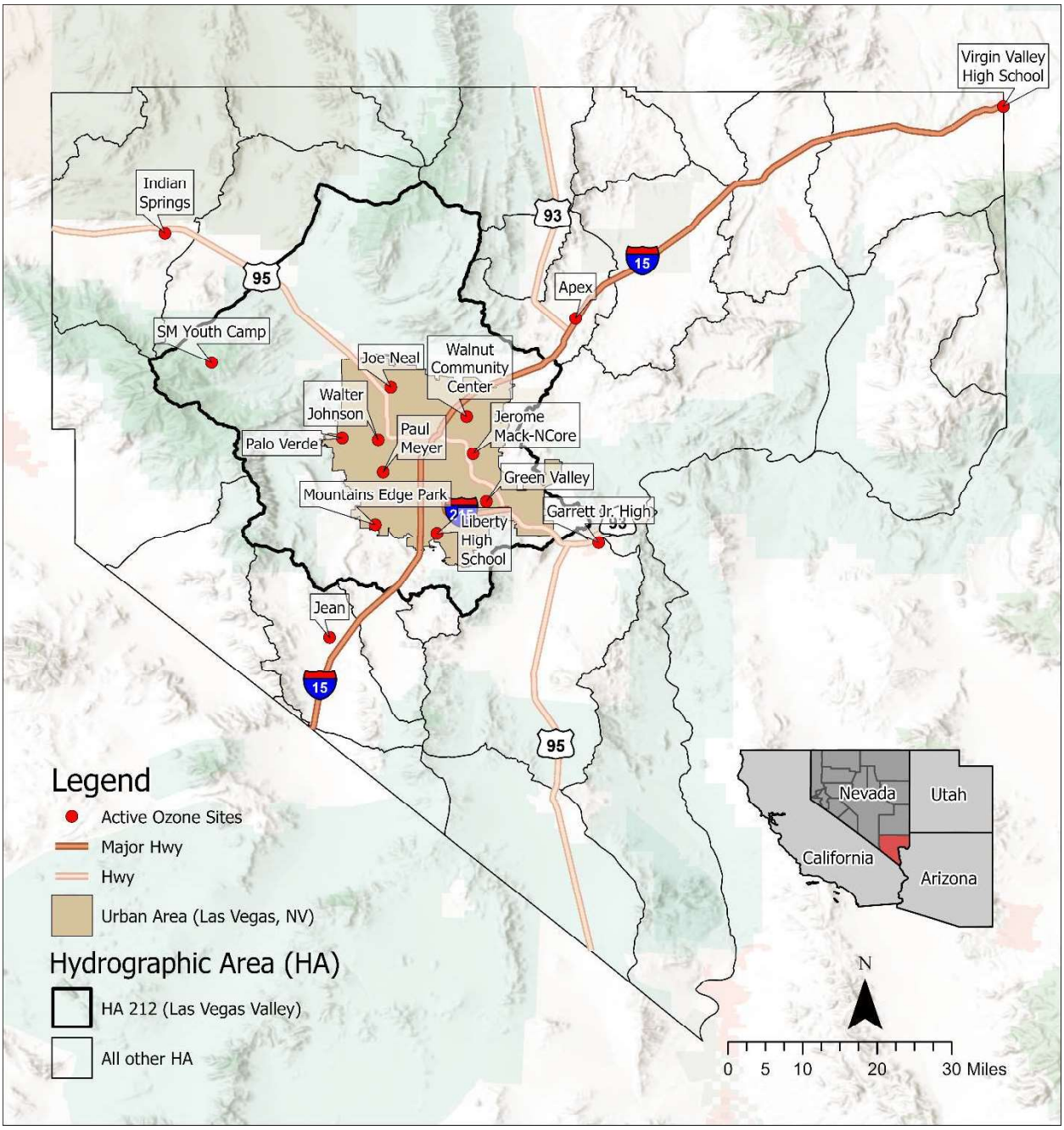

Figure 2. Active (as of 2025) ozone monitoring sites in Clark County, Nevada. The red-shaded area in the inset map indicates Clark County, Nevada.

1.3.3 Historical Ozone Summary

This section is partially based on the historical ozone and ozone trends analysis conducted by Ramboll Americas Engineering Solutions and Eastern Research Group (2026). Figure 3 shows the 23-yr history of peak 8-hr ozone design values (DVs) in Clark County along with the three ozone NAAQS that have been promulgated over the same period. The year 2020 was when attainment of the 2015

ozone NAAQS was required for Marginal NAAs to avoid reclassification to Moderate. Areas of Clark County have been designated nonattainment for the 1997 and 2015 standards. Over this period, peak ozone levels have decreased, particularly during the recession years of 2008-2011. Since that period, however, ozone concentrations have remained fairly constant with small variations caused by interannual variability in summer weather and external uncontrollable factors such as wildfires.

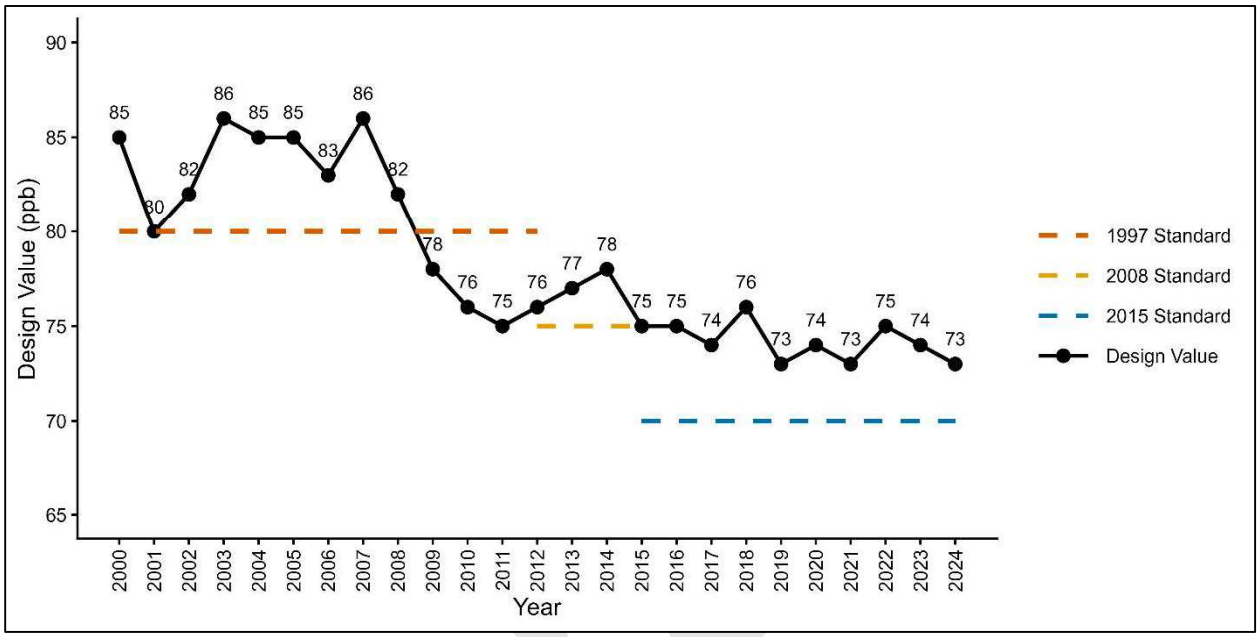

Figure 3. History of peak 8-hr ozone DVs in Clark County and the three ozone NAAQS that have been in effect since 2000. Data from **https://www.epa.gov/air-trends/air-quality-design-values#report**.

Table 3 lists the number of all 2015 ozone NAAQS Maximum Daily 8-hr Average (MDA8) exceedance days in Clark County partitioned by month and year, without any consideration for whether international transport played a role. The total number of exceedance days is indicated in the bottom right cell. Only sites with continuous ozone monitoring over the past 10 years of complete data from 2015-2024 were included in this analysis. The greatest number of exceedance days occurs from June through August, with July exhibiting the maximum number of exceedance days from 2015-2024 (i.e., 70). The annual count of exceedance days exhibits variation from year to year, with a minimum of six in 2019 and a maximum of 37 in 2018.

Table 3. Number of all days by month and year when MDA8 ozone concentrations exceeded the 2015 ozone NAAQS of 70 ppb at any ozone monitoring site in Clark County for sites with continuous ozone monitoring from 2015-2024. Concurred exceptional event ozone concentrations were excluded from this analysis.

Month	2015	2016	2017	2018	2019	2020	2021	2022	2023	2024	Exceedance Total (Month)
January	0	0	0	0	0	0	0	0	0	0	0
February	0	0	0	0	0	0	0	0	0	0	0
March	0	0	0	0	0	0	0	0	0	0	0
April	0	0	0	0	0	0	0	0	1	0	1
May	0	0	1	3	0	3	3	1	3	7	21
June	10	9	9	12	4	3	7	1	3	2	60
July	1	11	10	13	0	2	4	4	10	15	70
August	4	3	3	9	2	7	14	5	0	2	49
September	0	0	0	0	0	3	1	2	0	1	7
October	0	0	0	0	0	0	0	0	0	0	0
November	0	0	0	0	0	0	0	0	0	0	0
December	0	0	0	0	0	0	0	0	0	0	0
Exceedance Total (Year)	**15**	**23**	**23**	**37**	**6**	**18**	**29**	**13**	**17**	**27**	**208**

Table 4 lists the 8-hr ozone DVs at all applicable ozone monitoring sites within Clark County. Apex (EPA AQS Site ID 320030025) and SM Youth Camp (EPA AQS Site ID 320037771) do not have valid DVs during these periods and are not included in this table. As shown in the table, period-to-period variability in DVs is relatively low. Six sites exceed the 2015 ozone NAAQS during the 2022-2024 DV period. Joe Neal, Paul Meyer, and Walter Johnson have exceeded the NAAQS every DV period since the 2018-2020 DV period. However, DVs have generally been decreasing over the past few DV periods.

Table 4. 8-hr ozone DVs from end year 2020-2024 in Clark County. Bolded numbers indicate an exceedance of the 2015 8-hr ozone NAAQS of 70 ppb. Blank cells indicate that there is no DV for that site and DV period. Blue rows indicate sites within HA 212. Data from https://www.epa.gov/air-trends/air-quality-design-values#report.

Site Code	Local Site Name	2018-2020 DV (ppb)	2019-2021 DV (ppb)	2020-2022 DV (ppb)	2021-2023 DV (ppb)	2022-2024 DV (ppb)
320030602	Garrett Jr. High	67	67	67	67	68
320030298	Green Valley	**72**	**71**	70	70	70
320037772	Indian Springs	69	68	68	68	68
320031019	Jean	69	68	68	68	68
320030540	Jerome Mack-NCore	69	68	68	68	67
320030075	Joe Neal	**74**	**73**	**74**	**72**	**72**
320030299	Liberty High School	--	--	--	**71**	70
320030044	Mountains Edge Park	--	--	--	**74**	**73**
320030073	Palo Verde	67	68	**71**	**72**	**71**
320030043	Paul Meyer	**73**	**73**	**75**	**73**	**72**
320030024	Virgin Valley High School	--	--	--	64	65
320032003	Walnut Community Center	--	--	--	**72**	**72**
320030071	Walter Johnson	**73**	**73**	**74**	**72**	**71**

Figure 4 shows the spatial distribution of 2020 DVs, which corresponds to when attainment was required for Marginal NAAs, at the 10 ozone monitoring sites within and immediately surrounding HA 212 (sites without a DV in 2020 were not included in this map). Four sites within the greater U.S. Census-designated Las Vegas urban area, as indicated by the light brown outline, exceeded the 2015 ozone NAAQS of 70 ppb for the 2018-2020 DV period. The figure indicates the highest ozone levels in the basin occur over a distinct urban-oriented spatial pattern. The spatial pattern of slightly higher ozone levels in the urban area of Las Vegas persists during subsequent DV years (Figure 5). Although the spatial pattern of higher DVs within the urban area is persistent throughout the DV years, the average absolute difference between urban and rural sites is low; this is consistent with local emissions within the urban area not being the main driver of high ozone across the entirety of Clark County and instead suggests outside influence of concentrations.

Figure 6 shows 2024 DVs throughout the southwestern U.S., including California, Nevada, Utah, and Arizona. High (> 71 ppb) DVs are ubiquitous throughout southern California, specifically inland in the lower Central Valley and Los Angeles Basin. DVs in central Arizona are also elevated but to a lesser magnitude (i.e., between 71 and 80 ppb) than in southern California. Inverse distance-weighted (IDW) spatially interpolated 2024 DVs in the southwestern U.S. show low ozone concentrations along the west coast of California that increase eastward into the lower Central Valley and Los Angeles basin extending to Mexico (Figure 7). High (> 71 ppb) DVs extend into Clark County, as indicated by purple contours.

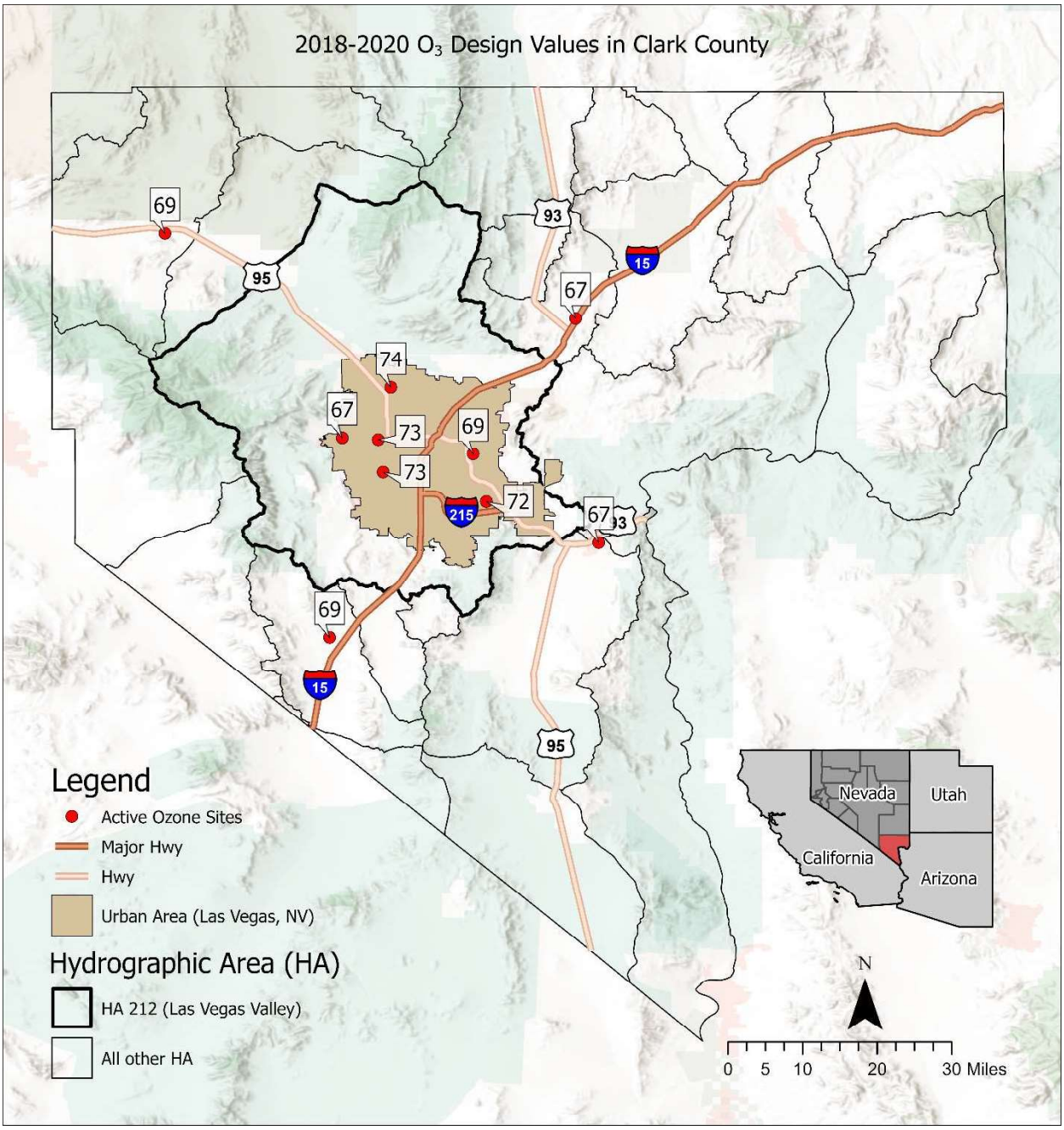

Figure 4. Spatial distribution of 2020 DVs at 10 ozone monitoring sites within and immediately surrounding HA 212. Sites without a 2020 DV are not included in this map. Data from https://www.epa.gov/air-trends/air-quality-design-values#report.

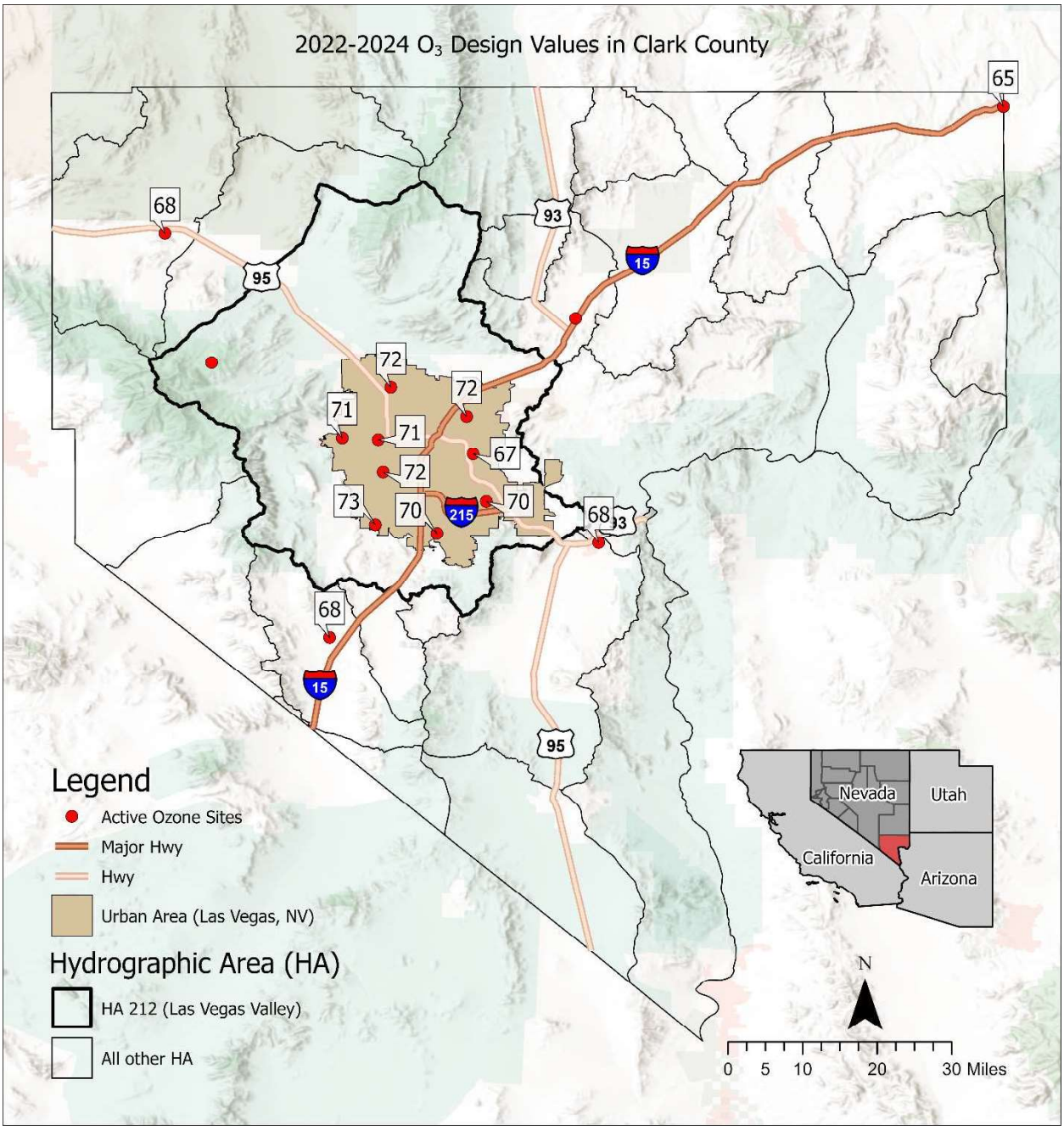

Figure 5. Spatial distribution of 2024 DVs at 13 ozone monitoring sites within and immediately surrounding HA 212. Sites without a 2024 DV are not included in this map. Data from https://www.epa.gov/air-trends/air-quality-design-values#report.

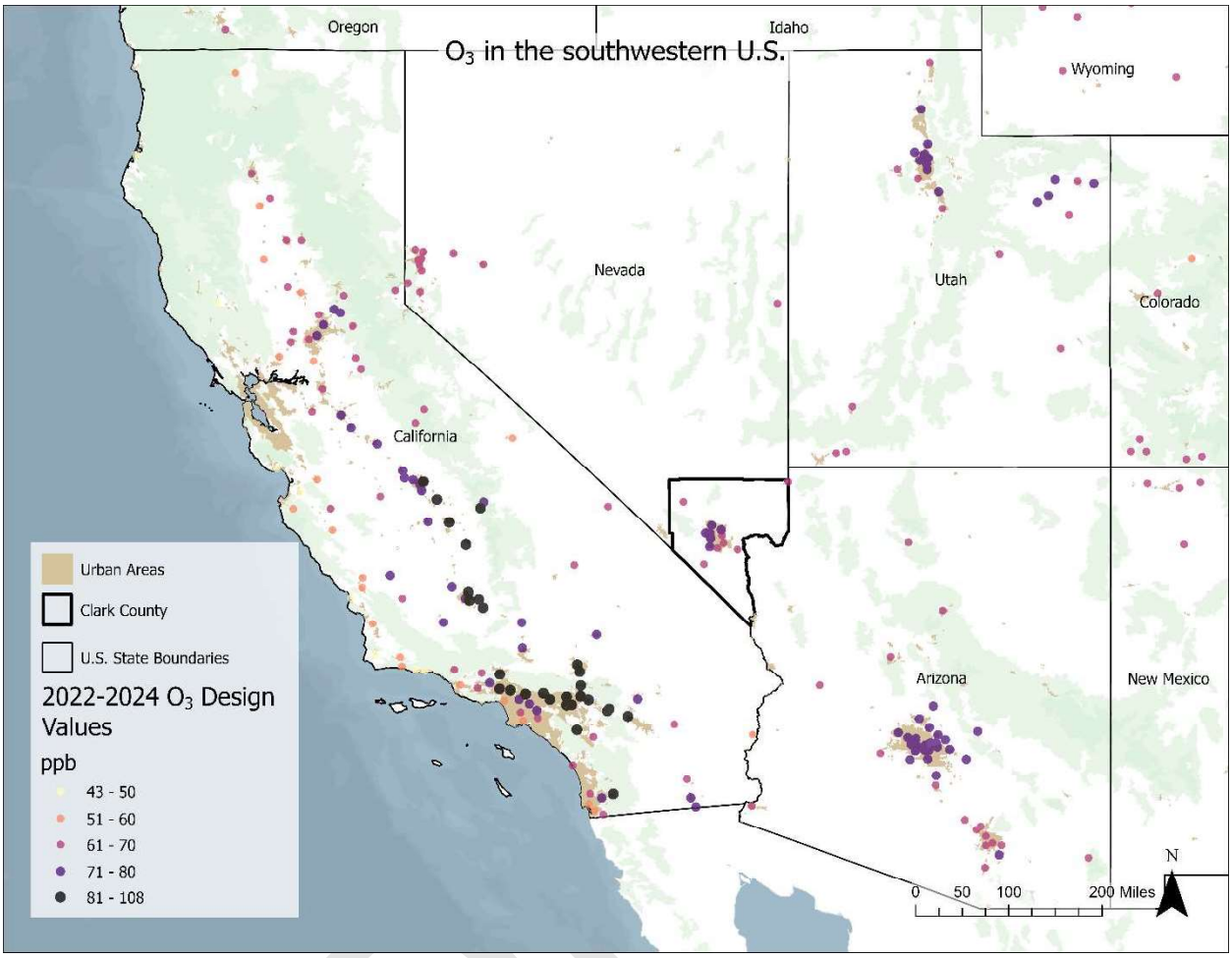

Figure 6. Spatial distribution of 2024 DVs at all ozone monitoring sites in the southwestern U.S. Sites without a 2024 DV are not included in this map. Data from https://www.epa.gov/air-trends/air-quality-design-values#report.

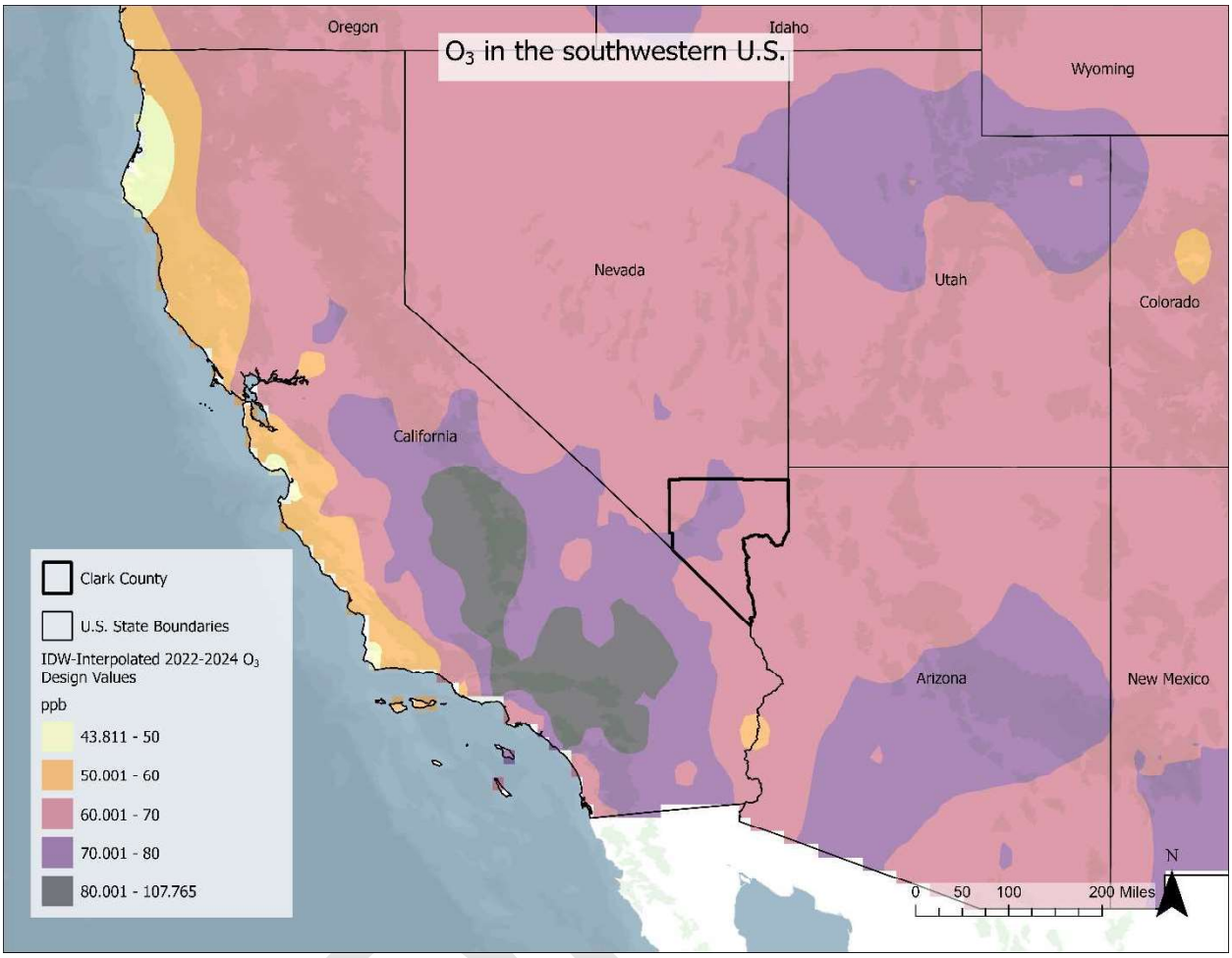

Figure 7. IDW-interpolated 2022-2024 ozone DVs in the southwestern U.S. Sites without a 2024 DV are not included in this analysis. Data from **https://www.epa.gov/air-trends/air-quality-design-values#report**.

1.4 Overview of HYSPLIT Analysis

1.4.1 Back-Trajectory Clustering

Multi-year back-trajectory simulations from the National Oceanic and Atmospheric Administration's (NOAA) Hybrid Single-Particle Lagrangian Integrated Trajectory (HYSPLIT) model were used to characterize the air masses reaching Las Vegas from 2016-2024. An eight-cluster configuration was selected to identify representative transport patterns. The clustered results consistently showed a small number of dominant transport pathways and were grouped into transport regimes based on their spatial patterns: local transport regime (LOC), Mexico transport regime (MEX), and long-range international transport regime (LNR). Overall, the MEX and LNR clusters accounted for 23.3% of all

trajectories entering Las Vegas. These aggregated regime categories were used to evaluate how different transport patterns relate to the observed air masses reaching Las Vegas.

1.4.2 Backward Dispersion Modeling

Backward dispersion modeling was performed using NOAA's HYSPLIT model to determine the likely origin and transport pathways of the air masses in Clark County prior to the exceedance day. This analysis presents backward dispersion results for 30 ozone exceedance dates (10 for each transport regime) that occurred from 2016-2024. Ozone exceedance dates were identified as when the MDA8 for ozone concentrations at any monitoring site in Clark County exceeded the 2015 ozone NAAQS of 70 ppb.

The result of the backward dispersion analysis is spatial data corresponding to the Normalized Potential Emissions Sensitivity (NPES), which is a normalized measure of particle frequency and residence time within each grid cell over the model duration. When plotted, NPES produces a spatial "heat map" indicating regions of higher or lower NPES values, reflecting where air masses more frequently resided during the transport period. NPES values across the entire model domain sum to one and can be analyzed geographically to determine the contribution on ozone from different regions.

Results show distinct spatial patterns in NPES, which point to different synoptic weather patterns. The MEX and LNR transport regimes have a higher proportion of international NPES than the LOC transport regime. The percentage of international NPES was approximately 75% for the LNR transport regime under a longer model duration (-10 days) and averaged throughout the entire troposphere (0-5,000 m).

The Las Vegas Ozone Study (LVOS), conducted in 2013 (Langford et al., 2015), and the Fires, Asian, and Stratospheric Transport-Las Vegas Ozone Study (FAST-LVOS), conducted in 2017 (Langford et al., 2022), examined sources of ozone impacting Clark County and found that stratospheric transport (STT) contributed more than 30 ppbv to ozone concentrations during exceedance events, while Asian transport contributed less than 10 ppbv and wildfire impacts were generally minimal. FAST-LVOS results showed that stratospheric intrusions are the most consistent and influential driver of elevated background ozone in late spring, with Asian pollution often co-transported and occasionally enhancing ozone levels. Overall, background ozone concentrations in Clark County are shaped by frequent stratospheric influences and episodic contributions from transported pollution, while neither study evaluated emissions from Mexico.

Both the LVOS, and FAST-LVOS studies found that stratospheric air masses were the dominant contributor to high ozone levels in Clark County, while transported Asian pollution contributed smaller but noticeable concentrations. The later FAST-LVOS work showed that stratospheric intrusions consistently elevated background ozone concentrations each spring and were often accompanied by additional ozone from distant pollution sources. Overall, ozone conditions in the

region were shaped by frequent stratospheric influence combined with occasional increases from transported pollution.

1.5 Synoptic Pattern Analysis

Three distinct transport regimes—LNR, MEX, and LOC—contribute to pollutant movement and ozone formation in Clark County. The synoptic meteorological characteristics were analyzed across all 30 ozone exceedance dates (10 for each transport regime) that occurred from 2016-2024. LNR events are driven by high pressure over the Pacific and strong west-to-east winds, enabling cross-Pacific transport, while low pressure over the western U.S. enhances vertical mixing. MEX transport is characterized by a thermal trough over the Colorado River Valley and a south-to-north pressure gradient that carries pollutants from northwestern Mexico, with warm surface temperatures and high pressure aloft promoting deep mixing and ozone production, compounded by light winds that limit dispersion. LOC transport features high pressure over the western U.S., sunny skies, and warm conditions that favor ozone formation, with pollutants arriving from California and ozone-rich air masses mixing to the surface; regional smoke may further amplify local ozone concentrations.

The seasonal profile of MDA8 ozone grouped by the three transport regimes reflects the meteorological conditions throughout the year: LOC transport days occur throughout the year and are less dependent on synoptic patterns, but are most numerous during the primary ozone production season in Clark County, MEX transport days occur during June-September, consistent with warm thermal troughing over the desert Southwest and enhanced southerly flow during the monsoonal season. LNR transport days occur from October-May, consistent with cool-winter season circulation patterns.

Average diurnal ozone profiles exhibit differences between the three regimes; notably, mean hourly ozone profiles on LNR transport days are typically flatter, feature a maximum concentration later in the day, and concentrations remain elevated relative to LOC ozone profiles; this may indicate sustained transport of ozone and ozone precursors from non-local sources into Clark County.

The spatial pattern of MDA8 ozone on LOC and MEX transport days shows an urban/non-urban distinction, where MDA8 ozone is generally higher within the Las Vegas urban area than outside, relative to MDA8 ozone on LNR transport days.

1.6 Overview of Emission Analysis

Ramboll Americas Engineering Solutions and Eastern Research Group (2026) compiled historical and projected Clark County anthropogenic emission inventories (beyond just the HA 212 NAA) to develop NO_x and VOC emission trendlines.

These emission inventories revealed a substantial 56% reduction in NO_x emissions between 2008 and 2023, with continued declines projected through 2033 for a total 2008–2033 reduction of 64%. These NO_x decreases are primarily driven by large reductions in on-road and nonroad mobile sources.

VOC emissions have also generally declined, decreasing by 25% from 2008 to 2023, with a net 26% reduction projected by 2033. While VOC decreases are largely attributable to reductions in on-road and nonroad sectors, they are partially offset by increases in nonpoint emissions associated with population and commercial growth.

Emissions from the airport sector are projected to increase over the 2008–2033 period, contributing to upward pressure on both NO_x and VOC totals.

Despite overall reductions in NO_x and VOC emissions within HA 212, ozone DVs have been stagnant since around 2015.

1.7 Overview of Photochemical Modeling

Source apportionment (SA) modeling was performed for the 2023 moderate attainment-year scenario to quantify and rank ozone contributions from specific source sectors and geographic regions affecting high ozone in HA 212. The analysis included tagging emissions from other U.S. states, international anthropogenic (IA) sources, and regional wildfires to assess the relative influence of upwind and international contributions.

IA contributions determined by Comprehensive Air Quality Model with extensions (CAMx) and Goddard Earth Observing System - Chemistry (GEOS-Chem) modeling account for approximately 8–23% of ozone concentrations at the HA 212 monitoring sites. This range of IA contribution is consistent with the cluster analysis showing 23% of trajectories from international sources and EPA Community Multiscale Air Quality model (CMAQ) modeling indicating 8-13% IA contribution. When these contributions are removed, the adjusted 2026 DVs indicate attainment of the 2015 ozone NAAQS at all monitors in Clark County (see Table 5).

These results demonstrate that HA 212 would attain the 2015 ozone NAAQS by the 2026 Serious attainment date but for contributions from foreign anthropogenic sources.

Table 5. Projected 2026 DVs and projected 2026 DVs with IA contributions removed at each monitoring site within Clark County according to calculations from the Software for the Modeled Attainment Test – Community Edition (SMAT-CE) program and a 2023 GEOS-Chem modeling run. Red values indicate exceedances of the 2015 ozone NAAQS; green indicate values below the NAAQS. DV values are in ppb.

Site ID	Site Name	2026 DV Avg 3 x 3	IA Contribution	Adjusted 2026 DV Avg 3 x 3
320030024	Virgin Valley High School	63.9	8-20%	51.1-58.8
320030043	Paul Meyer	72.7	8-19%	58.9-66.9
320030044	Mountains Edge Park	72.8	8-19%	59.0-67.0
320030071	Walter Johnson	71.8	8-19%	58.2-66.1
320030073	Palo Verde	70.5	8-19%	57.1-64.7
320030075	Joe Neal	71.6	8-19%	58.0-65.9
320030298	Green Valley	69.5	8-21%	54.9-63.9
320030299	Liberty High School	69.9	8-21%	55.2-64.3
320030540	Jerome Mack-NCore	67.3	8-20%	53.8-61.9
320030602	Garrett Jr. High School	66.7	8-21%	55.2-61.4
320031019	Jean	67.3	8-23%	51.8-61.9
320032003	Walnut Community Center	71.4	8-20%	57.1-65.7
320037772	Indian Springs	66.8	8-20%	53.4-61.5

1.8 Conclusions for International Transport

HA 212, which encompasses the greater Las Vegas, Nevada, urban area, is designated as Serious nonattainment for the 2015 ozone NAAQS of 70 ppb despite historic declines in ozone and ozone precursors. The ambient observation analysis identified two international transport pathways: air transport from Mexico and cross-Pacific transport from eastern Asia. The two international transport pathways occur under dissimilar meteorological conditions and during distinct times of the year: summertime monsoonal weather patterns for MEX transport days, and winter and spring hemispheric circulation patterns for LNR transport days. Emissions modeling showed clear decreases in local anthropogenic emissions of ozone precursors, including NO_x and VOCs, from 2008-2023 and continued reductions through 2033. Photochemical and trajectory modeling indicate that IA contributions account for up to 8-23% of ozone concentrations in HA 212. Removing the IA contribution from the 2026 future DV shows all sites within HA 212 and Clark County would have a DV of ≤ 67.0 ppb. The results from these analyses suggest that but for international transport, HA 212 would achieve attainment of the 2015 ozone NAAQS by the 2026 Serious attainment date.

2. International Transport Pathways

To assess the impact of international emissions on Clark County, we must first determine the typical international transport pathways into the area. We determine these pathways by first clustering back-trajectories for the time period spanning all emissions and modeling efforts (2016-2024). This process determines the dominant transport pathways entering Clark County. Dispersion modeling is performed for selected high ozone days within each regime spanning all years to confirm international transport. Additionally, we examine the meteorological characteristics of each pathway to confirm that transport of ozone and ozone precursors is possible. Finally, we review the influence of international emissions on the selected high ozone days from each regime. These analyses determine the dominant transport pathways for international emissions to impact ozone concentrations in Clark County.

2.1 HYSPLIT Analysis

2.1.1 Back-Trajectory Clustering

Back-trajectory simulations were conducted using the HYSPLIT model on a Linux platform. Trajectories were computed for the period 2016-2024, with four daily starting times at 00:00, 06:00, 12:00, and 18:00 UTC (16:00, 22:00, 4:00, and 10:00 PST). Each trajectory was calculated backward in time for 120 hours (5 days) to investigate the origin and transport pathways of air masses reaching internationally. Meteorological input data were obtained from the NOAA Global Data Assimilation System (GDAS), which provides data at a spatial resolution of 1° by 1° in latitude and longitude and a temporal resolution of 3 hours.

The starting location for all simulations was 36.0831°N, 115.1482°W (i.e., Las Vegas, Nevada, United States). Trajectories were initialized at a height of 500 m above ground level, and the model vertical domain extended to 10,000 m, capturing both boundary layer and free tropospheric transport.

To examine dominant transport pathways influencing air quality at Las Vegas, HYSPLIT cluster analysis was applied to the 5-day back-trajectories. The trajectory clustering was conducted using the built-in cluster analysis module within the HYSPLIT modeling framework, which groups trajectories based on their spatial similarity by minimizing the total spatial variance (TSV) within each cluster (Stein et al., 2015). The optimal number of clusters was determined by examining the reduction in TSV as a function of cluster number and identifying the point beyond which additional clusters resulted in diminishing improvements, consistent with established HYSPLIT clustering practice. This approach ensures that the selected clusters capture the dominant transport pathways while maintaining statistical robustness and interpretability.

This analysis focused on daytime trajectories, specifically those starting in the late morning (10:00-11:00 PST) and late afternoon (16:00-17:00 PST), corresponding to periods when photochemical ozone formation and MDA8 levels are most pronounced. This selection also facilitated tractable cluster analysis of the large trajectory dataset and reduced the inclusion of hours when the planetary boundary layer is likely to be shallower than the 500 m release height. Given the extended duration of the 120 h backward trajectories, which increases pathway dispersion and the diversity of potential source regions, an eight-cluster solution was chosen to balance separation of distinct synoptic-scale transport regimes with statistical stability of the clusters. Fewer clusters tended to merge physically distinct long-range pathways, whereas additional clusters primarily subdivided existing pathways without yielding substantial reductions in TSV. The results revealed several dominant transport pathways, including local or regional recirculation, transport from northern Mexico, and long-range, cross-Pacific transport, providing insights into the origins of air masses associated with elevated ozone concentrations. This analysis also resulted in a dataset of trajectories for each calendar day categorized by the cluster.

Figure 8 shows the mean 5-day backward trajectories from Las Vegas, Nevada, calculated using HYSPLIT cluster analysis with eight clusters. Trajectories illustrate dominant transport patterns contributing to air masses arriving at the site and highlight international influences from Mexico and long-range transport from Asia. Clusters 1 and 3 were characterized by short-to-moderate transport distances over the southwestern United States, coastal California, and the eastern Pacific, and were grouped into the LOC transport regime, accounting for 56.7% of all trajectories. Cluster 4 was classified as the MEX transport regime and accounts for 7.8% of transport pathways. Clusters 5, 7, and 8 were combined to form the LNR transport regime and account for 15.5% of transport pathways. Combined international transport clusters account for 23.3% of the total trajectories that were run in the analysis. Clusters 2 and 6 exhibited transport pathways that did not consistently align with the defined LOC, MEX, or LNR regimes, and were therefore retained as separate categories representing mixed or transitional transport conditions. Results of the cluster analysis for individual years from 2016 to 2022, including the corresponding back trajectories, are provided in Individual-Year Cluster Analysis Plots. Individual-year cluster analyses (2016–2024) were largely consistent with the multi-year mean, with transport dominated by LOC pathways and recurring contributions from MEX and LNR transport.

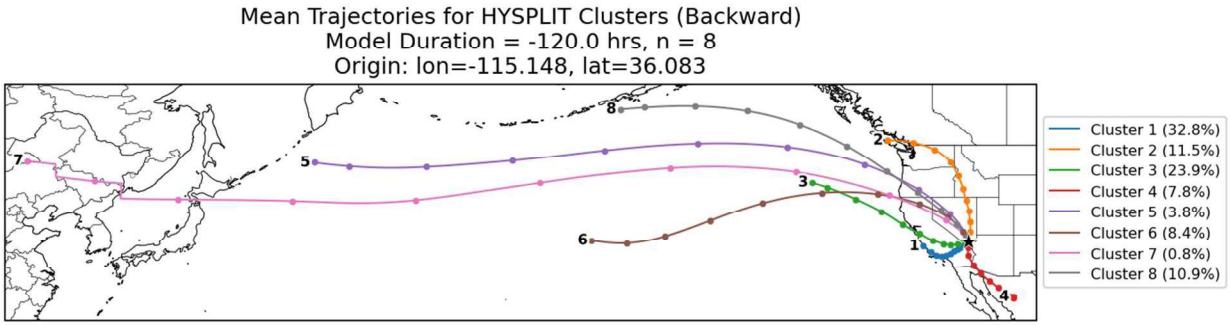

Figure 8. Mean 5-day backward trajectories from Las Vegas, Nevada (36.0831°N, 115.1482°W), calculated using HYSPLIT cluster analysis with eight clusters. Each colored line represents the mean pathway of a cluster, and the percentages in the legend indicate the fraction of trajectories assigned to each cluster. Trajectories illustrate dominant transport patterns contributing to air masses arriving at the site, highlighting both regional and long-range influences on air quality.

2.1.2 Backward Dispersion Modeling

As discussed in Section 1.4.2, backward dispersion modeling was conducted using HYSPLIT to determine the likely origin and transport pathways of air masses prior to the exceedance. This analysis presents backward dispersion results for 30 exceedance dates between 2016 and 2024, 10 for each of the three identified air transport regimes: MEX, LOC, and LNR. Exceedance dates were selected based on when an ozone monitoring site in Clark County, Nevada exceeded the 2015 ozone NAAQS MDA8 value of 70 ppb, using AQS data (**Error! Reference source not found.**).

Table 6. Dates that correspond to the identified air transport regimes.

Transport Regime	Dates
LOC	June 17, 2017; July 4, 2017; August 31, 2017; August 11, 2018; July 9, 2020; May 29, 2021; August 15, 2021; August 19, 2022; July 14, 2023; May 14, 2024
MEX	July 2, 2016; July 14, 2017; July 22, 2018; May 14, 2021; August 12, 2021; July 15, 2022; August 2, 2022; May 17, 2023; July 20, 2024; August 9, 2024
LNR	July 14, 2016; August 13, 2016; May 20, 2021; June 10, 2021; May 9, 2023; May 11, 2023; May 19, 2024; May 23, 2024; May 31, 2024; June 17, 2024

Results from the back-trajectory clustering guided the categorization of exceedance dates for initial modeling. Exceedance dates were matched with back-trajectory clusters using the back-trajectory nearest to the final MDA8 hour of each exceedance date. Clusters 1 and 3 were identified as the LOC air transport regime, due to the short transport distances and mean trajectory paths through the Los

Angeles and San Francisco Bay areas, respectively. Cluster 4 was identified as the MEX air transport regime since its mean trajectory passes through Mexico. Clusters 5, 7, and 8 were identified as LNR, since these mean trajectories extend over the Pacific Ocean and end near Asia.

HYSPLIT backward dispersion modeling is computationally intensive. As a result, a subset of exceedance days was modeled, with the initial backward dispersion modeling consisting of 22 MEX dates, 26 LOC dates, and 14 LNR dates. An additional subset of model runs (10 of each air transport regime) is presented in this analysis to show the most characteristic examples for each transport regime. These final dates were selected to prioritize (1) representation of air transport regime, (2) days on which the greatest number of monitors recorded exceedances, and (3) exceedance days that were not adjacent in time to other days with exceedances predominated by another air transport regime.

Table 7 includes information about how the HYSPLIT backward dispersion models were parameterized. The emission source for modeling was initialized to represent the PBL (layers of air that can freely mix with air near the surface) during the MDA8 averaging period for each exceedance date: a vertical line source between 0 and 1,000 m, emitting for 8 hours from the end to the start of the MDA8. HYSPLIT was initialized to output average concentrations between 0-100 m, 100-1,000 m, and 1,000-5,000 m. These results were aggregated to yield average concentration datasets between 0-1,000 m and 0-5,000 m that represented air within the PBL and air within the entire troposphere, respectively. To represent the movement of air, rather than a particular pollutant, HYSPLIT was initialized to treat the particles as an inert tracer gas with no deposition, decay, or resuspension characteristics. Finally, a model grid spacing of 0.05° latitude by 0.05° longitude and a particle-release rate of 10,000 particles/hour (i.e., 80,000 particles total) were selected following sensitivity testing to maximize model resolution without requiring excessive computation. LOC and MEX dates were modeled using North American Mesoscale Forecast System meteorological data, which has a spatial resolution of 12 km by 12 km and a temporal resolution of 1 hour (NAM12). LNR dates were modeled using NCEP GDAS 0.25 Degree Global Tropospheric Analyses and Forecast Grids meteorological data, which has a spatial resolution of 0.25° by 0.25° in latitude and longitude and temporal resolution of 6 hours.

Table 7. HYSPLIT backward dispersion model parameterization.

Parameter	Description
Location	Clark County, Nevada
Source Latitude, Longitude	36.16°, -115.15°
Meteorological Data	NAM12: MEX and LOC runs GDAS0.25: LNR runs
Source Type	Vertical line, 100-1,000 m
Starting Date, Time	Exceedance date, final MDA8 hour
Model Duration	-5 days (-120 hours): all model runs -10 days (-240 hours): additional to LNR runs
Emission Duration	8 hours
Grid Spacing Lat, Lon	0.05°, 0.05°
Concentration Levels	0-100 m 100-1,000 m 1,000-5,000 m
Deposition Characteristics	Insert tracer gas No dry or wet deposition No radioactive decay No resuspension
Particle Release Rate (hr^{-1})	10,000
Total Number of Particles	80,000

Two sample back-trajectories are included for the individual MEX and LOC backward dispersion plots to provide insight into the elevation of the air masses (see Backward Dispersion Daily Plots). These two trajectories used a model duration of -5 or -10 days, a release time corresponding to the final MDA8 hour, and release elevations of 100 and 1,000 m, respectively. Back-trajectory modeling was conducted using the same meteorological data as the backward dispersion modeling above (NAM12 for LOC and MEX days, and GDAS0.25 for LNR days). Back-trajectories were not included in plots that compiled backward dispersion results for a particular air transport regime since these plots depict data over multiple days (with multiple start times). Back-trajectories were not included in any LNR plots since the trajectories generally did not span the entire retroplume and therefore did not provide any useful information.

The result of the backward dispersion modeling is spatial data for NPES, which represents a normalized measure of particle frequency and residence time within each grid cell over the model duration. To calculate NPES, Potential Emissions Sensitivity (PES) is calculated for each model grid cell by summing its value over all time steps. NPES is determined by dividing the PES of each grid cell by

the summed PES values for all grid cells, thereby normalizing the PES data. NPES only depicts atmospheric transport patterns and does not represent actual sources of ozone or its precursors.

Figure 9, Figure 10, and Figure 11 show composite NPES for each of the three air transport regimes based on average concentration between 0 and 5 km. The composite backward dispersion results for MEX and LOC days depict a retroplume centered around Clark County; on the other hand, the retroplume for LNR days originates from the west. The composite results for MEX and LOC days have a similar appearance, with the continental portion of the LOC retroplume only located over the United States, while the continental portion of the MEX retroplume covers a large part of Mexico and is shifted roughly 1,000 km south in comparison. Percentages in the figures are calculated by summing NPES values within and outside of the US. As a result, 72.4% of the composite LOC retroplume occurs within the U.S., compared to 60.9% on MEX days. This corresponds to 11.5% more NPES contribution from outside of the U.S. on MEX days than on LOC days.

The 5-day cumulative LNR retroplume extends west of Clark County, covering the states of Nevada, California, Oregon, and Washington; much of the Pacific Ocean; and Japan, and reaching parts of eastern Russia. As a result, 45.5% of the NPES for the composite 5-day LNR retroplume occurs within the U.S., which is 26.9% less than on LOC days. When modeled over 10 days, the composite LNR retroplume covers a large part of eastern Asia, including Japan, Russia, Korea, and China, as well as western Canada. Only 26.0% of the 10-day LNR retroplume occurs within the U.S.

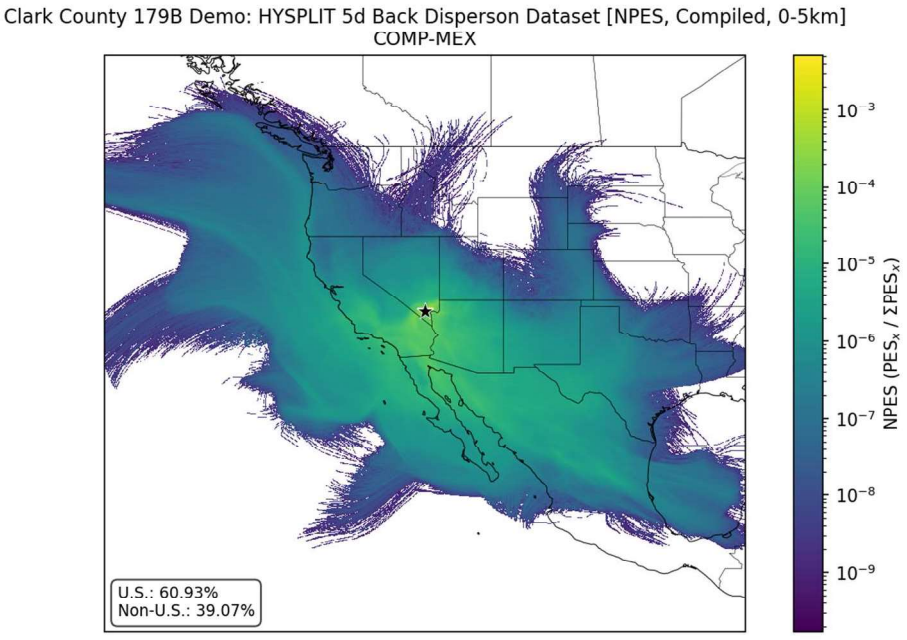

Figure 9. Clark County 5-day back dispersion-based NPES; the results are compiled for the 10 selected exceedance days (see **Table 6**) with the international transport from the Mexico (MEX) air transport regime. NPES is based on the average concentration of a generic, inert tracer gas between 0 and 5 km.

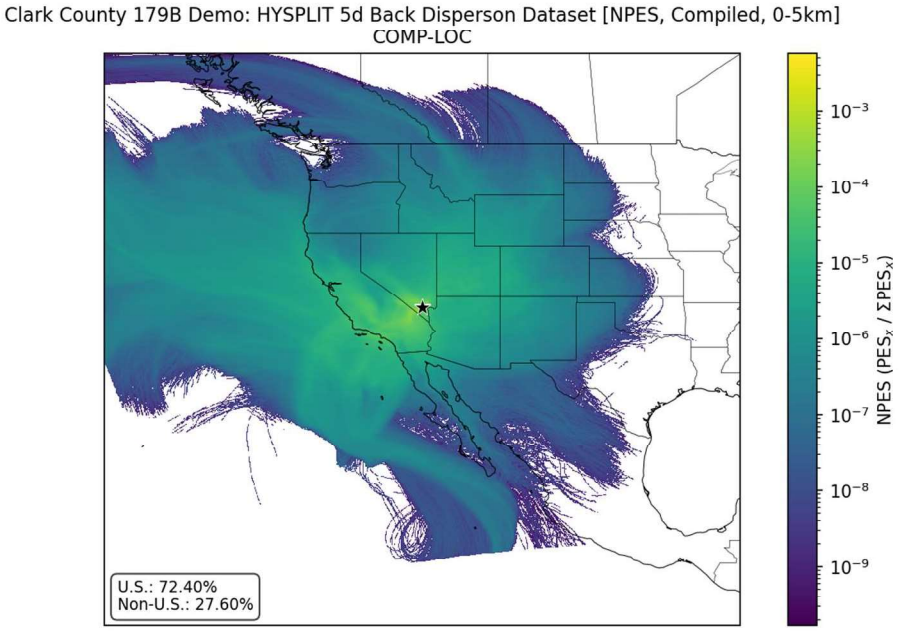

Figure 10. Clark County 5-day back dispersion-based NPES; the results are compiled for the 10 selected exceedance days (see **Table 6**) with the local transport (LOC) air transport regime. NPES is based on the average concentration of a generic, inert tracer gas between 0 and 5 km.

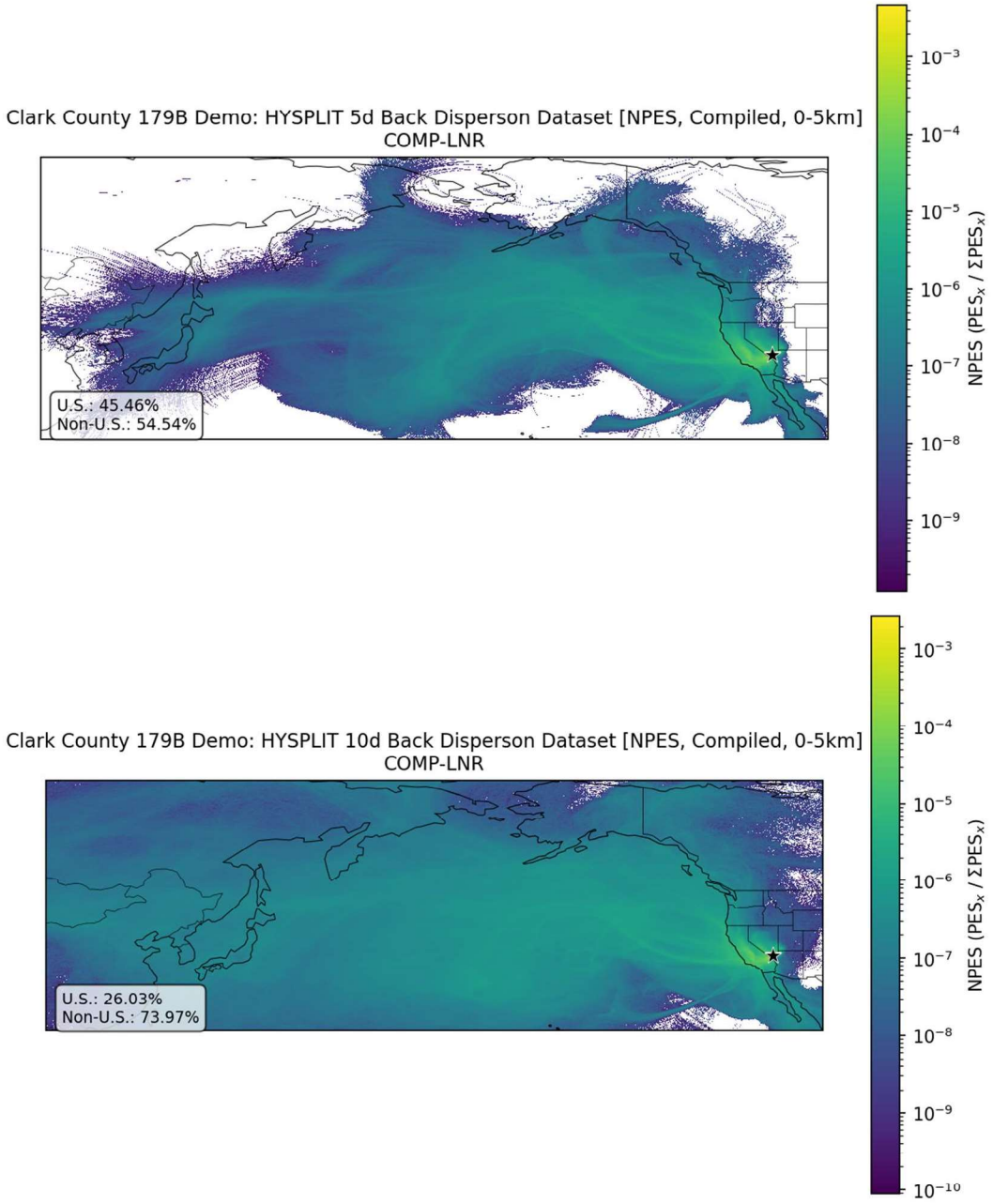

Figure 11. Clark County 5-day (top) and 10-day (bottom) back dispersion-based NPES; the results are compiled for the 10 selected exceedance days (see **Table 6**) with the long-range international transport (LNR) air transport regime. NPES is based on the average concentration of a generic, inert tracer gas between 0 and 5 km.

Figure 12, **Figure 13**, and **Figure 14** show composite NPES for each of the three air transport regimes based on average concentration between 0 and 1 km. The retroplumes in the composite 0-1 km NPES figures are similar to their 0-5 km counterparts but extend a shorter distance, with a larger percentage of NPES occurring within the United States for all transport regimes. This finding indicates that air transport within the PBL occurs over shorter distances, while longer-distance air

movement more often occurs within the free troposphere. Individual daily backward dispersion plots can be found in Backward Dispersion Daily Plots.

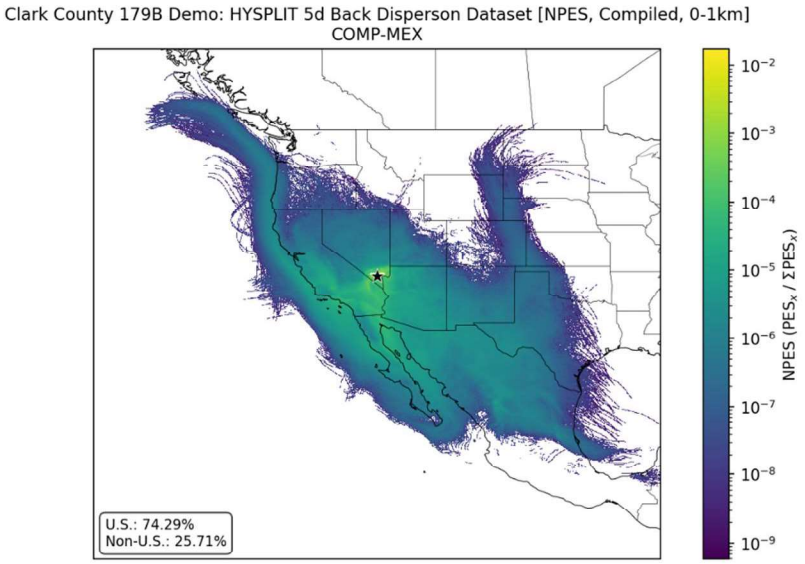

Figure 12. Clark County 5-day dispersion-based NPES; results are compiled for the 10 selected exceedance days (see **Table 6**) with the international transport from the Mexico (MEX) air transport regime. NPES is based on the average concentration of a generic, inert tracer gas between 0 and 1 km.

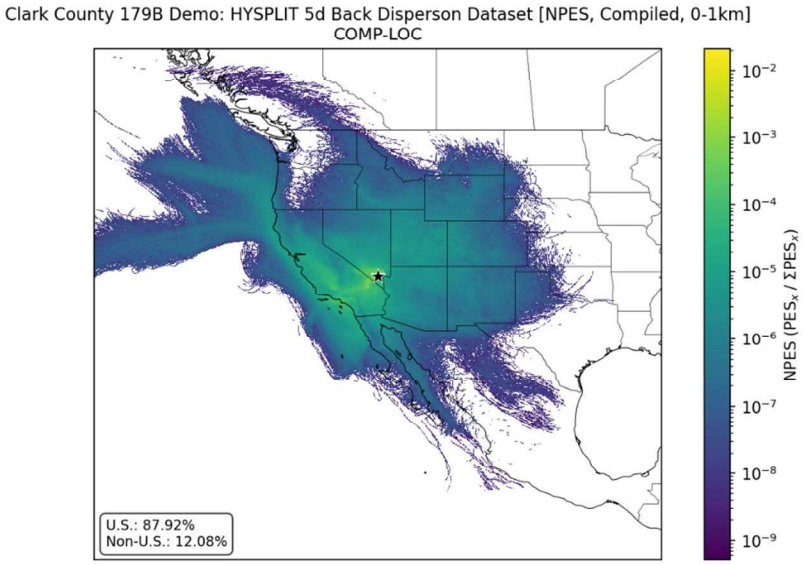

Figure 13. Clark County 5-day dispersion-based NPES; the results are compiled for the 10 selected exceedance days (see **Table 6**) with the local transport (LOC) air transport regime. NPES is based on the average concentration of a generic, inert tracer gas between 0 and 1 km.

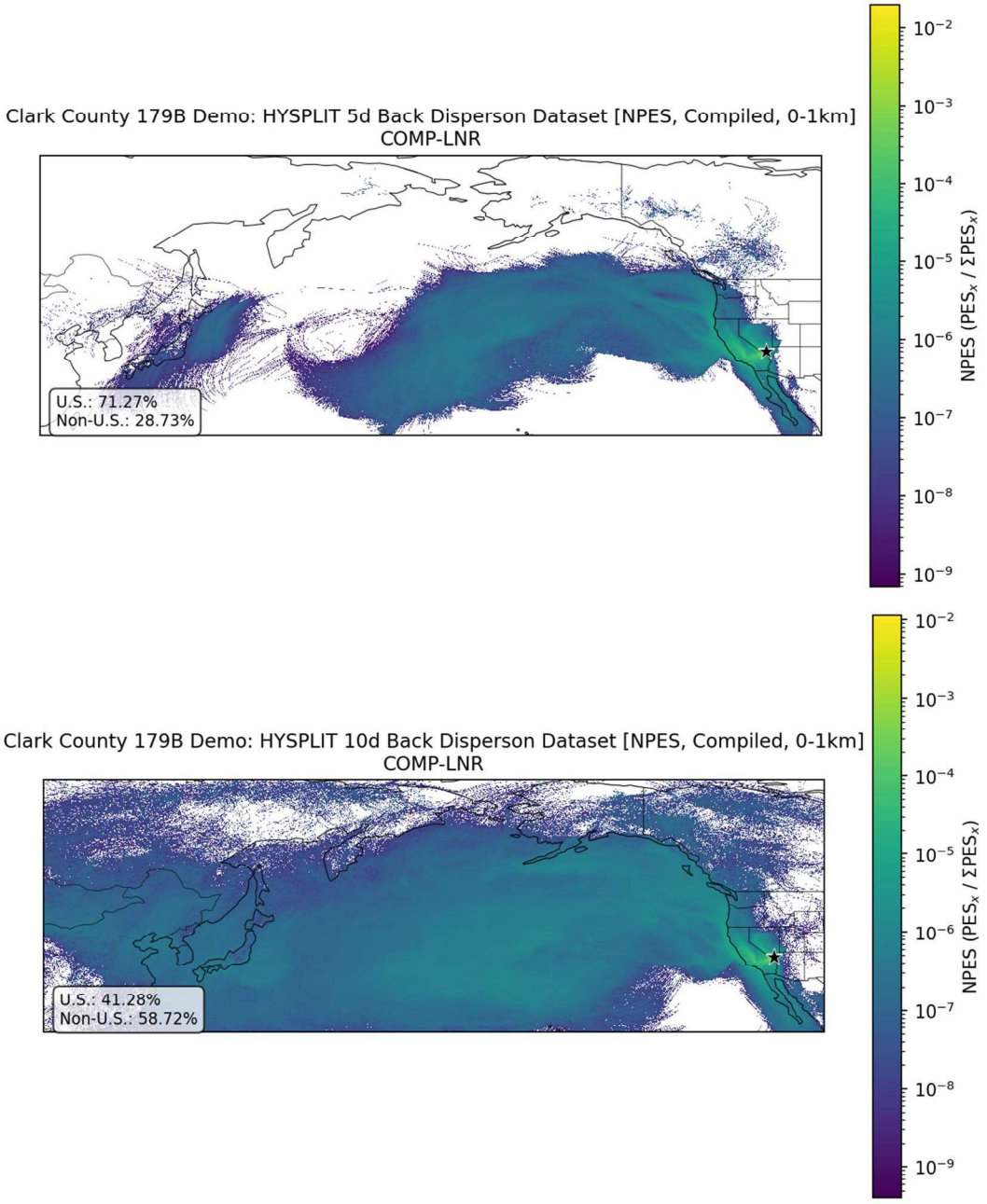

Figure 14. Clark County 5-day (a) and 10-day (b) back dispersion-based NPES; the results are results for the 10 selected exceedance days (see **Table 6**Error! Reference source not found.) with the long-range international transport (LNR) air transport regime. NPES is based on the average concentration of a generic, inert tracer gas between 0 and 1 km.

Summary data provides similar conclusions about the three air regimes as the composite backward dispersion plots (Table 8). In general, the MEX and LNR air regimes have a higher proportion of non-U.S. NPES than the LOC air regime. For LNR, non-U.S. NPES increased from 28.0-83.7% to 59.1-91.3% when the model duration was increased from -5 to -10 days. This increase in non-U.S. NPES is visible in the dispersion plots, which show -10-day retroplumes covering greater portions of the Pacific Ocean and eastern Asia.

Table 8. Summary NPES data for backward dispersion models. This table includes the percentage of NPES from the United States and outside of the United States (for example, from international sources or the ocean). Minimum and maximum percentage as presented, as well as the result from the aggregated composite figure. Each regime, model duration, and height category combination consisted of 10 model runs (i.e., 10 dates).

			% United States			% Non-United States		
Regime	Model Duration	Height Category	Min	Composite	Max	Min	Composite	Max
MEX	-5 days	0-5 km	44.9%	60.9%	79.4%	20.6%	39.1%	55.1%
MEX	-5 days	0-1 km	57.8%	74.3%	88.4%	11.6%	25.7%	42.2%
LOC	-5 days	0-5 km	35.6%	72.4%	98.0%	2.0%	27.6%	64.4%
LOC	-5 days	0-1 km	69.2%	87.9%	99.7%	0.3%	12.1%	30.8%
LNR	-5 days	0-5 km	16.3%	45.5%	72.0%	28.0%	54.5%	83.7%
LNR	-5 days	0-1 km	29.9%	71.3%	96.7%	3.3%	28.7%	70.1%
LNR	-10 days	0-5 km	8.7%	26.0%	40.9%	59.1%	74.0%	91.3%
LNR	-10 days	0-1 km	15.3%	41.3%	66.9%	33.1%	58.7%	84.7%

Several recent observational and modeling efforts have been conducted to characterize ozone sources affected Clark County, Nevada. The LVOS, conducted in late spring 2013, and the FAST-LVOS, conducted in late spring 2017 as a follow-up to LVOS, are summarized in the following sections.

Las Vegas Ozone Study (LVOS) 2013

The LVOS was conducted during late May through June 2013 to assess the seasonal contribution of STT and long-range transport on surface ozone concentrations in Clark County, Nevada. The measurement campaign took place at the Angel Peak Radar Camp and consisted of light detection and ranging (LiDAR) measurements and in-situ measurements.

Model analysis was performed using NOAA/GFDL Atmospheric Model version 3 (AM3) and FLEXible PARTicle dispersion model (FLEXPART). FLEXPART was used diagnostically to characterize transport pathways and air mass origins, while AM3 provided quantitative attribution of stratospheric ozone contributions to surface concentrations. FLEXPART 10-day backwards dispersion modeling was run using a global model domain, released from a 1° x 1° domain centered over Angels Peak, and at a

release rate of 20,000 particles per hour. AM3, a chemistry-climate model, was used to quantify the contribution of stratospheric ozone to surface concentrations in the western U.S. AM3 was applied using a cube-sphere grid resolution of 100 x 100 km^2, daily resolved fire and anthropogenic emissions, and a stratospheric ozone tracer defined relative to a dynamically varying e90 tropopause.

Measurements and modeling were used to draw conclusions about the sources contributing to ozone exceedances during the study period. STT directly contributed over 30 ppbv to surface ozone concentrations during each of the three exceedances. Long range Asian transport contributed to two exceedances during the study by <10 ppbv. Finally, wildfires had a negligible impact on the exceedances during the study; however, it was noted that they were found to be a major factor during exceedance events before and after LVOS. The LVOS study did not assess international emissions originating from Mexico.

Fires, Asian, and Stratospheric Transport – Las Vegas Ozone Study (FAST-LVOS) 2017

The FAST-LVOS was a follow-up study to LVOS that was conducted during late May through June 2017. The goal of FAST-LVOS was to assess the representativeness of the original LVOS results, characterize the distribution of ozone above southern Nevada, and assess the influence of STT, wildfires, and local, regional, and Asian pollution on surface ozone concentrations. The measurement campaign consisted of LiDAR, ozonesonde, aircraft, and in situ measurements.

Measurements from the study found elevated ozone layers above Las Vegas on more than 75% of days, which contributed to regional background ozone concentrations of 50-55 ppbv. These high levels of background ozone pose challenges to meeting the current NAAQS standards and would be especially challenging to reconcile with more strict NAAQS standards. The FAST-LVOS study did not assess international emissions originating from Mexico.

A companion study conducted by Zhang et al. (2020) included modeling using FAST-LVOS data with the goal of quantifying the drivers of springtime surface ozone and model differences. Modeling was performed using two global chemistry models: NOAA/GFDL Atmospheric Model version 4 (AM4) and GEOS-Chem. AM4 simulations were initialized at a horizontal resolution of 50 x 50 km^2, with a stratospheric ozone tracer defined relative to a dynamically varying e90 tropopause and included chemical loss and deposition. AM4 was run for a variety of simulations from January-June 2017:

1. Base simulation with all emissions included;
2. Sensitivity simulation without anthropogenic emissions over North America;
3. Sensitivity simulation without anthropogenic emissions over the U.S.;
4. Sensitivity simulation without Asian anthropogenic emissions;
5. Sensitivity simulation without wildfire emissions;

GEOS-Chem modeling was performed to conduct simulations over North America at 0.25° x 0.3125° horizontal resolution, using a one-way nested-grid. GEOS-Chem uses fully coupled troposphere chemistry mechanism and a simplified stratosphere chemistry mechanism. Initial and boundary conditions consisted of the AM4 base simulation and GEOS-Chem global simulations at 2° x 2.5° resolution for January-June 2017.

The results of FAST-LVOS indicate that stratospheric intrusions are the most pervasive driver of elevated background ozone in Clark County during late spring. These stratospheric intrusions result in elevated background ozone concentration which, in combination with regional pollution, drive NAAQS exceedances. Asian pollution was commonly co-transported with stratospheric air masses and enhanced background ozone. Wildfire influences were episodic, sometimes contributing substantially to surface ozone. These results highlight that background ozone in Clark County is driven by a combination of frequent stratospheric influence and episodic enhancements from transported pollution. FAST-LVOS did not assess international emissions originating from Mexico.

2.2 Meteorological Analysis of Local and Internationally Influenced Days

During the summer ozone season in Clark County, ozone production is influenced by the transport of air from outside sources, including international transport. To identify characteristic air transport patterns, average transport pathways were identified based on cluster analysis initiated on ozone exceedance days from 2016-2024. Exceedance days were selected to prioritize days on which the largest number of monitors recorded ozone exceedances; days that were adjacent in time to exceedance days predominated by another transport pathway were also avoided (see Sections 1.4 and 2.1 for the full methodology). Three different air transport regimes were identified that may lead to enhanced ozone in HA 212: LOC, MEX, and LNR. Thirty dates (10 for each transport regime) with a characteristic transport regime during the annual peak of ozone production (i.e., May-August) were selected (Table 6). The following sections describe analyses conducted to characterize typical synoptic and mesoscale meteorological conditions during the respective transport regimes, including analysis of upper-level geopotential heights and winds and anomalies, skew-T diagrams, surface temperatures, winds, sea level pressure, and sky conditions.

2.2.1 Local Transport

Due to the elevated terrain around the city of Las Vegas, increased mixing heights are an important factor in transporting air into the region from surrounding areas. In addition, wind speeds generally increase with height due to reduced friction with the surface. Therefore, deeper mixing can often tap into air masses that have traveled longer distances before reaching southern Nevada. In a dry desert atmosphere with high pressure aloft and light surface winds, deeply mixed PBLs are most likely to form from the surface upward. As the air in contact with the surface heats by conduction during the

day, the air parcels near the surface become warmer than the surrounding air, causing them to become buoyant and rise convectively. As the air rises and pressure decreases, the parcel of air cools at the dry adiabatic lapse rate of approximately 10°C per kilometer of elevation. Air moving downward to replace the rising air also warms at the rate of 10°C per kilometer. As this mixing air cools and warms at the dry adiabatic lapse rate, it creates a layer of air in contact with the surface, with nearly constant potential temperature. If temperatures above the PBL remain the same, the warmer the surface temperature gets, the deeper the potential mixing heights will be. As a result, as surface temperatures reach their maximum during the late afternoon hours, the PBL also generally reaches its maximum depth during the late afternoon, near the time when the late afternoon upper-air soundings are measured in Las Vegas. Mixing heights can therefore be easily diagnosed by looking for the depth of the atmosphere with constant potential temperature in contact with the surface on the afternoon soundings. These heights indicate the potential for aloft air and pollutants to mix to the ground level.

Mixing heights for the LOC transport days were established via upper-air sounding data from the Las Vegas upper-air weather station (VEF). Using the VEF upper-air data valid for 16:00 PST on LOC transport days, the mean PBL height was estimated to be 3,190 m (10,466 ft) above ground level (AGL), which is higher than the majority of the surrounding terrain. In all cases, ground level is taken to be the elevation at Harry Reid International Airport in Las Vegas (KLAS) (approximately 700 m above sea level). The range of the PBL heights on local transport days was 2,338 m (7,671 ft) AGL at a pressure level of 712 mb (July 9, 2020) to 4,970 m (16,306 ft) AGL at a pressure level of 506 mb (May 14, 2024). This fact indicates the top of the PBL was approximately within the 700-500 mb layer, with 850 mb representing the lower-to-middle portion of the PBL.

Based on the 850 mb average height pattern and the associated trajectory of the 850 mb winds, average winds on LOC transport days generally moved from the Bay Area and San Joaquin Valley of northern California southward toward Los Angeles before turning inland across the Mojave Desert and into Las Vegas (Figure 15). To confirm this pattern, the HYSPLIT model was run for each LOC transport day from the time and location of hourly maximum ozone at the bottom, middle, and top of the boundary layer determined by the upper-air sounding analysis. The trajectories were run backwards over the previous 48 hours to determine the origin of the air masses arriving on the local transport dates. The boundary layer air masses on the majority of these days originated either from southern California near the Los Angeles Basin or from near the Bay Area and the Sacramento Valley. However, two days had origins across far southeastern California, while one back-trajectory came from Reno, Nevada and far northern California. There were three cases in which air at the top of the boundary layer originated in western Utah. HYSPLIT back-trajectories run for all 10 days can be found in LOC Transport Back-Trajectories.

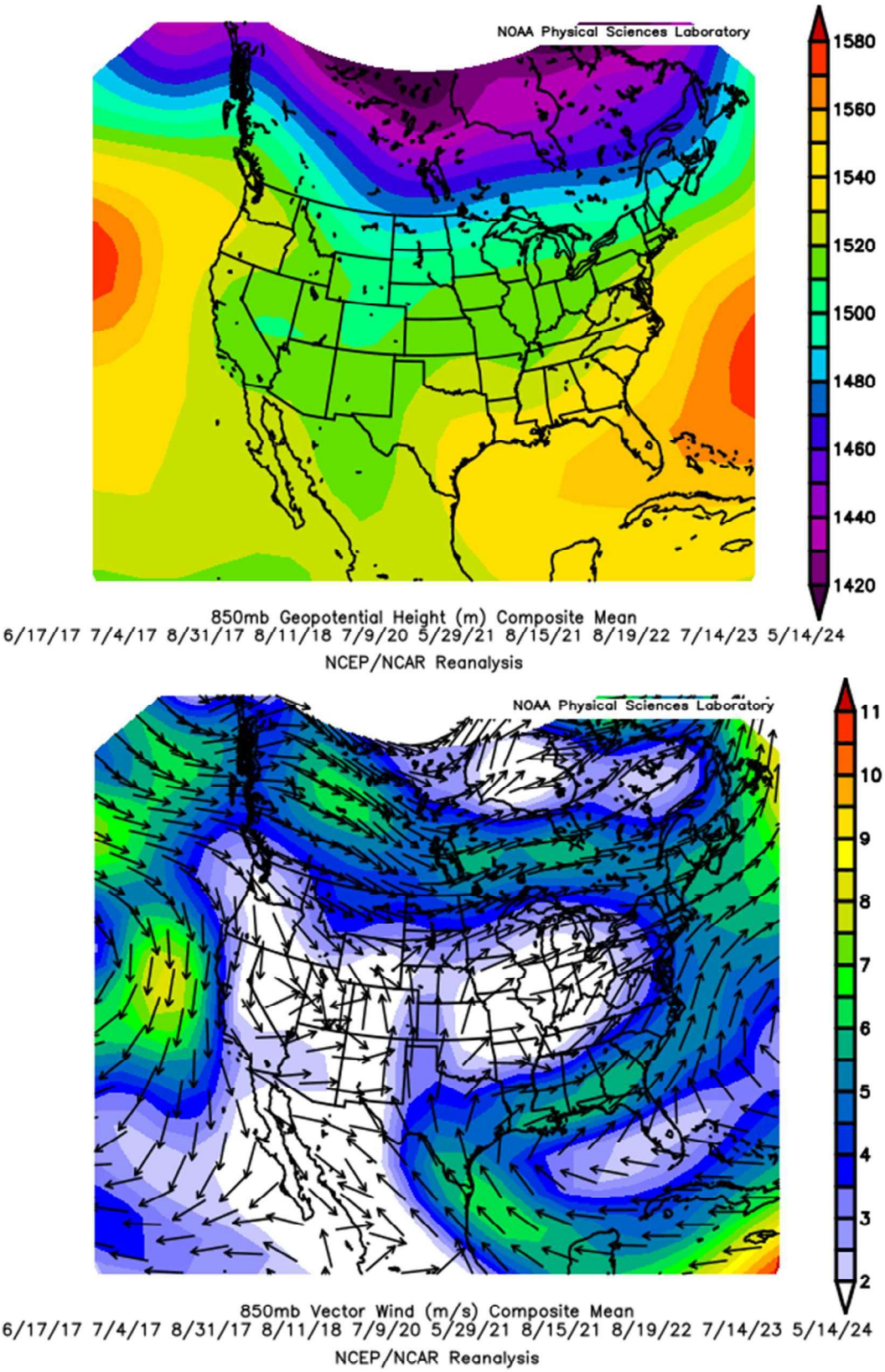

Figure 15. Mean heights (top) and wind vectors (bottom) at 850 mb on LOC transport days. Source: NOAA.

As a result of the mean wind and boundary layer HYSPLIT analysis, the aloft portion of this analysis will focus on the region from far northern California to western Utah, and southward to far southern California. The images in Figure 16 show a comparison of the average May-to-August 500 mb (top left) and 700 mb (top right), and the 500 mb (bottom left) and 700 mb (bottom right) geopotential heights on the 10 LOC transport days. There is a more pronounced ridge of high pressure over the western United States on the LOC transport days compared with the average seasonal patterns.

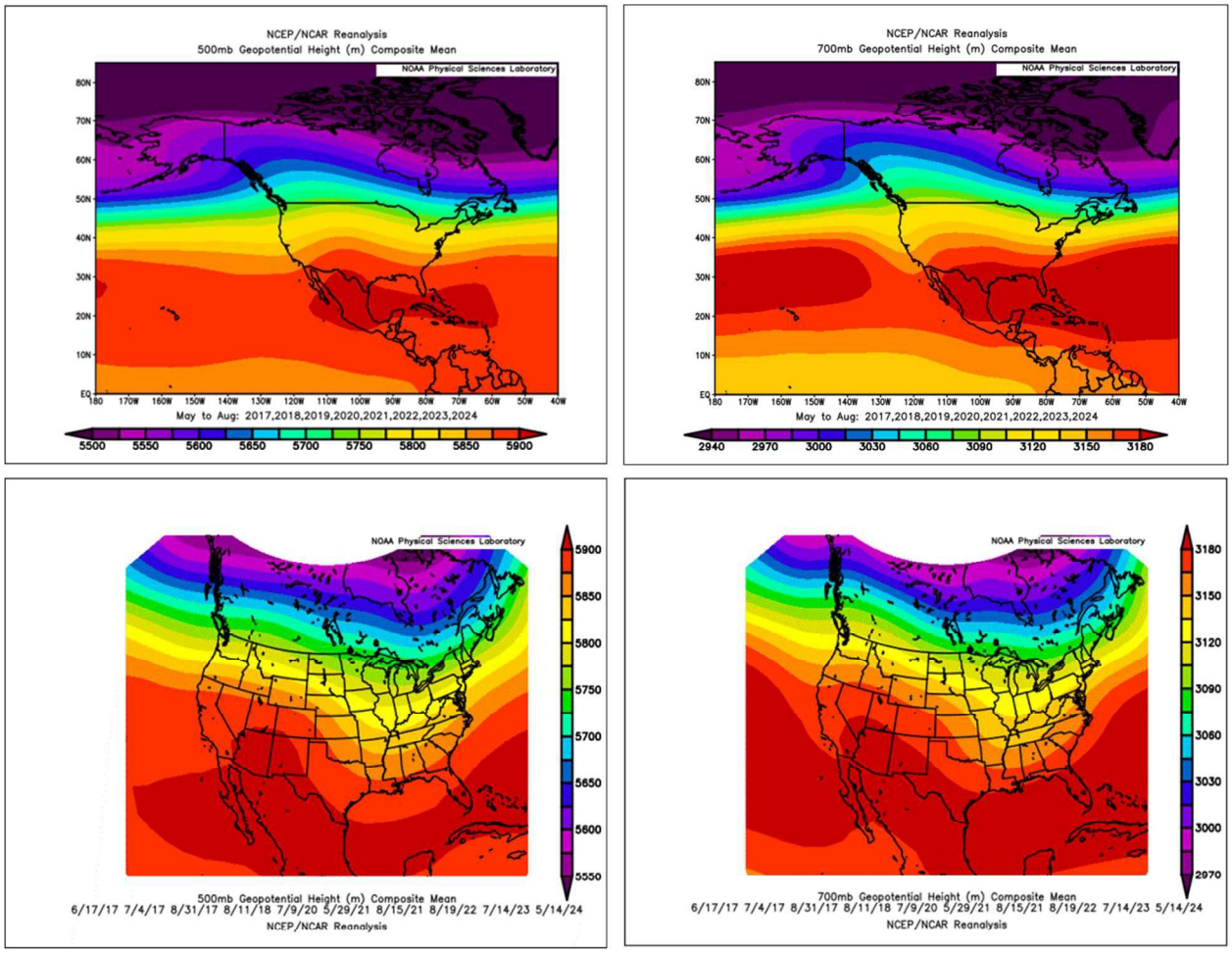

Figure 16. Mean heights (m) at 500 mb and 700 mb from May to August (2017-2024) (top) and mean heights (m) at 500 mb and 700 mb for the LOC transport days (bottom). Source: NOAA.

The above-normal heights extend from the Desert Southwest into the Rockies and into the Pacific Northwest (Figure 17); this area encompasses the area identified as the origin for air masses on the LOC transport days.

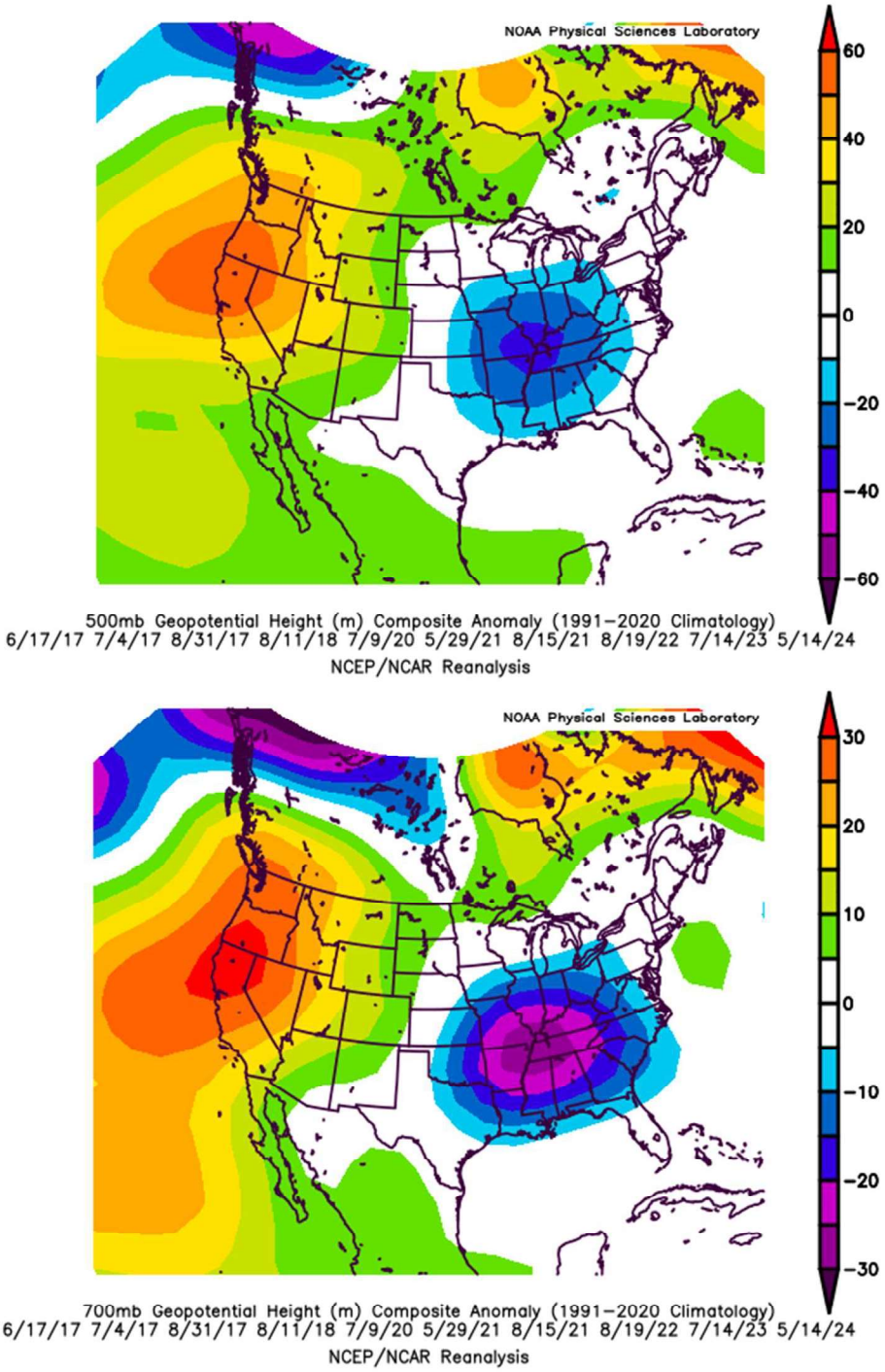

Figure 17. Geopotential height anomalies at 500 mb (top) and 700 mb (bottom) for the LOC transport days. Source: NOAA.

These anomalously high heights corresponded with generally sunny skies and hot temperatures near the surface; such conditions aid regional ozone development in upwind areas and enhance local

mixing heights. Figure 18 shows the average 2-meter temperature anomalies over the 48 hours preceding each local transport event.

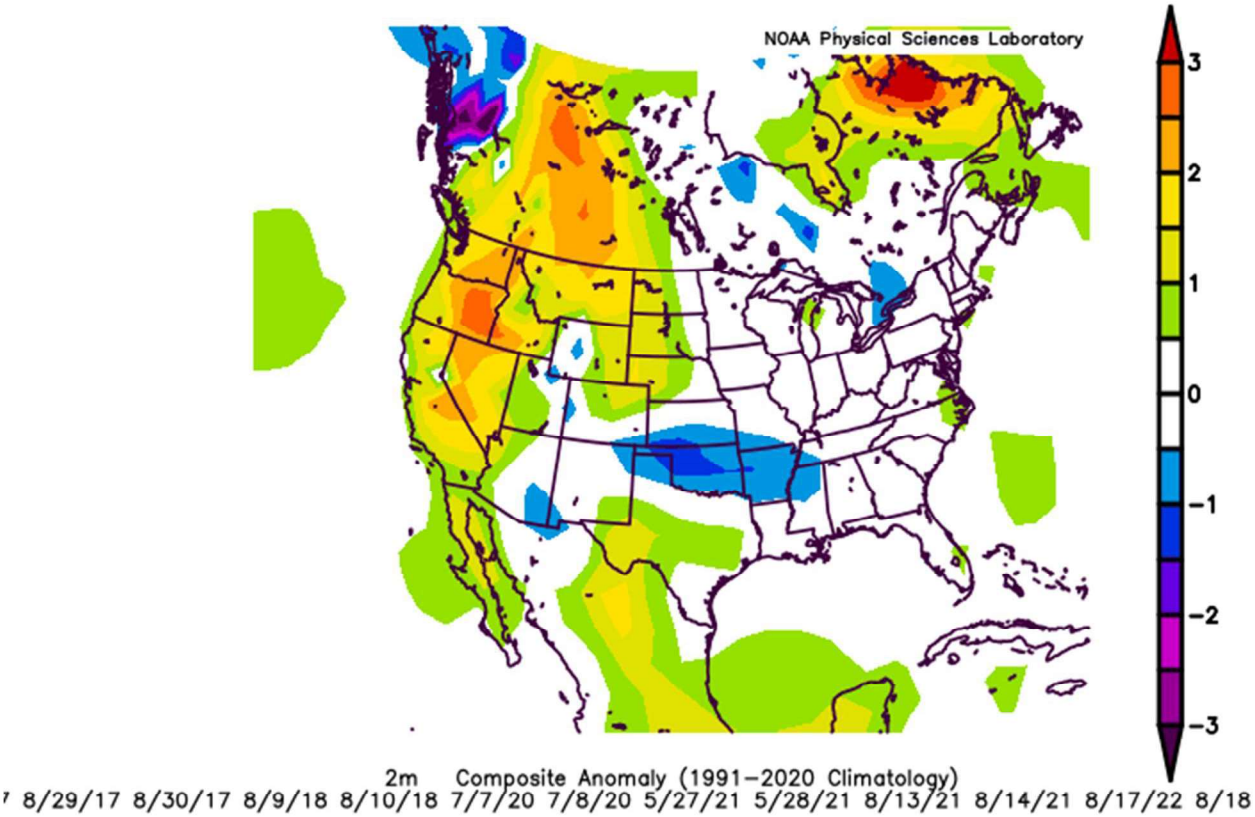

Figure 18. 2-m temperature anomalies over the 48 hours preceding each LOC transport event. Source: NOAA.

The positive surface temperature anomalies indicate the potential for increased ozone production across the air mass origin region, including the Bay Area, Sacramento, the San Joaquin Valley, and the Los Angeles Basin. In the HYSPLIT analysis, USG daily maximum 8-hr ozone AQI levels were noted near the 48-hr back-trajectories outside of the Las Vegas area in 9 out of the 10 cases. Dry and warm conditions also correspond with fire activity around the region. The transport paths from HYSPLIT crossed or passed near regions with fire and smoke on Hazard Mapping System (HMS) satellite imagery (not shown) on 7 out of the 10 LOC transport days, with smoke potentially contributing to regional ozone precursors.

As the air masses with elevated ozone entered Las Vegas from around the region and mixed to the surface, local conditions were conducive to further ozone production (Table 9). Due to weak gradients of surface pressure, surface winds at Harry Reid International Airport in Las Vegas averaged only 6 mph on the local transport days. As a result, once the regional pollutants arrived in Las Vegas, limited dispersion allowed the pollutants to linger. In addition, high temperatures averaged 105˚F

(40.6°C) on the LOC transport days under mostly sunny skies. These local conditions further supported ozone formation, leading to USG ozone AQI levels in the Las Vegas area.

Table 9. Surface weather conditions at KLAS on local transport days.

Local transport date	Mean Wind Speed (m/s) at KLAS	Max. Temp (°C)
6/17/2017	2.2	43.3
7/4/2017	2.7	42.8
8/31/2017	3.6	39.4
8/11/2018	4.0	41.7
7/9/2020	4.0	41.1
5/29/2021	1.8	34.4
8/15/2021	1.8	42.2
8/19/2022	2.7	37.8
7/14/2023	1.8	43.9
5/14/2024	2.7	36.1
Average	**2.7**	**40.6**

On the 10 days with LOC transport into Clark County, there was deep mixing in the PBL due to hot surface temperatures that allowed air transported into the region to mix down to the surface. Aloft winds transported air masses from areas in California such as the Los Angeles Basin, the Bay Area, Sacramento, and southeastern California into the Las Vegas area on the majority of the LOC transport days, as evidenced by winds at 850 mb and 48-hr HYSPLIT back-trajectories. Due to anomalously high pressure aloft, sunny and dry conditions led to above-normal temperatures in upwind areas, enhancing ozone formation. HYSPLIT back-trajectories crossed areas with USG ozone AQI levels outside of Las Vegas during the preceding days for 9 out of the 10 LOC transport days. Regional smoke was identified near the transport paths on 7 out of the 10 LOC transport days, which may have contributed to additional ozone precursors. Once regional pollutants arrived in Las Vegas, local conditions supported continued ozone development, including limited dispersion due to light winds and high average temperatures of 40.6°C.

2.2.2 Transport from Mexico

Figure 19 shows the mean 500 mb (5,500 m AGL) and 700 mb (3,000 m AGL) geopotential height patterns for the MEX transport days. The typical pattern at each level consists of a ridge of high pressure aloft across California, Nevada, Utah, and Arizona.

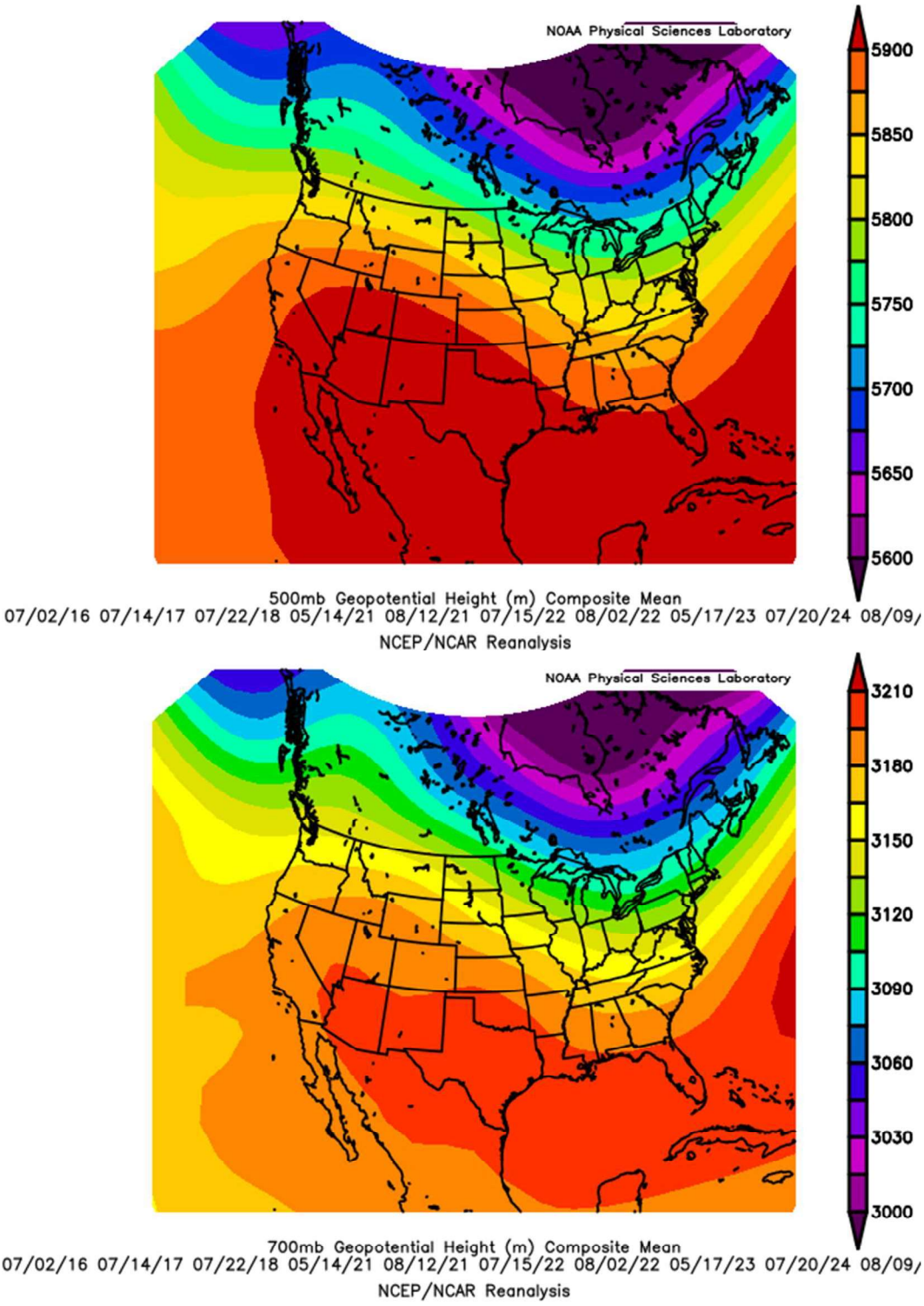

Figure 19. Mean geopotential heights at 500 mb (top) and 700 mb (bottom) on MEX transport days. Source: NOAA.

When comparing the 500 mb and 700 mb geopotential heights on MEX transport days to geopotential heights on these same dates in other years, a positive geopotential height anomaly was found across much of the western United States, including Nevada (Figure 20). These positive height anomalies were associated with persistent high pressure aloft, caused by an abnormally warm layer of air from the surface up to the analysis heights. As described in Section 2.2.1, the warm surface temperatures and sunny skies associated with upper-level high pressure can enhance atmospheric mixing as well as ground-level ozone formation.

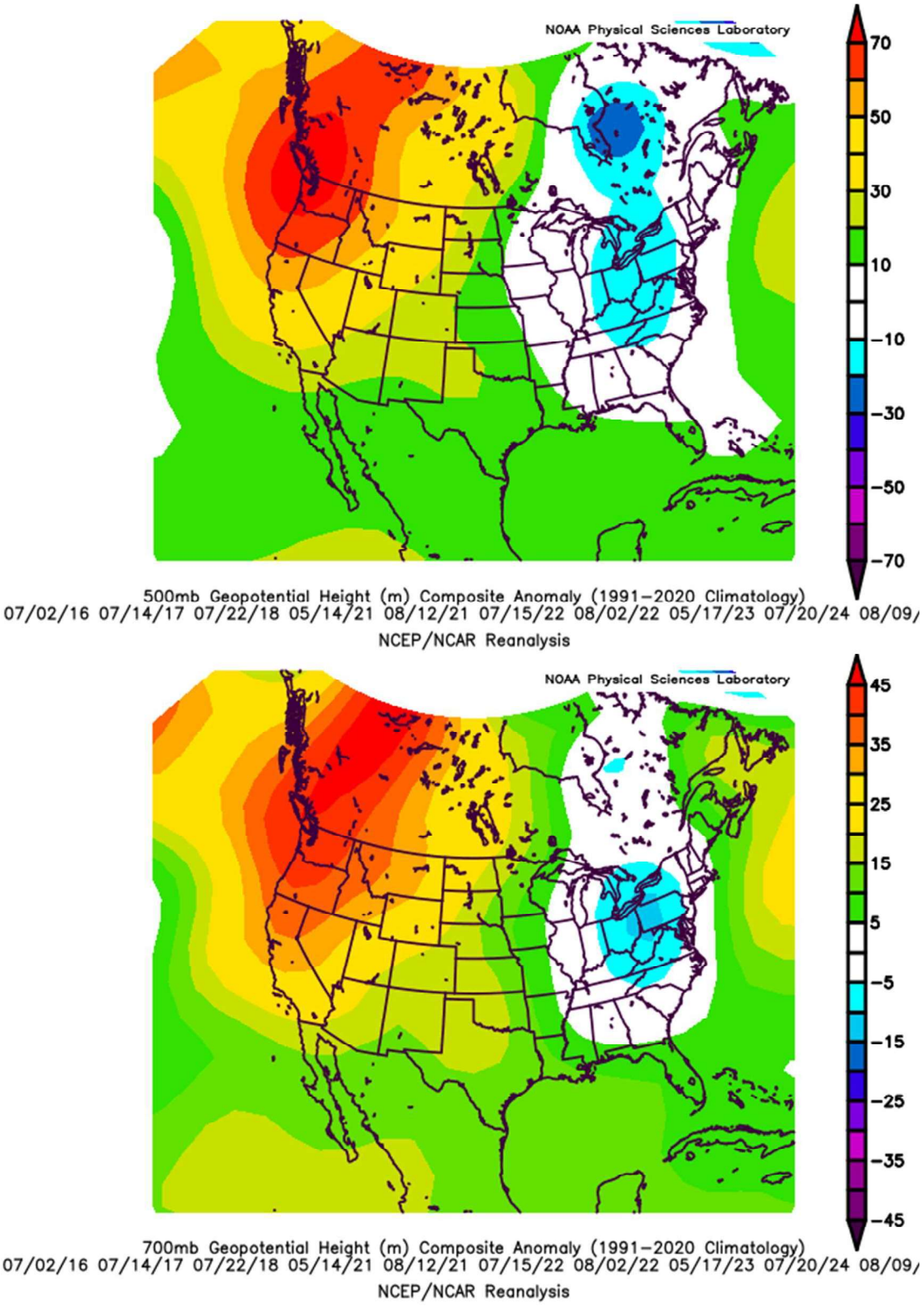

Figure 20. Geopotential height anomalies at 500 mb (top) and 700 mb (bottom) on MEX transport days. Source: NOAA.

Atmospheric conditions were also established via upper-air skew-T diagrams from the Las Vegas upper-air weather station (KVEF). These diagrams can determine the height of the PBL, which indicates the extent of the vertical transfer of air (and any pollutants) from aloft down to ground level. Using the KVEF upper-air data (valid for 16:00 PST) on MEX transport days, the mean PBL was estimated to be around 4,000 m (13,123 ft) AGL, which is a height greater than the surrounding terrain. The range of the PBL on MEX transport days was 2,500 m (8,202 ft) AGL (July 2, 2016) to 4,900 m (16,706 ft) AGL (May 14, 2021, and July 20, 2024). The mean and range in the PBL indicate deep mixing, allowing aloft air to be transferred vertically to the surface.

Transport patterns were assessed at the 700 mb and 850 mb level (1,500 m AGL) to determine whether aloft air from Mexico could reach Clark County. Figure 21 shows the mean 700 mb and 850 mb wind speed and direction for MEX transport days. It was found that southerly to southwesterly winds aloft were common over southern Nevada; upwind, southerly to south-southeasterly winds were present over the Colorado River Valley and northern Baja California. This wind pattern suggests aloft air being carried from Mexico into Clark County.

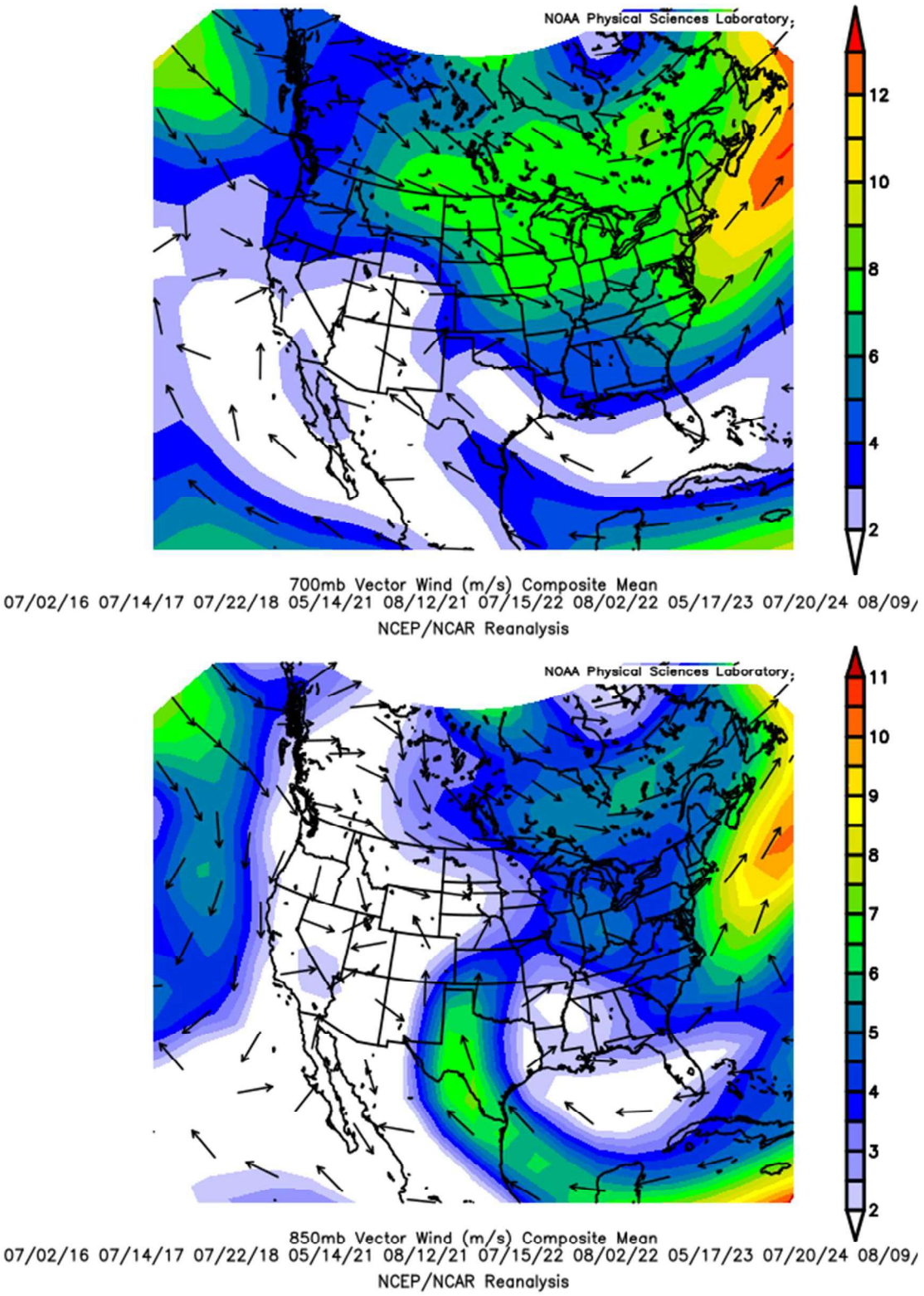

Figure 21. Mean wind vectors at 700 mb (top) and 850 mb (bottom) on MEX transport days. Source: NOAA.

The prevailing wind pattern at 700 mb was dictated by a ridge of high pressure over California, Nevada, Utah, and Arizona. Winds at 850 mb on MEX transport days were driven by high pressure over the northern Gulf of America and an area of low pressure off the Baja California spur (**Figure 22**). Additionally, 850 mb height anomalies also shown in Figure 23 were positive across the western United States, which was consistent with the anomaly findings at 700 mb and 500 mb.

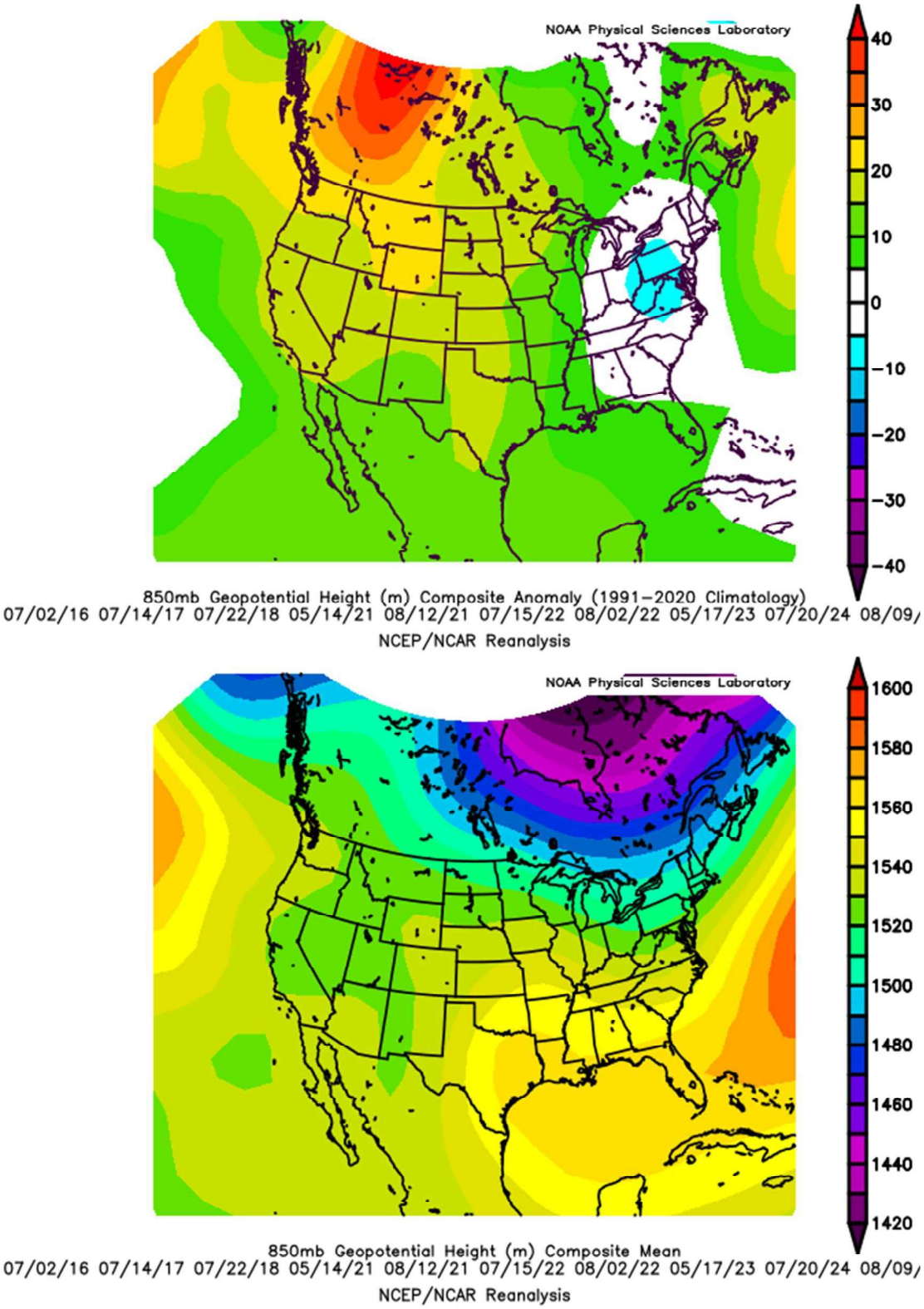

Figure 22. 850 mb geopotential heights (bottom) and height anomalies (top) for MEX transport days. Source: NOAA.

At the surface, ozone production is driven by sunshine, warm afternoon temperatures, and light winds. For the 10 MEX transport days, these surface meteorological conditions were present. Afternoon high temperatures at both KLAS and the North Las Vegas Airport (KVGT) were at or above 38°C on most days, while a few days recorded afternoon high temperatures in the mid- to upper-30s°C. These temperatures, combined with partly to mostly sunny skies each day, were sufficient to promote deep mixing and ozone development with the transported precursors.

Hot temperatures during the summer months can also lead to the development of a thermal low across southern Nevada and the Colorado River Valley. A thermal low is an area of low pressure at the surface, formed by hot temperatures generating rising air parcels from the ground to the upper levels of the atmosphere. These rising parcels produce a persistent area of surface low pressure. The thermal low can be further enhanced by the relatively cooler waters of the Gulf of California, where an area of high pressure develops at the surface. Because of the pressure difference between the Gulf of California-induced surface high and thermal low over the Colorado River Valley, a southerly wind can develop at the surface from the Gulf of California into Clark County. This wind can be a conduit for pollutant transport from Mexico.

Figure 23 shows the average sea level pressure at the surface on MEX transport days. Lower sea level pressure is noted across southern Nevada, the Colorado River Valley, and northwestern Mexico. This configuration suggests the presence of a thermal low and potential for southerly winds.

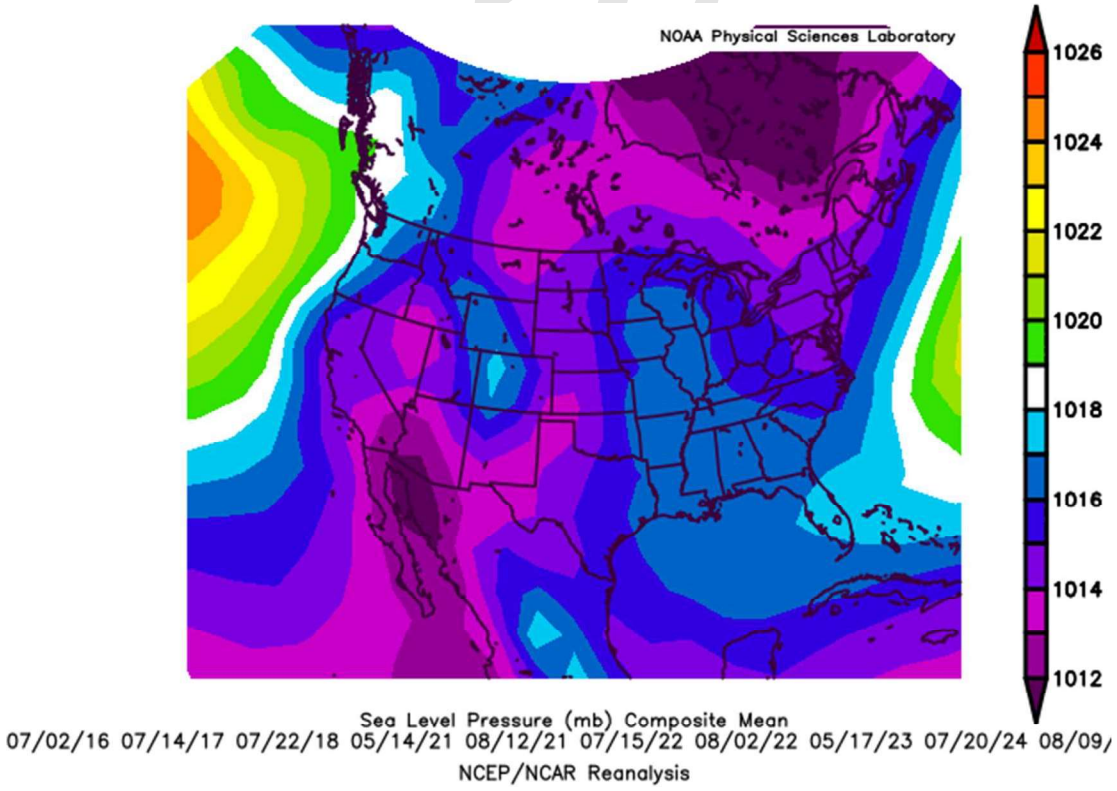

Figure 23. Mean surface sea level pressure on MEX transport days. Source: NOAA.

Figure 24 shows the wind roses for MEX transport days at KLAS (top) and KVGT (bottom). When comparing both sites, the wind directions varied. Even though KLAS and KVGT are located nine miles apart, the varying wind directions captured between the two Automated Surface Observing Systems (ASOS) sites are common. Figure 25 contains the historical wind roses for the 2016-2024 period between May 14 and August 12, which also show varying wind directions when comparing each ASOS site. This variation in wind direction is a result of regional terrain influences that lead to lower-level and surface winds being channeled through mountain gaps and other terrain features. Regarding wind speeds on MEX transport days, the average wind speed was calculated to be less than 6 mph. As a result of these light winds, dispersion of pollutants and ozone precursors was inhibited.

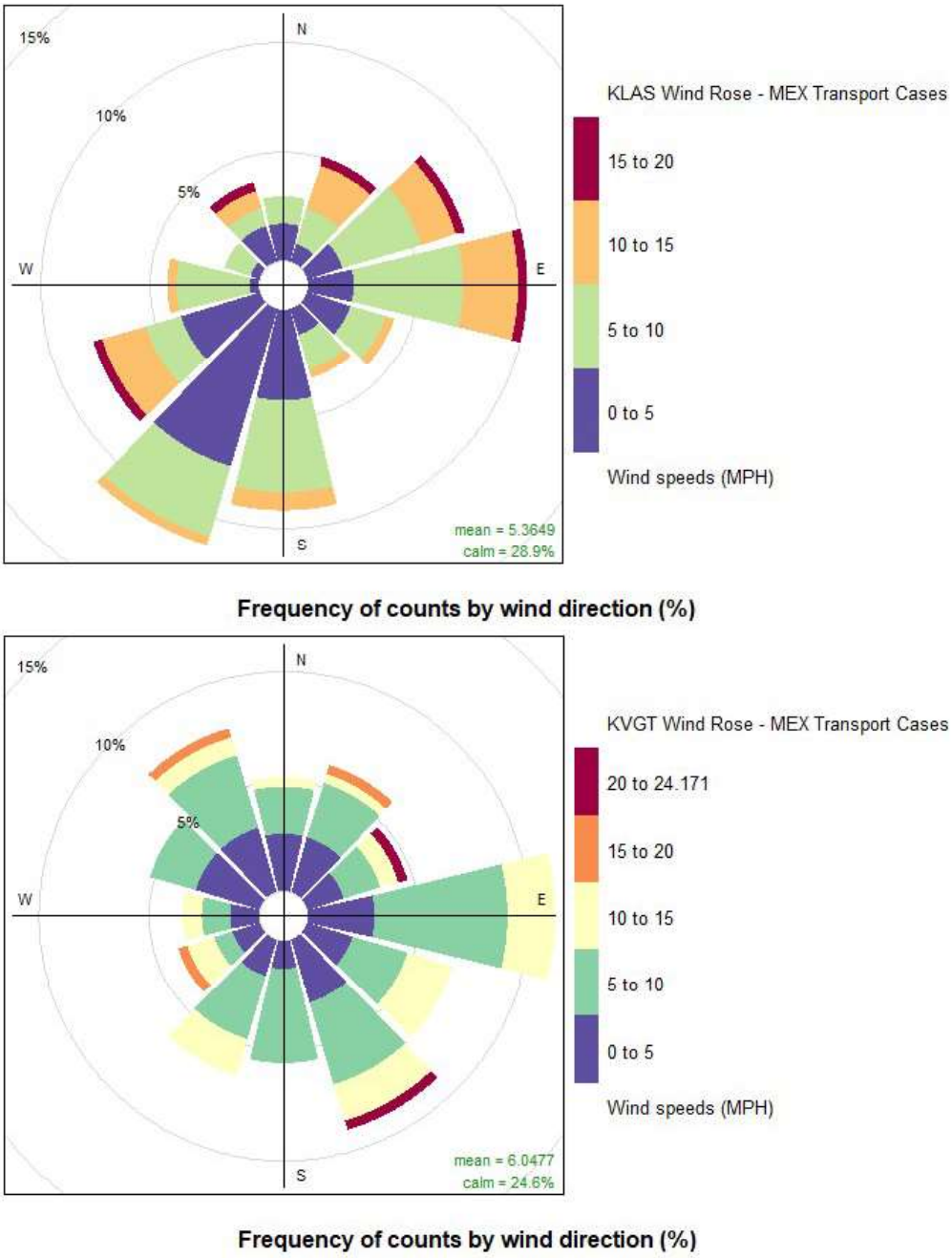

Figure 24. Wind rose diagrams on MEX transport days at KLAS (top) and KVGT (bottom). Data source: Iowa State Mesonet.

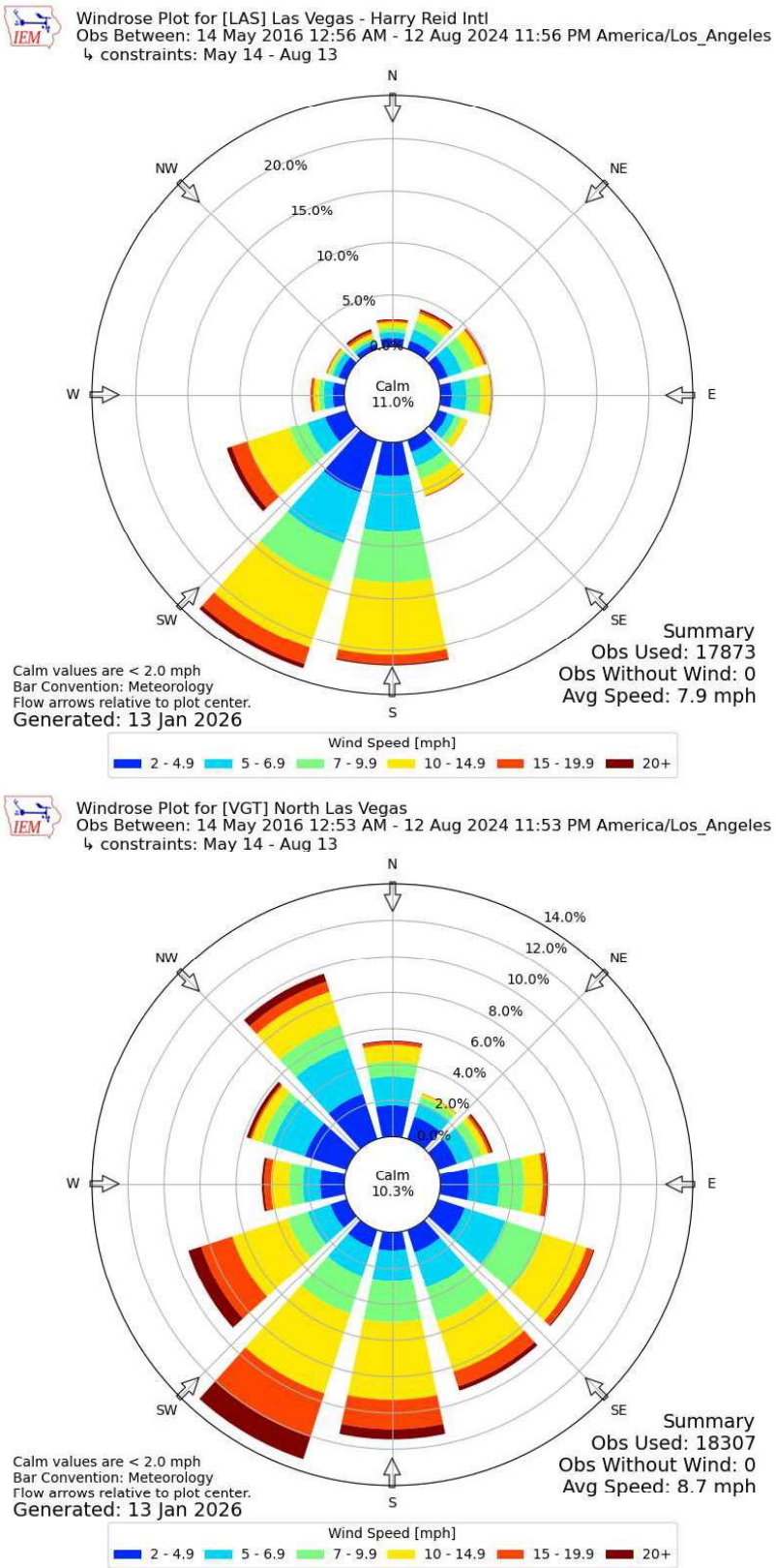

Figure 25. Historical wind rose diagrams for KLAS (top) and KVGT (bottom) for the May 14-August 12 period between 2016 and 2024. Data source: Iowa State Mesonet

Figure 26 shows the diurnal pattern for wind speed and direction on MEX transport days at KLAS (top) and KVGT (bottom), without periods of calm winds to better identify any potential periods for transport. In the left panels, a higher density (more red colors) indicates a higher frequency of wind directions during a given hour, whereas a lower density (more blue colors) indicates a lower frequency of wind directions during a given hour. On average, wind speeds throughout the diurnal period were generally less than 4.4 m/s, indicating a reduction in pollutant dispersion. When comparing the two ASOS sites, the diurnal wind direction on MEX transport days varied, due to the aforementioned terrain influences. Southerly to southwesterly winds were common at KLAS during the evening and overnight hours, which suggests transport of pollutants and ozone precursors from the south into Clark County. At KVGT, northwesterly winds were common during the overnight hours. The convergent pattern of northwesterly overnight winds at KVGT with southerly to southwesterly overnight winds at KLAS would allow transported pollutants to accumulate in Clark County. By the late morning and continuing through the late afternoon on MEX transport days, winds at KVGT shifted from northwesterly to easterly to south-southeasterly. Given this wind shift, there is evidence on MEX transport days that pollutants and ozone precursors carried toward KLAS during the overnight hours would reach KVGT as soon as the late morning, resulting in enhanced ozone formation.

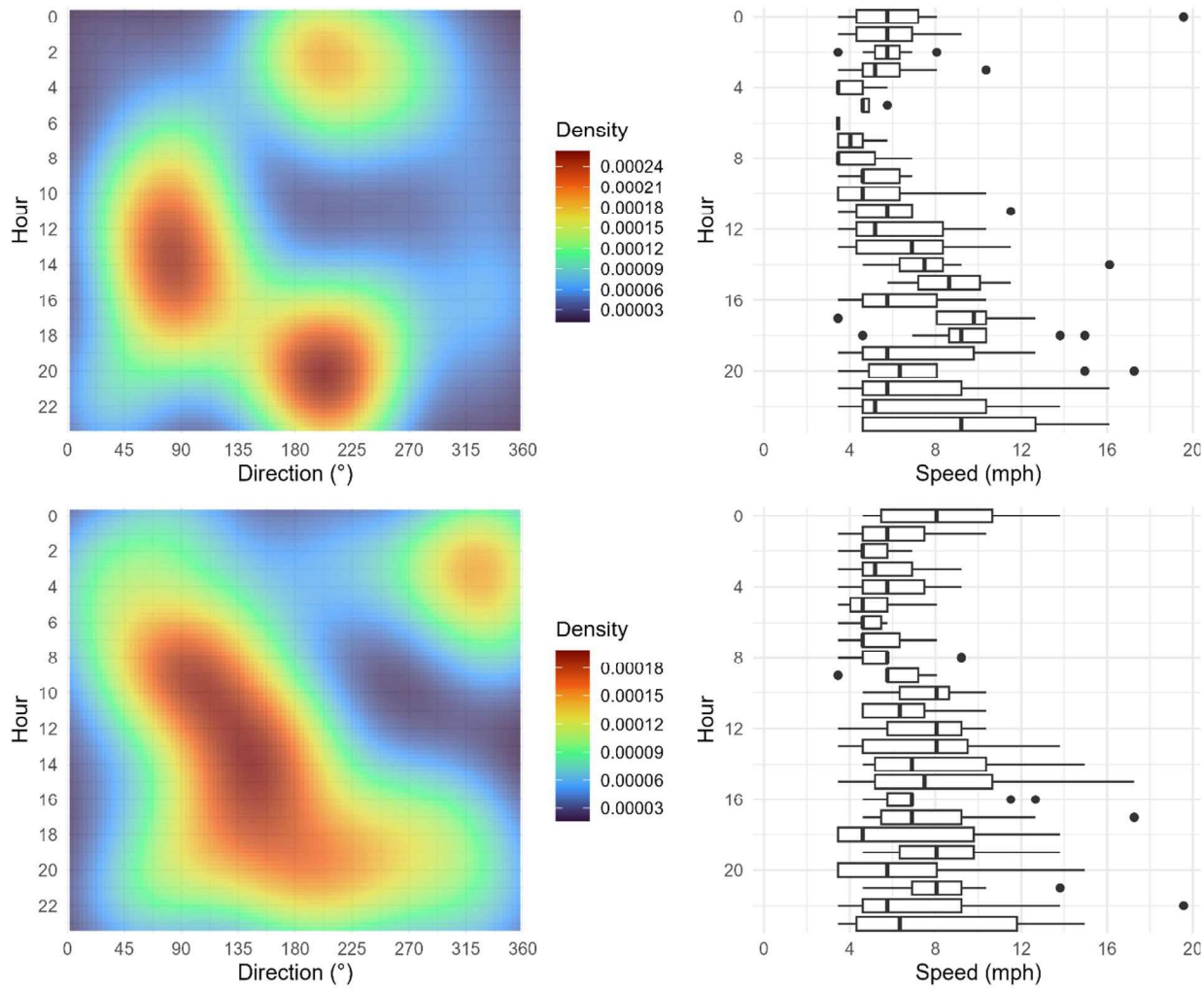

Figure 26. Frequency density of hourly wind direction (left) and hourly wind speeds (right) for KLAS (top) and KVGT (bottom) on MEX transport days. Data source: Iowa State Mesonet.

On the 10 days with MEX transport into Clark County, upper-level high pressure over the southwestern United States resulted in warm temperatures aloft and at the surface, conditions that are conducive to ozone formation. Winds at 700 mb and 850 mb on MEX transport days were southerly to south-southeasterly over northern Baja California, shifting to southerly to southwesterly over Clark County. This wind pattern allows aloft pollutants to reach southern Nevada. Deep mixing due to warm surface temperatures led to high PBL heights averaging around 4,000 m AGL on MEX transport days, which indicates the vertical transfer of aloft air (and any lofted pollutants) to the surface. Partly to mostly sunny skies and hot afternoon temperatures of at least 32°C and sometimes above 38°C promoted ozone formation. The development of surface thermal low pressure over the Colorado River Valley, coupled with an area of surface high pressure over the Gulf of California, suggests the development of a southerly wind from northwestern Mexico into Clark County. Light

surface winds on MEX transport days inhibited dispersion of pollutants and ozone precursors. Additionally, converging winds overnight primarily due to terrain influences allowed pollutants transported from the south into Clark County to accumulate. Late morning to late afternoon winds at KVGT were easterly to south-southeasterly on MEX transport days, which allowed pollutants carried into KLAS overnight to reach KVGT, further enhancing ozone development.

2.2.3 Long-Range International Transport

Atmospheric conditions were established via upper-air sounding data from the KVEF station. Vertical profiles of potential temperature can be used to determine the height of the PBL, which indicates the extent of the vertical transfer of air (and pollutants) from aloft down to ground level. Using the KVEF upper-air data valid for 16:00 PST on LNR transport days, the mean PBL height was estimated to be 3,400 m (11,155 ft) AGL. In all cases, ground level is taken to be the elevation at Harry Reid International Airport in Las Vegas (approximately 700 m above sea level). The range of the PBL heights on LNR transport days was 2,030 m (6,660 ft) AGL (May 20, 2021) to 4,610 m (15,125 ft) AGL (May 31, 2024). The height levels in the next sections were selected based on the range of PBL heights for the LNR transport days.

The relatively deep mixing on these days was driven, in part, by the consistent pattern of upper-level troughing, wherein an area of low pressure was observed over the West Coast of the United States. The dynamics behind deep mixing on the LNR transport days differs from the LOC and MEX transport cases in that the deep mixing on the LOC and MEX days is not primarily driven by surface heating. Deep mixing associated with upper-level troughing is also supported by the vertical motion caused by an increase in cyclonic atmospheric spin aloft known as positive vorticity advection, and also by cooling upper-level temperatures. While surface heating can still aid atmospheric mixing on these days, those convective processes are aided by the upper-level weather system cooling temperatures above the PBL. The combination of the cooling aloft and surface heating can result in deep PBLs similar to the LOC and MEX cases, without the heat observed on those days. In fact, the average maximum surface temperature on the LNR transport days at KLAS was only 91°F (33°C) compared to 104°F (40°C) for the MEX cases and 105°F (40°C) for the LOC cases. However, the range of mixing heights on the LNR transport days was nearly identical to the mixing heights on the hotter days.

The mean pattern of 500 mb geopotential heights (a proxy for pressure) for these days is shown in Figure 27, with a pronounced trough of low pressure over the western United States. Figure 27 also shows the 500 mb geopotential height anomaly for these days, indicating that, on average, pressure was anomalously low over much of the western United States on LNR transport days.

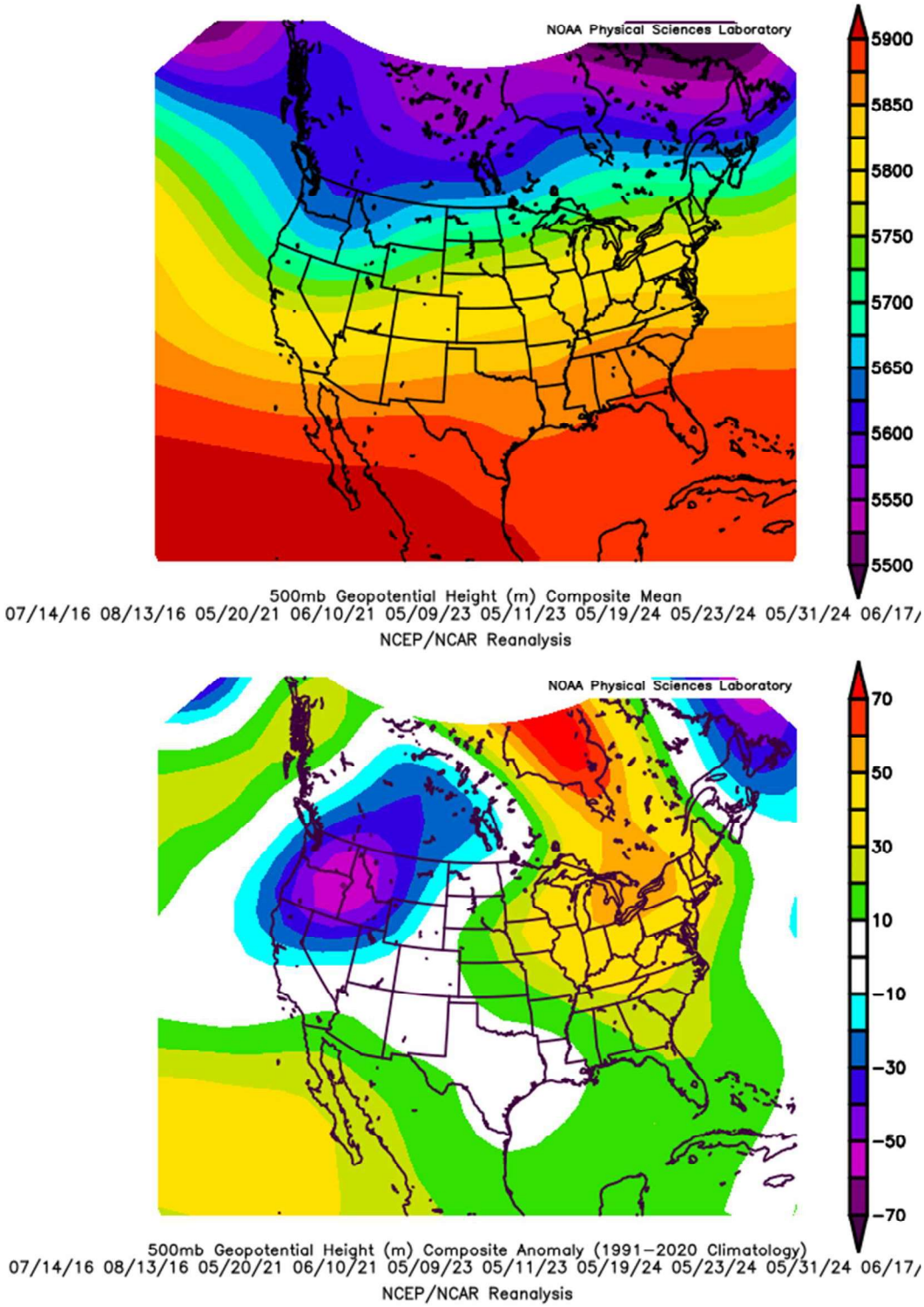

Figure 27. Mean geopotential height (top) and anomalies (bottom) at 500 mb on LNR transport days. Source: NOAA.

On LNR transport days, daily maximum mixing heights fell between 2,030 m and 4,610 m AGL; those heights correspond to approximately 725 mb and 535 mb pressure levels, respectively. The average height was 3,400 m AGL (612 mb). Accordingly, pressure patterns and winds were analyzed at the following pressure levels and corresponding approximate heights AGL:

- 700 mb, 2,630 m AGL
- 850 mb, 800 m AGL

Figure 28 shows the mean and anomaly geopotential height patterns at 700 mb for the LNR transport days. The observed geopotential heights and height anomalies at the 700 mb level on LNR transport dates indicate strong aloft high pressure over the Pacific Ocean, with a positive geopotential height anomaly observed across much of the central and western Pacific Ocean. This high-pressure pattern at 700 mb is associated with enhanced west-to-east upper-level wind flow along the northern edge of the aloft high pressure. This wind flow pattern supports LNR cross-Pacific transport and the corresponding transport of any pollutants contained within that air mass.

Similar geopotential height patterns were observed at lower levels as well, including the 850 mb level (Figure 29). However, at the 850 mb level, the mean geopotential height pattern had a pronounced maximum centered over the east-central Pacific. This pattern is consistent with a low-level wind pattern of anti-cyclonic (clockwise) flow around the high-pressure center, corresponding to westerly (west-to-east) winds over the eastern Pacific at around 40-45°N latitudes, shifting to more northwesterly (northwest-to-southeast) to northerly along the North American West Coast. This wind pattern would facilitate transport across the northeastern Pacific and into the western and southwestern continental United States.

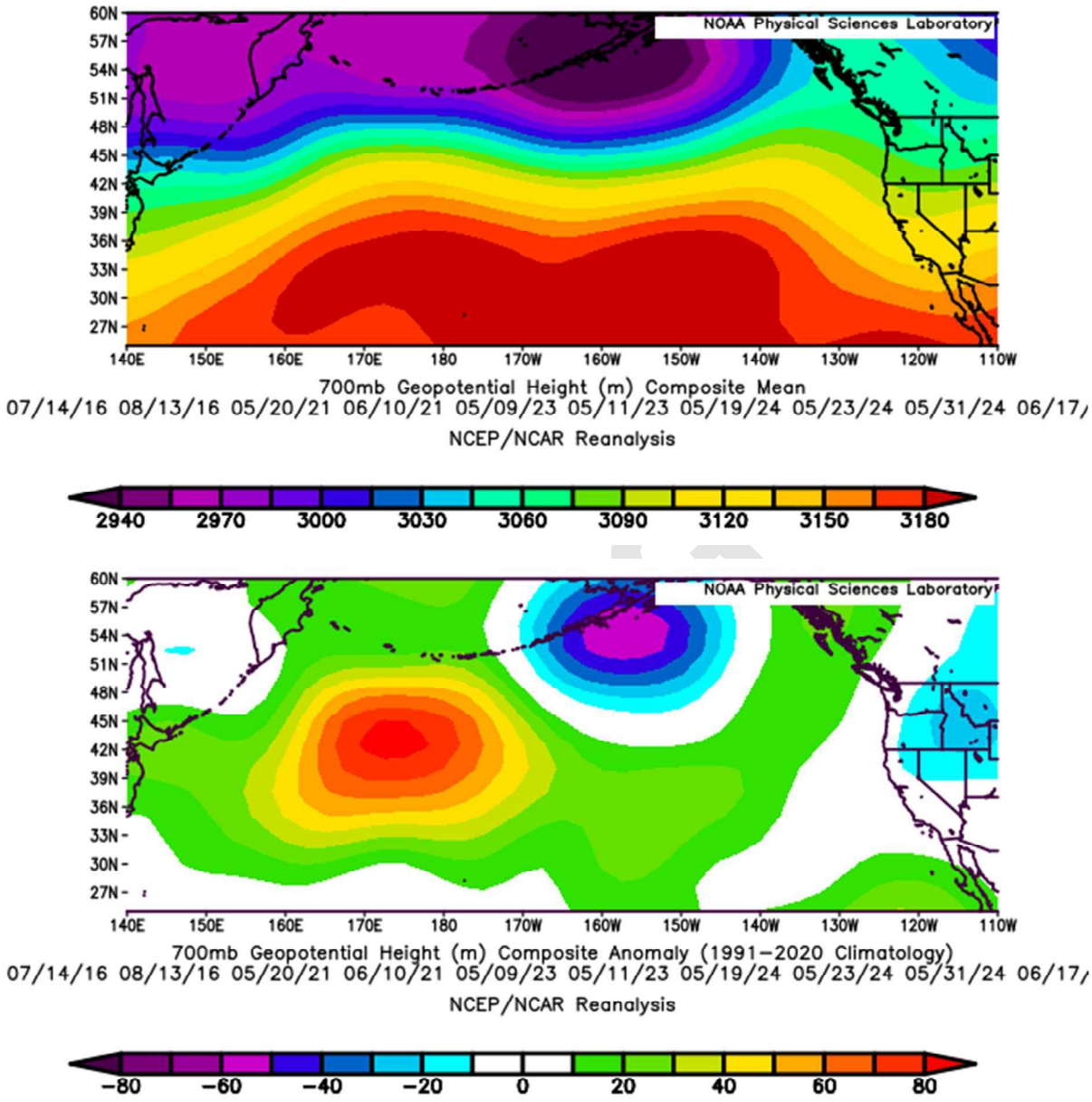

Figure 28. Mean geopotential height (top) and anomalies (bottom) at 700 mb on LNR transport days. Source: NOAA.

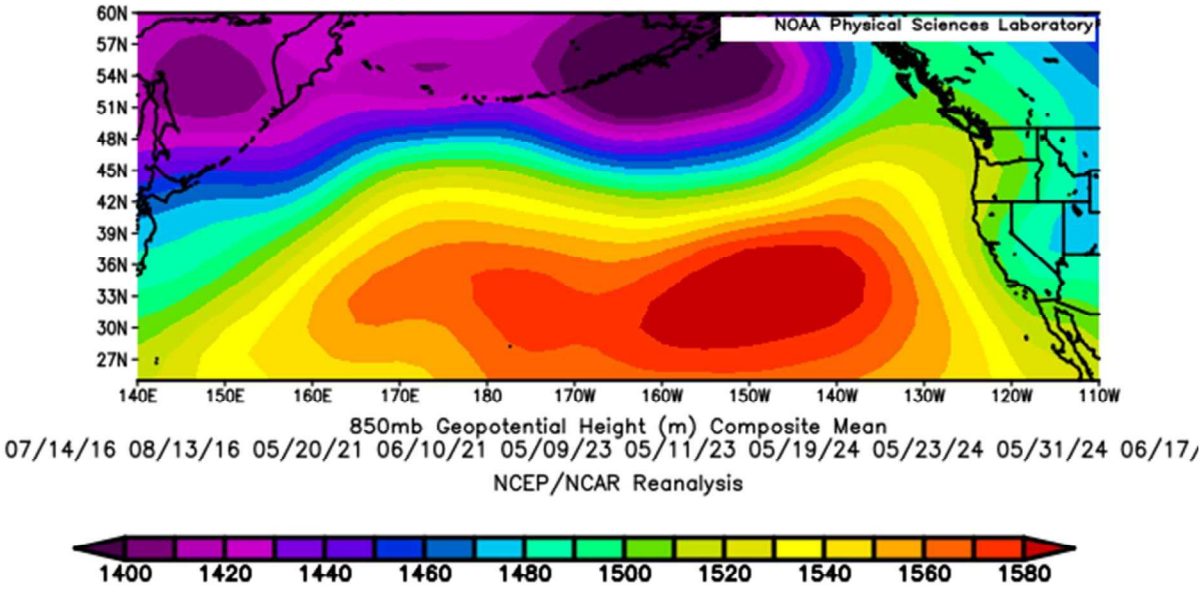

Figure 29. Mean geopotential height at 850 mb on LNR transport days. Source: NOAA.

The aloft geopotential height patterns at 700 mb and 850 mb both exhibited anomalously high pressure over much of the north Pacific Ocean. This pattern suggests enhanced west-to-east wind flow through much of the troposphere, facilitating LNR transport across the northern Pacific. The aloft geopotential height patterns furthermore suggest northwesterly flow along the West Coast, from the northeastern Pacific Ocean into the southwestern United States.

A more detailed view of the 700 mb geopotential height pattern over the continental United States reveals a trough of low pressure along the West Coast (Figure 30), which is consistent with the trough of low pressure observed at the 500 mb level. The expected wind flow along the base of this trough would be southwest-to-northeast, into Clark County.

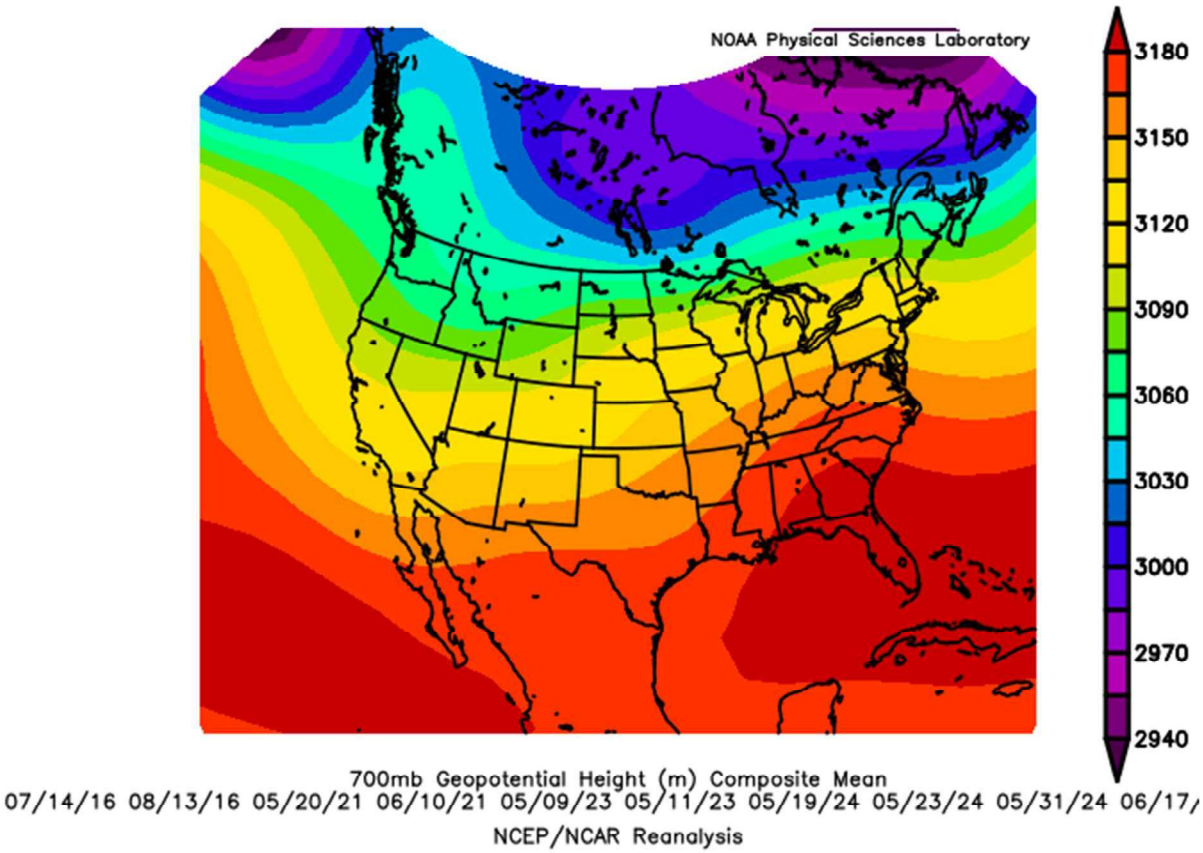

Figure 30. Mean geopotential heights at 700 mb on LNR transport days. Source: NOAA.

Mean wind patterns and wind anomaly patterns were analyzed at 700 mb and 850 mb for LNR transport days to identify wind flow patterns within the mixed layer. Figure 30 shows the mean and anomaly vector wind patterns at the 700 mb level (2,630 m AGL). Figure 32 shows the mean and anomaly vector wind patterns at the 850 mb level (800 m AGL).

The mean wind patterns at both 700 mb (Figure 31, top panel) and 850 mb (Figure 32, top panel) both indicate strong west-to-east wind flow pattern across the north Pacific, consistent with the geopotential height patterns found at those levels in Figure 6. Furthermore, these westerly winds were anomalously strong, generally by 5-7 m/s. Additionally, the 750 mb and 850 mb wind patterns over the far eastern Pacific on these days both indicated pronounced northwesterly flow, which directed that transport toward the southwestern United States.

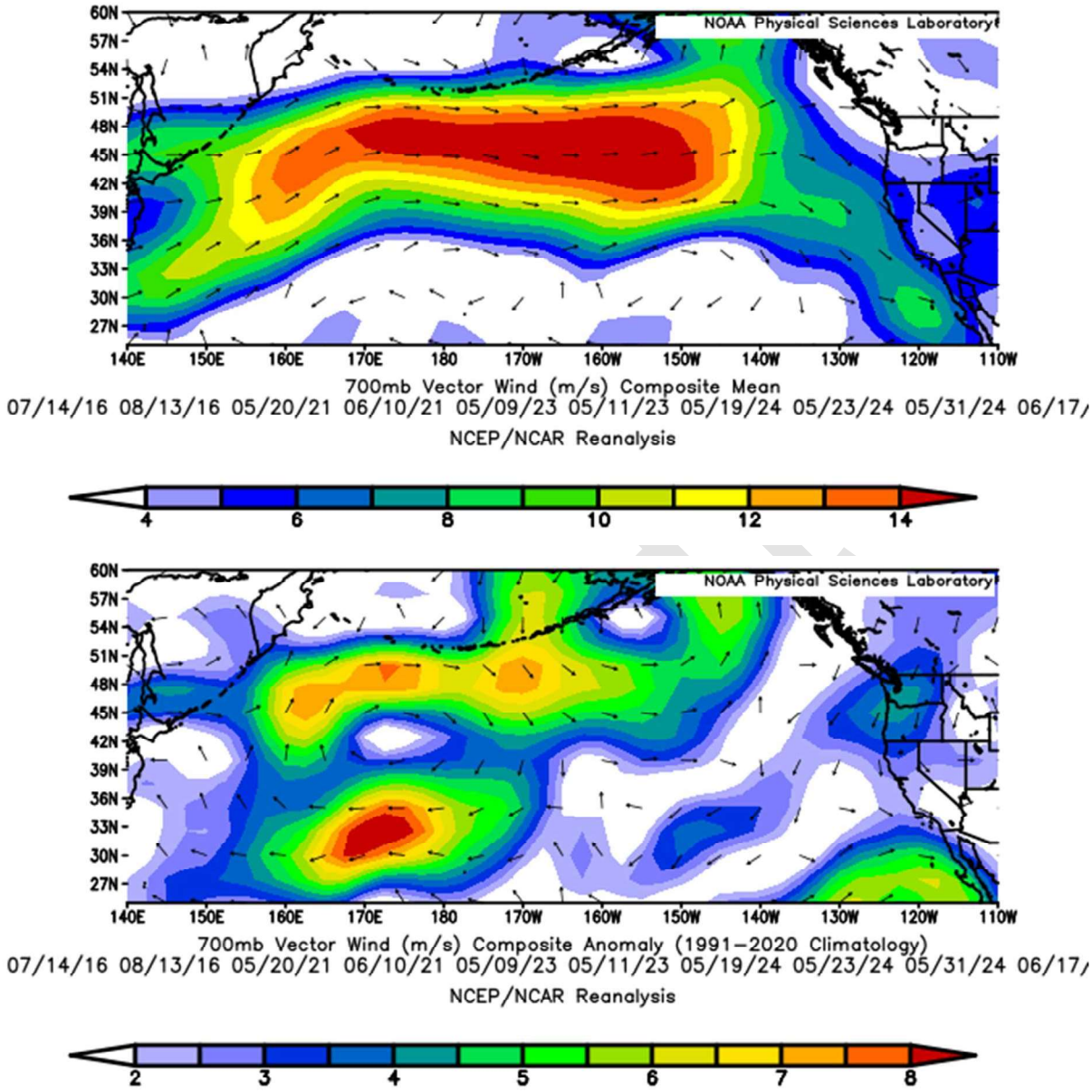

Figure 31. Mean wind vectors (top) and wind anomalies (bottom) at 700 mb on LNR transport days. Source: NOAA.

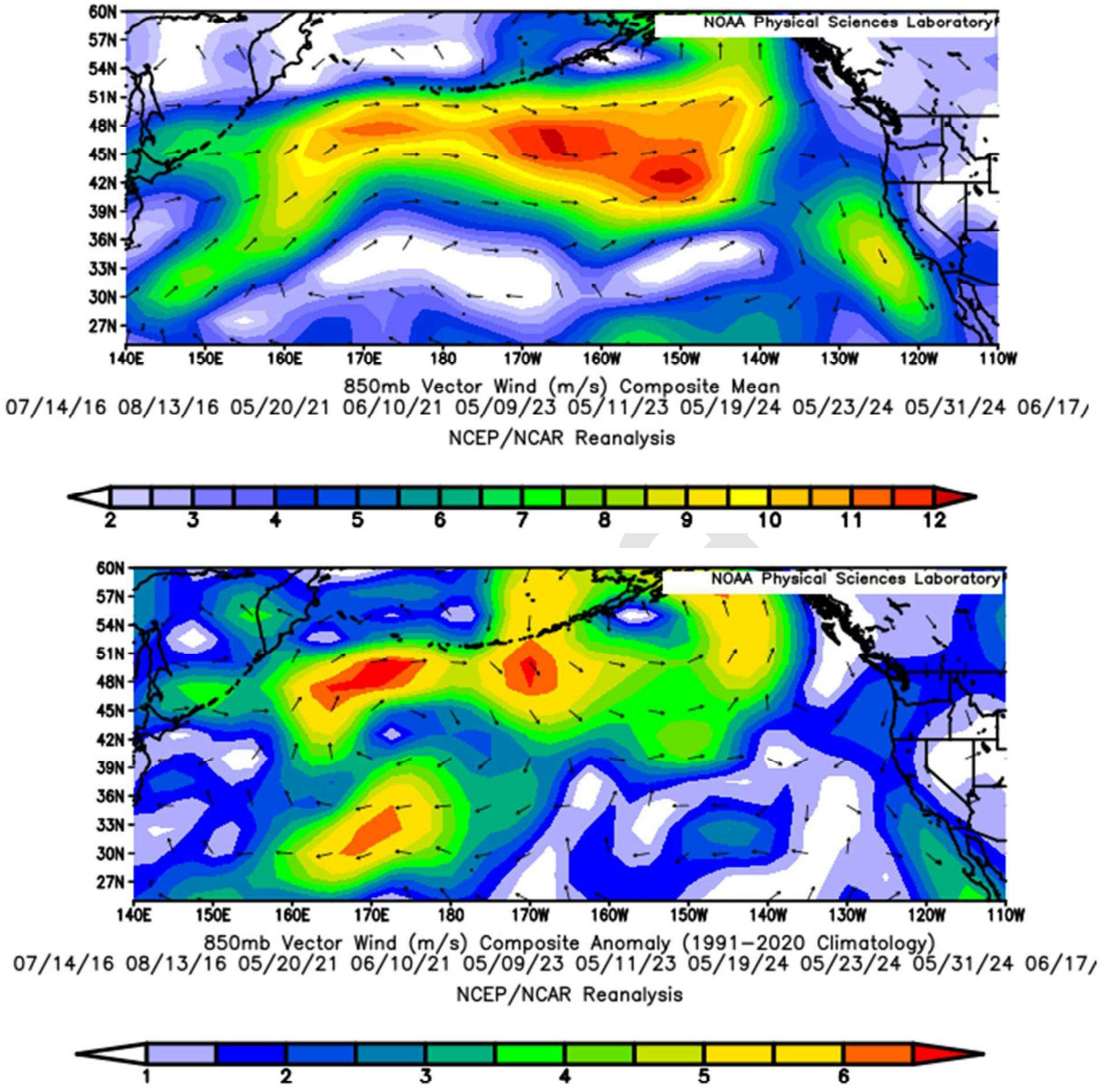

Figure 32. Mean wind vectors (top) and wind anomalies (bottom) at 850 mb on LNR transport days. Source: NOAA.

In addition to the 700 mb and 850 mb wind patterns supporting LNR transport on these days, the wind pattern over the southwestern United States at 700 mb indicated southwesterly winds from the southern California Coast into the Clark County region (Figure 33). This wind pattern is consistent with the trough of low pressure along the West Coast at 700 mb.

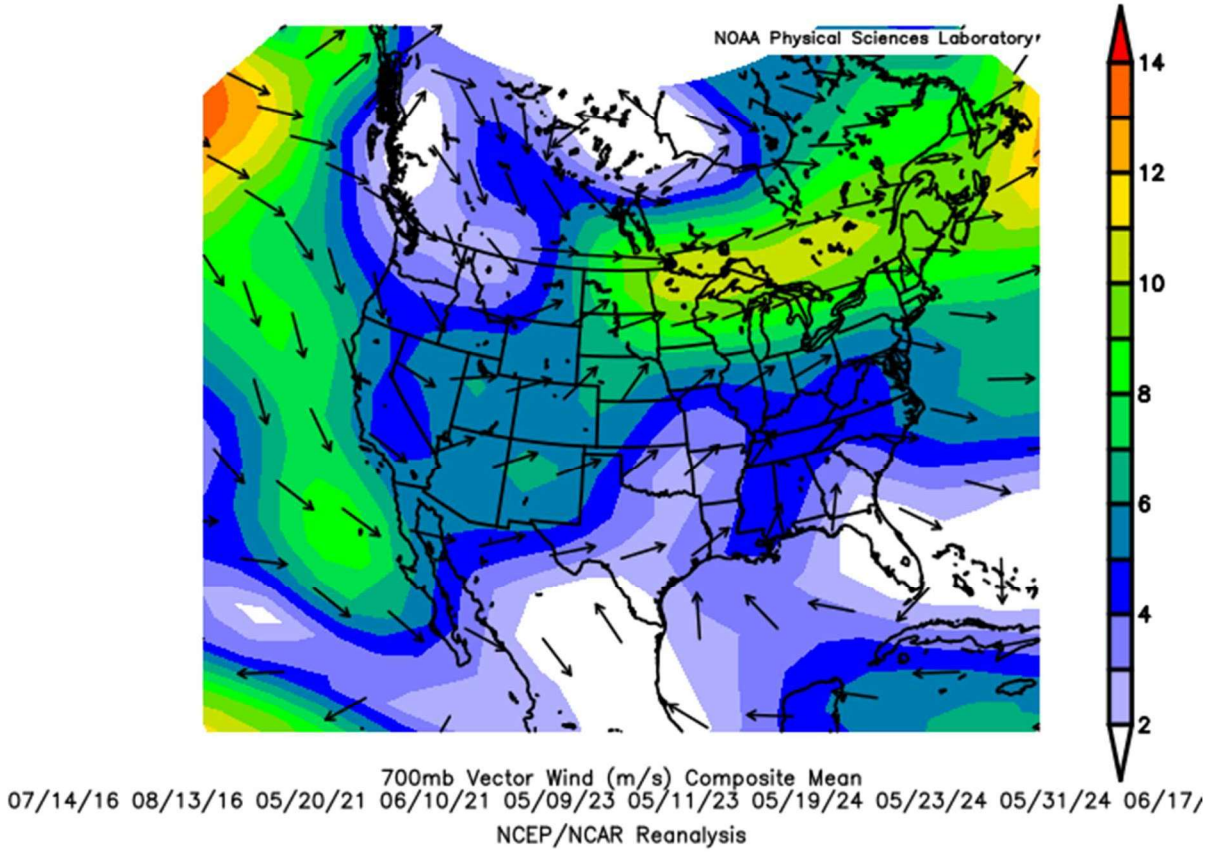

Figure 33. Mean wind vectors at 700 mb on LNR transport days. Source: NOAA.

Surface wind observations at the KLAS and KVGT stations were analyzed on LNR transport days to determine whether there were any consistent local wind patterns that were associated with these days, and whether those patterns were anomalous compared with climatology. Figure 34 shows the wind roses for LNR transport days at KLAS (top) and KVGT (bottom).

The dominant wind direction at KLAS on LNR transport days was out of the south or southwest. However, the dominant wind direction at the KVGT station varied, with pronounced components from the south, southwest, and northwest. It should be noted that surface winds patterns in and around Las Vegas are driven largely by terrain surrounding the region, with lower-level and surface winds being channeled through mountain gaps and other terrain features. Indeed, when compared with the climatological winds for all May days from 2016-2024 (Figure 35), the wind patterns in Figure 34 do not appear to be anomalous.

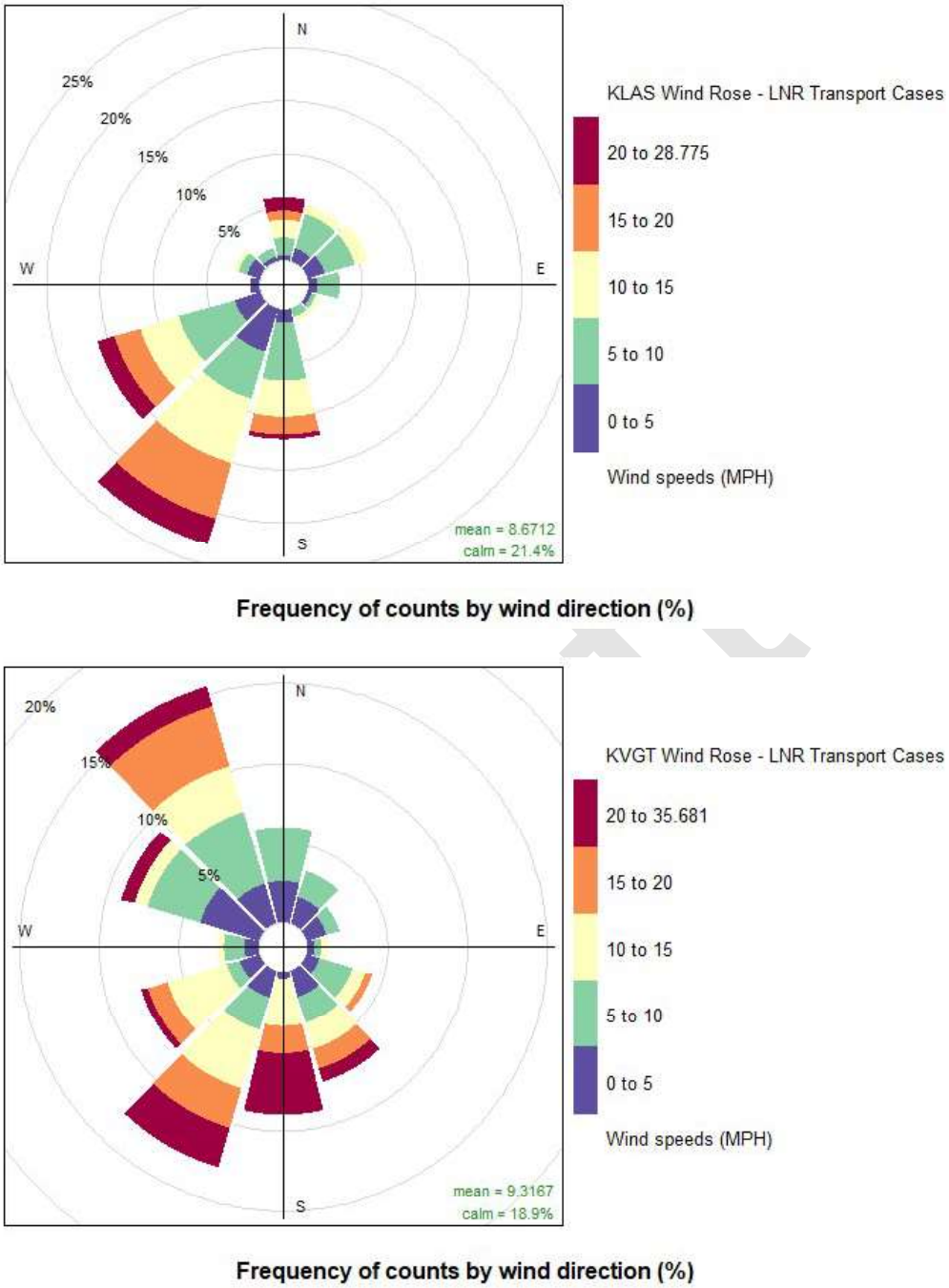

Figure 34. Wind rose diagrams on LNR transport days at KLAS (top) and KVGT (bottom). Data source: Iowa State Mesonet.

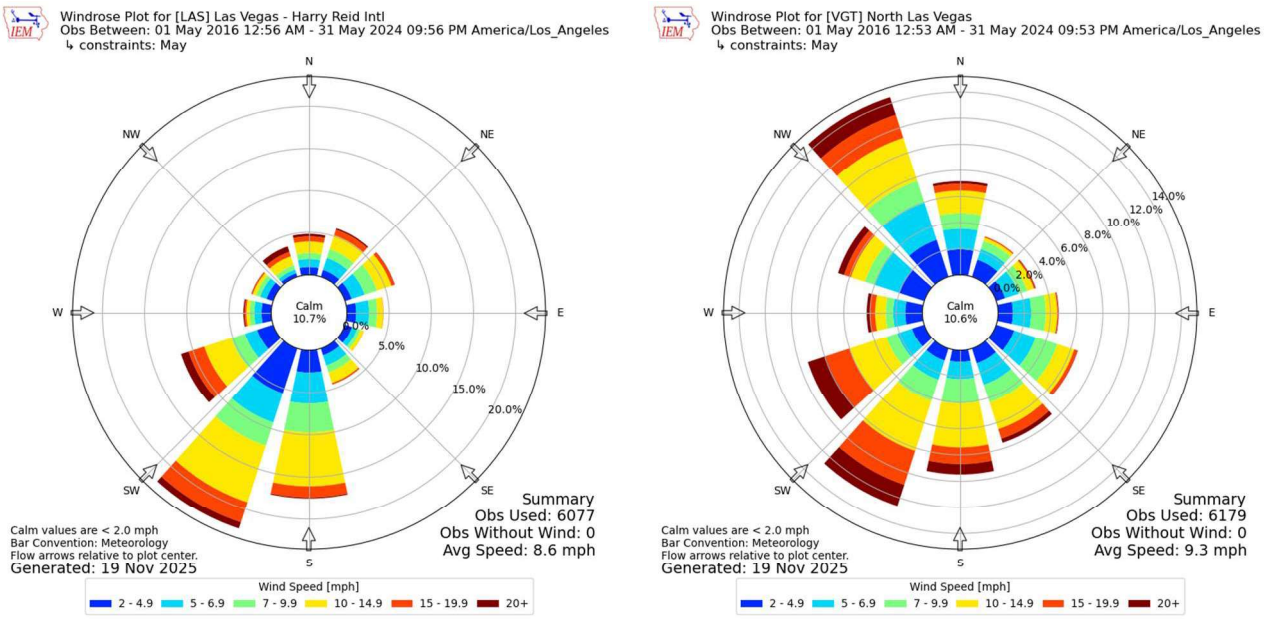

Figure 35. Wind rose diagrams for all May days from 2016-2024 at KLAS (left) and KVGT (right). Data source: Iowa State Mesonet.

Aloft winds at 850 and 700 mb appear to be the main drivers in LNR transport on these days, with pollutants then being mixed to the surface under mid-level low pressure troughs. However, the relatively high frequency of southwesterly winds at the surface, especially at KLAS, is consistent with the regional-scale 700 mb wind pattern, which indicates a similar transport pattern in the Clark County region.

Both geopotential height patterns and wind flow patterns on the 10 LNR transport days indicate anomalously strong west-to-east flow across the northern Pacific Ocean toward the West Coast of the United States. These wind flows were driven by strong high pressure over the northern Pacific. Furthermore, aloft geopotential height and wind patterns indicate winds that veered from westerly to northwesterly as they reached the northeastern Pacific and approached the West Coast, further facilitating transport into the southwestern United States. Additionally, an aloft trough of low pressure along the West Coast steered winds from the southern California coast into Clark County. The consistent pattern of aloft low pressure over the western United States on these days enhanced vertical mixing on LNR transport days, bringing aloft air masses—and pollutants therein—down to the lower levels of the atmosphere. The aloft west-to-east transport driven by strong high pressure over the Pacific Ocean, combined with the subsequent vertical mixing over the western United States, were the main drivers in LNR pollutant transport into Clark County.

2.3 Comparison of International Transport with Locally Influenced Days

Three air transport regimes—LOC, MEX, and LNR—each exhibit distinct patterns that contribute to pollutant transport and localized ozone production in HA 212.

LNR transport synoptic patterns exhibited anomalously high pressure through multiple vertical levels of the atmosphere (i.e., 700 and 850 mb) over the Pacific Ocean. Consistent with the high-pressure patterns, anomalously strong west-to-east winds were observed across the northern Pacific Ocean, directly contributing to cross-Pacific transport at multiple vertical levels in the atmosphere. Over the western United States, anomalously low pressure was observed at the 500 mb level, which directed transport along the West Coast and into southern Nevada and enhanced atmospheric mixing through the atmosphere, facilitating the vertical transfer of aloft pollutants to the surface.

On days with MEX transport, a thermal trough of surface low pressure over the Colorado River Valley, coupled with surface high pressure over the Gulf of California, produced a south-to-north pressure gradient. Consistent with the surface pressure pattern, 850 mb winds were southerly over northern Baja California, shifting to southwesterly in southern Nevada. This wind configuration is evidence of pollutant transport from northwestern Mexico directly into the Clark County region. Very warm surface temperatures resulted in deep atmospheric mixing (around 4,000 m AGL on average) over Clark County, which facilitated the vertical transfer of aloft air and pollutants to the surface. In addition to the potential for transport from Mexico, anomalously high pressure aloft (at 500 mb) over the southwestern United States on these days produced ample sunshine and warm surface temperatures, sufficient for ground-level ozone formation. Ozone production was also influenced by light local winds at the surface, which hindered dispersion of transported pollutants and related ozone precursors in Clark County.

LOC transport exhibited anomalously high pressure at 500 mb and 700 mb over the western United States that produced sunny skies and anomalously warm temperatures at the surface and aloft over the Clark County region, enhancing ground-level ozone formation. Winds within the boundary layer indicated transport from multiple sources (the Los Angeles Basin, the Bay Area, Sacramento, and southeastern California) but did not indicate significant transport from either Mexico or across the Pacific during the 48 hours leading up to each case. Deep atmospheric mixing allowed aloft air masses that were transported into the Clark County region to be mixed to the surface. Of the 10 cases with local transport, there were nine instances in which air mass source regions intersected areas with high (over 100 AQI) ozone levels outside of Nevada on the days prior to the high-pollution event, indicating transport of ozone-rich air masses into the Clark County region. Regional smoke was also present along or near the transport paths in 7 out of 10 cases. This smoke may have further enhanced ozone formation. Meteorological surface conditions in Clark County supported local ozone production, with light winds limiting dispersion and temperatures of at least 37.8°C promoting ozone formation.

The highest MDA8 ozone concentration across all AQS sites in Clark County for each day from 2016-2024 were grouped by identified cluster categories (see Section 2.1.1) and labeled as LOC, MEX, LNR, and "other" (i.e., trajectory clusters not defined in this analysis); these concentrations are plotted in Figure 36 to visualize the seasonal variation in MDA8 ozone grouped by transport regime. The MEX transport regime primarily occurs during the months of June-September, consistent with warm-season thermal troughing over the desert Southwest and enhanced southerly flow from the Gulf of California (i.e., weather patterns indicative of the North American Monsoon). In contrast, the LNR transport regime primarily occurs from October-May, which is consistent with cool-season circulation patterns such as strengthened Pacific westerly winds and more frequent low-pressure systems affecting the western US. The LOC transport regime occurs throughout the year but are most numerous during the primary ozone production season in Clark County, reflecting regional and local transport patterns that are less dependent on large-scale seasonal circulation patterns and can occur under a range of synoptic conditions.

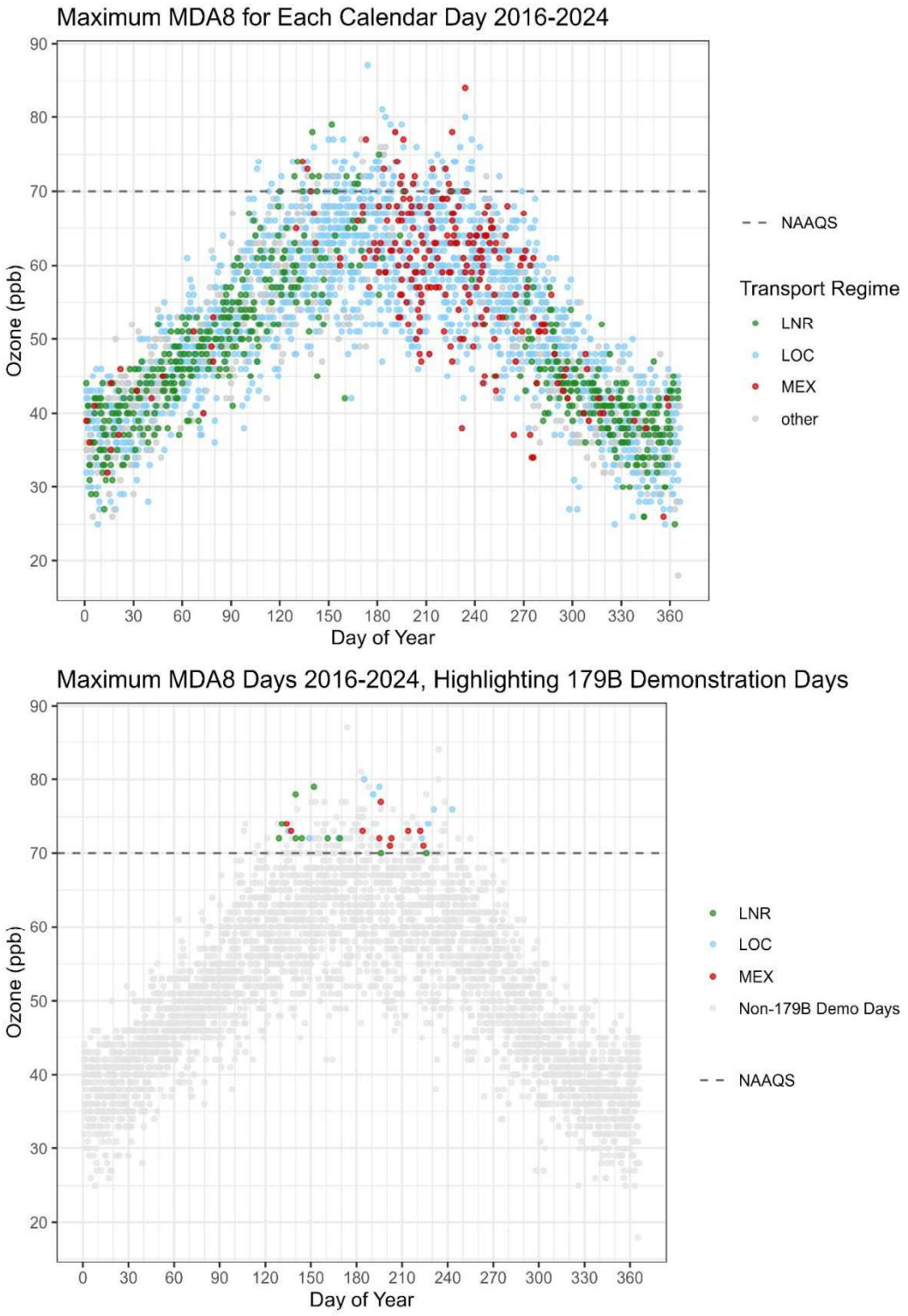

Figure 36. (Top) MDA8 ozone as a function of day-of-year for all days between 2016-2024. Each point depicts the maximum MDA8 ozone for a given calendar day, taken from all of the Clark County AQS ozone monitoring sites. (Bottom) Same as the top figure but only highlighting days from this analysis.

Figure 37 shows average hourly ozone profiles at eight sites in Clark County with data from the 30 days characterized by the LOC, MEX, and LNR transport regimes. A box indicates the hour(s) of maximum hourly ozone concentrations for each site and for each transport regime. LNR transport ozone profiles are generally flatter, exhibit a maximum concentration later in the day, and remain elevated relative to LOC ozone profiles. Mean hourly ozone towards the end of the day (e.g., hours 20-23) on LNR transport days are up to approximately 10 ppb higher than on LOC transport days. For MEX transport days, overnight concentrations tend to be lower than LOC days with ozone increasing to near LOC levels during the early morning production period. This could point to transport of ozone precursors fueling ozone production despite the day starting at lower levels. These observations indicate transport of ozone and/or ozone precursors from non-local sources into Clark County.

Figure 38, Figure 39, and Figure 40 show MDA8 ozone levels overlaid onto Clark County and the U.S. Census-designated Las Vegas urban area, on LOC, MEX, and LNR transport regime days, respectively. The spatial pattern of MDA8 ozone levels on LOC and MEX transport days shows an urban/non-urban distinction, where the MDA8 ozone level is generally higher within the Las Vegas urban area than outside, relative to MDA8 ozone levels on LNR transport days. This may be due to more favorable conditions for ozone production given local and/or transported ozone precursors within the Las Vegas urban area on LOC and MEX transport days. In contrast, the LNR days show uniform high concentrations around the county at both urban and rural sites. Boxplots of the MDA8 ozone levels (Figure 41) show the MDA8 ozone concentrations for each transport regime. LOC and MEX days show statistically significantly higher urban MDA8 ozone concentrations than non-urban MDA8 ozone concentrations, as indicated by the non-overlapping notches in the boxplots, while LNR days are not statistically different between urban and non-urban sites.

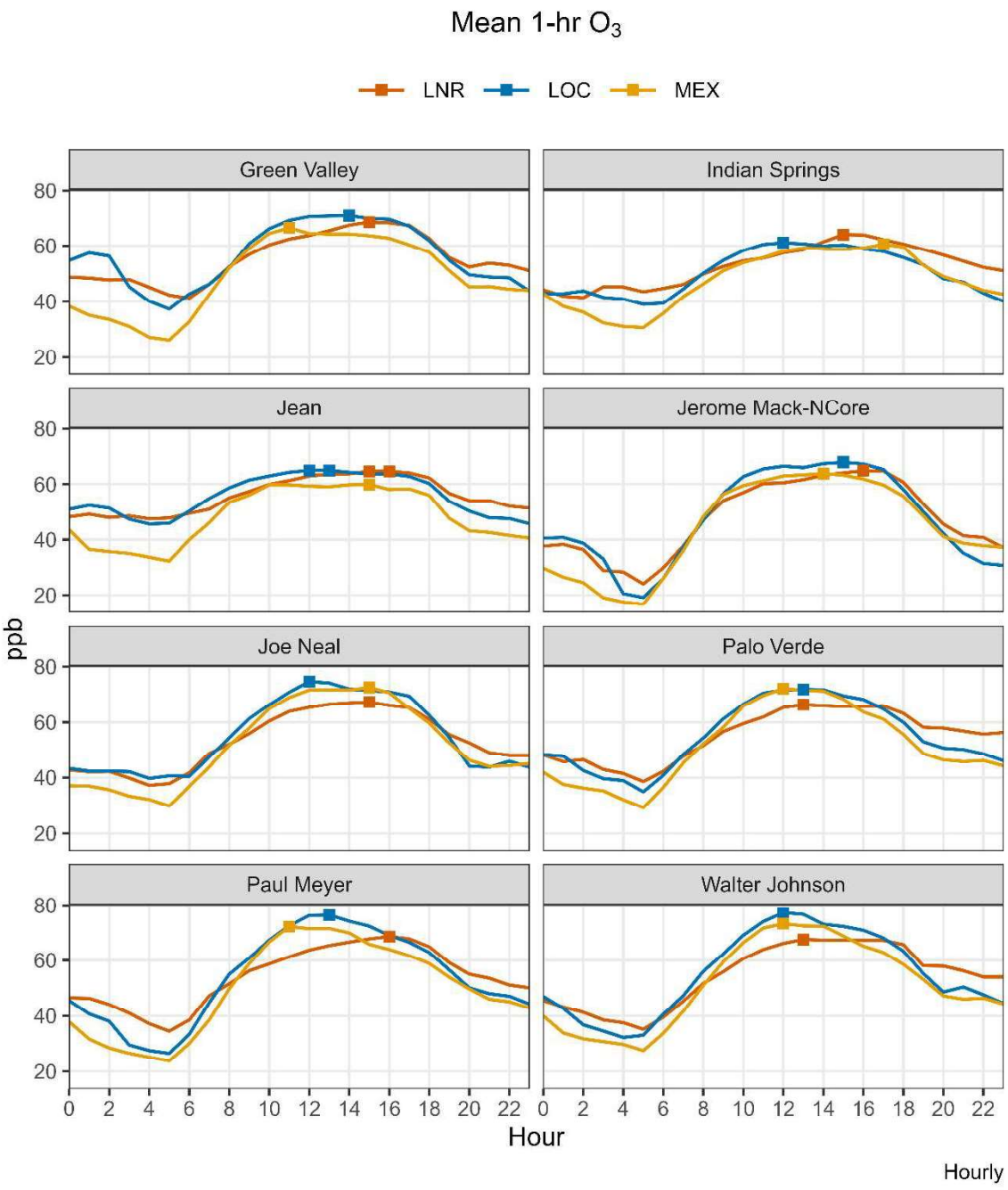

Figure 37. Mean hourly ozone concentrations during each hour for the three transport regimes. Squares imposed on the ozone profile indicate the hour(s) of maximum hourly ozone concentrations.

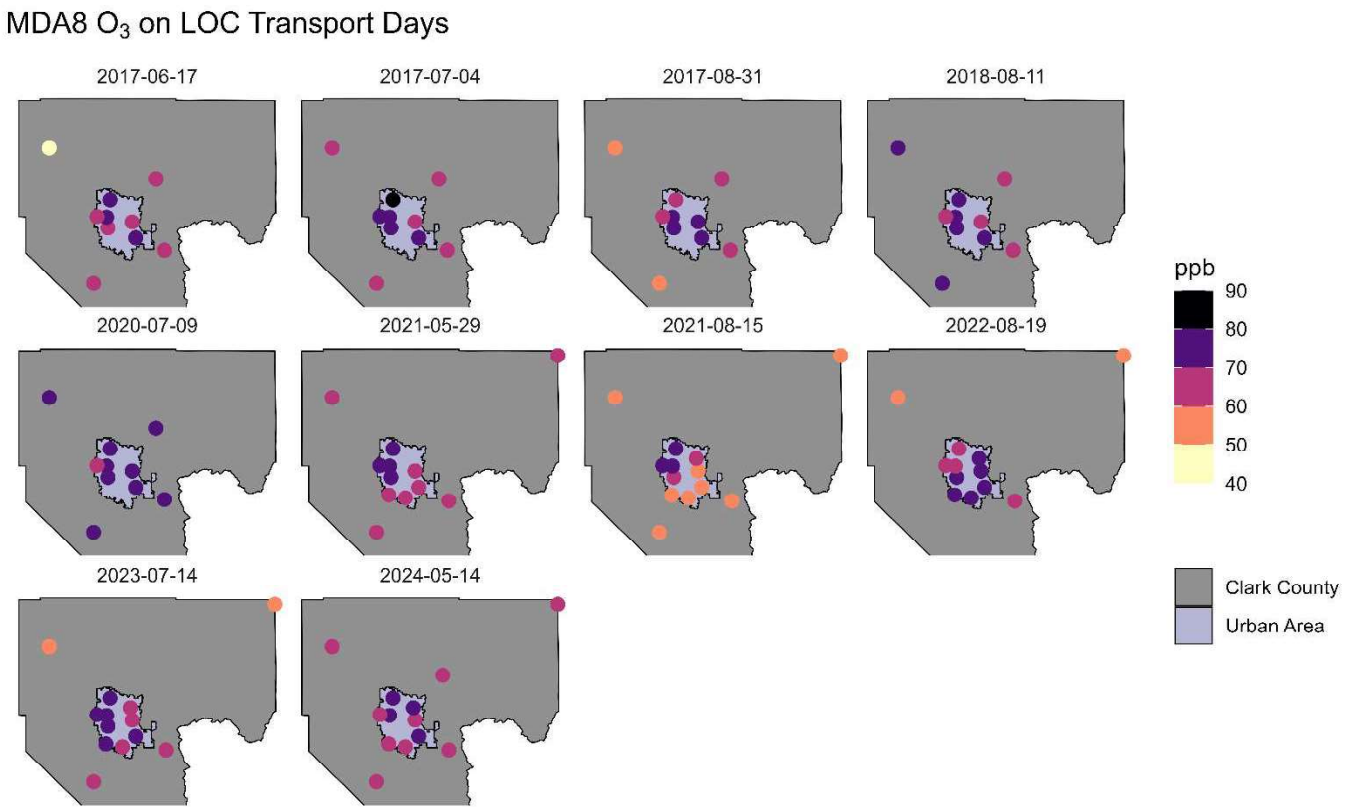

Figure 38. MDA8 ozone levels on LOC transport days overlaid onto Clark County, Nevada, and the U.S. Census-designated Las Vegas urban area.

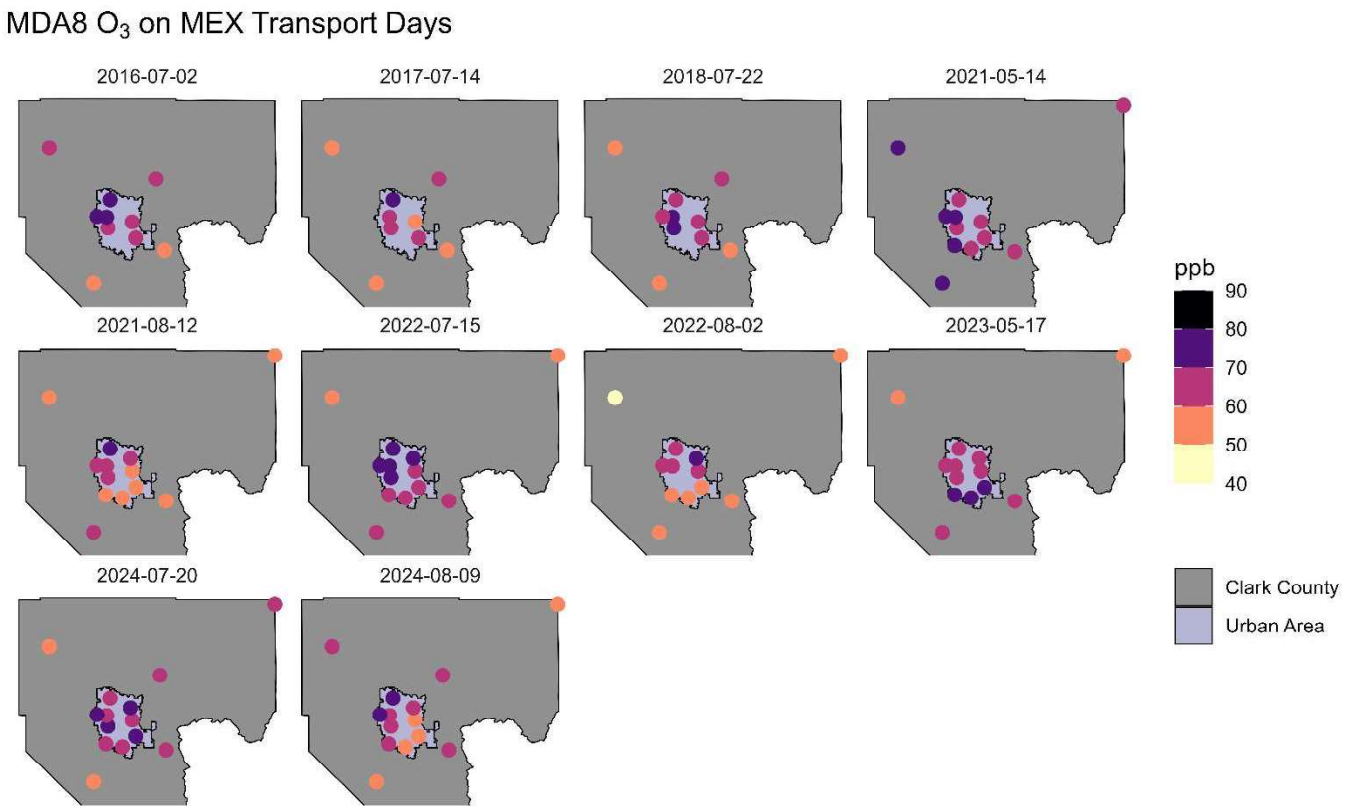

Figure 39. MDA8 ozone levels on MEX transport days overlaid onto Clark County, Nevada, and the U.S. Census-designated Las Vegas urban area.

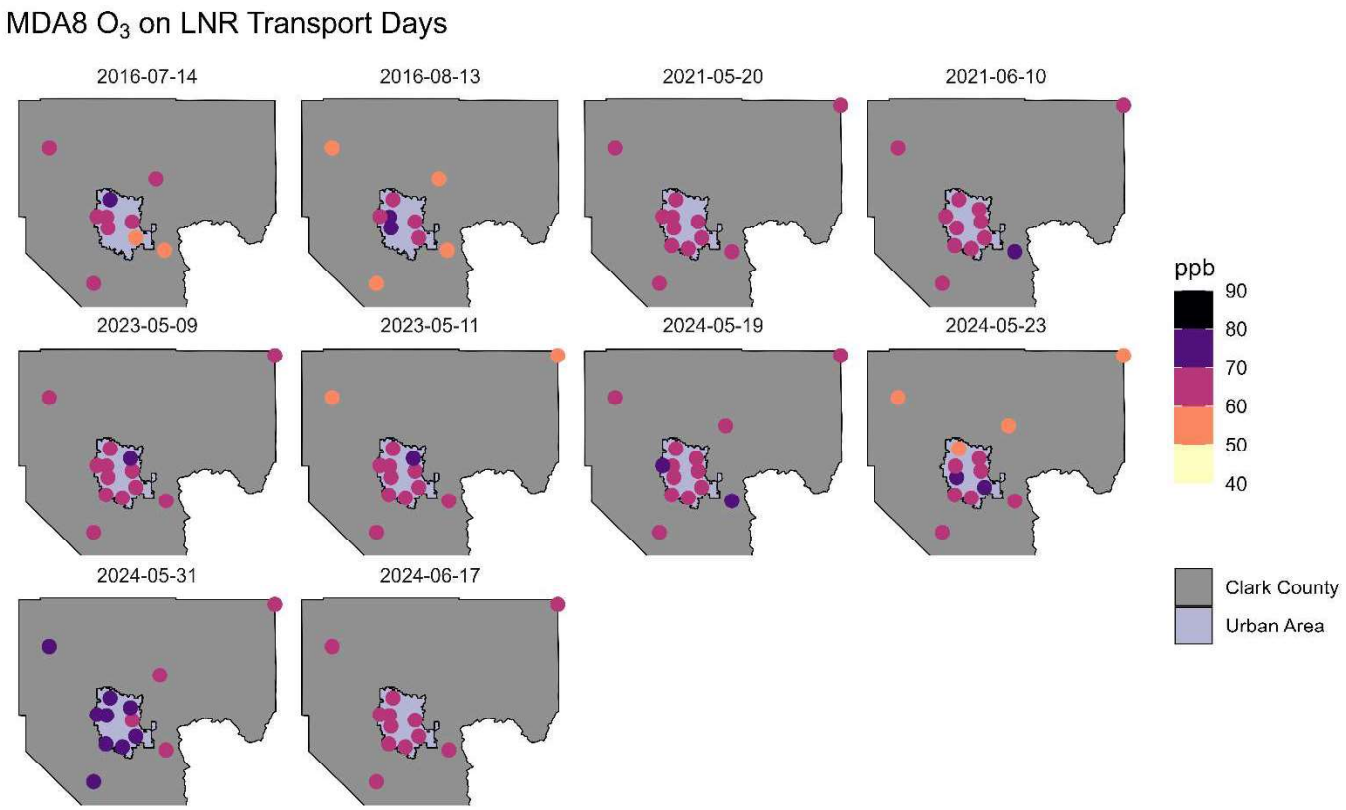

Figure 40. MDA8 ozone levels on LNR transport days overlaid onto Clark County, Nevada, and the U.S. Census-designated Las Vegas urban area.

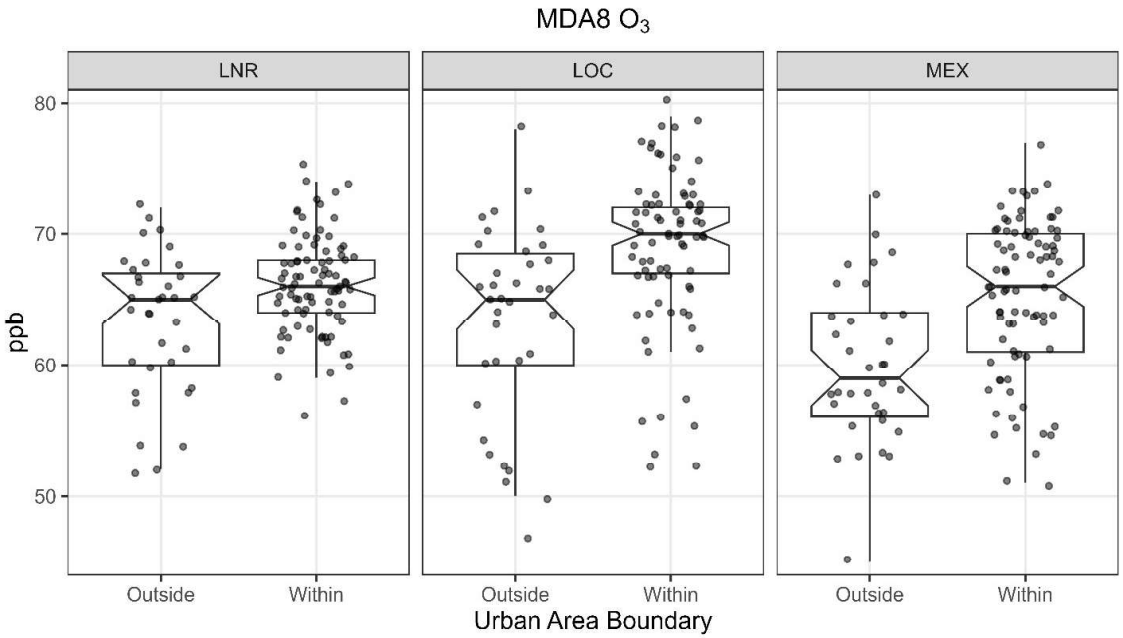

Figure 41. Boxplot graphs of MDA8 ozone levels with points overlaid on LNR, LOC, and MEX transport days grouped by whether the site is within or outside of the U.S. Census-designated Las Vegas urban area.

2.4 Percentile Rank for International Influence

The percentile rank of each LOC, MEX, and LNR date is listed in Table 10. An empirical cumulative distribution function (ECDF) is established for MDA8 ozone concentrations recorded in Clark County between January 1, 2016, and December 31, 2024. MDA8 ozone data are obtained from the AQS daily data product. Omitted from this ECDF are exceptional events (deferred review status), potential wildfire smoke-impacted days, and dates corresponding to international ozone transport regimes (i.e., MEX and LNR dates). By omitting these dates, the ECDF better represents "typical" ozone conditions in Clark County without potential influence from wildfire smoke and international transport. The MDA8 value per date is identified as the maximum MDA8 (rounded to the nearest ppb) recorded in Clark County on each date (see Table 2 for a list of Clark County ozone monitors). The ECDF is used to determine the percentile rank of each LOC, MEX, and LNR date.

LOC dates tend to have higher percentile MDA8 ozone concentrations than dates with an international transport regime. Six out of the 10 LOC dates have an MDA8 concentration in the 99th or 100th percentile of "typical" daily observations, with a percentile range of 97-100. Among the dates with an international transport regime, LNR dates tend to fall into lower percentile rankings of MDA8 ozone than MEX dates. Half of all LNR dates have an MDA8 concentration in the 97th percentile or lower, with a percentile range of 95-99 (likely due to more dispersion of ozone precursors across long distances). Most MEX dates have an MDA8 concentration in the 98th percentile, with a percentile range of 98-100.

Table 10. Percentile rank of each LOC, MEX, and LNR date. The percentile is calculated across 2016-2024 with concurred exceptional events and dates with international transport (MEX and LNR dates) omitted. The listed MDA8 ozone is the maximum MDA8 across Clark County sites per date.

Transport Type	Date	MDA8 Ozone (ppb)	Percentile Rank (%)
LOC	6/17/2017	72	98
	7/4/2017	80	100
	8/31/2017	76	99
	8/11/2018	72	98
	7/9/2020	78	100
	5/29/2021	71	97
	8/15/2021	74	99
	8/19/2022	76	99
	7/14/2023	79	100
	5/14/2024	73	98
MEX	7/2/2016	73	98
	7/14/2017	72	98
	7/22/2018	72	98
	5/14/2021	73	98
	8/12/2021	71	97
	7/15/2022	77	100
	8/2/2022	73	98
	5/17/2023	73	98
	7/20/2024	71	97
	8/9/2024	73	98
LNR	7/14/2016	70	97
	8/13/2016	70	97
	5/20/2021	68	95
	6/10/2021	72	98
	5/9/2023	71	97
	5/11/2023	74	99
	5/19/2024	70	97
	5/23/2024	72	98
	5/31/2024	75	99
	6/17/2024	69	96

Additional analysis of MDA8 ozone concentrations for all days from 2016-2016, not just those selected for modeling in this study (listed in Table 10), is listed in Table 11 and Table 12. These analyses omit exceptional events and potential wildfire smoke-impacted days in order to more accurately represent "typical" ozone conditions in Clark County. Table 11 includes average full-year and ozone-season MDA8 ozone concentrations and the ECDF of each, for all data and each of the three transport regimes. Table 12 includes average full-year and ozone-season MDA8 ozone concentrations and the ECDF of each calendar year from 2016 to 2024.

As depicted in Figure 36, there are seasonal differences in the transport regimes, with MEX days mainly occurring from June-September and LNR days from October-May. These seasonal differences are reflected in Table 11; on average, MEX transport days have higher MDA8 ozone concentrations compared to LNR days. When considering whole-year data, MEX days have higher MDA ozone concentrations than LOC days on average; however, when considering only ozone season data, MEX days have lower MDA8 ozone concentrations than LOC days on average. Table 12 depicts the annual full-year and ozone-season average MDA8 ozone concentrations from 2016 to 2024. Average MDA8 ozone concentration has been increasing between 2016 and 2024.

Table 11. Full-year and ozone season average MDA8 ozone concentrations and percentiles for all data and each transport regime from 2016 to 2024.

Regime	Full Year Avg MDA8 (ppbv)	Full Year MDA8 Percentile	Ozone Season Avg MDA8 (ppbv)	Ozone Season MDA8 Percentile
All Data	47.2	48.0%	55.1	73.4%
LNR	42.2	33.9%	53.0	64.1%
LOC	49.5	54.3%	55.7	73.4%
MEX	52.0	60.7%	54.5	70.3%
other	42.8	33.9%	53.8	67.3%

Table 12. Full-year and ozone season average MDA8 ozone concentrations and percentiles for each year from 2016 to 2024.

Year	Full Year Avg MDA8 (ppbv)	Full Year MDA8 Percentile	Ozone Season Avg MDA8 (ppbv)	Ozone Season MDA8 Percentile
2016	45.6	42.2%	54.0	67.3%
2017	47.6	48.0%	55.0	70.3%
2018	46.9	45.1%	57.1	79.3%
2019	46.8	45.1%	53.8	67.3%
2020	45.6	42.2%	53.2	67.3%
2021	47.8	48.0%	56.0	73.4%
2022	47.2	48.0%	54.7	70.3%
2023	48.0	48.0%	55.5	73.4%
2024	48.6	51.0%	56.7	76.2%

3. International Ozone Contribution

Regional- and global-scale modeling was performed to assess the international contribution on ozone concentrations observed in Clark County. Before discussing these results, we first introduce the domestic and international emissions inventories to provide context and include extensive analysis on uncertainties in the source apportionment modeling. This includes an evaluation of international transport pathways and the comparison of 2016 and 2022 meteorological data for use in source apportionment modeling.

3.1 Domestic Emissions Inventories

Ramboll Americas Engineering Solutions and Eastern Research Group (2026) compiled historical and projected anthropogenic emission inventories in Clark County (all HAs, including HA 212) to develop NO_x and VOC emission trendlines. Centered on 2017, the resulting trendlines span nine years prior and 16 years forward. Historical emissions in 2008 and 2015 were taken from the Ozone Redesignation Request and Maintenance Plan for the 1997 Ozone NAAQS (Clark County Department of Air Quality, 2018); 2017 anthropogenic emissions and projections to 2023 and 2033 were taken from the second Maintenance Plan (Clark County Department of Environment and Sustainability, 2021). Note that the emission inventories that Ramboll Americas Engineering Solutions and Eastern Research Group (2026) generated for Serious Ozone SIP are focused on the NAA (HA 212) and therefore cannot be directly compared with the Clark County Maintenance Plan inventories, which cover the full geographic region of the County.

It is important to note that the historical inventories reported here for 2008, 2015, and 2017 were developed using different data sources, methods, and models unique to each inventory year. This situation leads to some inconsistencies in trendlines for those sectors affected by substantial updates, improvements, or refinements (e.g., the evolution of MOBILE, NONROAD, and EPA's Motor Vehicle Emission Simulator (MOVES) models, and associated local data used to estimate emissions for the on-road and nonroad motor vehicle sectors). Additionally, substantial methodological and data updates for other sectors have occurred and are anticipated, such as the use of new information from field research and models from which to estimate emissions from volatile chemical products (VCPs) that comprise a major fraction of the nonpoint VOC emissions sector. Nevertheless, the trendlines developed here provide a general sense for the evolution of NO_x and VOC emissions over a 25-yr span.

Table 13 and Table 14 tabulate Clark County's anthropogenic emission estimates over 2008-2033 by major source sector, and Figure 42 shows the resulting trendline for total anthropogenic NO_x and VOCs. A substantial NO_x reduction of 56% occurred between 2008 and 2023. Continued reductions are projected out to 2033, with an overall 2008-2033 reduction of 64%. NO_x reductions over the

entire period are driven primarily by large decreases among the on-road and nonroad motor vehicle sectors but are curbed by increases in airport-related emissions.

VOC emissions have also decreased over the 2008-2023 period by 25% and are projected to continue decreasing through 2033 for an overall reduction of 26%. VOC decreases over the period are driven primarily by on-road and nonroad mobile sources but are curbed by growth in the nonpoint sector because of historical and future population and commercial activity. Recent growth in airport emissions has also contributed to increasing VOCs since 2017.

Table 13. Clark County anthropogenic NO_x emissions trends in tons per day (TPD) by major source category. Data from 2008 and 2015 are reported by Clark County Department of Air Quality (2018); data from 2017-2033 are reported by Clark County Department of Environment and Sustainability (2021). Sectors noted in green (red) exhibit a net reduction (increase) from 2008-2023 and beyond to 2033.

Sector	2008	2015	2017	2023	2033
Point Source	28.97	11.6	12.34	11.41	11.33
Nonpoint Source	6.6	5.94	4.69	5.03	4.78
Mobile: On-road	89.5	64.3	42.2	22.22	11.13
Mobile: Nonroad	40.63	27.69	38.87	24.48	16.33
Aviation: Commercial	12.68	13.35	11.9	15.53	19.77
TOTAL	**178.38**	**122.88**	**110**	**78.67**	**63.34**

Table 14. Clark County anthropogenic VOC emissions trends in TPD by major source category. Data from 2008 and 2015 are reported by Clark County Department of Air Quality (2018); data from 2017-2033 are reported by Clark County Department of Environment and Sustainability (2021). Sectors noted in green (red) exhibit a net reduction (increase) from 2008-2023 and beyond to 2033.

Sector	2008	2015	2017	2023	2033
Point Source	1.5	2.42	2.95	2.62	2.63
Nonpoint Source	67.56	60.12	64.69	67.83	71.31
Mobile: On-road	42.46	33.04	26.27	17.85	11.5
Mobile: Nonroad	42.07	31.1	28.93	27.29	27.86
Aviation: Commercial	3.39	3.75	1.96	2.64	3.05
TOTAL	**156.98**	**130.43**	**124.08**	**118.23**	**116.35**

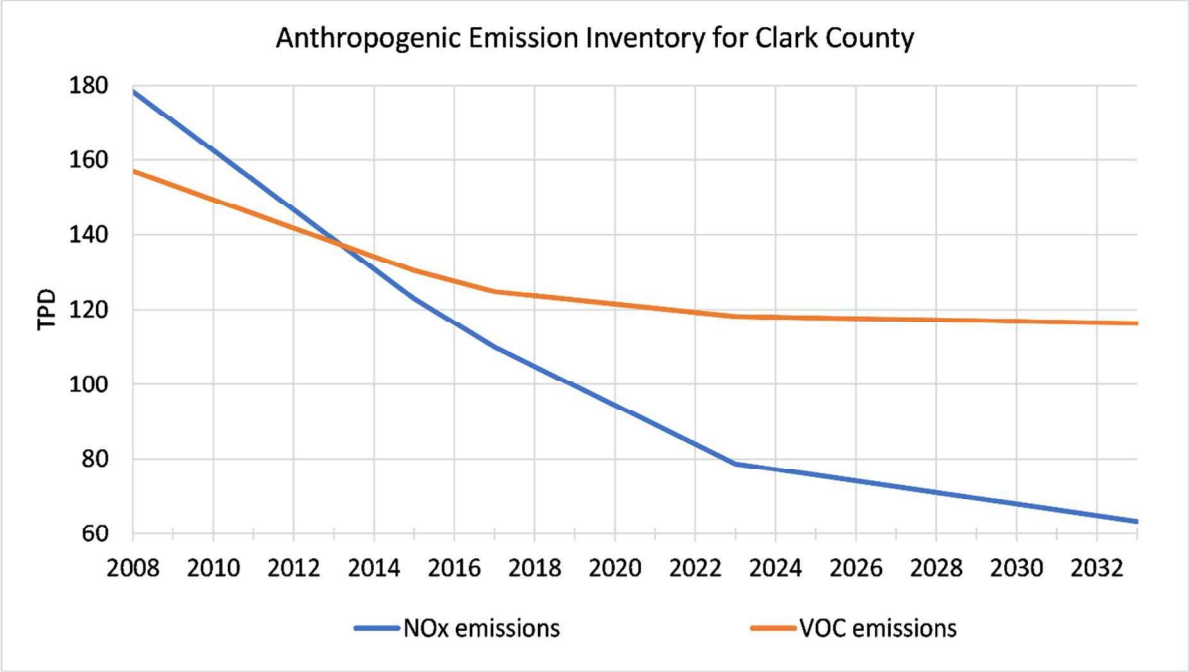

Figure 42. Clark County total anthropogenic NO_x and VOC emission trends in TPD from 2008 through 2033. Data from 2008 and 2015 are reported by Clark County Department of Air Quality (2018); data from 2017-2033 are reported by Clark County Department of Environment and Sustainability (2021).

3.2 Evaluation of International Transport and Emissions Uncertainty

Two key factors influence contributions from international emissions: the transport mechanisms, and the level of international emissions. As a summer phenomenon, ozone episodes in Clark County coincide with the seasonal North American monsoonal circulation pattern. This lower-level atmospheric flow pattern brings humid air northward from Mexico into the Sonoran Desert and Great Basin states during July and August. This establishes a common transport corridor for pollutants emitted in Mexico to rapidly reach Clark County.

There is another common transport pattern in the mid to upper atmosphere linking Asia to the western US, which is a more significant source of IA contributions during late spring through early summer. There is overwhelming evidence from more than a decade of scientific literature, including from EPA, that trans-Pacific transport of air pollution from Asia has raised background ozone levels in the western U.S. (Dentener et al., 2010; Baker et al., 2015; Jiang et al., 2016; Langford et al., 2017; Huang et al., 2017; Nopmongcol et al., 2017; Jaffe et al., 2018; Zhang et al., 2020; Mathur et al., 2022). Seasonally persistent global circulation patterns establish a direct transport route within the upper troposphere that brings pollutant-laden air from Asia to North America within days to weeks (Figure 43). Over eastern Asia, a persistent low-pressure trough lofts pollutants to the upper troposphere.

While rapidly transported across the Pacific, the chemical lifetimes of ozone and precursors increase because low temperatures minimize destruction. Sinking air within the persistent high-pressure dome over the western US brings transported ozone and precursors toward the surface, while complex topography and deep boundary layer mixing enhances vertical transport. Thus, high-altitude locations throughout the western US experience the greatest ozone impacts from intercontinental transport. Therefore, the long-range trans-Pacific transport of air pollution is a persistent feature of natural atmospheric circulation, regardless of year.

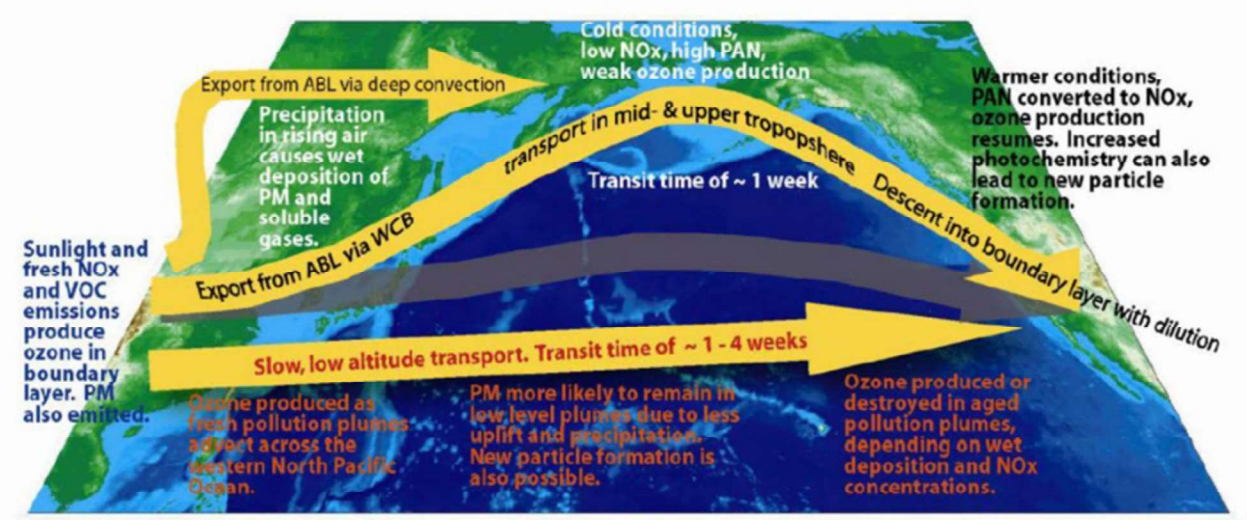

Figure 43. Schematic conceptual model of pollutant transport from Asia to North America (from HTAP, 2010). Blue text on left refers to Asian continental boundary layer processes, red text along bottom refers to low level transport, and black/white text along top and right refers to high altitude transport.

As for international emissions, a simple assumption is that foreign emissions have scaled with population growth. According to the United Nations Department of Economic and Social Affairs, Population Division, population trends for Asia and Central America show growth rates of 5-10% between 2016 and 2025 (United Nations, 2026). That tracks for Mexico, where the Maricopa Association of Governments reports precursor emission increases in three northern Mexican border states of 6% for NOx and 2% for VOC between 2017 and 2023 (Maricopa Association of Governments, 2025). It can reasonably be assumed that similar increases have occurred throughout Mexico.

Emission trends in East Asia demonstrate that air pollution emissions are not necessarily coupled with population change. From 2016 to 2025, the populations of China, Japan, and the Republic of Korea (South Korea) remained relatively stable, changing by approximately 1.5%, -2.5%, and 1.0%, respectively (World Bank Group). In the 2000s-2010s, each of these countries began implementing targeted air pollution control programs, leading to notable reductions in NO_x emissions (Lee et al., 2021). Despite successful NO_x abatement, surface ozone concentrations have continued to increase

or remained unchanged across the region (Lee et al., 2021). In South Korea, an analysis of surface, aircraft, and satellite observations showed that surface NO_x concentrations declined by 23% between 2015 and 2021, while the 90th percentile MDA8 ozone levels from May-June increased by an average of 0.9 ppbv yr^{-1} during the same period (Oak et al., 2025). Similarly, emissions inventory data indicate that Japan reduced NO_x emissions by more than 20% between 2000 and 2018 (Kim et al., 2023), yet mean national MDA8 ozone levels during the warm season (April-September) remained relatively unchanged during that over that period (Li et al., 2025). Finally, Silver et al. (2025) analyzed 10 years of air quality data from approximately 1,200 monitoring stations across China and found that between 2017 and 2024, average NO_2 concentrations decreased by 27%, while local ozone levels increased by 30% (likely due to lifting a substantial NO_x inhibition effect in urban areas – a NO_x disbenefit).

The Emissions Database for Global Atmospheric Research (EDGAR) Hemispheric Transport of Air Pollution (HTAP) is a program led by the European Commission that compiles national global emission inventories and trends for criteria pollutants, precursors, and greenhouse gases. **Figure 44** shows 2000-2020 NO_x and non-methane volatile organic compound (NMVOC) emissions trends for China, Canada and Mexico reported by HTAP v3.2 (Guizzardi et al., 2025). Note that 2020 emission estimates are likely influenced by reduced activities at the start of the COVID-19 pandemic.

Reported NO_x and NMVOC emissions in North America have consistently trended downward throughout the 20-year period, despite evidence discussed above for recent increases in emissions from the northern states of Mexico from 2017 through 2023. We expect the majority of anthropogenic emissions in Canada and Mexico that influence Clark County, Nevada, are explicitly simulated within the CAMx domain, and thus simulated impacts from those counties are fairly represented in the modeled 2026 emissions inventory.

Reported NO_x emissions in China increased substantially through 2012 and then steadily declined by 30% out to 2020. A linear extrapolation from 2016 to 2026 yields a 38% NO_x reduction. Reported NMVOC emissions in China also increased substantially through 2016 and then decreased out to 2020. A linear extrapolation from 2016 to 2026 yields a 24% NMVOC reduction.

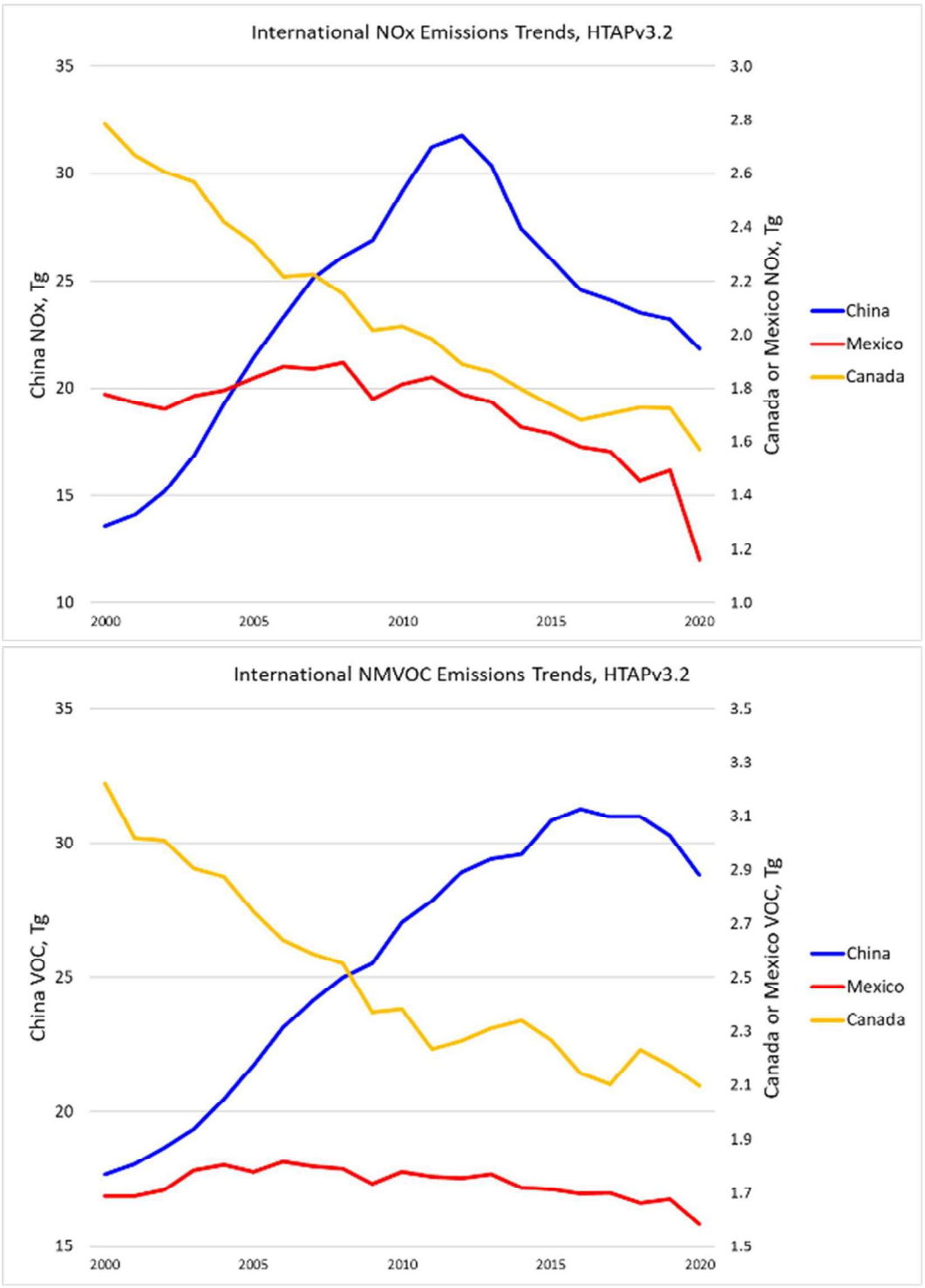

Figure 44. Twenty-year emissions trends of NOx (top) and NMVOC (bottom) in China, Mexico, and Canada compiled by HTAP v3.2.

It is not clear, however, what effect regional NO_x reductions have on the larger-scale, longer-term export of ozone from China. Applying a linearity argument, it is reasonable to assume that a 30%

NO_x reduction could result in a commensurate reduction in exported ozone despite the localized increases. Of course, East Asia is not the only contributor to ozone concentrations across the Northern Hemisphere, so the impact of reduced East Asian precursor emissions on total anthropogenic ozone transport into the U.S. is likely much smaller than 30%. Regardless, as a conservative approximation, applying a 30% reduction to modeled background IA ozone concentrations would reduce the modeled 2026 IA contribution in the Clark County NAA by about 5 ppb (14% contribution rather than 20%, or 10 ppb contribution rather than 15 ppb). Removal of this smaller IA contribution is still sufficient for all 2026 DVs to attain the NAAQS by a wide margin.

3.3 Analysis of 2016 vs 2022 Meteorological Data

In addition to the analysis of domestic vs international emissions and transport, uncertainty in the modeling results may arise from the use of 2016 meteorological data used in conjunction with 2022 emissions to model future DVs. This section discusses the comparability of 2016 and 2022 meteorological conditions to determine if 2016 data can be effectively used in place of 2022 data.

3.3.1 Transport Pathways

The existence of seasonally consistent transport pathways that develop year after year allows for the use of the 2016 meteorology in support of global chemical transport modeling for this demonstration. These pathways include transport of pollutants from the Asian continent into the southwestern U.S. via westerly winds across the central and northern Pacific, and the transport of pollutants northward from Mexico via the southerly winds associated with the North American Monsoon. As described in Section 3.2, the cross-Pacific transport pattern generally develops during the late spring and early summer, while the monsoon winds are most prevalent during the mid- to late-summer months. If these transport pathways are consistent from year-to-year, it can reduce the burden of selecting a particular year of meteorological data for use in modeling these transport patterns for future years.

3.3.2 Long-Range International Transport

From the analysis performed in Section 2.2.3, the pressure levels most relevant to pollutant transport into the southwestern U.S. on LNR days were the 700 mb (2,630 m AGL), and 850 mb (800 m AGL) pressure levels, with most cases occurring in May and June. Consistent with that analysis, 700 mb and 850 mb average wind patterns were analyzed for the months of May and June of 2016. These winds patterns were then compared to the wind patterns in those same months in 2022, which is the year of the emissions inventory selected for this modeling demonstration. In addition, the climatological wind data for May and June 2016 were compared to data for those same months from 1991-2020 to see if 2016 winds could be more widely applicable when modeling future years, assuming climatologically consistent winds in the future.

As seen in Figure 45, 700 mb average winds depict a clear west-to-east transport pathway from eastern Asia into the southwestern U.S. during the months of May and June of 2016. The jet of westerly winds travels from eastern Asia, east-northeastward across the central and northern Pacific, before turning southeastward along the California Coast. As the winds move inland over southern California, they turn back to the northeast and into southern Nevada.

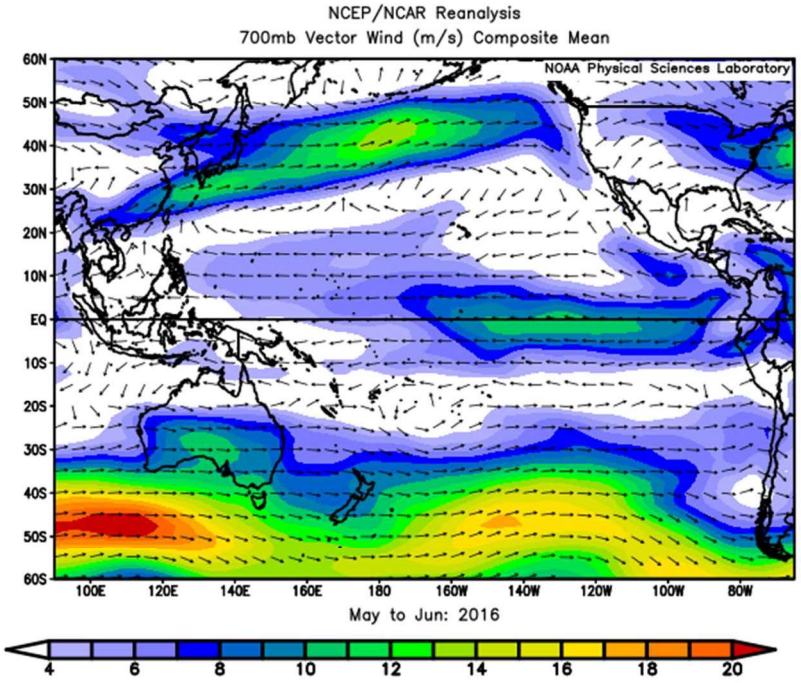

Figure 45. Average 700 mb vector wind (m/s) for May and June of 2016. Source: National Oceanic and Atmospheric Administration (NOAA)

A similar wind pattern was observed for May and June of 2022 (Figure 46). However, while the transport path is similar, winds were slightly stronger and more direct between eastern Asia and the southwestern U.S. in 2022 compared to 2016.

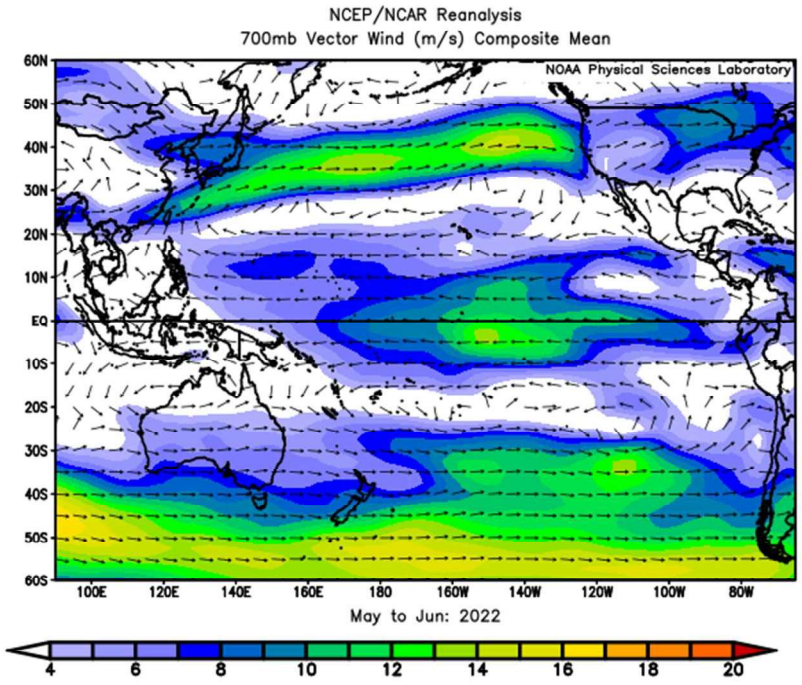

Figure 46. Average 700 mb vector winds (m/s) for May and June of 2022. Source: NOAA.

The 700 mb wind patterns for May and June of 2016 and 2022 are also representative of 1991-2020 climatological 700 mb winds across the Pacific Basin, as shown in Figure 47, with a similar west-to-east transport pattern and similar wind speeds during the climatological period.

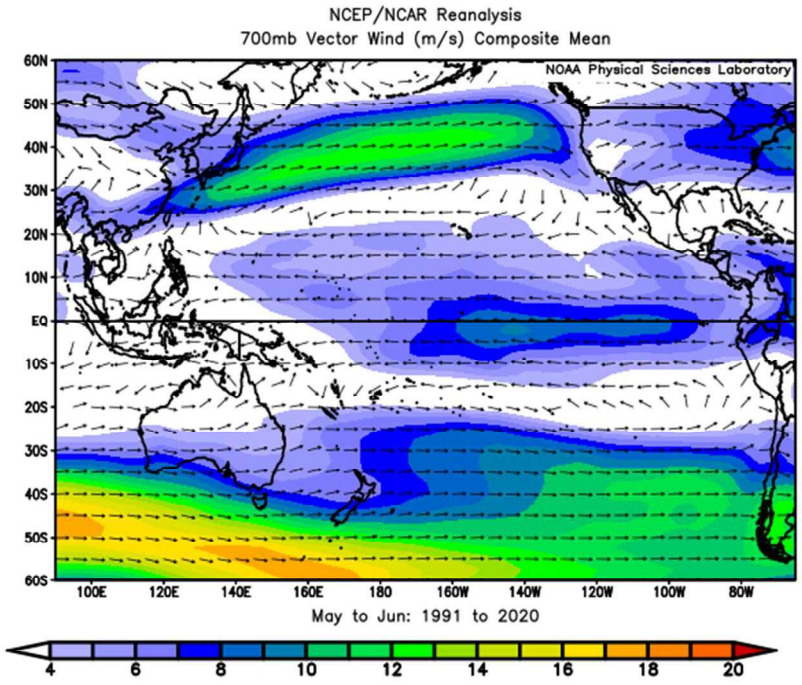

Figure 47. Climatological average 700 mb vector winds (m/s) for May and June 1991 to 2020. Source: NOAA.

Moreover, with 700 mb winds in 2016 showing a slightly weaker and less direct transport pattern, 2016 meteorological conditions may represent a conservative estimate of cross-Pacific transport compared to 2022 and climatological records. The 700 mb wind speed anomalies for May and June of 2016 in **Figure 48** confirm that the 700 mb transport pattern in 2016 was generally weaker than normal across the north-central Pacific.

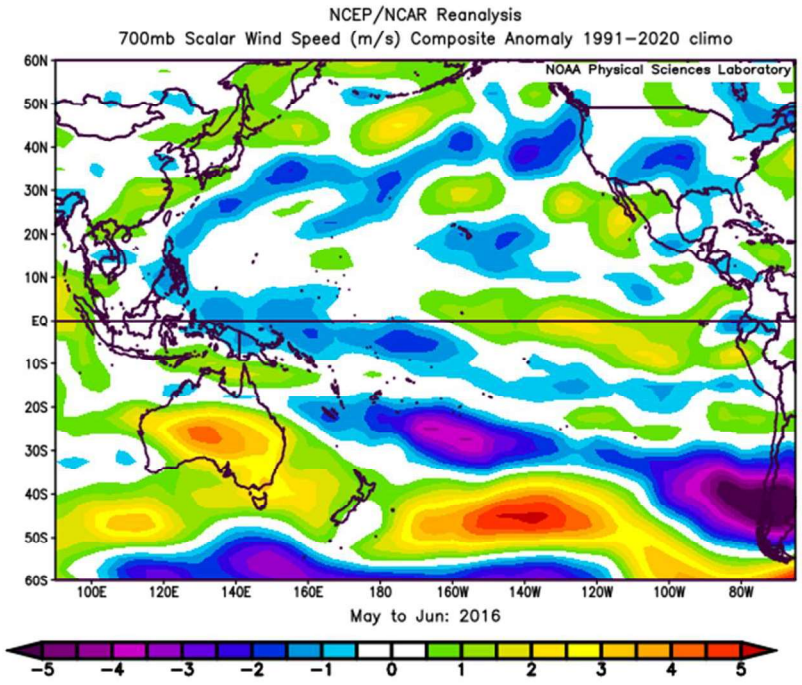

Figure 48. 2016 May-June 700 mb wind anomalies (m/s) compared to the 1991-2020 climatological period. Cool colors indicate wind speed reductions compared to the 1991-2020 climatological records, while warm colors indicate wind speed increases. Source: NOAA.

In Figure 48, there is one notable area of increase in winds south of the Aleutian Islands where the maximum 700 mb westerly winds were observed in 2016. However, there is a consistent region of lower-than-normal wind speeds along the more direct climatological transport path connecting the two continents.

The LNR transport path winds at the 850 mb level in 2016 also compare favorably to those from 2022 and climatological records. In May and June of 2016, a transport path from eastern Asia moves east-northeastward into the north Pacific, before turning southeastward along the West Coast. The wind field becomes diffluent offshore of Southern California, with southwesterly winds over southern Nevada and northeasterly winds west of Baja California (Figure 49).

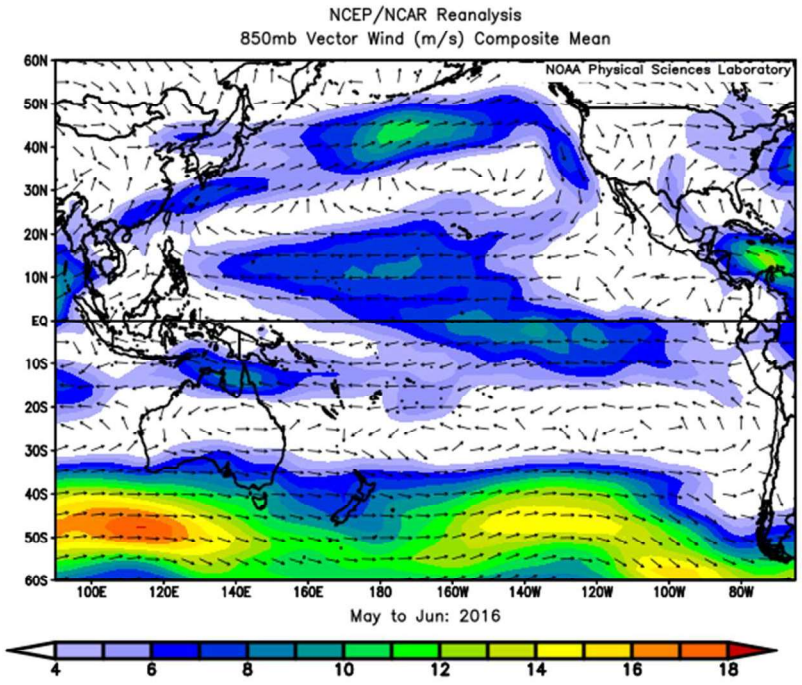

Figure 49. Average 850 mb vector winds (m/s) for May and June of 2016. Source: NOAA.

Similar to the pattern at 700 mb, 850 mb LNR transport winds in May and June of 2022 were farther south than those in 2016 (**Figure 50**), providing a more direct transport path into the southwestern U.S. However, the configuration of the transport paths and the overall magnitude of wind speeds are similar for both years.

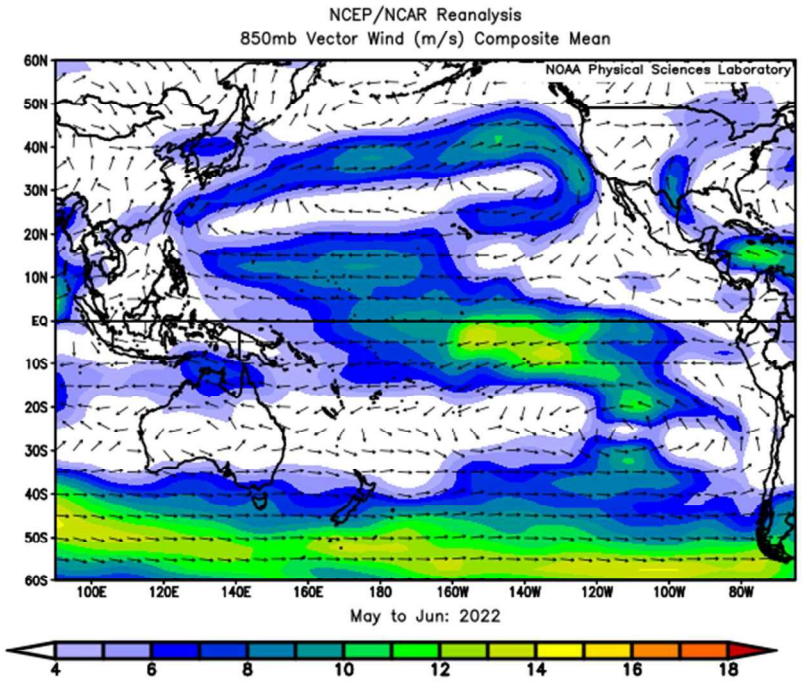

Figure 50. Average 850 mb vector winds (m/s) for May and June of 2022. Source: NOAA.

The 850 mb wind patterns for May and June of 2016 and 2022 are also similar to the climatological wind pattern for May and June over the period from 1991-2020, as shown in **Figure 51**. The latitude of the climatological 850 mb westerly jet appears to lie between the more direct southern path of 2022 and the more northern path seen in 2016.

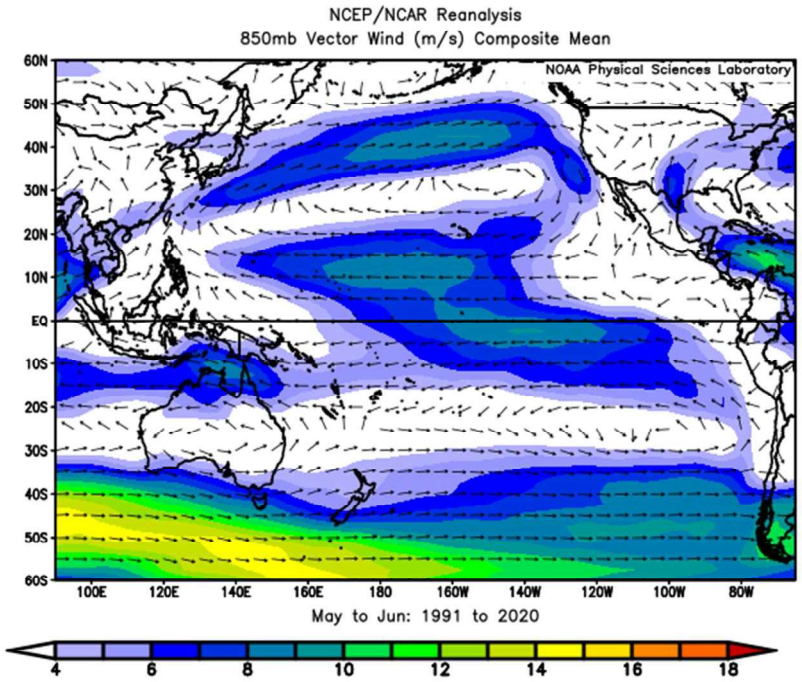

Figure 51. Average 850 mb vector winds (m/s) for May and June of 1991 to 2020. Source: NOAA.

The 850 mb wind speed anomalies in Figure 52 show that the 2016 LNR transport path was similar in speed, but north of the more direct climatological route, with the increase in winds across the northern Pacific similar in magnitude to the decreases farther south.

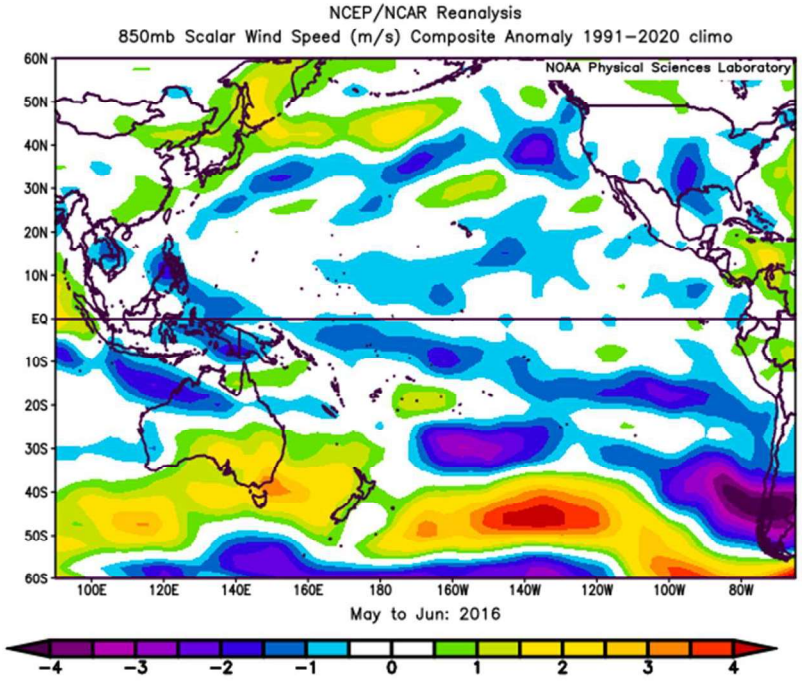

Figure 52. 850 mb wind speed anomalies for May and June of 2016 compared to climatological 850 mb wind speeds from 1991-2020. Source: NOAA.

In summary, when considering the LNR component of this photochemical modeling demonstration, the cross-Pacific transport wind patterns from eastern Asia into the southwestern U.S. during the months of May and June at 700 mb and 850 mb appear to be seasonally consistent when comparing data from 2016 to both 2022 and climatological records. In addition, the generally below-normal wind speeds across the central Pacific Basin at 700 mb, and a less direct transport path at 700 mb and 850 mb in 2016, indicate that the use of 2016 meteorological data could represent a conservative estimate of cross-Pacific long-range pollutant transport. As a result, when considering LNR pollutant transport winds in May and June 2016 meteorological data appears to be a representative and potentially conservative dataset to use in modeling LNR transport for 2022 or future years.

3.3.3 Mexico Transport Days

From the analysis performed in Section 2.2.2, the pressure levels most relevant to pollutant transport into Clark County on MEX transport days were the 700 mb (2,630 m AGL) and 850 mb (800 m AGL) pressure levels. Most MEX transport days in Section 2.2.2 occurred in July and August, coinciding with the annual development of the North American Monsoon. To remain consistent with the previous analysis, mean wind patterns at 700 mb and 850 mb were analyzed for the months of July and August of 2016. These winds patterns were then compared to the wind patterns in July and August of 2022, which is the year of the emissions inventory selected for this modeling

demonstration. In addition, the 700 mb and 850 mb wind patterns in 2016 were compared to the July-August climatological wind patterns from 1991-2020 to see if 2016 wind patterns could be applicable when modeling future years.

Figure 53 shows the 700 mb mean wind patterns for the July-August period for 2016 and 2022. In 2016, a ridge of high pressure over the Four Corners region produced a clockwise wind pattern across the southwestern United States and northern Mexico. In Clark County, winds were southwesterly, while winds over northwestern Mexico were easterly to southeasterly. From the configuration of the ridge and its associated wind pattern, it can be inferred that 700 mb winds in the Colorado River Valley were generally southerly, on average, which would allow pollutants from Mexico to be carried into Clark County.

The July-August 2022 mean wind pattern was similar to the same period in 2016. The ridge of high pressure over the Four Corners was more amplified in 2022, leading to southerly winds in Clark County and easterly winds in northwestern Mexico. The clockwise configuration of the 700 mb wind pattern in 2022 also suggests pollutant transport from Mexico into Clark County.

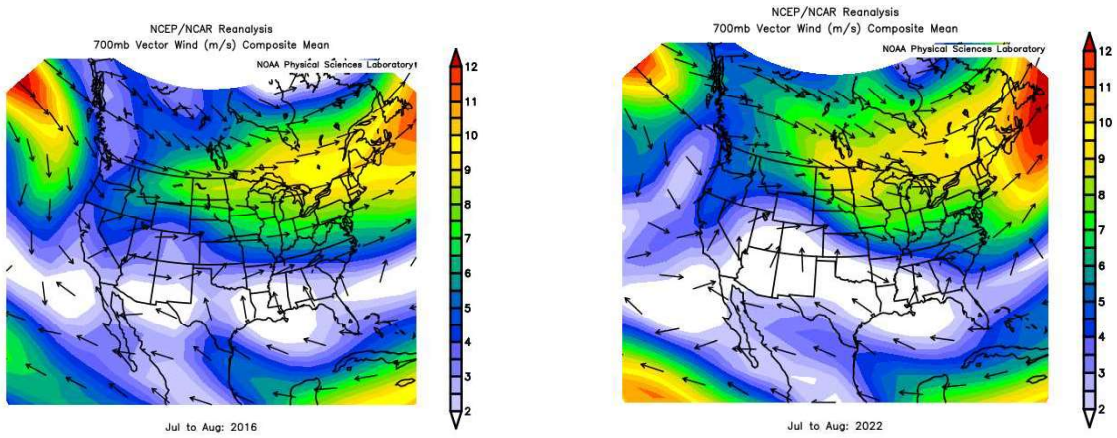

Figure 53. July-August 700 mb mean wind patterns for 2016 (left) and 2022 (right). Source: NOAA.

Figure 54 displays the July-August climatological mean 700 mb wind patterns from 1991-2020. The July-August 2016 mean 700 mb wind patterns shown in Figure 53 compare favorably to the climatological mean wind patterns in Figure 54, with a ridge of high pressure generating a clockwise wind pattern across the southwestern U.S. and northern Mexico. Specific to Clark County, wind patterns for the 2016 and climatological periods were southwesterly in each case. Therefore, it could be acceptable for the July-August 2016 700 mb wind patterns to be used as a proxy when modeling July-August winds and transport patterns for future years, provided those future years match reasonably with these climatological conditions.

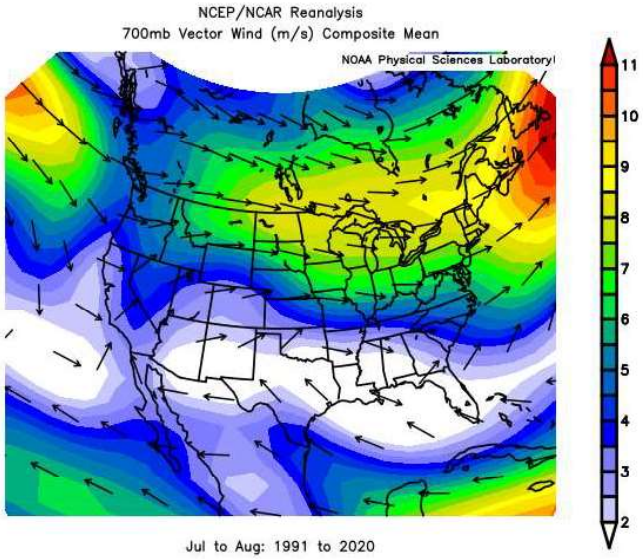

Figure 54. July-August 700 mb mean wind patterns for the 1991-2020 climatological period. Source: NOAA.

Similarities were also found when comparing the mean 850 mb wind patterns for the July-August timeframes in 2016 and 2022 (**Figure 55**). In 2016, an area of low pressure was analyzed off the Baja California Coast, with high pressure positioned across the northern Gulf Coast. These features resulted in southerly winds over northern Baja California, with winds shifting to southwesterly in southern Nevada. This wind pattern would be conducive to transport pollutants from Mexico into Clark County.

Similarly, during July-August 2022, high pressure over the northern Gulf Coast and low pressure off the Baja California coast yielded a southeasterly wind in northern Baja California. Winds then shifted to southwesterly in southern Nevada. Like 2016, the 2022 winds would also favor pollutant transport from Mexico into Clark County.

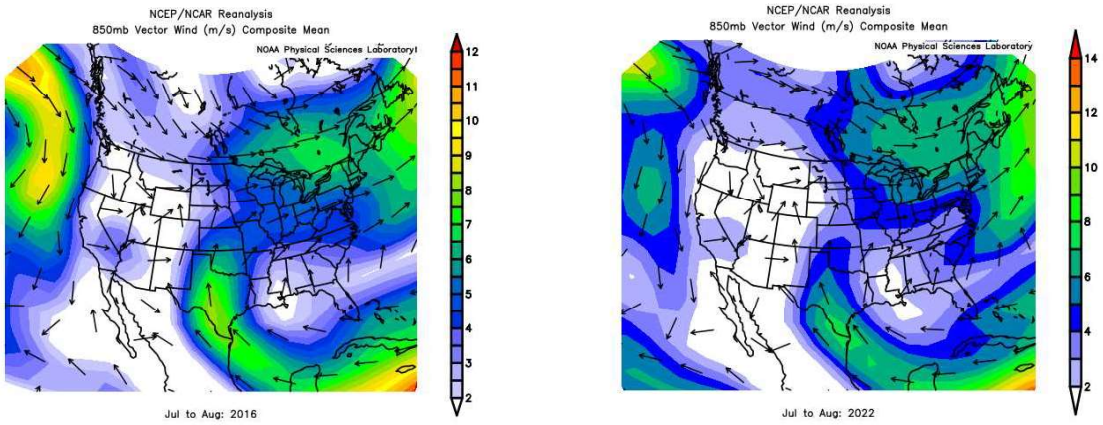

Figure 55. July-August 850 mb mean wind patterns for 2016 (left) and 2022 (right). Source: NOAA.

July-August 2016 mean 850 mb wind patterns were also compared to the July-August climatological mean 850 mb wind patterns for the 1991-2020 period. Figure 56 displays the 1991-2020 mean 850 mb wind patterns for the July-August timeframe, which is a similar pattern to that seen in 2016: high pressure over the northern Gulf Coast, low pressure off the Baja California coast, and a southerly wind in northern Baja California that shifted to southwesterly in Clark County. The pattern of potential pollutant transport in the climatological mean, in conjunction with the potential pollutant transport path seen in Figure 55 for 2016, suggests that it may be suitable to use the July-August 2016 wind patterns when modeling future years.

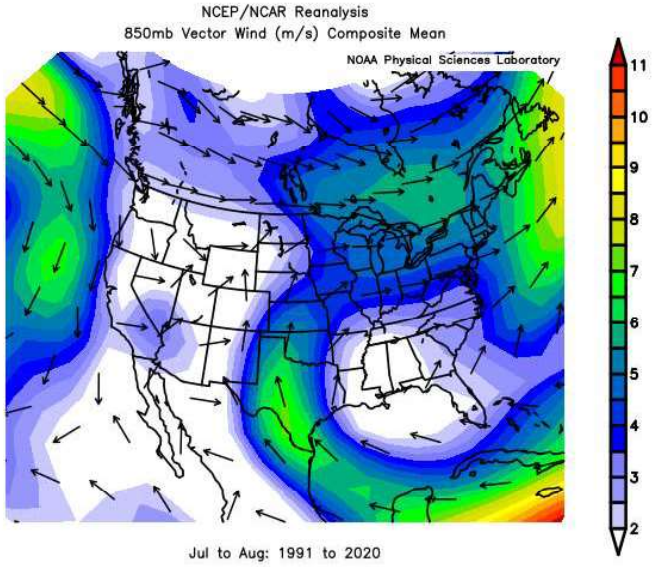

Figure 56. July-August 850 mb mean wind patterns for the 1991-2020 climatological period. Source: NOAA.

In summary, the 700 mb mean winds for the July-August period for 2016 and 2022 were comparable in their depiction of potential pollutant transport from Mexico into Clark County. Furthermore, the July-August 2016 mean wind patterns at 700 mb were similar to the 1991-2020 July-August climatological mean wind patterns. In addition, the 850 mb mean wind patterns for the July-August period for 2016 and 2022 were similar, with each showing a potential pollutant transport path into southern Nevada from northwestern Mexico. The July-August 2016 850 mb mean wind pattern also compared favorably to the 1991-2020 July-August climatological mean wind pattern. These wind results at 700 mb and 850 mb suggest that July-August 2016 may be a representative wind dataset that can be used as a proxy for modeling future years.

3.3.4 Local Meteorological Comparison of 2016 and 2022

In addition to comparing large-scale upper-level wind patterns to assess meteorological similarity between years, it may be helpful to compare local surface and upper-level weather observations across several parameters. These parameters include (but are not limited to):

- Surface daily average temperature (°F)
- Surface daily average wind speed (mph)
- Surface daily precipitation (inches)
- Surface mean sea level pressure (MSLP [mb])
- 500 mb heights (meters) measured twice daily at 4:00 and 16:00 PST

To identify patterns in the surface and upper-level meteorological parameters listed above, data was obtained from the ASOS weather station at KLAS for 2016 and 2022. Next, the surface meteorological data were aggregated on a daily basis for the parameters listed above. Twice-daily upper-air data was obtained for 500 mb heights from the KVEF station.

Using the April-September period (the defined ozone season for Clark County), two sample t-Tests (assuming unequal variances) were conducted to determine whether differences in meteorological data for 2016 and 2022 were statistically significant. When comparing the two years, a statistically significant difference in meteorological data is defined by the absolute value of the t-statistic being greater than 2, along with the value of P two-tail being less than 0.05. Meteorological parameters that *do not* exhibit statistically significant differences in means between two periods may indicate that weather conditions were sufficiently similar to allow a substitution of one year's meteorological conditions for another year's when modeling emissions.

Table 15 contains t-statistic and two-tail p-values when comparing the April-September 2016 and 2022 data for the meteorological parameters listed above. Green cells indicate the given meteorological parameter for 2016 and 2022 was statistically similar. Conversely, red cells highlight a statistically significant difference in the given meteorological parameter when comparing 2016 and 2022.

Table 15. t-Statistic and two-tail p-values when comparing 2016 and 2022 data for select surface and upper-air meteorological parameters at the KLAS and KVEF sites.

Daily Tavg	**t-Stat**	**P two-tale**
KLAS	-0.395	0.693
Daily precip	**t-Stat**	**P two-tale**
KLAS	0.900	0.369
Daily avg WS	**t-Stat**	**P two-tale**
KLAS	-0.027	0.979
500 mb heights	**t-Stat**	**P two-tale**
KVEF	-1.641	0.101
Daily avg mslp	**t-Stat**	**P two-tale**
KLAS	-1.709	0.088

When comparing the 2016 to 2022 meteorological data at KLAS, the differences for each parameter were not statistically significant. In addition, the differences in 500 mb heights at KVEF were not statistically significant between the two years.

Two sample t-Tests (assuming unequal variances) were also conducted using the KLAS surface meteorological parameters for 2016 and the 1991-2020 climatological averages covering the April-September period. A comparison of KVEF daily average 500 mb heights for 2016 and the 1991-2020 period were not calculated because KVEF has only been in operation since 2010. Table 16 shows that the differences in most surface meteorological parameters were not statistically significant. However, the difference in the daily average wind speed data at KLAS for the April-September 2016 period was statistically significant compared to the 1991-2020 April-September climatological average.

Table 16. t-Statistic and two-tail p-values when comparing April-September 2016 to April-September 1991-2020 climatological data for select surface meteorological parameters at the KLAS and KVEF sites.

Daily Tavg	**t-Stat**	**P two-tale**
KLAS	-1.09565	0.274595958
Daily precip	**t-Stat**	**P two-tale**
KLAS	-1.376	0.170476817
Daily avg WS	**t-Stat**	**P two-tale**
KLAS	5.580617	7.68865E-08
Daily avg mslp	**t-Stat**	**P two-tale**
KLAS	0.142504	0.886830459

The monthly distributions of daily average wind speeds were also compared for 2016, 2022, and the historic climatological period (1991-2020) at the KLAS ASOS site in Figure 57.

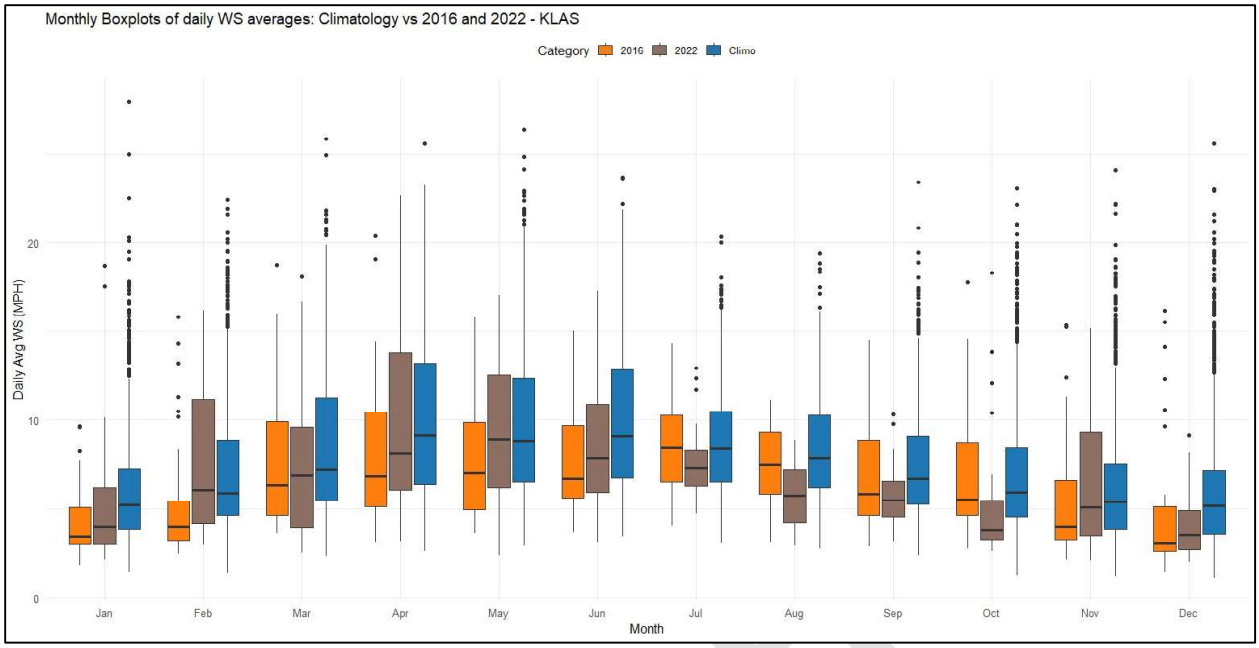

Figure 57. Monthly boxplots of daily wind speed averages at KLAS for 2016 (orange), 2022 (brown) and the 1991-2020 climatological records (blue).

In general, when focusing on the April-September ozone season, Figure 57 shows similar seasonal trends in wind speeds for 2016, 2022, and the 1991-2020 climatological records; higher daily average wind speeds in the spring and early summer, before decreasing to lower averages during the late summer and fall. There is significant overlap of the interquartile ranges for the three datasets from April through July, and again in September, signifying statistically comparable wind speeds during those months. While greater differences appear in August when comparing 2016 and 2022, the interquartile range in August 2016 remains similar to the climatological interquartile range for that month. Although most months at KLAS exhibited similarities in wind distributions between 2016 and the 1991-2020 climatological period (Figure 57), the comparison of April-September 2016 winds at KLAS versus the climatological records (Table 16) showed that differences in wind speeds were statistically significant.

To fully understand the surface meteorological conditions beyond the KLAS ASOS site, a regional analysis of the surface meteorological parameters listed above was also examined for the April-September period for 2016 and the 1991-2020 climatological average. Using reanalysis data from NOAA, Figure 58 contains anomaly maps for 1,000 mb temperature, wind speed, precipitation, and MSLP. The white shading over Clark County in top and left panels of Figure 58 indicates most surface meteorological parameters across southern Nevada in the April-September 2016 period were similar to the 1991-2020 climatological period. The lone exception was MSLP (bottom right of Figure 58), which was less than 1 mb higher than normal across most of Nevada in April-September 2016.

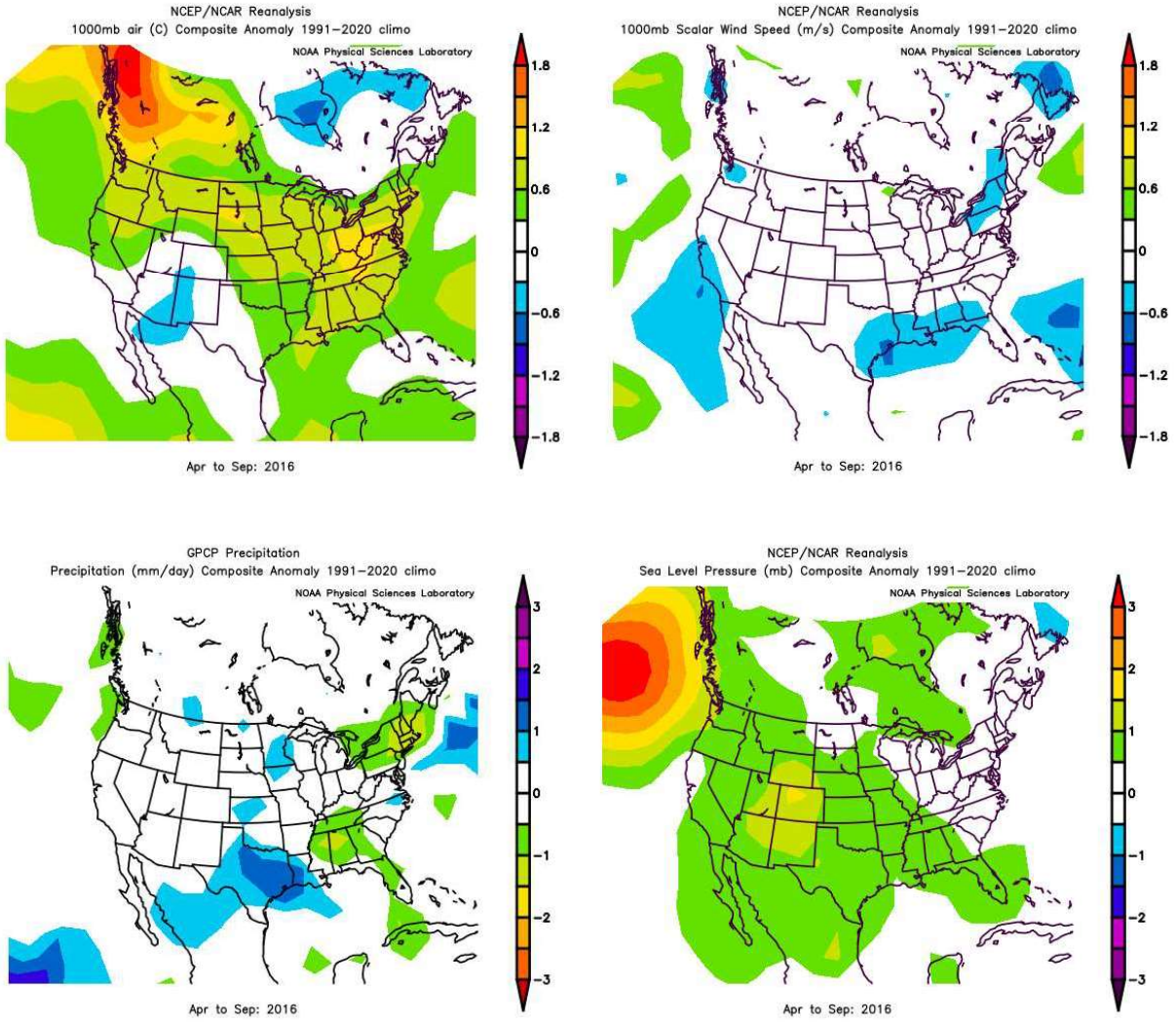

Figure 58. Clockwise from the top left, the April-September 2016 anomalies (compared to 1991-2020 climatological period) for 1,000 mb air temperature (°C), wind speed (m/s), sea level pressure (mb), and precipitation (mm/day). Source: NOAA.

In conclusion, the majority of the meteorological parameters analyzed in Clark County were similar when comparing 2016 and 2022. Additionally, most meteorological parameters in the April-September 2016 period were similar to the 30-year climatological averages for the same period. Thus, it can be concluded that, for the local and regional meteorological parameters above, the weather conditions in 2016 compared favorably to 2022 and the 1991-2020 climatological period in Clark County, Nevada, which may allow the dataset to be sufficiently representative for modeling future years. However, it is recommended that subsequent model years also be compared to both 2016 and the climatological records, if possible, to determine meteorological similarity before substituting one year's meteorological conditions for another year's when carrying out modeling.

3.4 Regional Model (CAMx) Source Apportionment

SA modeling results for the year 2023, developed under the Moderate ozone SIP (Ramboll Americas Engineering Solutions, 2024), were used to estimate ozone contributions from IA emissions to the projected 2026 ozone DV at monitoring sites throughout Clark County. No new SA model runs were conducted specifically for 2026.

The CAMx (Emery et al., 2024; Ramboll Environment and Health, 2024) was used to support both Moderate and Serious ozone attainment demonstrations for Clark County. Refer to the Serious Attainment Demonstration Technical Support Document (TSD) for details on CAMx selection, configuration, application, and results (Ramboll Americas Engineering Solutions and Eastern Research Group, 2026). CAMx contains the Ozone Source Apportionment Technology (OSAT) that tracks contributions from user-designated emission source categories and regions. As part of the modeled attainment demonstration for the Moderate ozone SIP, CAMx OSAT was run for the 2023 Moderate attainment year scenario to quantify and rank ozone contributions from specific source sectors and regions that contribute to high ozone levels in Clark County. This included tagging contributions from other states, international anthropogenic emissions, and regional wildfires to assess culpability of upstream and international contributions. Additional details on the OSAT configuration are provided in the Moderate attainment demonstration TSD (Ramboll Americas Engineering Solutions, 2024).

The 2023 OSAT simulation divided the modeling domain into six source regions along with stratified 2016 boundary conditions (Figure 59):

1. All of Clark County, including HA 212
2. The remaining areas of Nevada
3. California
4. The remaining areas of the United States, including the 200-mile United States coastal zone
5. Mexico
6. Other international areas, including Canada and beyond the 200-nautical-mile United States coastal zone
7. Global boundary conditions (BCs) stratified among non-United States (international) anthropogenic and other

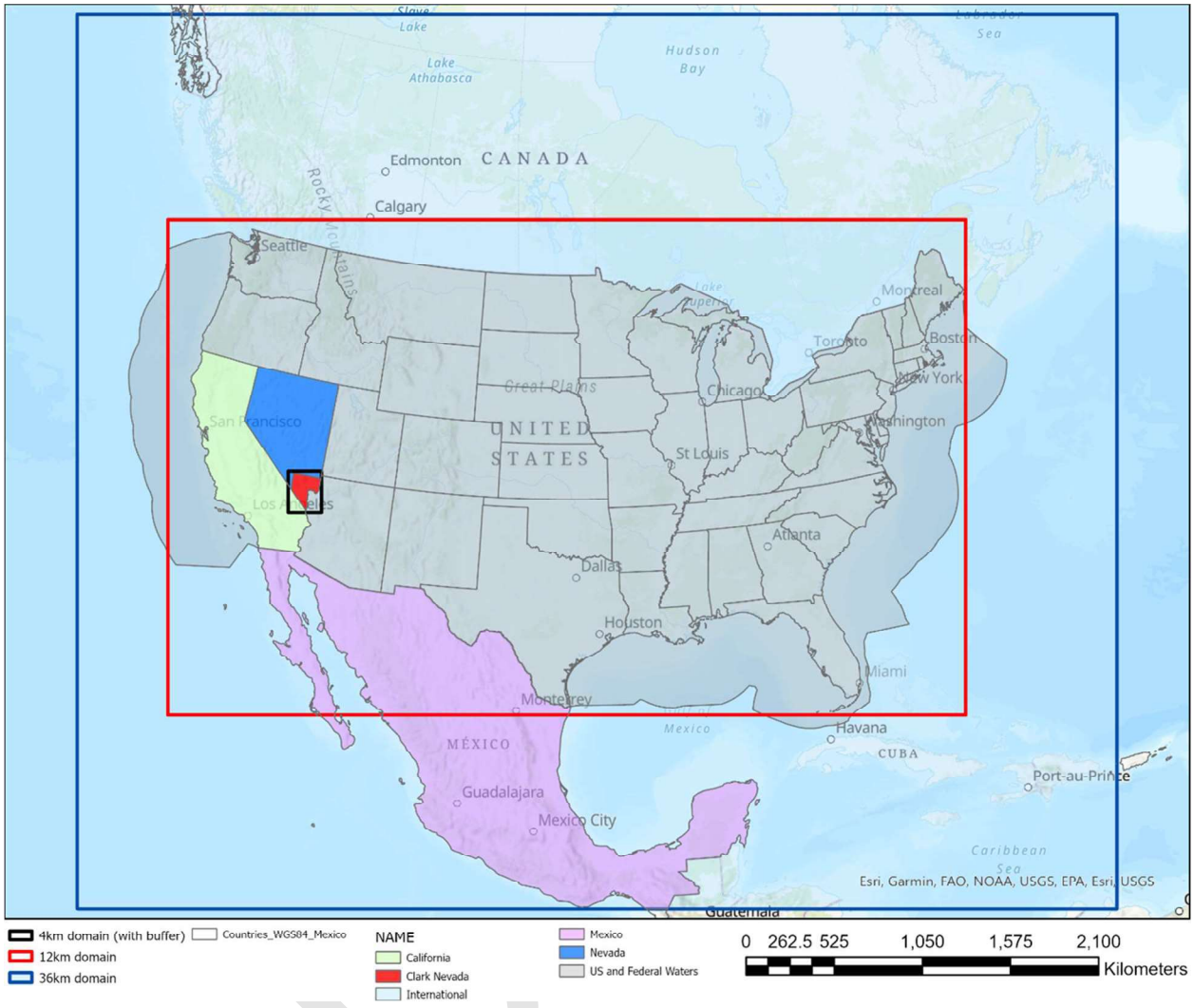

Figure 59. Source apportionment regions for the 2023 SA run.

The 2023 SA simulation tracked ozone contributions from the following seven source sectors:

1. Natural (biogenic, lightning NO_x, oceanic)
2. Open-land fires (all wildfires, prescribed fires, and agricultural fires)
3. On-road sources
4. Nonroad sources (including airports, rail, commercial marine vessels)
5. Point sources
6. Nonpoint solvent sector
7. Remaining nonpoint sectors

Two separate sets of BC tracers tracked global IA and remaining natural emissions as defined by two sets of global model output. The Clark County 2016 modeling platform employed BCs developed

from the publicly available Community Atmosphere Model with Chemistry (CAM-Chem) global model output datasets provided by the National Center for Atmospheric Research (NCAR). CAM-Chem includes all global anthropogenic and natural precursor emissions and stratospheric ozone. Therefore, another source of global model output was needed to define the IA contribution, which is normally determined from a "zero out rest of world" (ZROW) or natural-only scenario from the same global model. No such data was available from CAM-Chem. However, both total and ZROW scenarios were available from the hemispheric version of the EPA's Community Multiscale Air Quality (H-CMAQ) model applications, which were developed specifically for the 2016 modeling platform and have pedigree of prior use for similar purposes. Ramboll Americas Engineering Solutions and Eastern Research Group (2026) developed an approach to use EPA's H-CMAQ results to split CAM-Chem output into IA and other fractions for use in the SA application.

The use of 2016 global chemical transport modeling to characterize 2026 IA ozone levels and precursors entering the western U.S. carries uncertainty, primarily by assuming that non-U.S. emissions have held steady over the past 10 years. Further uncertainty is introduced by the complex method employed to translate estimated IA fractions from one global model (H-CMAQ) to the boundary conditions derived from another (CAM-Chem). Section 3.2 evaluates the potential range of contemporary IA impacts on Clark County.

Raw hourly ozone SA tracer data were postprocessed to represent contributions to total MDA8 ozone concentrations each day. In other words, the unique 8-hr period defining total MDA8 ozone concentrations at each grid cell on each day was used to time average all of the ozone tracers. The results were then compiled into a Microsoft Excel "dashboard" to facilitate interactive analyses in a way that maximizes choices by monitoring site, combinations of sectors, and combinations of regions. Total IA ozone levels were determined by summing SA tracers for Mexico, other non-U.S. areas within the modeling domain, and IA BCs representing the rest of the world. Using data archived in the dashboard, Ramboll Americas Engineering Solutions and Eastern Research Group (2026) determined the relative total IA ozone contributions to 2023 DVs at each of the Clark County monitoring sites that operated during the 2016-2018 DV period (i.e., sites with valid fourth-high MDA8 ozone levels during 2014-2018). Ramboll Americas Engineering Solutions and Eastern Research Group (2026) then scaled 2026-projected DVs at each of those sites (as determined by the 2022-2026 modeling conducted for the serious modeled attainment test) by the relative total IA contribution to yield the projected 2026 DVs that would occur without the influence from all IA emissions.

Table 17 lists the 2022-2024 base year DVs at all Clark County monitoring sites, the projected 2026 DVs from the serious attainment test, the relative contribution from IA sources from the SA dashboard, and the scaled 2026 DVs without IA contributions. Entries marked with an asterisk are newer sites since 2018 for which the original 2023 SA contributions were not calculated. IA relative contributions for those sites were assigned from legacy sites: the Virgin Valley HS site was assigned IA contributions from the Indian Springs site; the Mountains Edge Park site was assigned from the Paul Meyer site; the Liberty HS site was assigned from the Green Valley site; the Garrett Jr. HS site

was assigned from the Green Valley site; and the Walnut CC site was assigned from the Jerome Mack site. Relative IA contributions range from 19-23%. While the original projected 2026 DVs indicated continued exceedances according to Software for the Modeled Attainment Test – Community Edition (SMAT-CE) projections, the adjusted 2026 DVs with IA contributions removed all show attainment of the 2015 ozone NAAQS by more than 10 ppb.

Based on these results, we conclude that HA 212 would attain the 2015 ozone NAAQS by the 2026 serious attainment date but for contributions from foreign anthropogenic sources.

Table 17. 2022-2024 base DVs, projected 2026 DVs, and projected 2026 DVs with IA contributions removed at each monitoring site within Clark County according to SMAT-CE calculations. Red values correspond to exceedances of the 2015 ozone NAAQS; green values correspond to data below the NAAQS. DV values are in ppb.

Site ID	Site Name	2022-2024 DV Avg 3 x 3	2026 DV Avg 3 x 3	IA Contribution	Adjusted 2026 DV Avg 3 x 3
320030024	Virgin Valley High School	64.5	63.9	20%	51.1
320030043	Paul Meyer	73.3	72.7	19%	58.9
320030044	Mountains Edge Park	73.5	72.8	19%	59.0
320030071	Walter Johnson	72.3	71.8	19%	58.2
320030073	Palo Verde	71.3	70.5	19%	57.1
320030075	Joe Neal	72.7	71.6	19%	58.0
320030298	Green Valley	70	69.5	21%	54.9
320030299	Liberty High School	70.5	69.9	21%	55.2
320030540	Jerome Mack-NCore	67.7	67.3	20%	53.8
320030602	Garrett Jr. High School	67.3	66.7	21%	55.2
320031019	Jean	68.0	67.3	23%	51.8
320032003	Walnut Community Center	72.0	71.4	20%	57.1
320037772	Indian Springs	68.0	66.8	20%	53.4

3.5 Global Model (GEOS-Chem) Source Apportionment

Ozone chemistry is complex and non-linear. Because ozone's lifetime can range from a few hours to several weeks, depending on its source, season, and transport pathway, the contribution of international transport to the southwest U.S. can only be verified using a global model. To help bound the modeled 2026 IA impact described above, results from a 2023 GEOS-Chem application

were analyzed. GEOS-Chem output was available from two runs covering the period of July through August 2023: a full global emissions run, and an IA zero-out run. Surface ozone concentrations were extracted for the single 2 x 2.5° grid cell covering Clark County, and differences between the two runs were calculated to yield the IA contribution.

Results are shown in Figure 60 as a time series of daily-averaged ozone concentrations spanning July and August 2023. The modeled daily total ozone concentrations range from 36 to 72 ppb, which is reasonable for the summer season despite the coarse resolution. Modeled IA contributions range from 1 to 9 ppb, and this range is consistent between all modeled days and half the days that were simulated above 60 ppb. The IA contribution tends to decrease through the summer season, with a July average of 5.6 ppb (9%) and an August average of 4.0 ppb (7%).

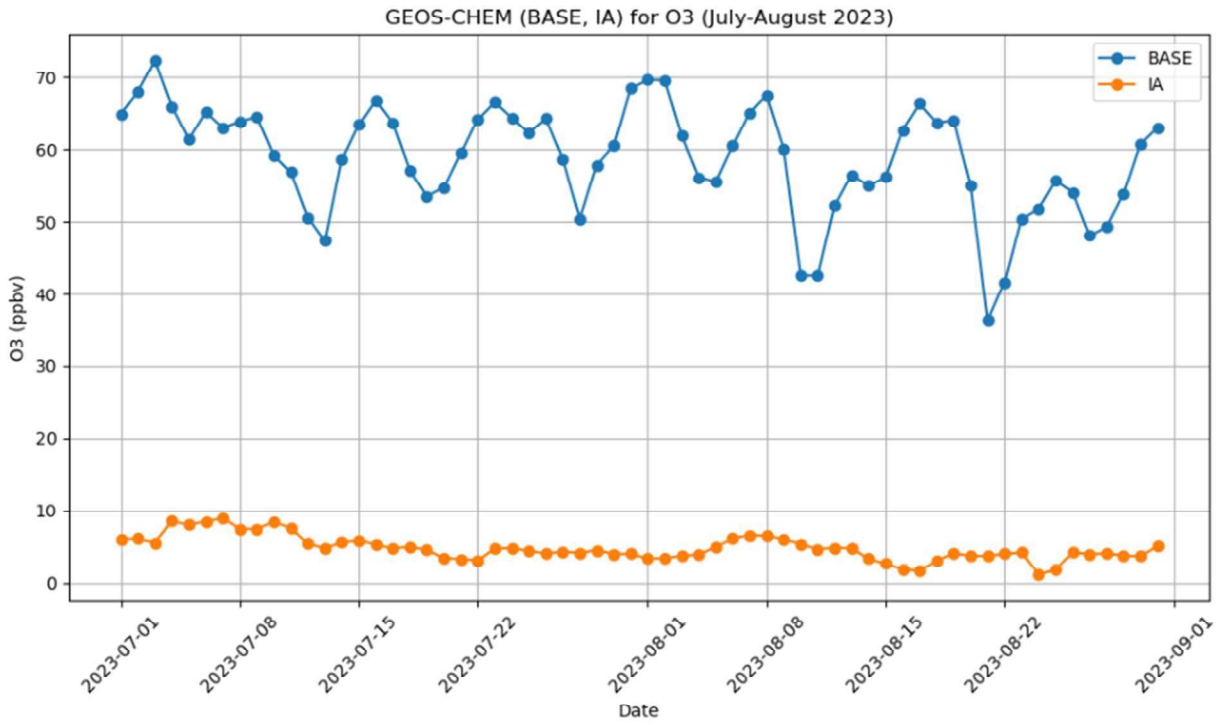

Figure 60. Time series of daily average surface ozone concentrations and IA contributions spanning July through August 2023 as simulated by GEOS-Chem from a single grid cell covering Clark County.

These results are much smaller than the 20% modeled IA contributions from the CAMx source apportionment simulation that used 2026 emissions with 2016-based boundary conditions. There are two likely causes for this. First, and probably most impactful, is the fact that GEOS-Chem exhibits less vigorous vertical transport dynamics and a greater tendency to underpredict surface ozone concentrations across the western U.S. than either CAMx or CAM-Chem. Differences in spatial resolution, sources of meteorological data, and transport algorithms could explain the variations in

vertical transport. This was a major reason why the 2016 CAM-Chem modeling resulted in higher ozone concentrations over the southwestern U.S and improved the negative bias exhibited by 2016 GEOS-Chem across rural background ozone monitoring sites (Clark County Department of Environment and Sustainability Division of Air Quality, 2024). Second, the 2023 GEOS-Chem simulation reflects reductions in the Asian precursor emissions inventory relative to 2016. The separate impacts from these two factors are difficult to quantify from the GEOS-Chem output alone. Nevertheless, when the July-August average 8% IA contributions derived from the 2023 GEOS-Chem results over Clark County are removed from the projected 2026 DVs, all DVs remain below the 70 ppb NAAQS (Table 18).

Table 18. 2022-2024 base DVs, projected 2026 DVs, and projected 2026 DVs that remove the relative IA contributions over Clark County from a 2023 GEOS-Chem run. Red values indicate exceedances of the 2015 ozone NAAQS; green indicate values below the NAAQS. DV values are in ppb

Site ID	Site Name	2022-2024 DV Avg 3 x 3	2026 DV Avg 3 x 3	2023 GEOS-Chem IA Contribution	Adjusted 2026 DV Avg 3 x 3
320030024	Virgin Valley High School	64.5	63.9	8%	58.8
320030043	Paul Meyer	73.3	72.7	8%	66.9
320030044	Mountains Edge Park	73.5	72.8	8%	67.0
320030071	Walter Johnson	72.3	71.8	8%	66.1
320030073	Palo Verde	71.3	70.5	8%	64.7
320030075	Joe Neal	72.7	71.6	8%	65.9
320030298	Green Valley	70	69.5	8%	63.9
320030299	Liberty High School	70.5	69.9	8%	64.3
320030540	Jerome Mack-NCore	67.7	67.3	8%	61.9
320030602	Garrett Jr. High School	67.3	66.7	8%	61.4
320031019	Jean	68.0	67.3	8%	61.9
320032003	Walnut Community Center	72.0	71.4	8%	65.7
320037772	Indian Springs	68.0	66.8	8%	61.5

3.6 Modeled U.S. and International Contributions for 2015 Ozone NAAQS in Nonattainment Areas

EPA performed national-scale photochemical modeling to attribute observed ozone concentrations at nonattainment-area monitors to natural background sources (Natural), U.S. anthropogenic emissions (US Anth), international anthropogenic emissions (Intl Anth), and ozone chemistry arising from both U.S. and international sources (Mixed Anth) (Henderson and Simon, 2021). Modeling was performed as follows:

- **Model:** CMAQ
- **Resolution:** 12 km with 35 vertical layers
- **Modeling year:** 2016

Modeling was performed for the following four scenarios:

1. Base case, which includes all emissions (Base)
2. Zero U.S. anthropogenic emissions (ZUSA)
3. Zero international anthropogenic emissions (ZROW)
4. Zero all anthropogenic emissions (ZANTH)

For each grid cell, the base CMAQ model was used to identify and select the top 10 days with the highest MDA8 ozone concentrations. These top 10 days and MDA8 periods were applied to each of the four modeling scenarios, and used to determine source attribution using a zero-out approach as follows:

- Natural = ZANTH
- US Anth = Base – ZUSA
- Intl Anth = Base – ZROW
- Mixed Anth = Base – Natural – US Anth – Intl Anth

For the 2018-2020 DVs, source attribution was estimated by scaling the observed DVs using the relative source contribution fractions (Natural, US Anth, Intl Anth, and Mixed Anth) developed from the 2016 CMAQ modeling at the corresponding grid cell.

In Clark County (Las Vegas, NV nonattainment area), source attribution for the 2018-2020 DV was based on data from the Joe Neal AQS site (ID 320030075). In 2016, the 4th highest MDA8 for the site was 77 ppb, while the mean of the 2016 CMAQ base model top 10 concentrations was 79.0 ppb. For the 2018-2020 DV in Clark County:

- DV = 74.0 ppb
- Natural = 28.6 ppb
- US Anth = 35.6 ppb
- Intl Anth = 6.0 ppb
- Mixed Anth = 3.8 ppb

Based on these results, EPA estimates the international anthropogenic contribution to be between 8.1 and 13.2% (range calculated as Intl Anth-only to Intl Anth + Mixed Anth). Comparing these results to the CAMx and GEOS-Chem modeling results, which ranged between 8 and 23%, we see that the current modeling results encompass and are generally consistent with the EPA modeling results. The CAMx model does indicate a higher international anthropogenic contribution (19-23%), but the IA contribution is sourced from the 2023 SA dashboard where DVs are lower than the EPA modeling period (2018-2020). If international emissions have increased (Maricopa Association of Governments, 2025) or remained steady since the EPA modeling period, the percentage of IA contribution would be higher relative to a more recent, lower DV level. Overall, the EPA modeling

results of IA contribution are generally consistent with the current CAMx and GEOS-Chem results, despite differences in model initiation and periods modeled.

4. Conclusions

HA 212, which encompasses the greater Las Vegas, Nevada, urban area, is designated as Serious nonattainment for the 2015 ozone NAAQS of 70 ppb despite historic declines in ozone and ozone precursors. Back-trajectory cluster analysis identified two international transport pathways: air transport from Mexico and cross-Pacific transport from eastern Asia. International transport clusters accounted for a total of 23% of all back-trajectories. The two international transport pathways occur under dissimilar meteorological conditions and during distinct times of the year: summertime monsoonal weather patterns for MEX transport days, and winter and spring hemispheric circulation patterns for LNR transport days. Backward dispersion modeling indicated that MEX transport dates had the highest overall percentage of international NPES (24.7% at 0-5 km initialization height with a 5-day model duration), and LNR transport dates had the second-highest overall percentage of international NPES (7.1% at 0-5 km initialization height with a 10-day model duration). Synoptic analysis of the 30 transport regime days (LOC, MEX, and LNR) characterized typical meteorological conditions that led to high ozone in Clark County; atmospheric anomalies in geopotential height, winds, temperature, and pressure are distinct for each transport regime, but all describe pathways in which pollutants (including ozone and/or ozone precursors) can be transported from sources outside of Clark County into HA 212.

Emissions modeling showed clear decreases in local anthropogenic emissions of ozone precursors, including NO_x and VOCs, from 2008-2023 and continued reductions through 2033. International emissions show an increase in ozone precursors from Mexico, while Asian precursor emissions decreased in the last decade. HTAP emissions suggest a decrease in precursor emissions from both sources, but this inventory ends in 2020 (and includes pandemic biases) and may not be as up-to-date as the more recent measurements. To determine the impact of international emissions, photochemical modeling via CAMx and GEOS-Chem was performed and indicated that IA contributions account for 8-23% of ozone concentrations in HA 212, which aligns with EPA's CMAQ modeling of 8-13% IA contribution and 23% of back-trajectories identified as international transport (i.e., MEX and LNR transport). Despite the range of modeled IA contribution, the calculated future DVs are lower than 70 ppb for all Clark County sites, including all sites within HA 212. The range of modeled 2026 MDA8 ozone DVs calculated by removing the IA contribution decreased from 63.9-72.8 ppb to 51.1-59.0 ppb when using CAMx, and to 58.8-67.0 ppb when using GEOS-Chem.

The results from these analyses show there are clear and present pathways for international transport of ozone and ozone precursors. International emissions of these precursors have shown increase in some areas (Mexico) and decreases in others (Asia). Additionally, emissions of ozone precursors within Clark County have decreased despite a nearly steady ozone DV over the last decade. Modeling of IA contributions shows a range of 8-23% impact on Clark County DVs, consistent with EPA modeling and transport pathway analyses. Removing the IA contribution from the 2026 future DV value shows that all sites within Clark County (and HA 212) are below the NAAQS. In summary, this

evidence suggests that but for international transport, HA 212 would achieve attainment of the 2015 ozone NAAQS by the 2026 Serious attainment date.

5. References

Baker K.R., Emery C., Dolwick P., and Yarwood G. (2015) Photochemical grid model estimates of lateral boundary contributions to ozone and particulate matter across the continental United States. *Atmospheric Environment*, 123(A), 49-62, December. Available at http://dx.doi.org/10.1016/j.atmosenv.2015.10.055.

Clark County Department of Air Quality (2018) Revision to motor vehicle emissions budgets in ozone redesignation request and maintenance plan: Clark County, Nevada, . Oct.

Clark County Department of Air Quality (2019) Ozone Advance program progress report update. August.

Clark County Department of Environment and Sustainability (2021) Second maintenance plan for the 1997 8-hour ozone NAAQS December.

Clark County Department of Environment and Sustainability (2025) Annual monitoring network plan. July.

Dentener F., Keating T., and Akimoto H. (2010) Hemispheric transport of air pollution 2010, Part A: ozone and particulate matter, air pollution studies no. 17. United Nations Publication prepared by the Task Force on Hemispheric Transport of Air Pollution. Available at https://unece.org/sites/default/files/2021-06/Air.Pollution%20Studies.No_.17_100.pdf.

Emery C., Baker K., Wilson G., and Yarwood G. (2024) Comprehensive Air Quality Model with Extensions: formulation and evaluation for ozone and particulate matter over the US. *Atmosphere*, 15(10), 1158. Available at https://www.mdpi.com/2073-4433/15/10/1158.

Fransioli P. (2021) Quality assurance project plan for ambient and NCore air quality monitoring. Quality assurance project plan by the Clark County Department of Environmental and Sustainability Division of Air Quality, Clark County, NV, Revision 0, February.

Guizzardi D., Crippa M., Butler T., Keating T., Wu R., Kaminski J., Kuenen J., and others (2025) The HTAP_v3.2 emission mosaic: merging regional and global monthly emissions (2000–2020) to support air quality modelling and policies. Available at https://doi.org/10.5194/essd-17-5915-2025.

Henderson B. and Simon H. (2021) Modeled U.S. and international contributions for 2015 ozone NAAQS nonattainment areas. Memorandum to the Ozone Determination of Attainment by the Attainment Date Rule Docket (EPA-HQ-OAR-2021-0742) by the U.S. Environmental Protection Agency, Office of Air Quality Planning and Standards, Research Triangle Park, NC, December.

Huang M., Carmichael G.R., Pierce R.B., Jo D.S., Park R.J., Flemming J., Emmons L.K., and others (2017) Impact of intercontinental pollution transport on North American ozone air pollution: an HTAP phase 2 multi-model study. *Atmos. Chem. Phys.*, 17(9), 5721-5750. Available at https://acp.copernicus.org/articles/17/5721/2017/.

Jaffe D.A., Cooper O.R., Fiore A.M., Henderson B.H., Tonnesen G.S., Russell A.G., Henze D.K., Langford A.O., Lin M., and Moore T. (2018) Scientific assessment of background ozone over the U.S.:

Implications for air quality management. *Elementa: Science of the Anthropocene*, 6. Available at https://doi.org/10.1525/elementa.309.

Jiang Z., Worden J.R., Payne V.H., Zhu L., Fischer E., Walker T., and Jones D.B.A. (2016) Ozone export from East Asia: The role of PAN. *Journal of Geophysical Research: Atmospheres*, 121(11), 6555-6563. Available at https://doi.org/10.1002/2016JD024952.

Kim J., Park J., Hu H., Crippa M., Guizzardi D., Chatani S., Kurokawa J., Morikawa T., Yeo S., Jin H., and Woo J.-H. (2023) Long-term historical trends in air pollutant emissions in South Korea (2000–2018). *Asian Journal of Atmospheric Environment*, 17(1), 12, October. Available at https://doi.org/10.1007/s44273-023-00013-w.

Langford A.O., Senff C.J., Alvarez R.J., Brioude J., Cooper O.R., Holloway J.S., Lin M.Y., Marchbanks R.D., Pierce R.B., Sandberg S.P., Weickmann A.M., and Williams E.J. (2015) An overview of the 2013 Las Vegas Ozone Study (LVOS): impact of stratospheric intrusions and long-range transport on surface air quality. *Atmospheric Environment*, 109, 305-322, doi: 10.1016/j.atmosenv.2014.08.040, 2015/05/01/. Available at http://www.sciencedirect.com/science/article/pii/S1352231014006426.

Langford A.O., Alvarez II R.J., Brioude J., Fine R., Gustin M.S., Lin M.Y., Marchbanks R.D., Pierce R.B., Sandberg S.P., Senff C.J., Weickmann A.M., and Williams E.J. (2017) Entrainment of stratospheric air and Asian pollution by the convective boundary layer in the southwestern U.S. *Journal of Geophysical Research: Atmospheres*, 122(2), 1312-1337. Available at https://doi.org/10.1002/2016JD025987.

Langford A.O., Senff C.J., Alvarez Ii R.J., Aikin K.C., Baidar S., Bonin T.A., Brewer W.A., and others (2022) The Fires, Asian, and Stratospheric Transport–Las Vegas Ozone Study (FAST-LVOS). *Atmos. Chem. Phys.*, 22(3), 1707-1737, doi: 10.5194/acp-22-1707-2022. Available at https://acp.copernicus.org/articles/22/1707/2022/.

Lee H.-J., Chang L.-S., Jaffe D.A., Bak J., Liu X., Abad G.G., Jo H.-Y., Jo Y.-J., Lee J.-B., and Kim C.-H. (2021) Ozone continues to increase in East Asia despite decreasing NO2: causes and abatements. *Remote Sensing*, 13(11), 2177, June 1. Available at https://doi.org/10.3390/rs13112177.

Li K., Tan R., Qiao W., Lee T., Wang Y., Zhang D., Tang M., and others (2025) Surface and tropospheric ozone over East Asia and Southeast Asia from observations: distributions, trends, and variability. *Atmos. Chem. Phys.*, 25(19), 11575-11596, doi: 10.5194/acp-25-11575-2025. Available at https://acp.copernicus.org/articles/25/11575/2025/.

Maricopa Association of Governments (2025) MAG 2025 Clean Air Act Section 179b(b) retrospective demonstration of the impact of international emissions on ozone concentrations in the Maricopa nonattainment area. Prepared by the Maricopa Association of Governments, Phoenix, AZ, September. Available at https://azmag.gov/portals/0/Environmental/Air-Quality/2025/MAG-2025-CAA-Section-179B(b)-Retrospective-Demonstration.pdf.

Mathur R., Kang D., Napelenok S.L., Xing J., Hogrefe C., Sarwar G., Itahashi S., and Henderson B.H. (2022) How have divergent global emission trends influenced long-range transported ozone to North America? *Journal of Geophysical Research: Atmospheres*, 127(16), e2022JD036926. Available at https://agupubs.onlinelibrary.wiley.com/doi/abs/10.1029/2022JD036926.

National Weather Service Forecast Office (2020) Las Vegas, NV: general climatic summary. Available at https://www.wrh.noaa.gov/vef/lassum.php.

Nopmongcol U., Liu Z., Stoeckenius T., and Yarwood G. (2017) Modeling intercontinental transport of ozone in North America with CAMx for the Air Quality Model Evaluation International Initiative (AQMEII) Phase 3. *Atmos. Chem. Phys.*, 17(16), 9931-9943, doi: 10.5194/acp-17-9931-2017. Available at https://acp.copernicus.org/articles/17/9931/2017/.

Oak Y.J., Jacob D.J., Pendergrass D.C., Dang R., Colombi N.K., Chong H., Lee S., Kuk S.K., and Kim J. (2025) Air quality trends and regimes in South Korea inferred from 2015–2023 surface and satellite observations. *Atmos. Chem. Phys.*, 25(5), 3233-3252. Available at https://acp.copernicus.org/articles/25/3233/2025/.

Ramboll Americas Engineering Solutions (2024) Technical support document: attainment demonstration for the Clark County ozone State Implementation Plan. Prepared for Clark County Department of Environment and Sustainability, Division of Air Quality, June. Available at https://www.clarkcountynv.gov/adobe/assets/urn:aaid:aem:3f3abc47-2bb5-411f-b314-15230eea1ff5/original/as/attb-attainment-demo-tsd.pdf.

Ramboll Americas Engineering Solutions and Eastern Research Group (2026) Technical support document: attainment demonstration for the Clark County Serious area ozone state implementation plan. Prepared for Clark County Department of Environment and Sustainability, Division of Air Quality, February.

Ramboll Environment and Health (2024) User's guide: Comprehensive Air quality Model with extensions, version 7.3. User's guide, June. Available at https://camx.com/Files/CAMxUsersGuide_v7.30.pdf.

Silver B., Reddington C.L., Chen Y., and Arnold S.R. (2025) A decade of China's air quality monitoring data suggests health impacts are no longer declining. *Environment International*, 197, 109318, March. Available at https://doi.org/10.1016/j.envint.2025.109318.

U.S. Census Bureau (2010) State & County QuickFacts. Available at http://quickfacts.census.gov/qfd/states/.html.

United Nations (2026) Population trends. Accessed February 25, 2026. Available at https://www.un.org/development/desa/pd/content/population-trends-0.

Wang N., McClure C., and DeWinter J. (2023a) Technical assistance document for sampling and analysis of ozone precursors for the photochemical assessment monitoring stations program - revision 3. Prepared for the U.S. Environmental Protection Agency Office of Air Quality Planning Standards Air Quality Assessment Division, Research Triangle Park, NC, by Sonoma Technology, Petaluma, CA, STI-7907, May.

Wang N., McClure C., and DeWinter J. (2023b) Quality assurance project plan for the photochemical assessment monitoring stations (PAMS) required site network for speciated volatile organic compounds, carbonyls, and meteorological parameters including mixing layer height - revision 1. Prepared for the U.S. Environmental Protection Agency Office of Air Quality Planning Standards Air Quality Assessment Division, Research Triangle Park, NC by Sonoma Technology, Petaluma, CA, STI-7906, May.

World Bank Group Population, total. Accessed February 25, 2026. Available at https://data.worldbank.org/indicator/SP.POP.TOTL.

Zhang L., Lin M., Langford A.O., Horowitz L.W., Senff C.J., Klovenski E., Wang Y., Alvarez R.J., II, Petropavlovskikh I., Cullis P., Sterling C.W., Peischl J., Ryerson T.B., Brown S.S., Decker Z.C.J., Kirgis G., and Conley S. (2020) Characterizing sources of high surface ozone events in the southwestern US with intensive field measurements and two global models. *Atmospheric Chemistry & Physics*, 20, 10379-10400, doi: 10.5194/acp-20-10379-2020. Available at https://acp.copernicus.org/articles/20/10379/2020/acp-20-10379-2020.pdf.

Attachment 1. Individual-Year Cluster Analysis Plots

This attachment presents the results of the HYSPLIT backward-trajectory cluster analysis for individual years from 2016 to 2024.

Table A-1. Summary of the dominant atmospheric transport pathways derived from HYSPLIT cluster analysis for the years of 2016 to 2024.

Year	LOC		MEX		LNR		Other	
	Cluster #	%	Cluster #	%	Cluster #	%	Cluster #	%
2016	1, 3	62.8%	4	7.4%	5, 7	10.2%	2, 6, 8	19.2%
2017	2, 3, 4	64.0%	1	9.1%	5, 7, 8	18.8%	6	8.0%
2018	1, 2	51.8%	8	12.7%	5, 6, 7	12.9%	3, 4	22.6%
2019	2, 7	48.2%	4	17.3%	1, 5, 8	12.3%	3, 6	22.2%
2020	1, 4, 5, 7	72.5%	8	5.7%	2, 3, 6	21.8%		
2021	1, 3, 4	56.1%	7	14.1%	6, 8	8.7%	2, 5	21.0%
2022	1, 3, 5	50.8%	8	15.6%	2 ,6	10.9%	4, 7	22.7%
2023	2, 5, 7	51.7%	1	17.1%	6, 8	11.6%	3, 4	19.6%
2024	1, 5, 8	46.0%	6	9.0%	2, 3	16.0%	4, 7	29.1%

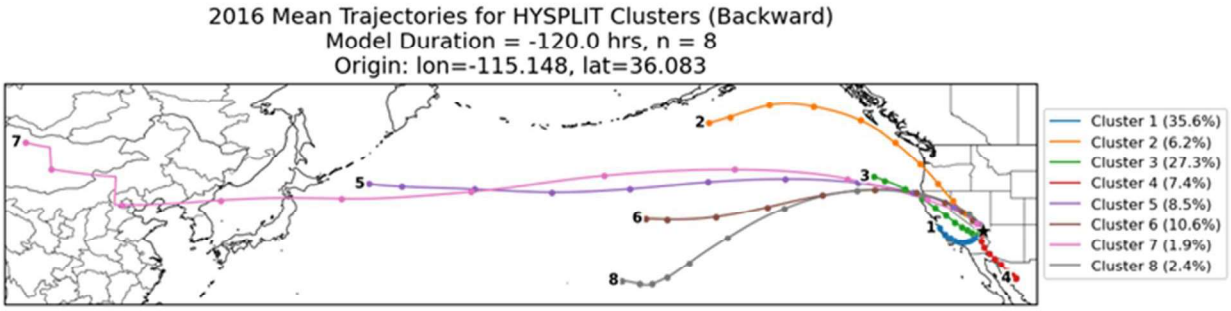

Figure A-1. Mean 5-day backward trajectories from Las Vegas, Nevada (36.0831°N, 115.1482°W), calculated using HYSPLIT cluster analysis with eight clusters for the year 2016. Each colored line represents the mean pathway of a cluster, and the percentages in the legend indicate the fraction of trajectories assigned to each cluster. Trajectories illustrate dominant transport patterns contributing to air masses arriving at the site, highlighting both regional and long-range influences on air quality.

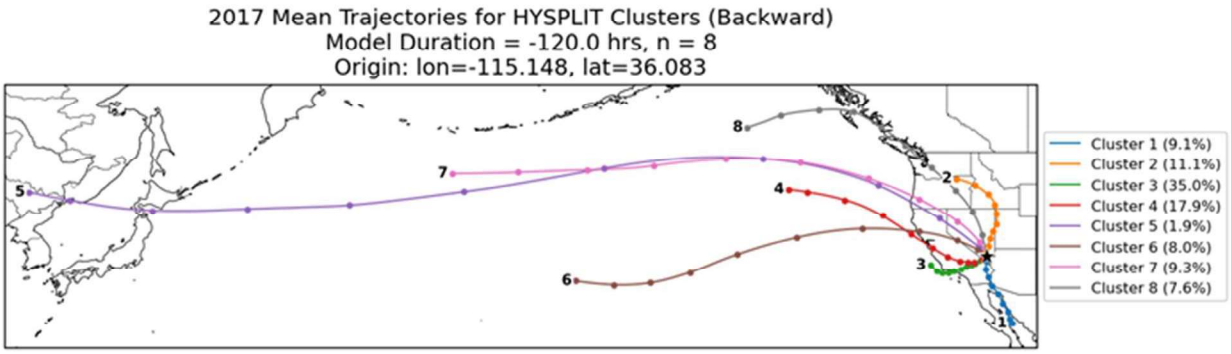

Figure A-2. Mean 5-day backward trajectories from Las Vegas, Nevada (36.0831°N, 115.1482°W), calculated using HYSPLIT cluster analysis with eight clusters for the year 2017. Each colored line represents the mean pathway of a cluster, and the percentages in the legend indicate the fraction of trajectories assigned to each cluster. Trajectories illustrate dominant transport patterns contributing to air masses arriving at the site, highlighting both regional and long-range influences on air quality.

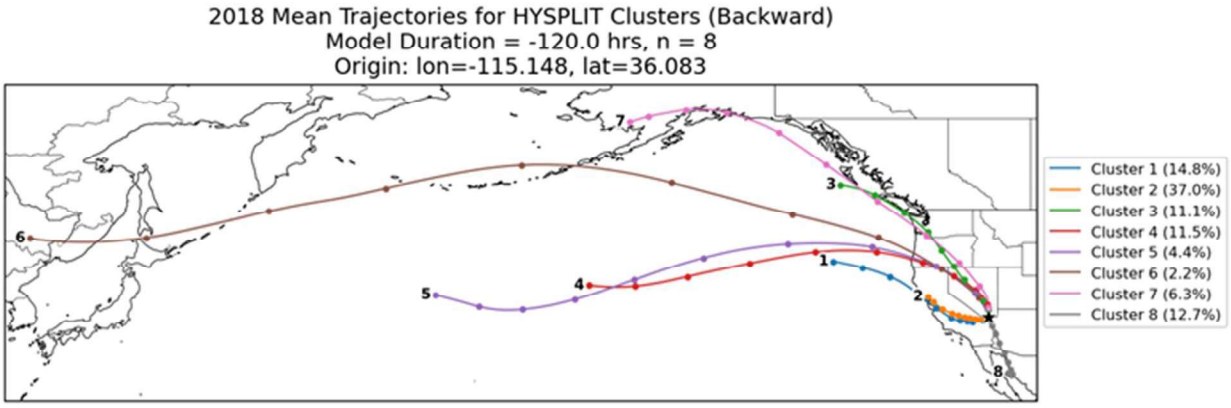

Figure A-3. Mean 5-day backward trajectories from Las Vegas, Nevada (36.0831°N, 115.1482°W), calculated using HYSPLIT cluster analysis with eight clusters for the year 2018. Each colored line represents the mean pathway of a cluster, and the percentages in the legend indicate the fraction of trajectories assigned to each cluster. Trajectories illustrate dominant transport patterns contributing to air masses arriving at the site, highlighting both regional and long-range influences on air quality.

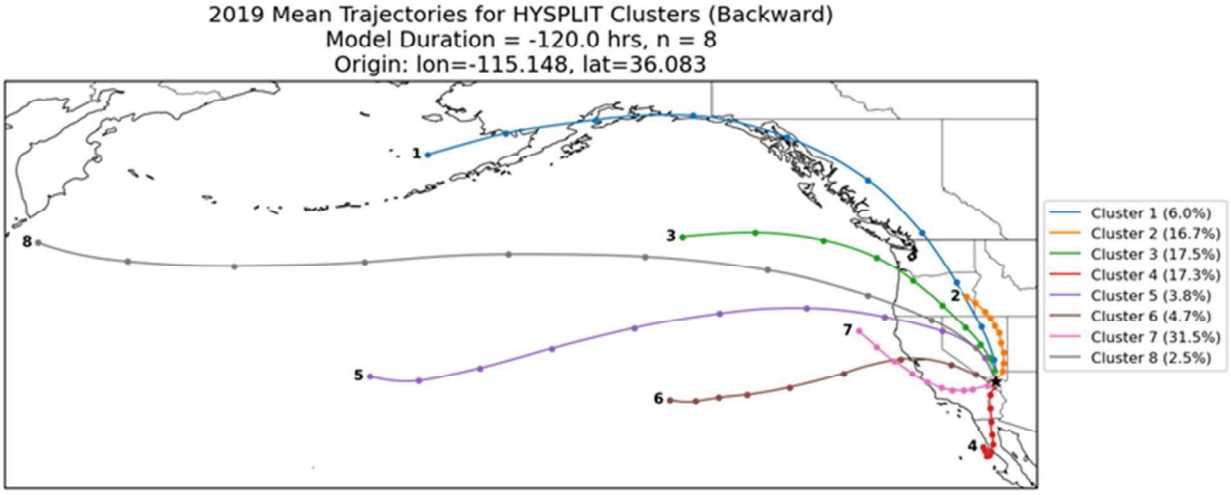

Figure A-4. Mean 5-day backward trajectories from Las Vegas, Nevada (36.0831°N, 115.1482°W), calculated using HYSPLIT cluster analysis with eight clusters for the year 2019. Each colored line represents the mean pathway of a cluster, and the percentages in the legend indicate the fraction of trajectories assigned to each cluster. Trajectories illustrate dominant transport patterns contributing to air masses arriving at the site, highlighting both regional and long-range influences on air quality.

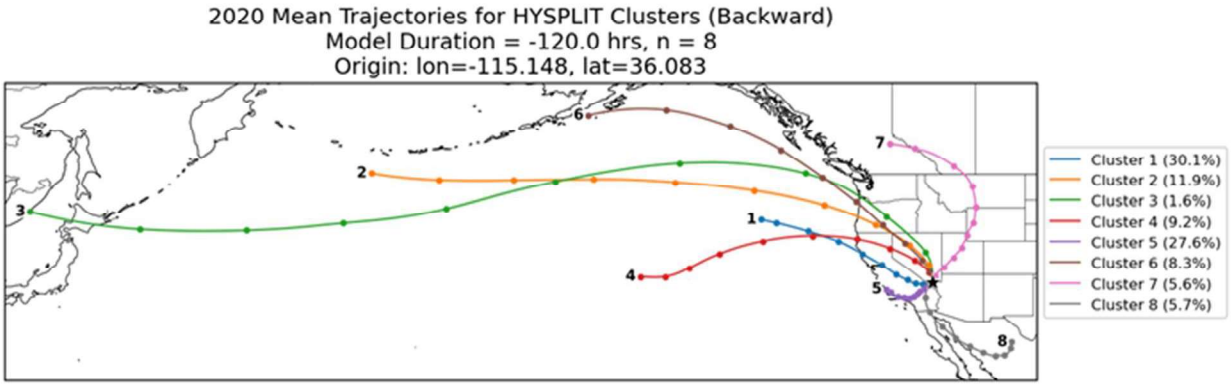

Figure A-5. Mean 5-day backward trajectories from Las Vegas, Nevada (36.0831°N, 115.1482°W), calculated using HYSPLIT cluster analysis with eight clusters for the year 2020. Each colored line represents the mean pathway of a cluster, and the percentages in the legend indicate the fraction of trajectories assigned to each cluster. Trajectories illustrate dominant transport patterns contributing to air masses arriving at the site, highlighting both regional and long-range influences on air quality.

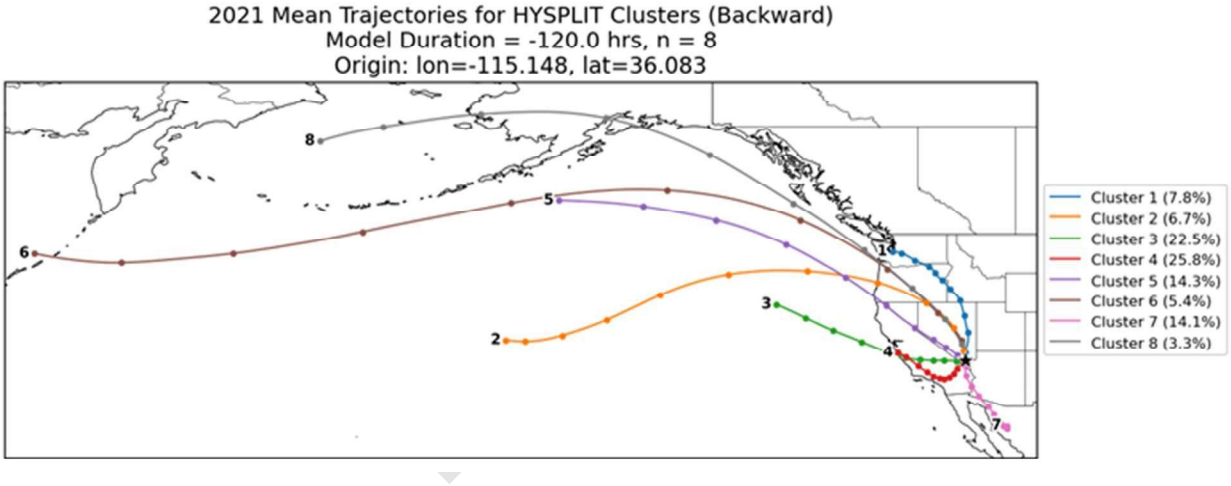

Figure A-6. Mean 5-day backward trajectories from Las Vegas, Nevada (36.0831°N, 115.1482°W), calculated using HYSPLIT cluster analysis with eight clusters for the year 2021. Each colored line represents the mean pathway of a cluster, and the percentages in the legend indicate the fraction of trajectories assigned to each cluster. Trajectories illustrate dominant transport patterns contributing to air masses arriving at the site, highlighting both regional and long-range influences on air quality.

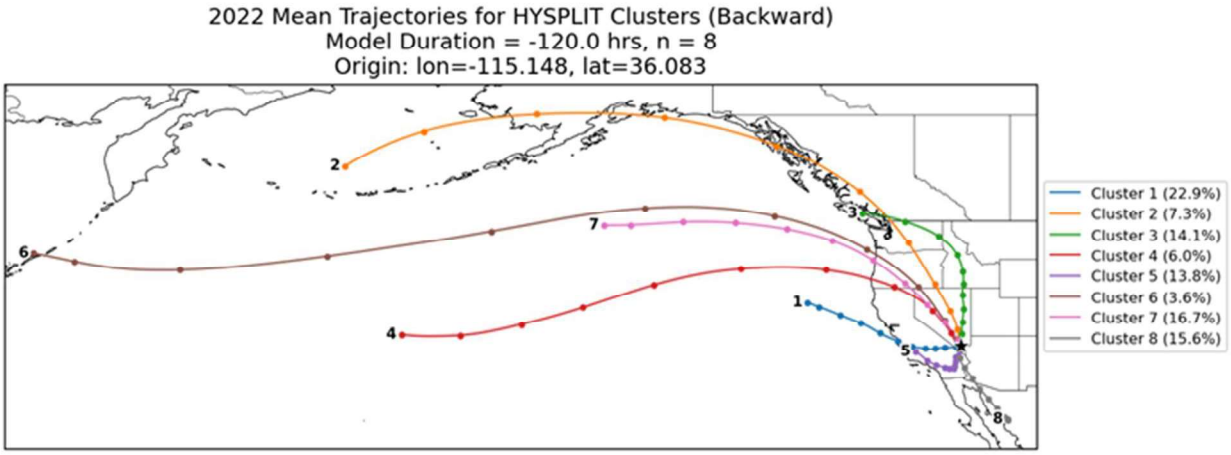

Figure A-7. Mean 5-day backward trajectories from Las Vegas, Nevada (36.0831°N, 115.1482°W), calculated using HYSPLIT cluster analysis with eight clusters for the year 2022. Each colored line represents the mean pathway of a cluster, and the percentages in the legend indicate the fraction of trajectories assigned to each cluster. Trajectories illustrate dominant transport patterns contributing to air masses arriving at the site, highlighting both regional and long-range influences on air quality.

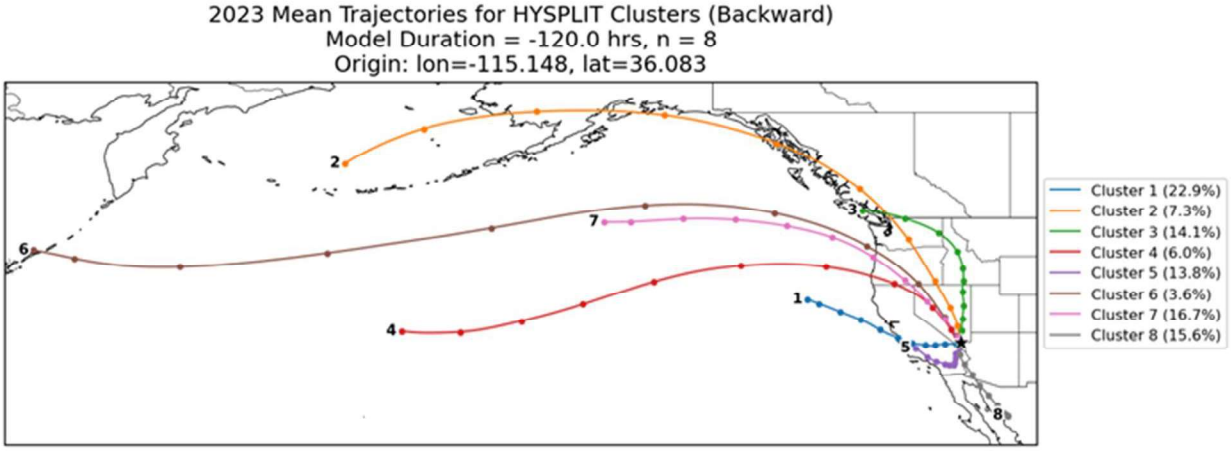

Figure A-8. Mean 5-day backward trajectories from Las Vegas, Nevada (36.0831°N, 115.1482°W), calculated using HYSPLIT cluster analysis with eight clusters for the year 2023. Each colored line represents the mean pathway of a cluster, and the percentages in the legend indicate the fraction of trajectories assigned to each cluster. Trajectories illustrate dominant transport patterns contributing to air masses arriving at the site, highlighting both regional and long-range influences on air quality.

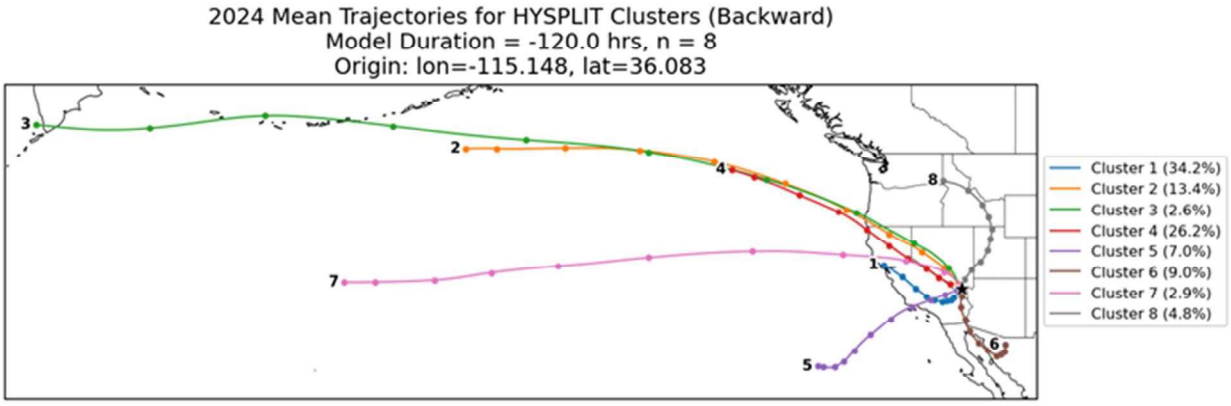

Figure A-9. Mean 5-day backward trajectories from Las Vegas, Nevada (36.0831°N, 115.1482°W), calculated using HYSPLIT cluster analysis with eight clusters for the year 2024. Each colored line represents the mean pathway of a cluster, and the percentages in the legend indicate the fraction of trajectories assigned to each cluster. Trajectories illustrate dominant transport patterns contributing to air masses arriving at the site, highlighting both regional and long-range influences on air quality.

Attachment 2. Backward Dispersion Daily Plots

This section contains backward dispersion plots for the 30 selected ozone exceedance dates (10 per air transport regime). Sets of plots are provided that either aggregate NPES between 0-1,000 m and 0-5,000 m, which represent air within the PBL and air within the entire troposphere, respectively. A model duration of -5 days is presented for all dates. LNR dates also include -10 day simulations to better visualize long-range movement of air across the Pacific Ocean.

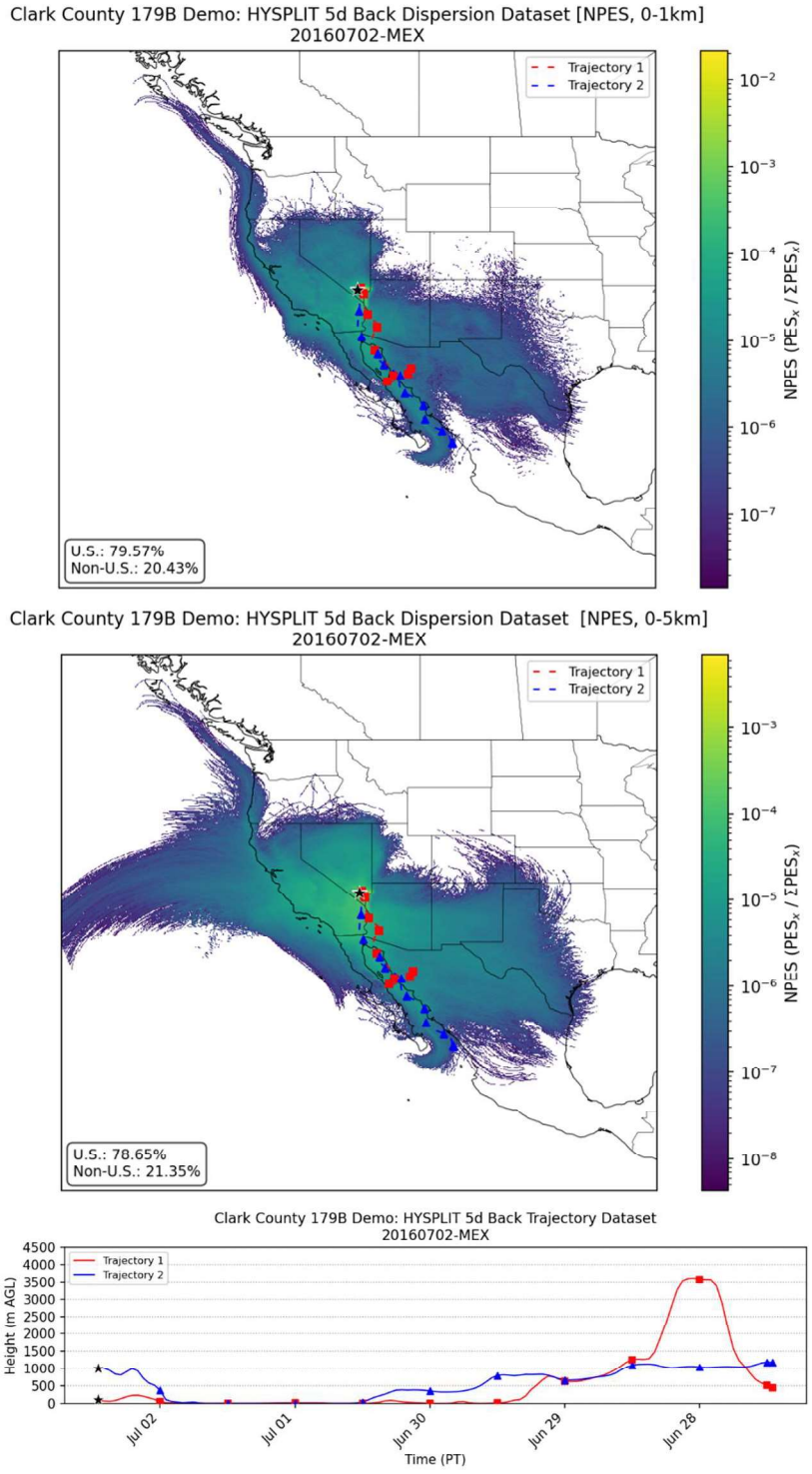

Figure B-1. Clark County 5-day back dispersion-based NPES. Results for July 2, 2016, with international transport from Mexico (MEX) air transport regime. NPES is based on the average concentration of a generic, inert tracer gas between 0 and 1 km (top panel) and 0 and 5 km (middle panel). Plots include sample back trajectories at 100 m and 1,000 m (red and blue), the elevation of which are also depicted (bottom panel).

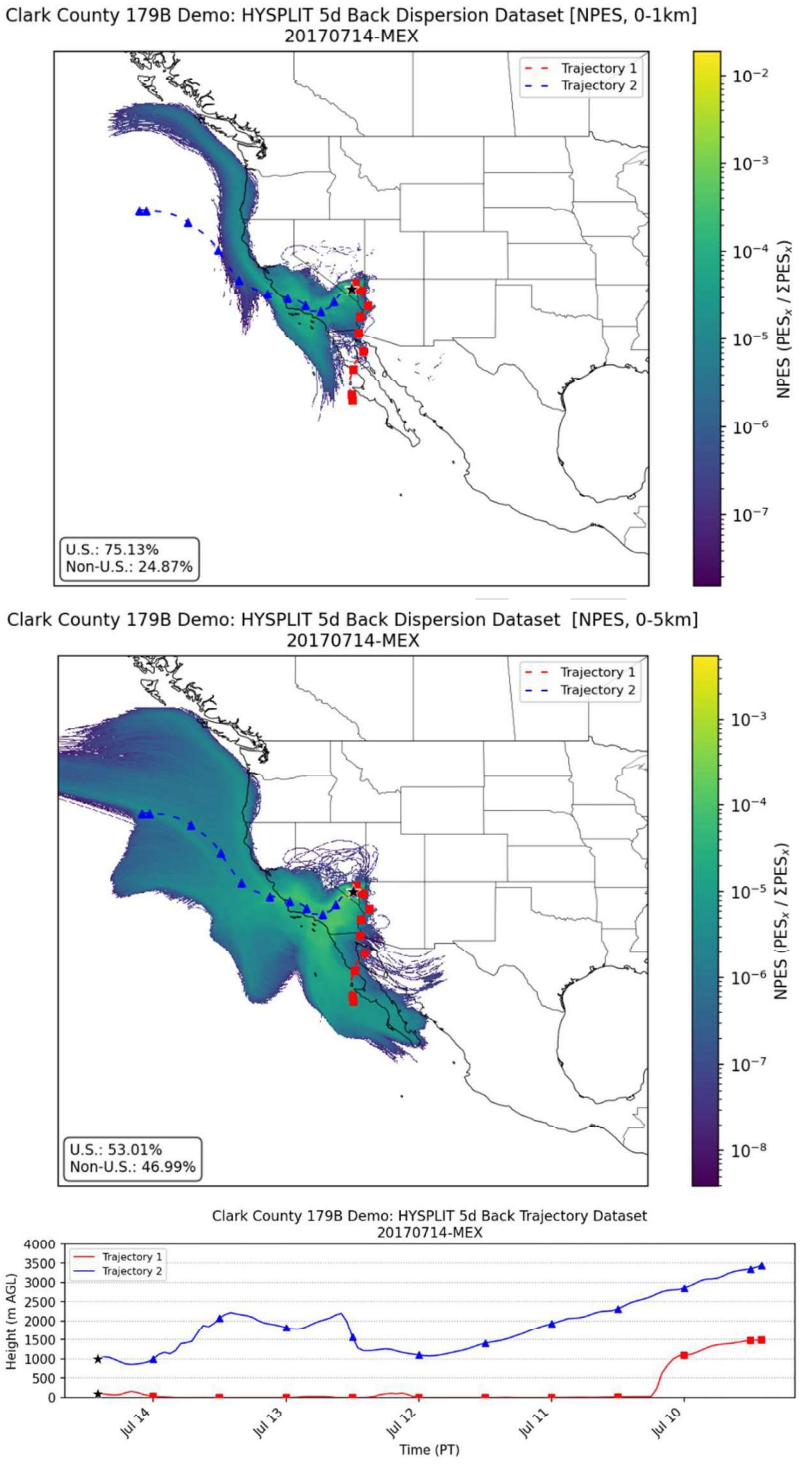

Figure B-2. Clark County 5-day back dispersion-based NPES. Results for July 14, 2017, with international transport from Mexico (MEX) air transport regime. NPES is based on the average concentration of a generic, inert tracer gas between 0 and 1 km (top panel) and 0 and 5 km (middle panel). Plots include sample back trajectories at 100 m and 1,000 m (red and blue), the elevation of which are also depicted (bottom panel).

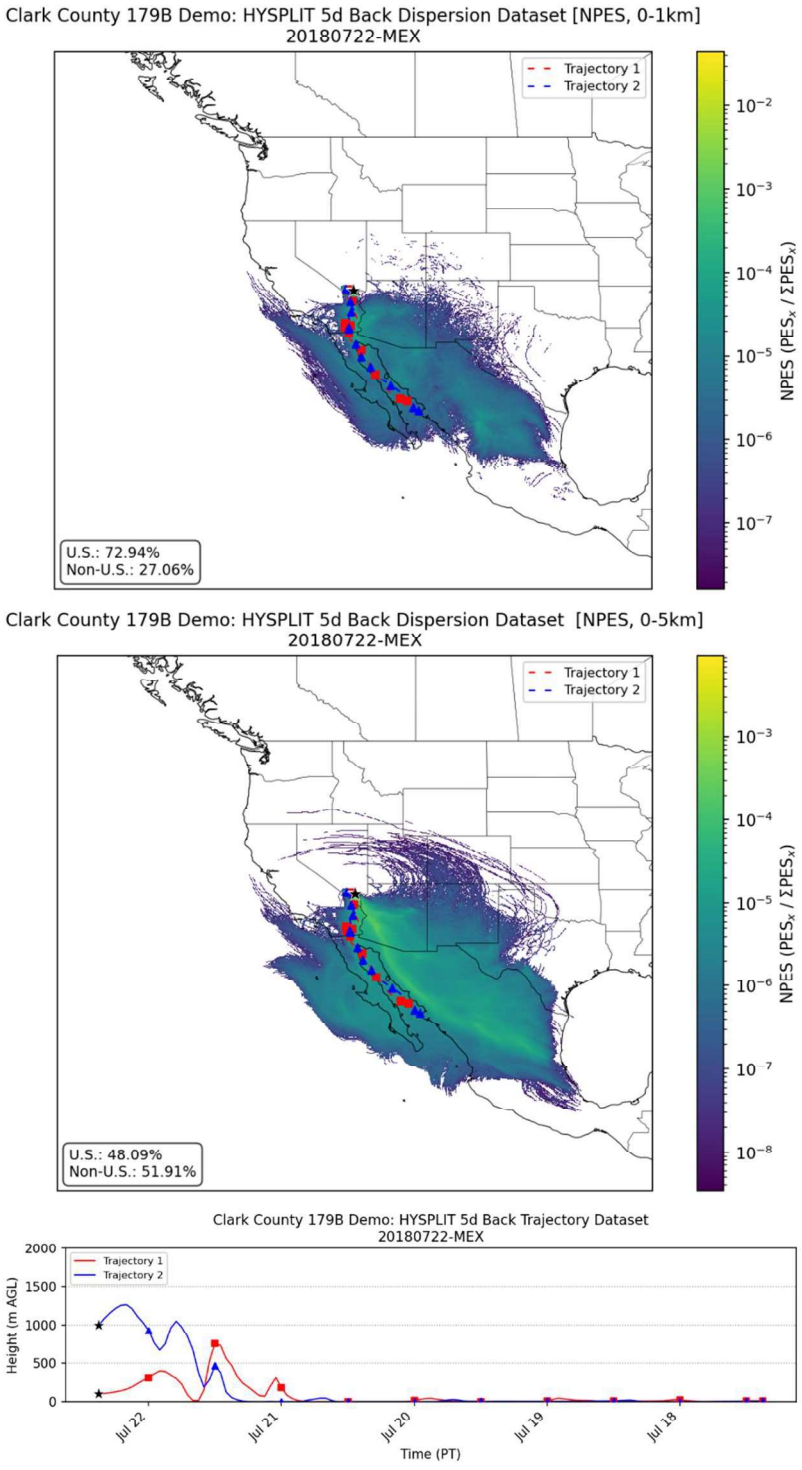

Figure B-3. Clark County 5-day back dispersion-based NPES. Results for July 22, 2018, with international transport from Mexico (MEX) air transport regime. NPES is based on the average concentration of a generic, inert tracer gas between 0 and 1 km (top panel) and 0 and 5 km (middle panel). Plots include sample back trajectories at 100 m and 1,000 m (red and blue), the elevation of which are also depicted (bottom panel).

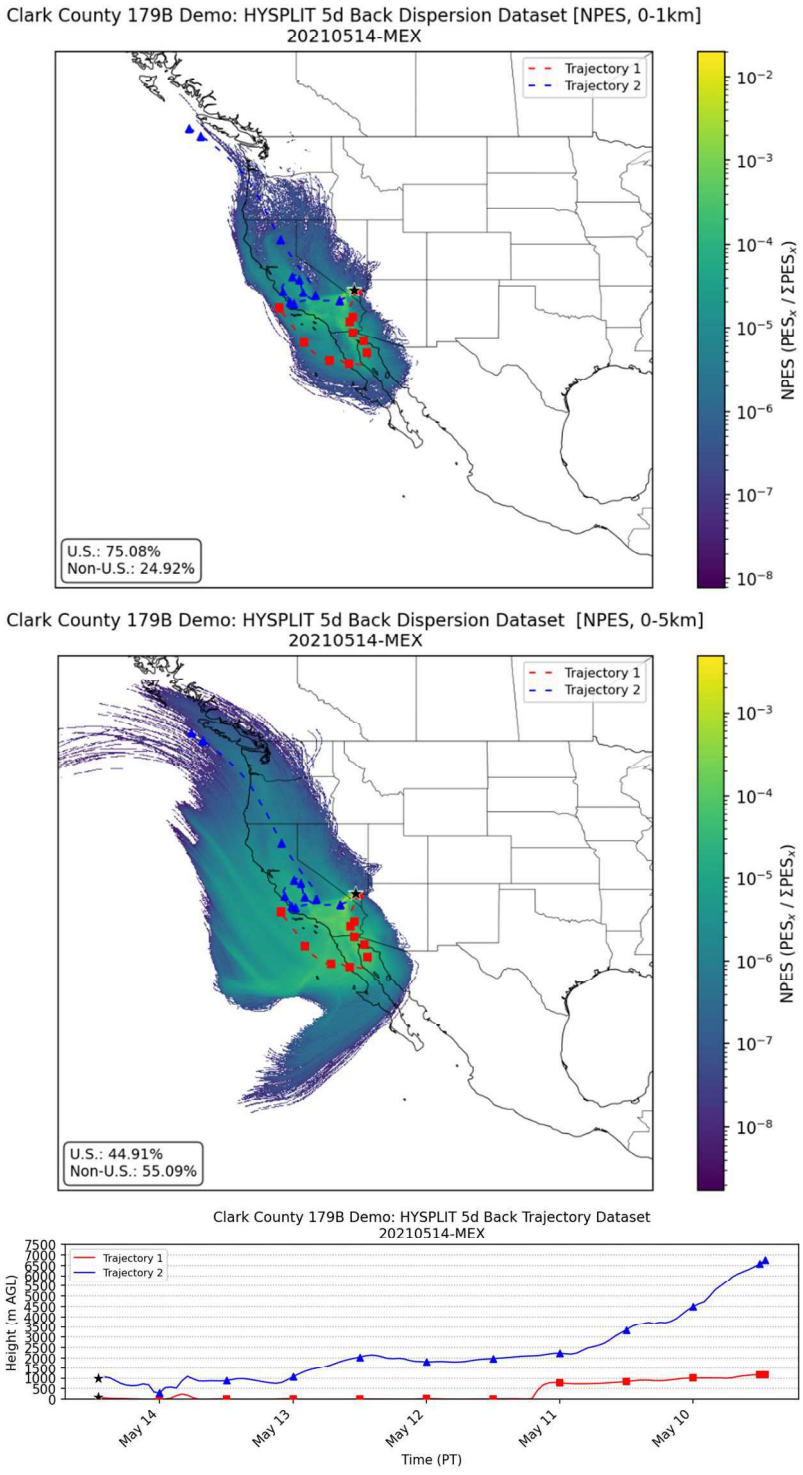

Figure B-4. Clark County 5-day back dispersion-based NPES. Results for May 14, 2021, with international transport from Mexico (MEX) air transport regime. NPES is based on the average concentration of a generic, inert tracer gas between 0 and 1 km (top panel) and 0 and 5 km (middle panel). Plots include sample back trajectories at 100 m and 1,000 m (red and blue), the elevation of which are also depicted (bottom panel).

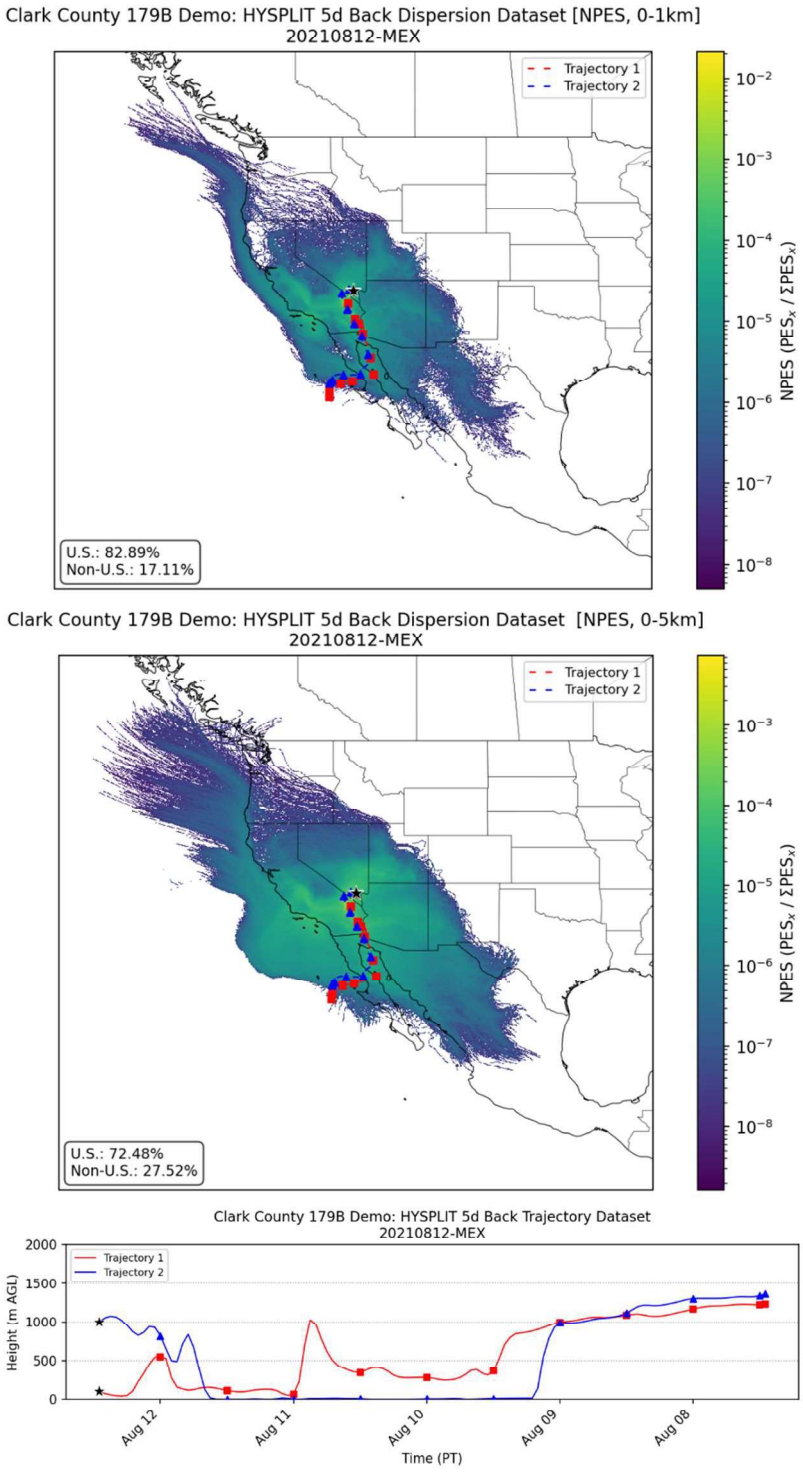

Figure B-5. Clark County 5-day back dispersion-based NPES. Results for August 12, 2021, with international transport from Mexico (MEX) air transport regime. NPES is based on the average concentration of a generic, inert tracer gas between 0 and 1 km (top panel) and 0 and 5 km (middle panel). Plots include sample back trajectories at 100 m and 1,000 m (red and blue), the elevation of which are also depicted (bottom panel).

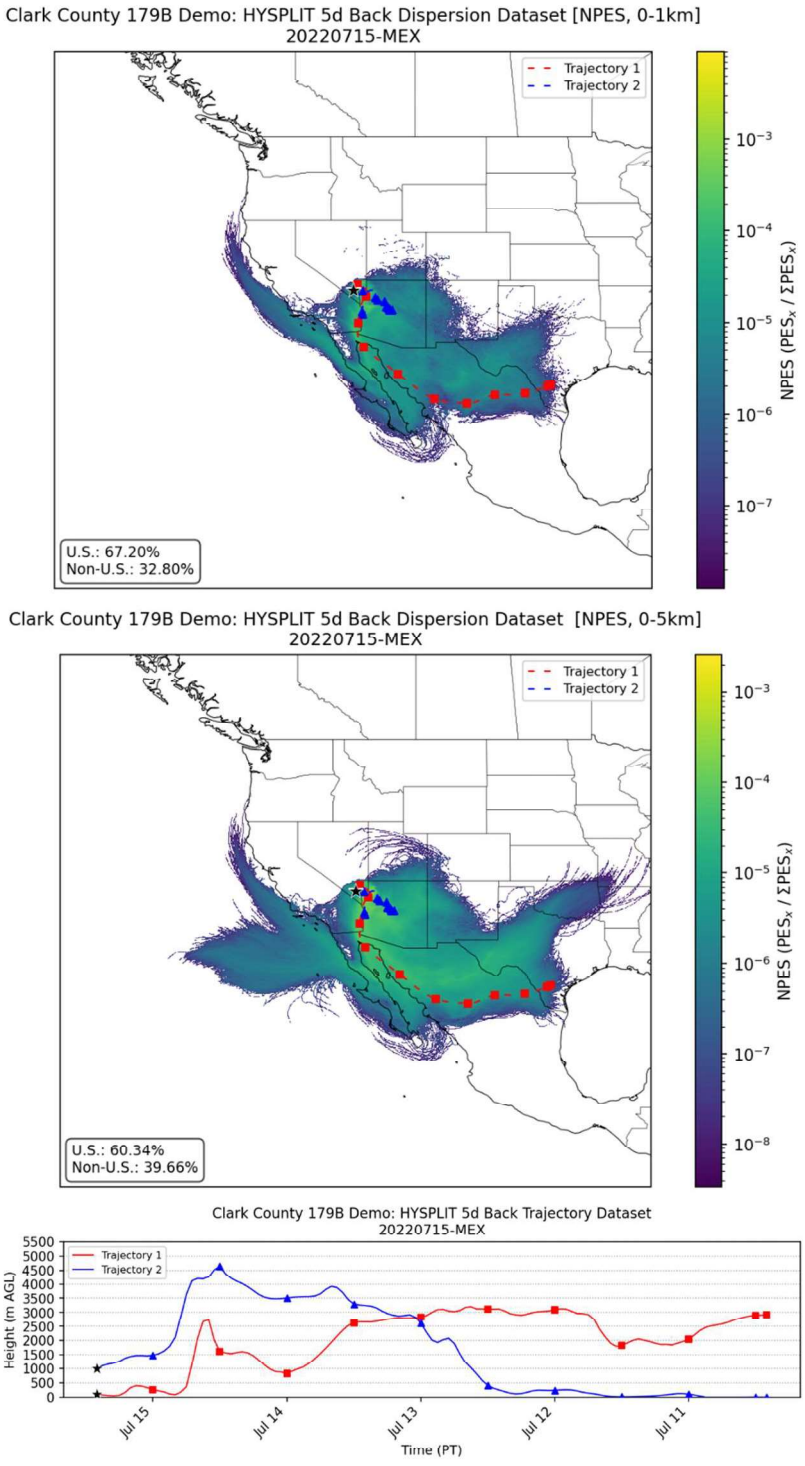

Figure B-6. Clark County 5-day back dispersion-based NPES. Results for July 15, 2022, with international transport from Mexico (MEX) air transport regime. NPES is based on the average concentration of a generic, inert tracer gas between 0 and 1 km (top panel) and 0 and 5 km (middle panel). Plots include sample back trajectories at 100 m and 1,000 m (red and blue), the elevation of which are also depicted (bottom panel).

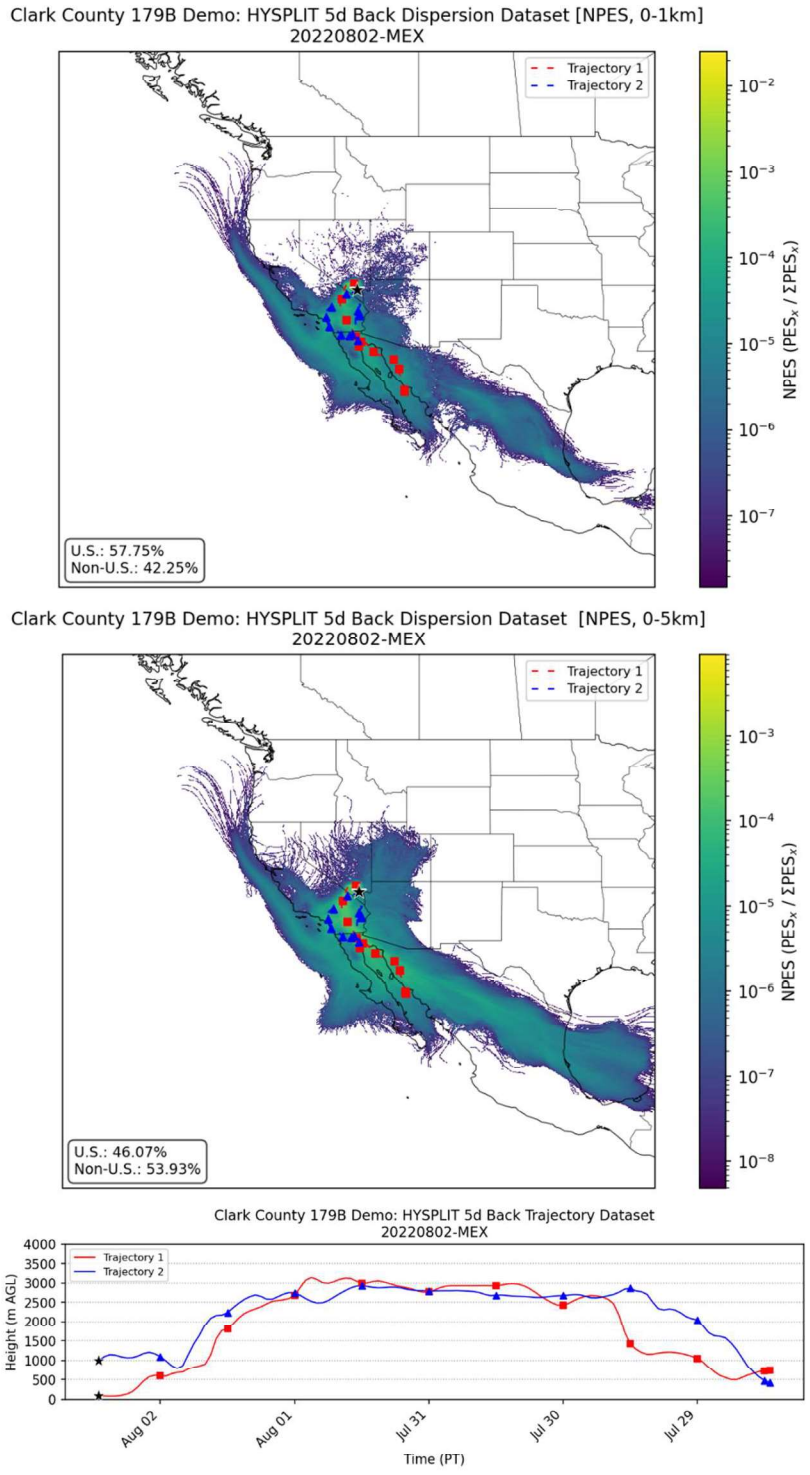

Figure B-7. Clark County 5-day back dispersion-based NPES. Results for August 2, 2022, with international transport from Mexico (MEX) air transport regime. NPES is based on the average concentration of a generic, inert tracer gas between 0 and 1 km (top panel) and 0 and 5 km (middle panel). Plots include sample back trajectories at 100 m and 1,000 m (red and blue), the elevation of which are also depicted (bottom panel).

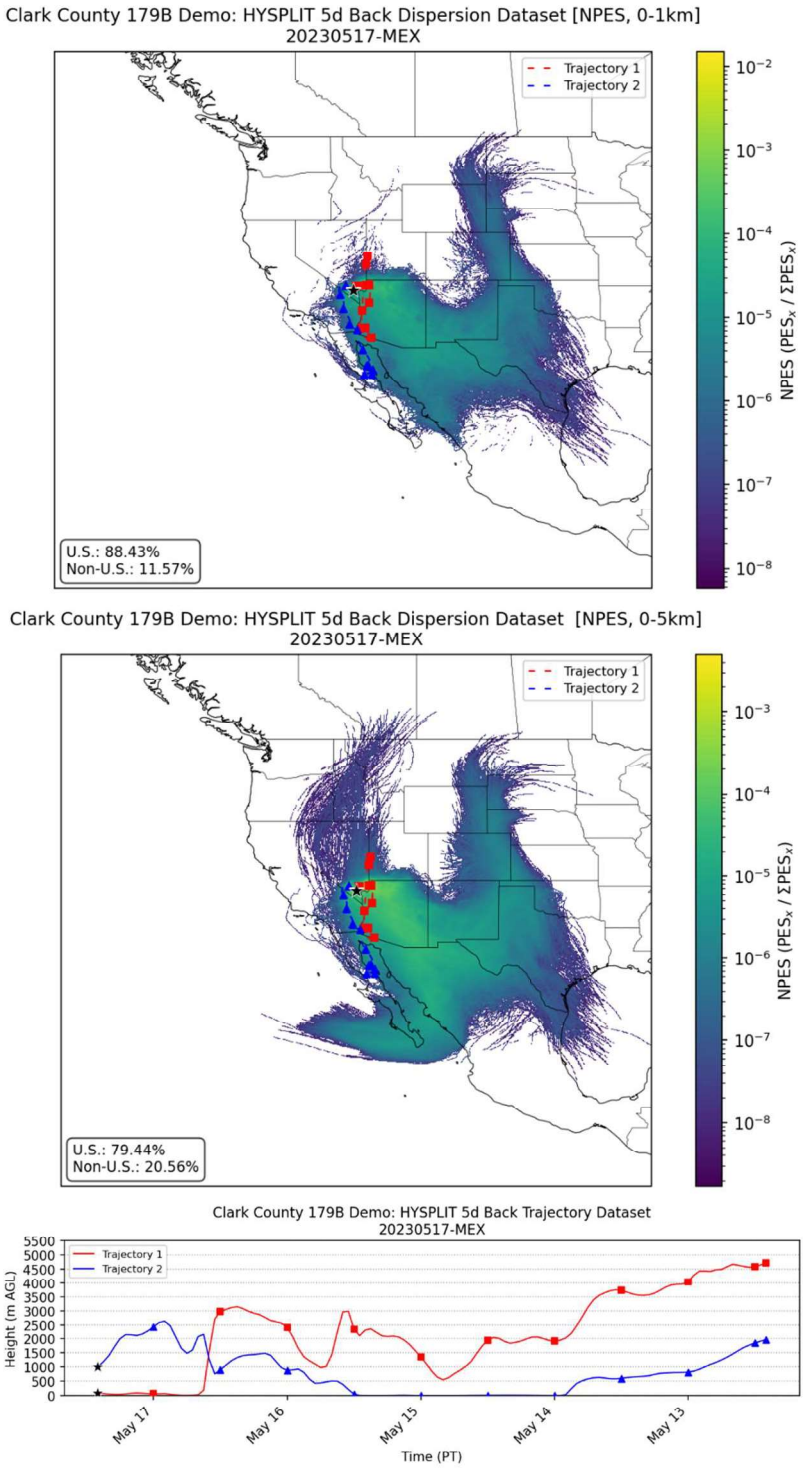

Figure B-8. Clark County 5-day back dispersion-based NPES. Results for May 17, 2023, with international transport from Mexico (MEX) air transport regime. NPES is based on the average concentration of a generic, inert tracer gas between 0 and 1 km (top panel) and 0 and 5 km (middle panel). Plots include sample back trajectories at 100 m and 1,000 m (red and blue), the elevation of which are also depicted (bottom panel).

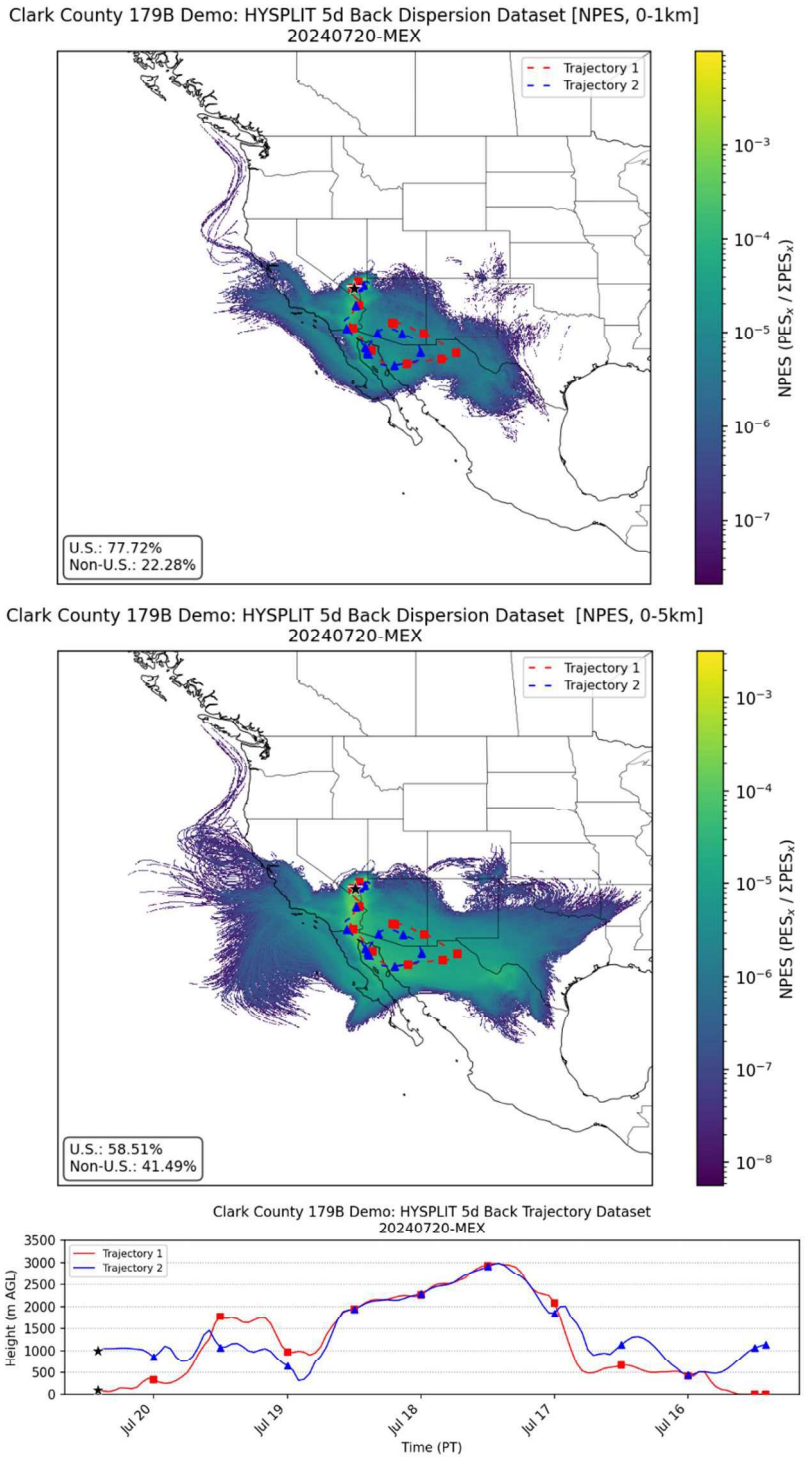

Figure B-9. Clark County 5-day back dispersion-based NPES. Results for July 20, 2024, with international transport from Mexico (MEX) air transport regime. NPES is based on the average concentration of a generic, inert tracer gas between 0 and 1 km (top panel) and 0 and 5 km (middle panel). Plots include sample back trajectories at 100 m and 1,000 m (red and blue), the elevation of which are also depicted (bottom panel).

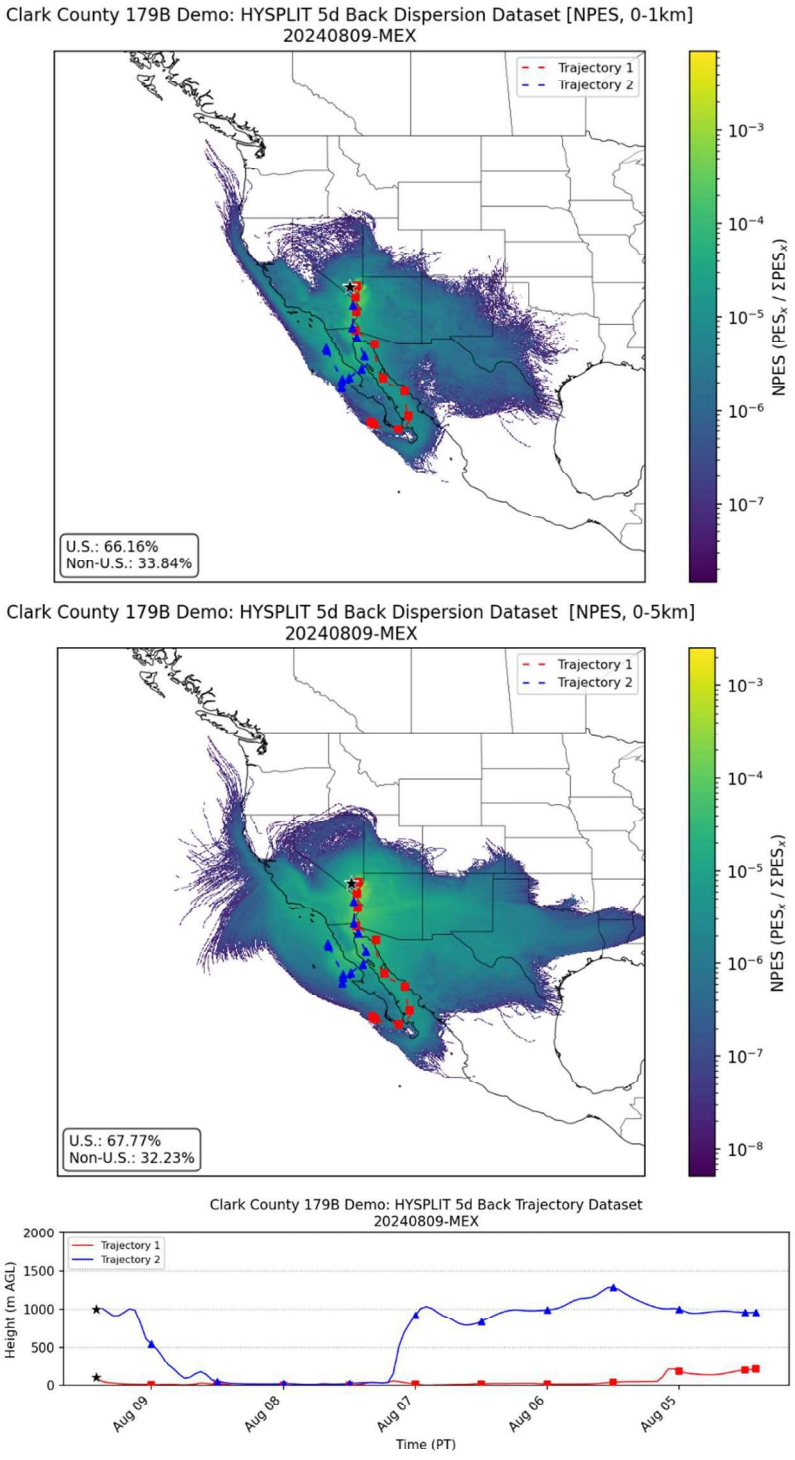

Figure B-10. Clark County 5-day back dispersion-based NPES. Results for August 9, 2024, with international transport from Mexico (MEX) air transport regime. NPES is based on the average concentration of a generic, inert tracer gas between 0 and 1 km (top panel) and 0 and 5 km middle panel). Plots include sample back trajectories at 100 m and 1,000 m (red and blue), the elevation of which are also depicted (bottom panel).

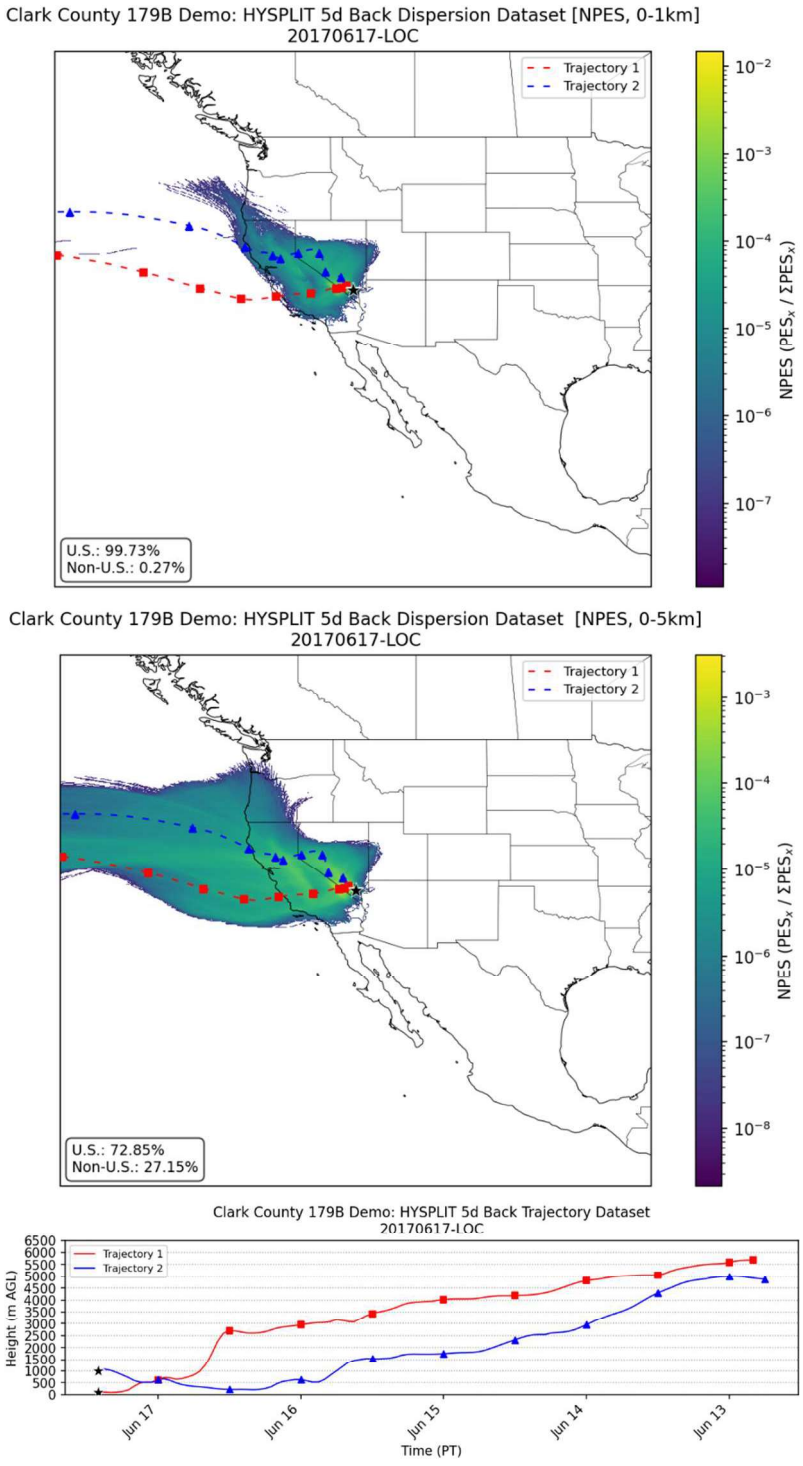

Figure B-11. Clark County 5-day back dispersion-based NPES. Results for June 17, 2017, with the local transport (LOC) air transport regime. NPES is based on the average concentration of a generic, inert tracer gas between 0 and 1 km (top panel) and 0 and 5 km (middle panel). Plots include sample back trajectories at 100 m and 1,000 m (red and blue), the elevation of which are also depicted (bottom panel).

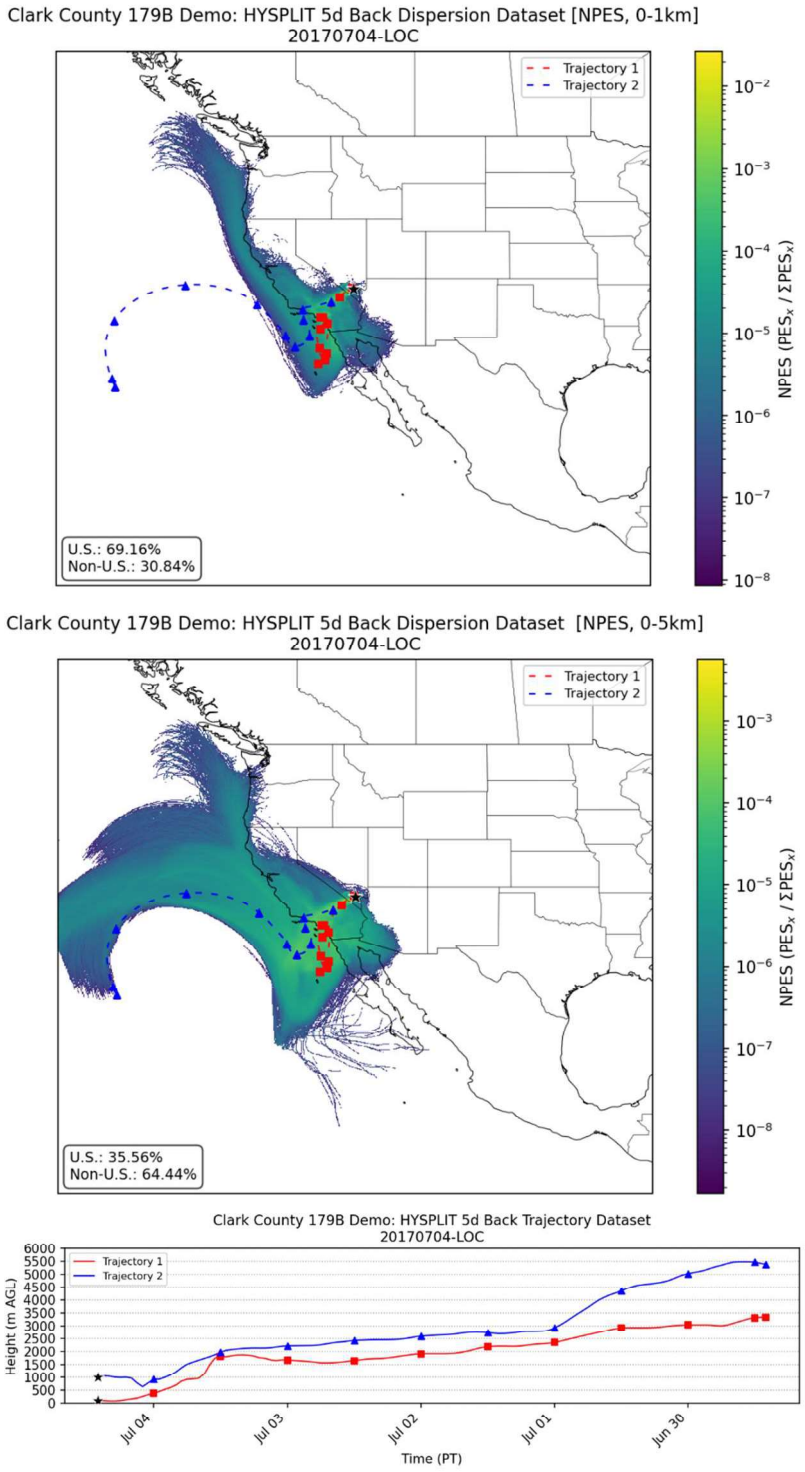

Figure B-12. Clark County 5-day back dispersion-based NPES. Results for July 4, 2017, with the local transport (LOC) air transport regime. NPES is based on the average concentration of a generic, inert tracer gas between 0 and 1 km (top panel) and 0 and 5 km (middle panel). Plots include sample back trajectories at 100 m and 1,000 m (red and blue), the elevation of which are also depicted (bottom panel).

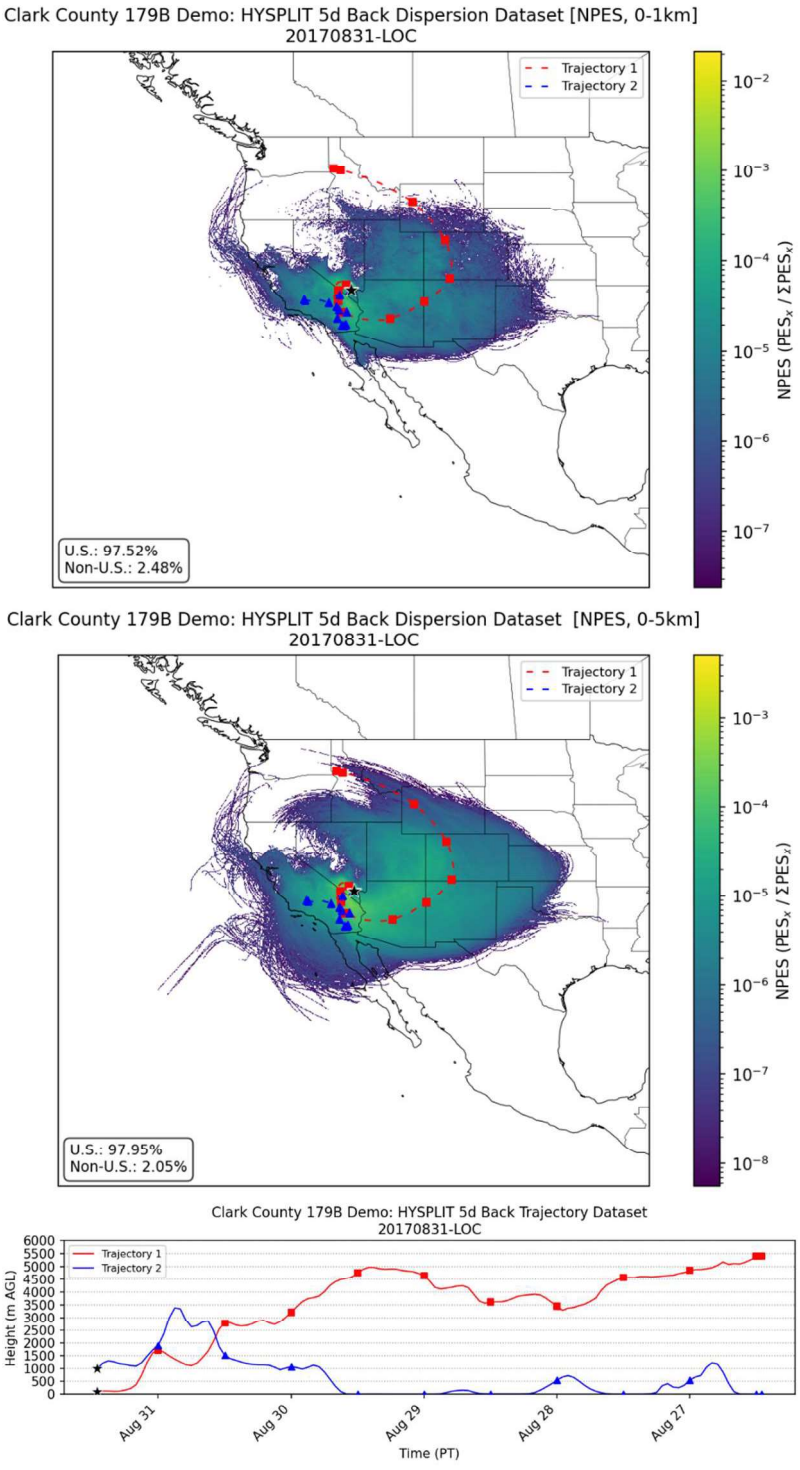

Figure B-13. Clark County 5-day back dispersion-based NPES. Results for August 31, 2017, with the local transport (LOC) air transport regime. NPES is based on the average concentration of a generic, inert tracer gas between 0 and 1 km (top panel) and 0 5 km (middle panel). Plots include sample back trajectories at 100 m and 1,000 m (red and blue), the elevation of which are also depicted (bottom panel).

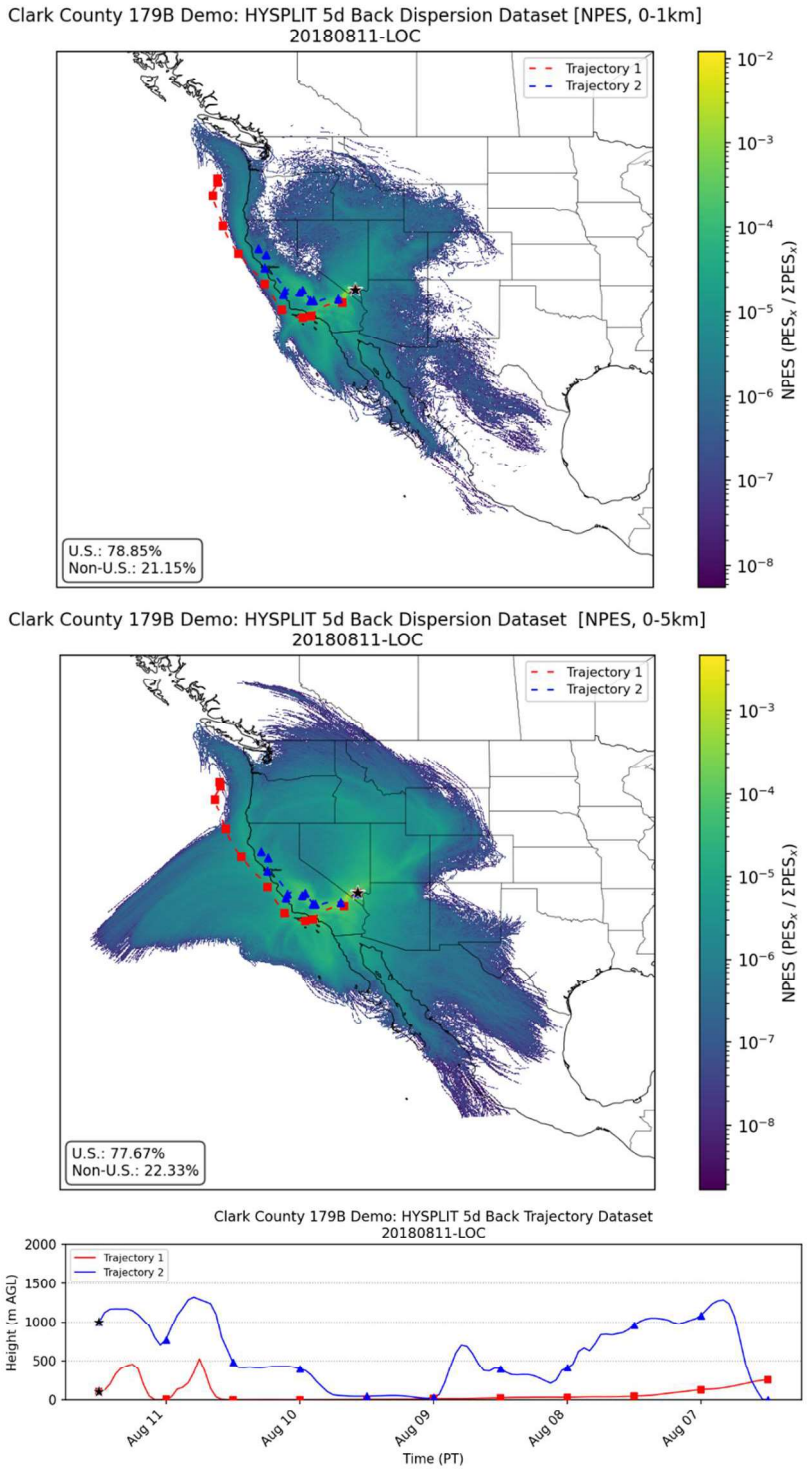

Figure B-14. Clark County 5-day back dispersion-based NPES. Results for August 11, 2018, with the local transport (LOC) air transport regime. NPES is based on the average concentration of a generic, inert tracer gas between 0 and 1 km (top panel) and 0 and 5 km (middle panel). Plots include sample back trajectories at 100 m and 1,000 m (red and blue), the elevation of which are also depicted (bottom panel).

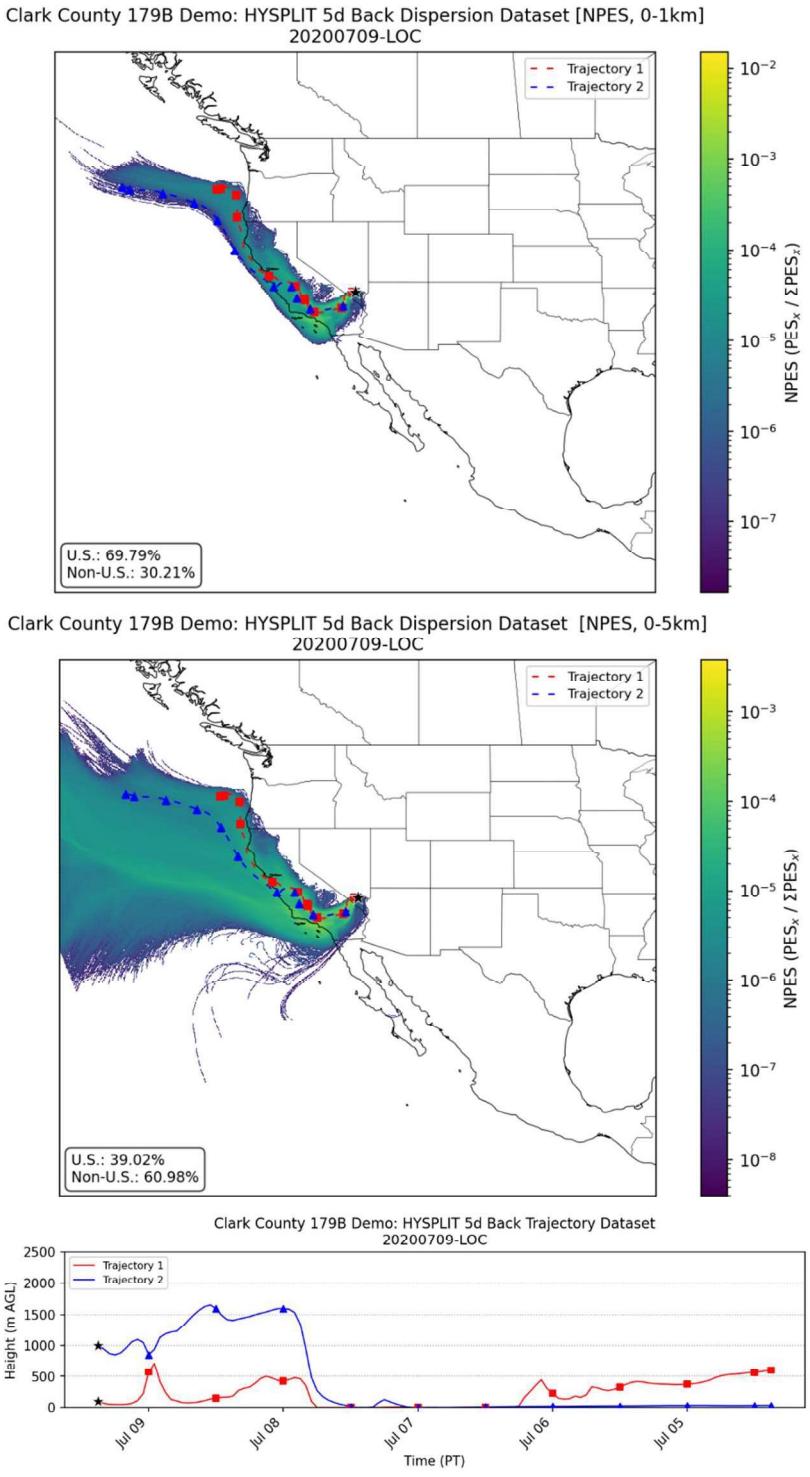

Figure B-15. Clark County 5-day back dispersion-based NPES. Results for July 9, 2020, with the local transport (LOC) air transport regime. NPES is based on the average concentration of a generic, inert tracer gas between 0 and 1 km (top panel) and 0 and 5 km (middle panel). Plots include sample back trajectories at 100 m and 1,000 m (red and blue), the elevation of which are also depicted (bottom panel).

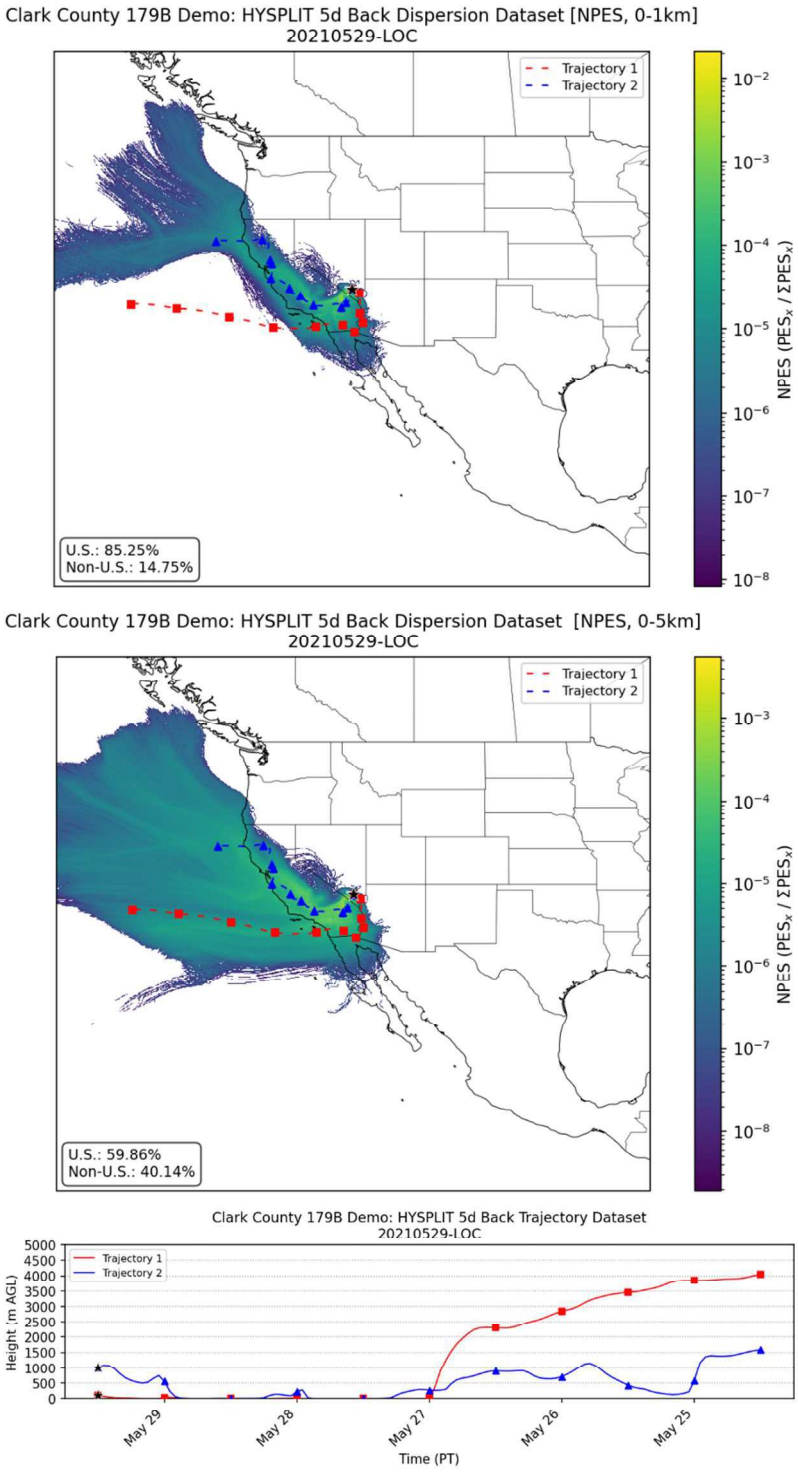

Figure B-16. Clark County 5-day back dispersion-based NPES. Results for May 29, 2021, with the local transport (LOC) air transport regime. NPES is based on the average concentration of a generic, inert tracer gas between 0 and 1 km (top panel) and 0 and 5 km (middle panel). Plots include sample back trajectories at 100 m and 1,000 m (red and blue), the elevation of which are also depicted (bottom panel).

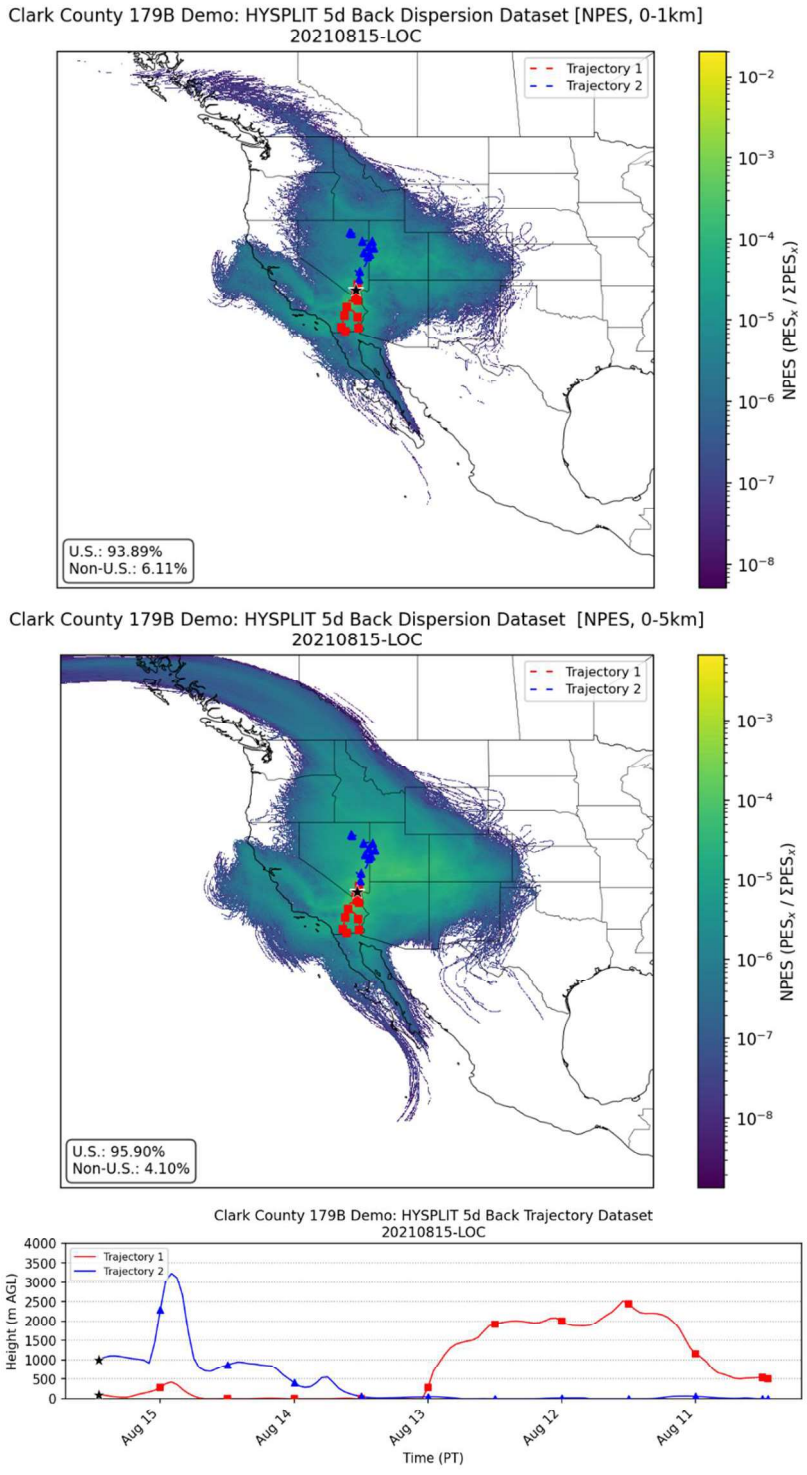

Figure B-17. Clark County 5-day back dispersion-based NPES. Results for August 15, 2021, with the local transport (LOC) air transport regime. NPES is based on the average concentration of a generic, inert tracer gas between 0 and 1 km (top panel) and 0 and 5 km (middle panel). Plots include sample back trajectories at 100 m and 1,000 m (red and blue), the elevation of which are also depicted (bottom panel).

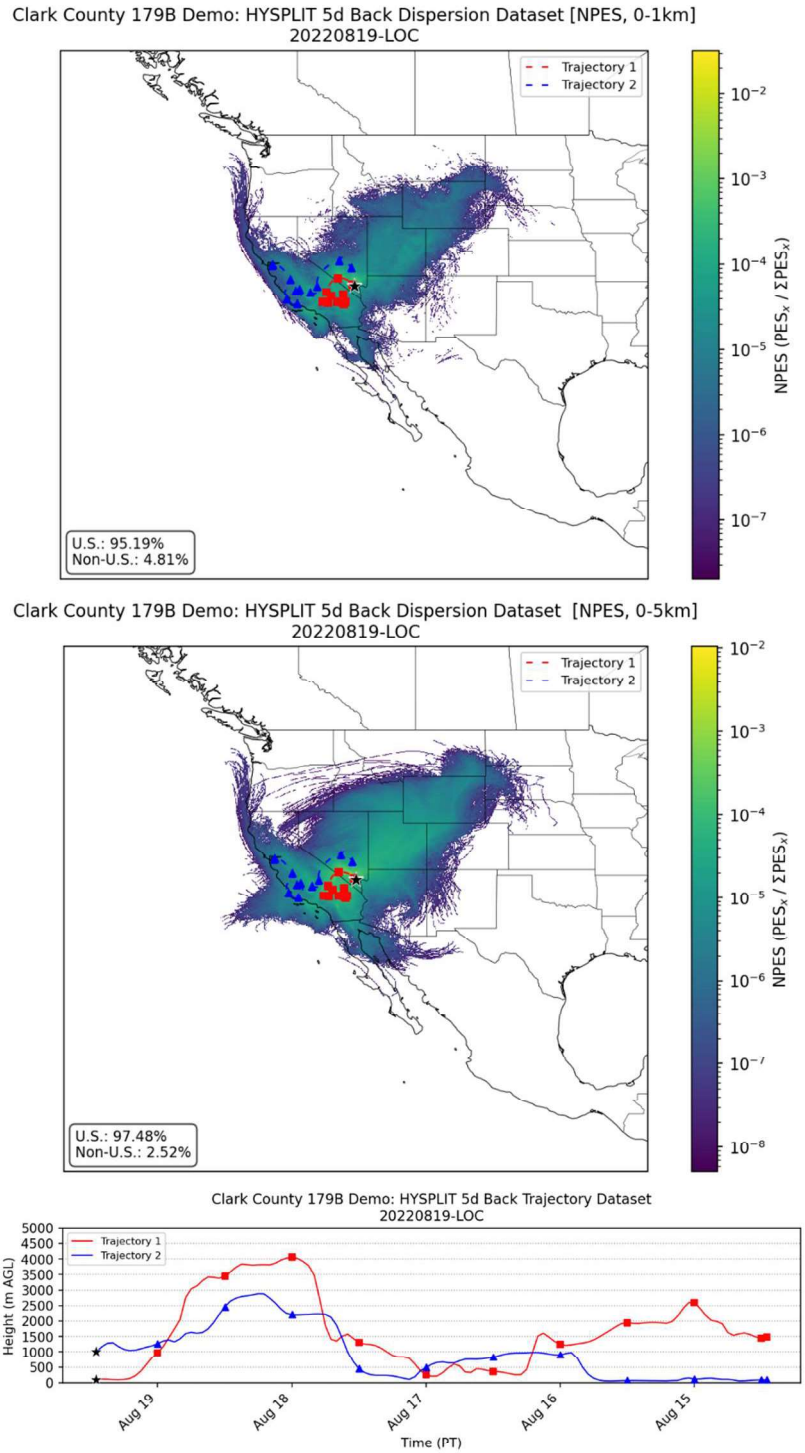

Figure B-18. Clark County 5-day back dispersion-based NPES. Results for August 19, 2022, with the local transport (LOC) air transport regime. NPES is based on the average concentration of a generic, inert tracer gas between 0 and 1 km (top panel) and 0 and 5 km (middle panel). Plots include sample back trajectories at 100 m and 1,000 m (red and blue), the elevation of which are also depicted (bottom panel).

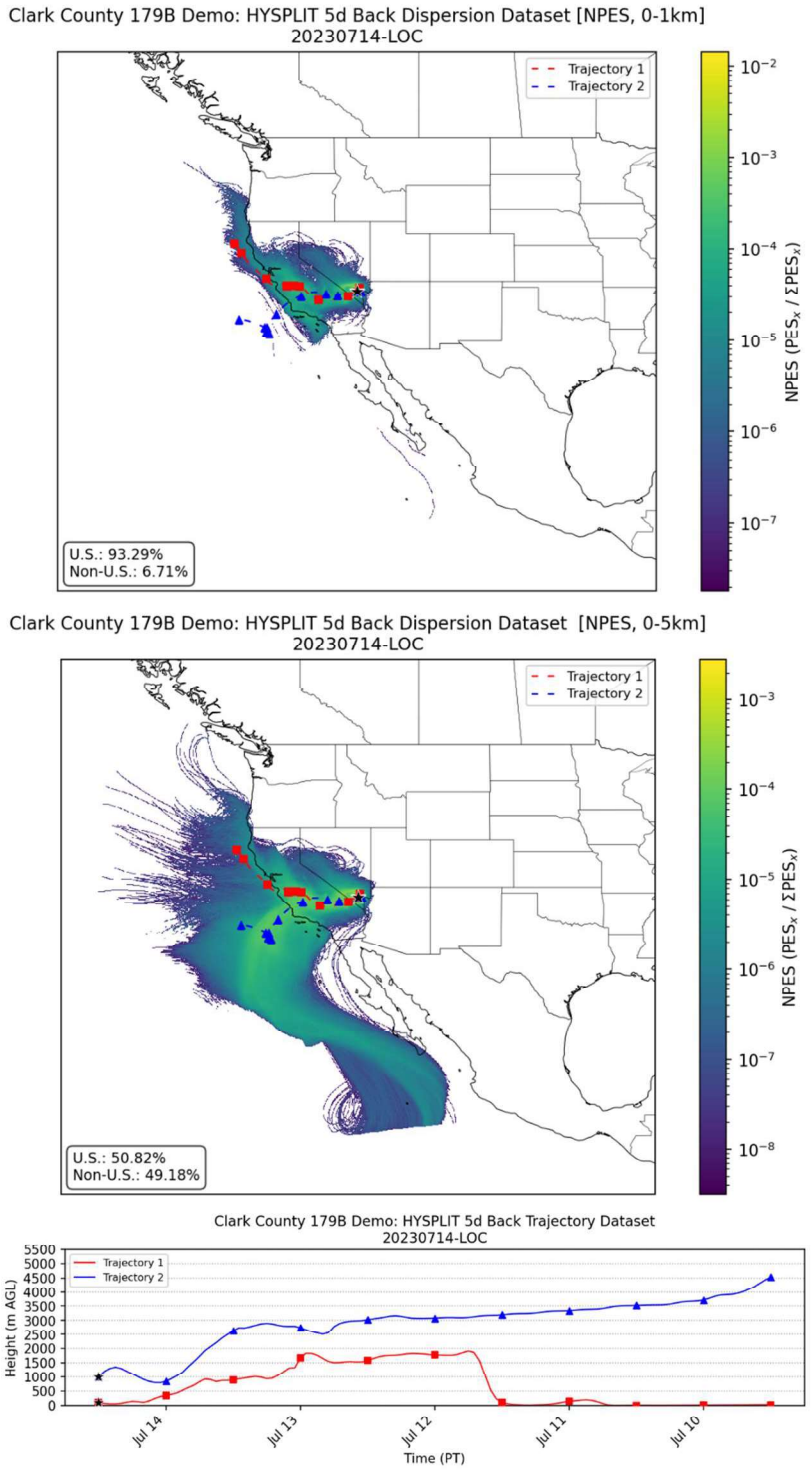

Figure B-19. Clark County 5-day back dispersion-based NPES. Results for July 14, 2023, with the local transport (LOC) air transport regime. NPES is based on the average concentration of a generic, inert tracer gas between 0 and 1 km (top panel) and 0 and 5 km (middle panel). Plots include sample back trajectories at 100 m and 1,000 m (red and blue), the elevation of which are also depicted (bottom panel).

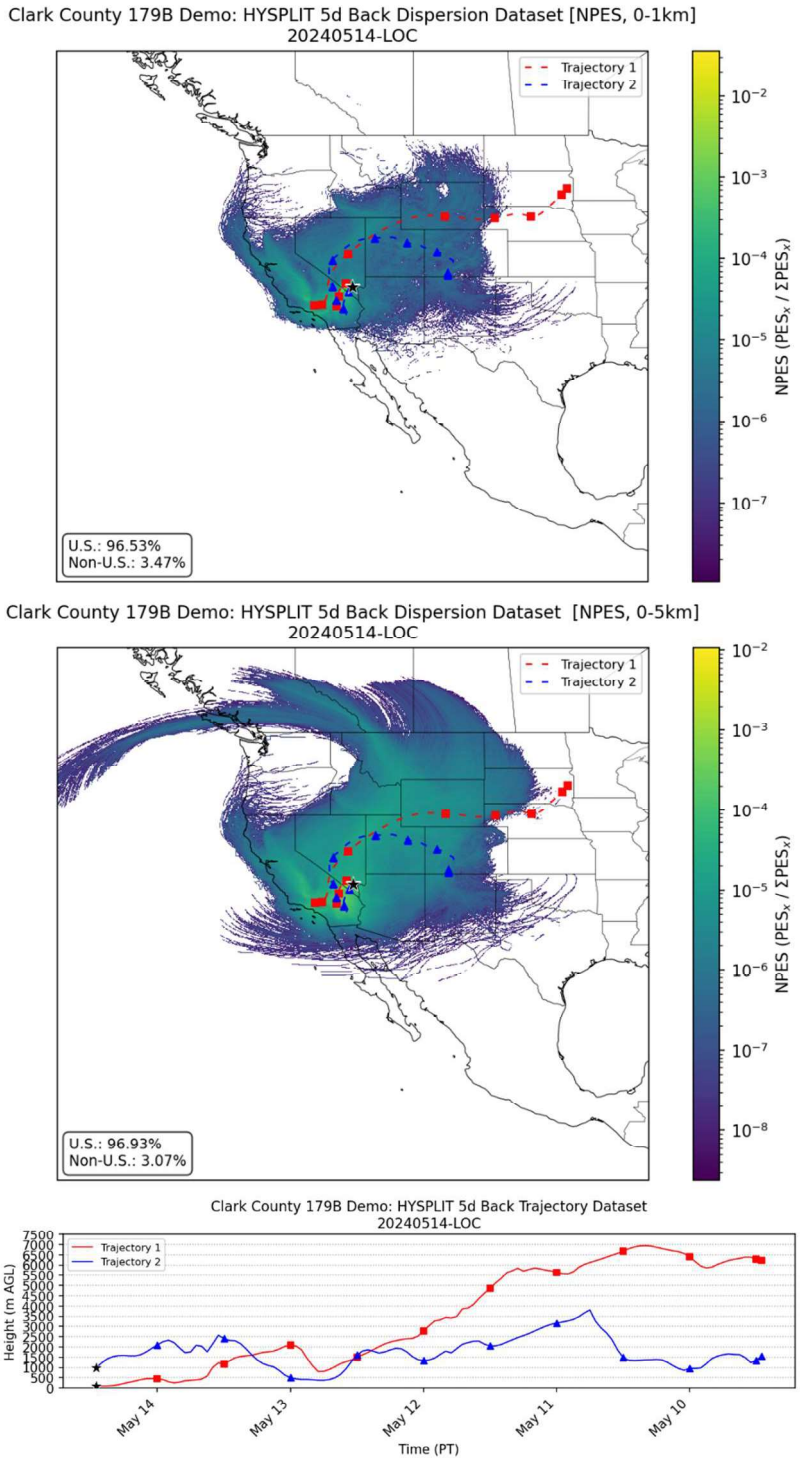

Figure B-20. Clark County 5-day back dispersion-based NPES. Results for May 14, 2024, with the local transport (LOC) air transport regime. NPES is based on the average concentration of a generic, inert tracer gas between 0 and 1 km (top panel) and 0 and 5 km (middle panel). Plots include sample back trajectories at 100 m and 1,000 m (red and blue), the elevation of which are also depicted (bottom panel).

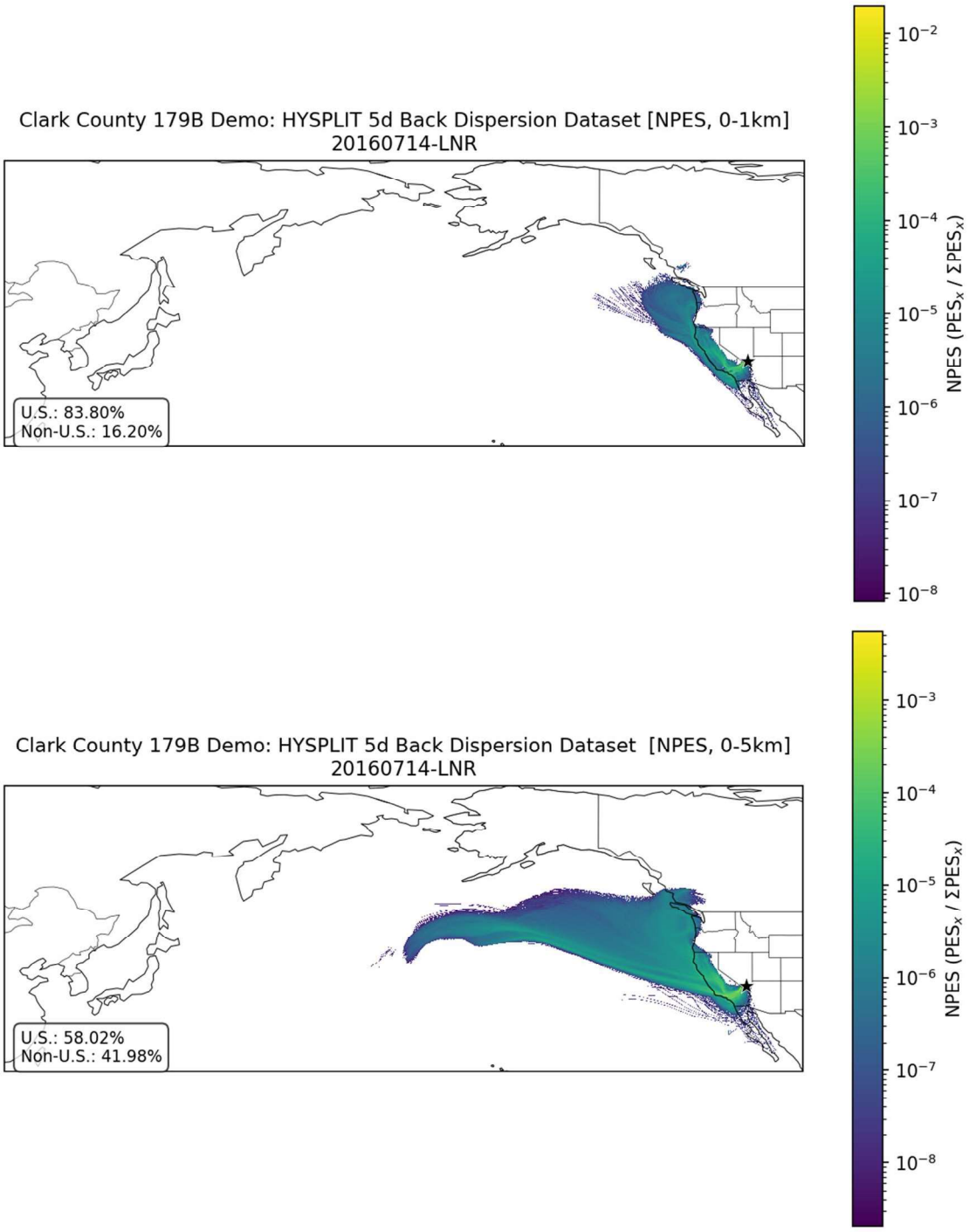

Figure B-21. Clark County 5-day back dispersion-based NPES. Results for July 14, 2016, with the long-range international transport (LNR) air transport regime. NPES is based on the average concentration of a generic, inert tracer gas between 0 and 1 km (top panel) and 0 and 5 km (bottom panel).

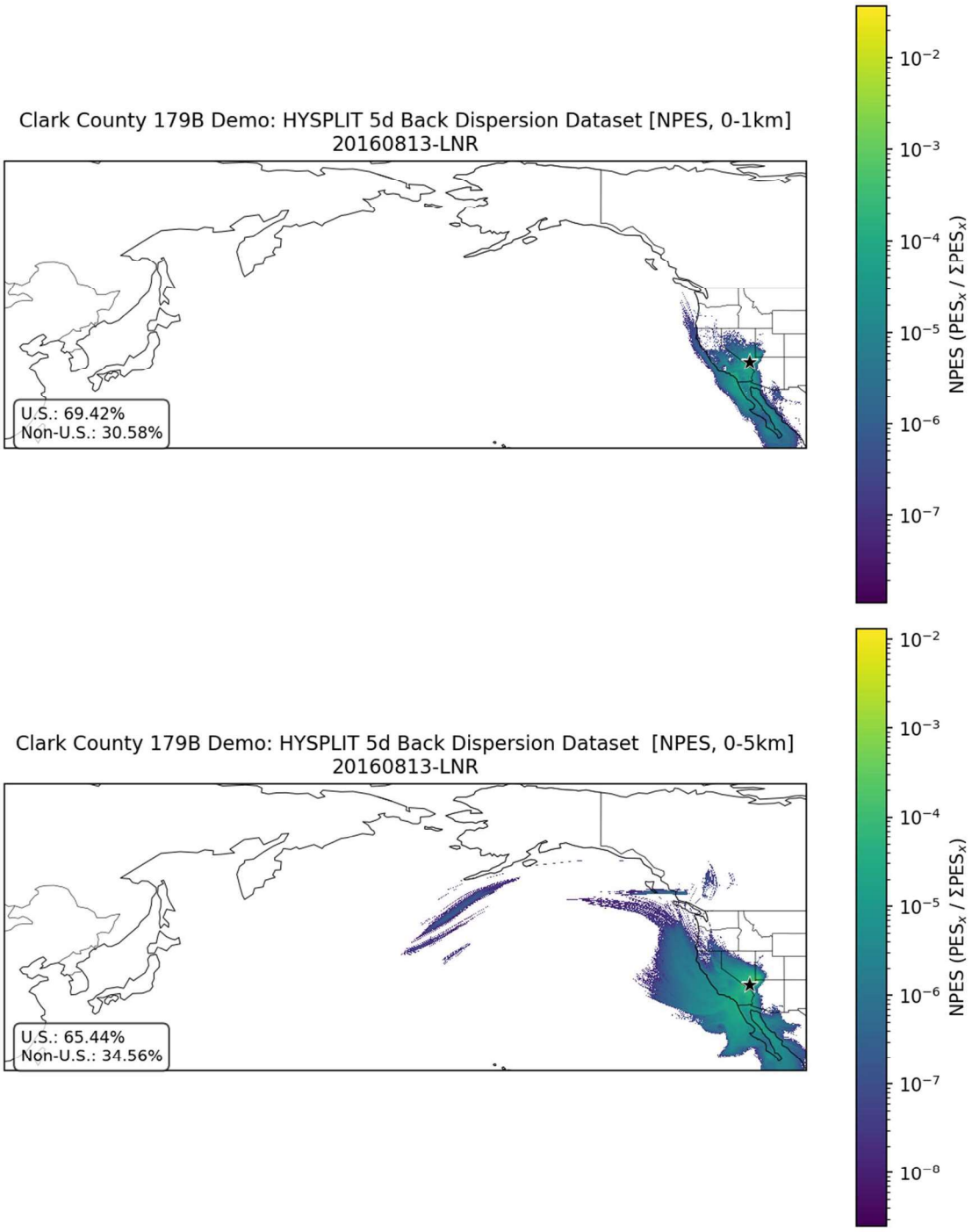

Figure B-22. Clark County 5-day back dispersion-based NPES. Results for August 13, 2016, with the long-range international transport (LNR) air transport regime. NPES is based on the average concentration of a generic, inert tracer gas between 0 and 1 km (top panel) and 0 and 5 km (bottom panel).

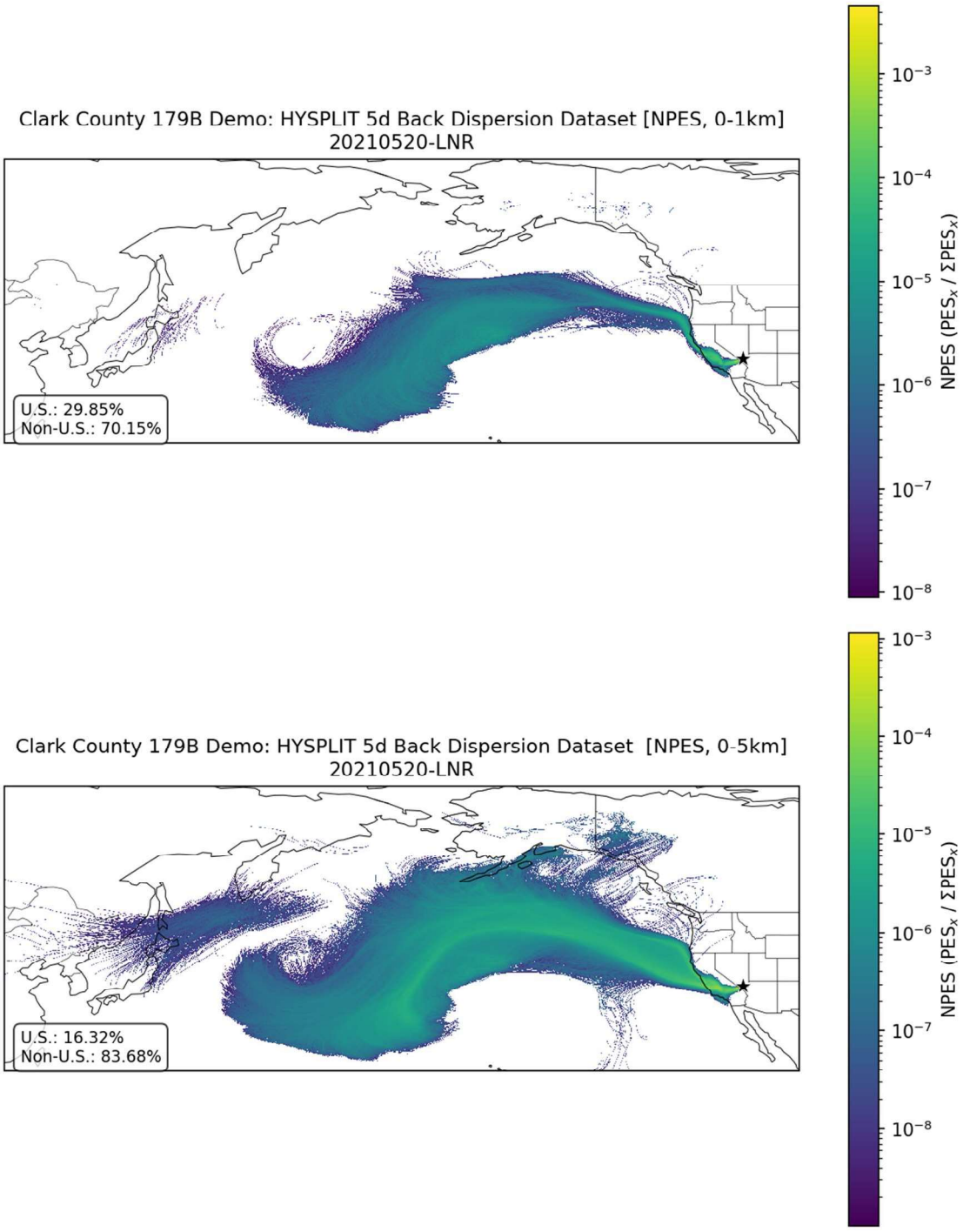

Figure B-23. Clark County 5-day back dispersion-based NPES. Results for May 20, 2021, with the long-range international transport (LNR) air transport regime. NPES is based on the average concentration of a generic, inert tracer gas between 0 and 1 km (top panel) and 0 and 5 km (bottom panel).

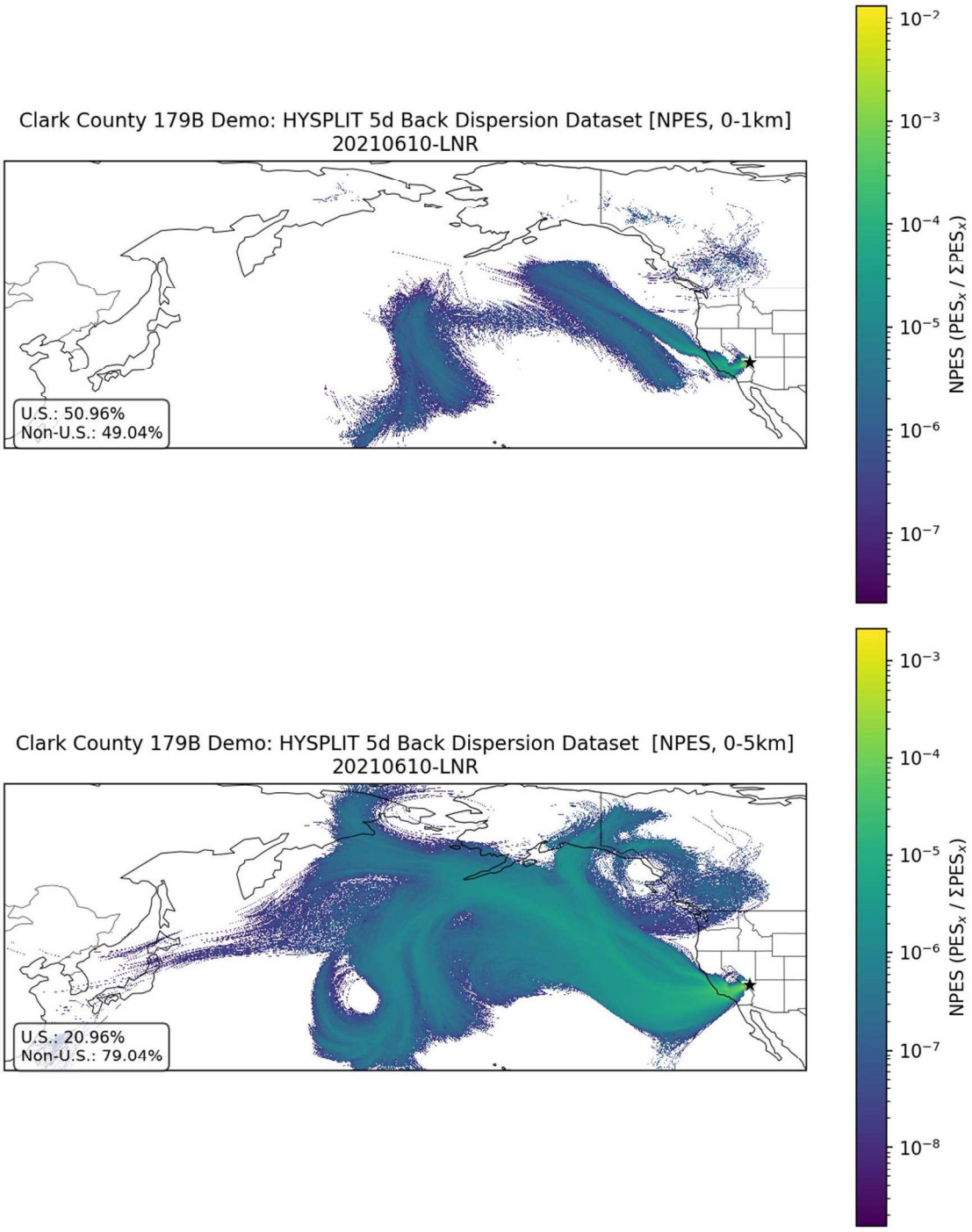

Figure B-24. Clark County 5-day back dispersion-based NPES. Results for June 10, 2021, with the long-range international transport (LNR) air transport regime. NPES is based on the average concentration of a generic, inert tracer gas between 0 and 1 km (top panel) and 0 and 5 km (bottom panel).

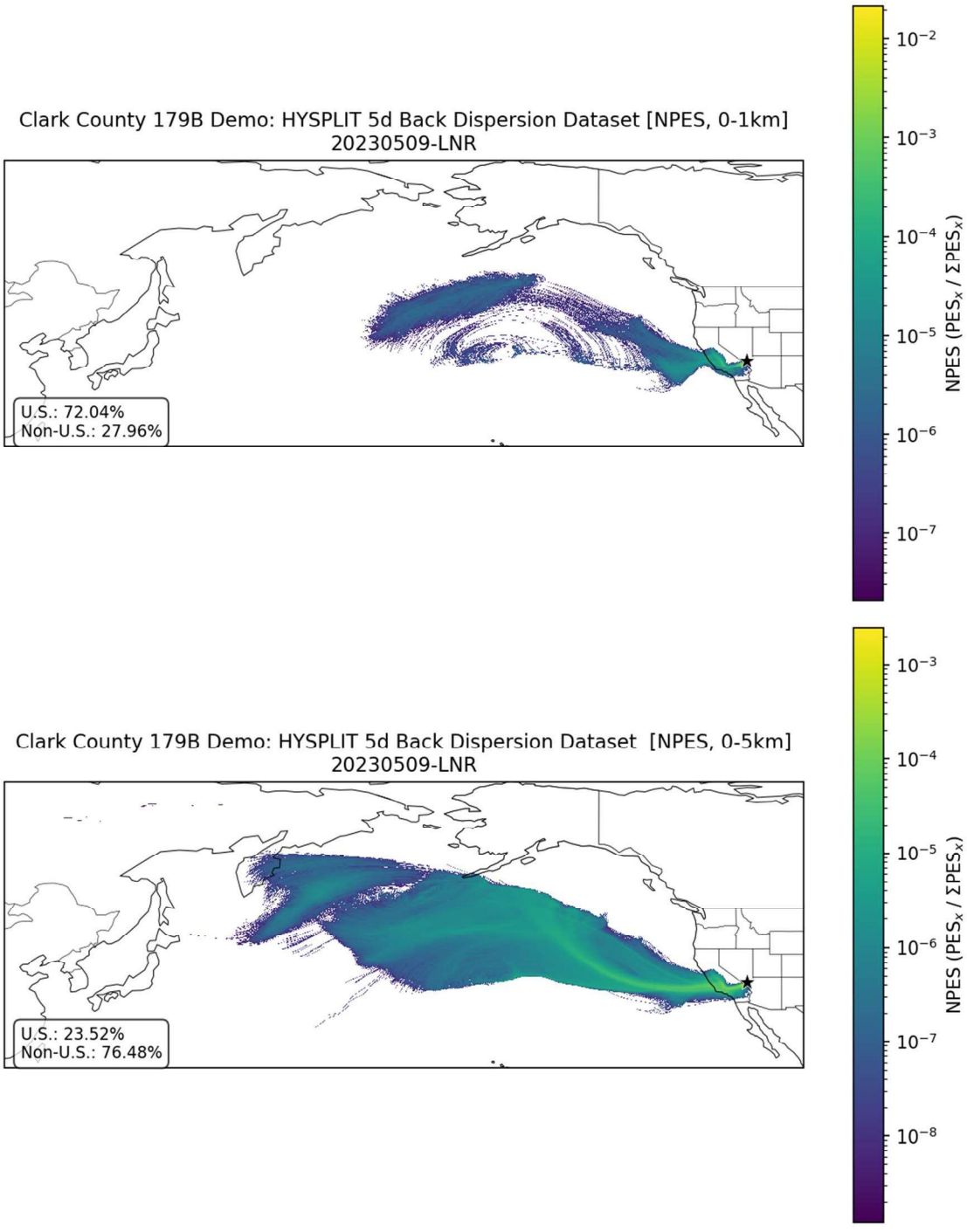

Figure B-25. Clark County 5-day back dispersion-based NPES. Results for May 9, 2023, with the long-range international transport (LNR) air transport regime. NPES is based on the average concentration of a generic, inert tracer gas between 0 and 1 km (top panel) and 0 and 5 km (bottom panel).

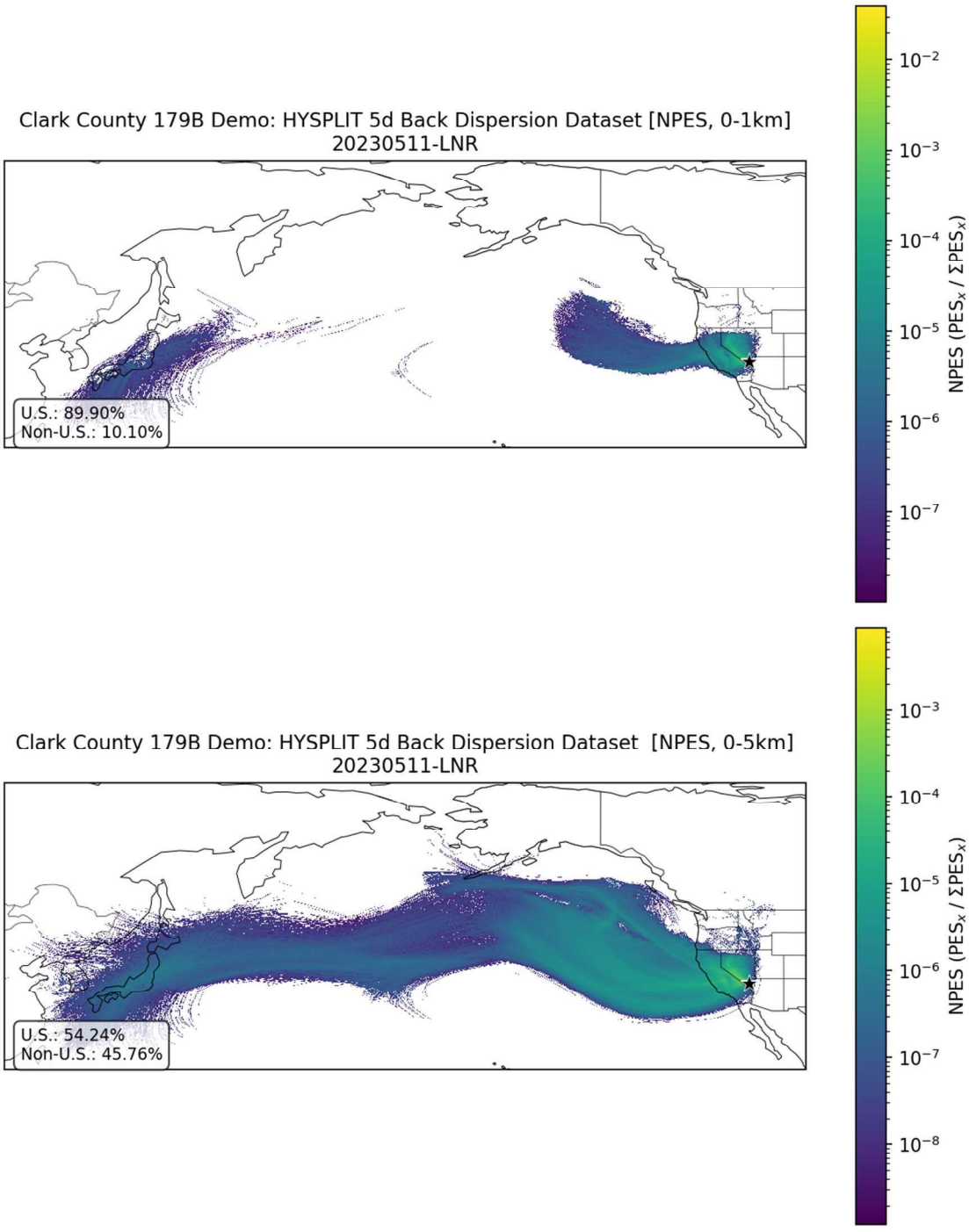

Figure B-26. Clark County 5-day back dispersion-based NPES. Results for May 11, 2023, with the long-range international transport (LNR) air transport regime. NPES is based on the average concentration of a generic, inert tracer gas between 0 and 1 km (top panel) and 0 and 5 km (bottom panel).

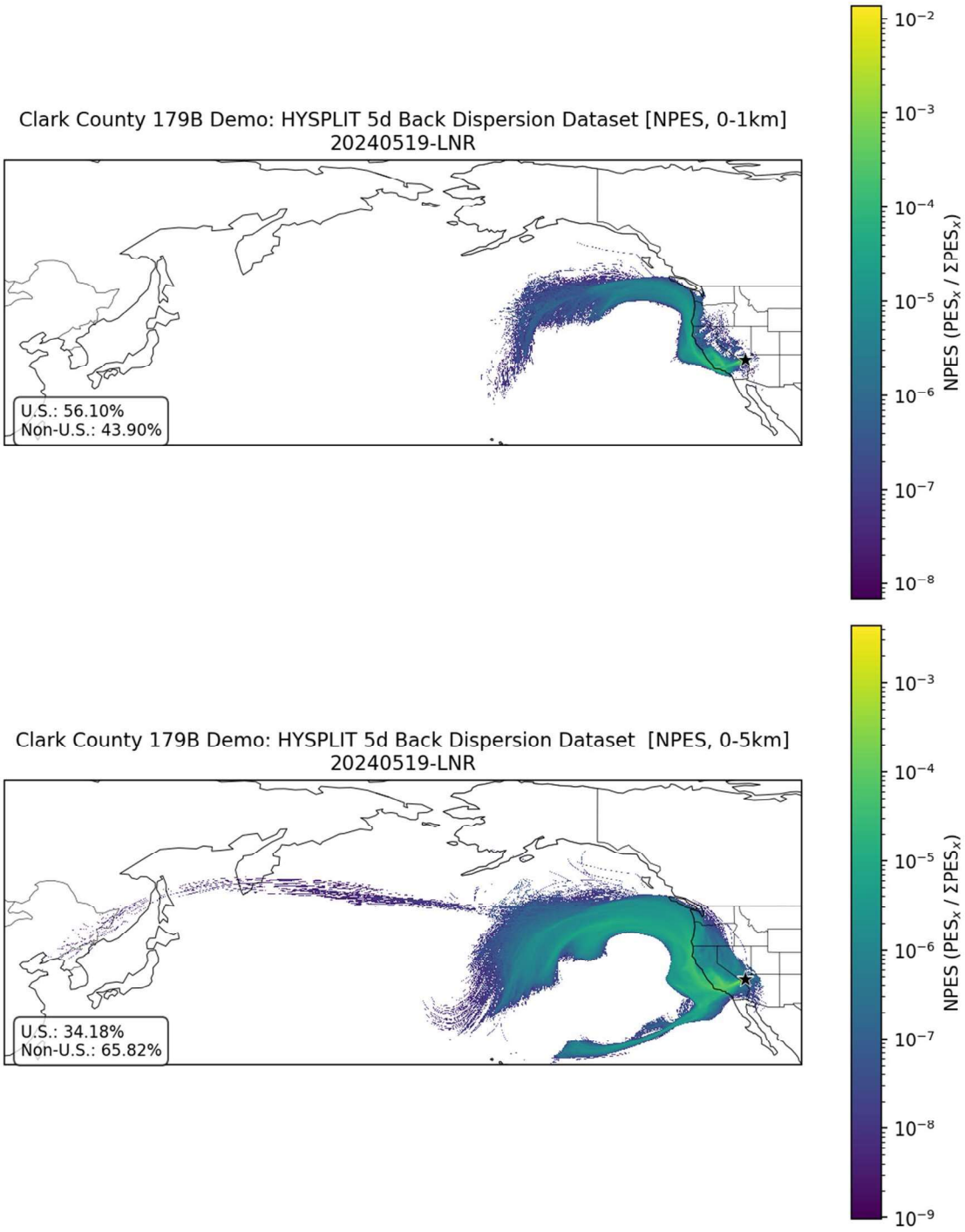

Figure B-27. Clark County 5-day back dispersion-based NPES. Results for May 19, 2024, with the long-range international transport (LNR) air transport regime. NPES is based on the average concentration of a generic, inert tracer gas between 0 and 1 km (top panel) and 0 and 5 km (bottom panel).

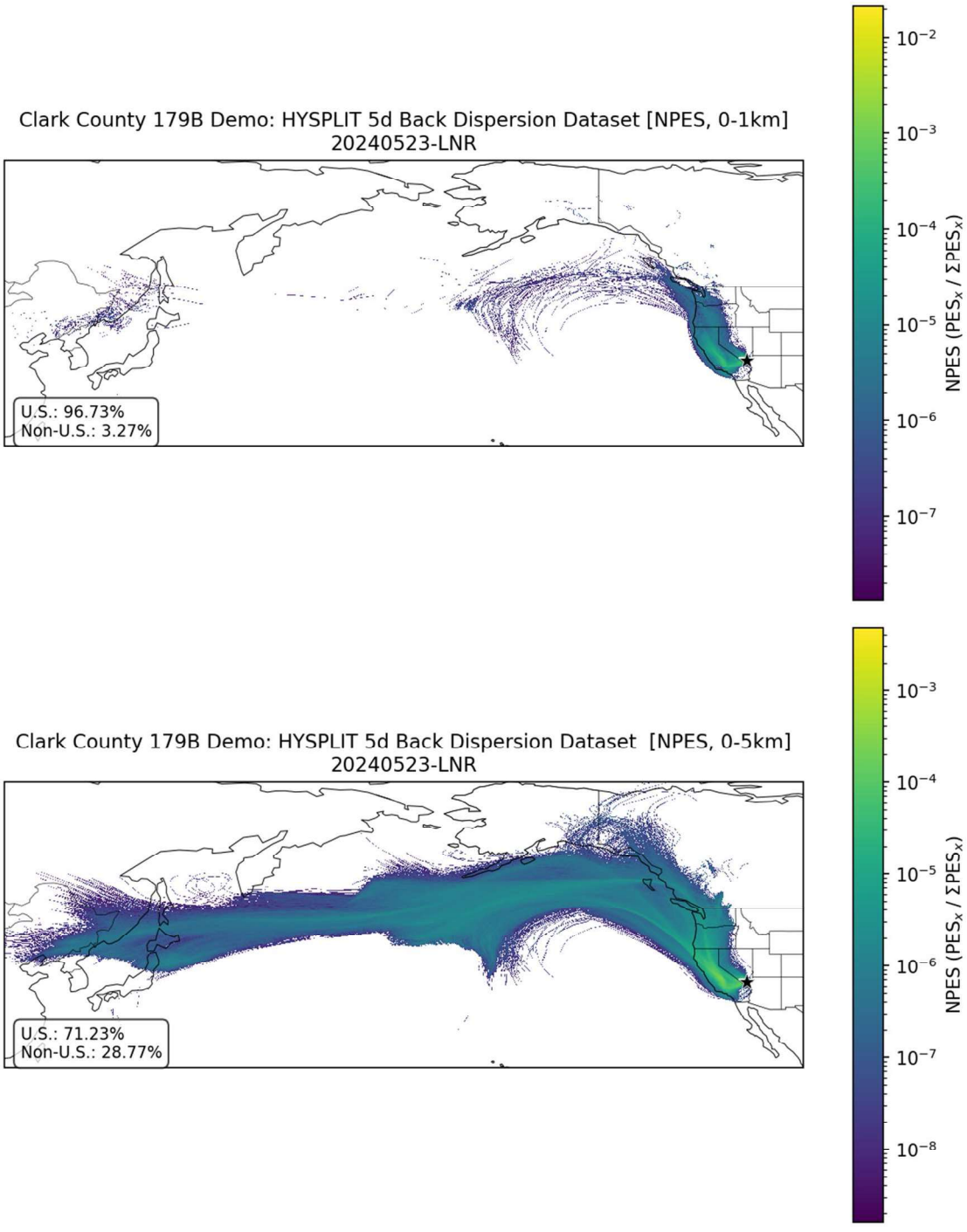

Figure B-28. Clark County 5-day back dispersion-based NPES. Results for May 23, 2024, with the long-range international transport (LNR) air transport regime. NPES is based on the average concentration of a generic, inert tracer gas between 0 and 1 km (top panel) and 0 and 5 km (bottom panel).

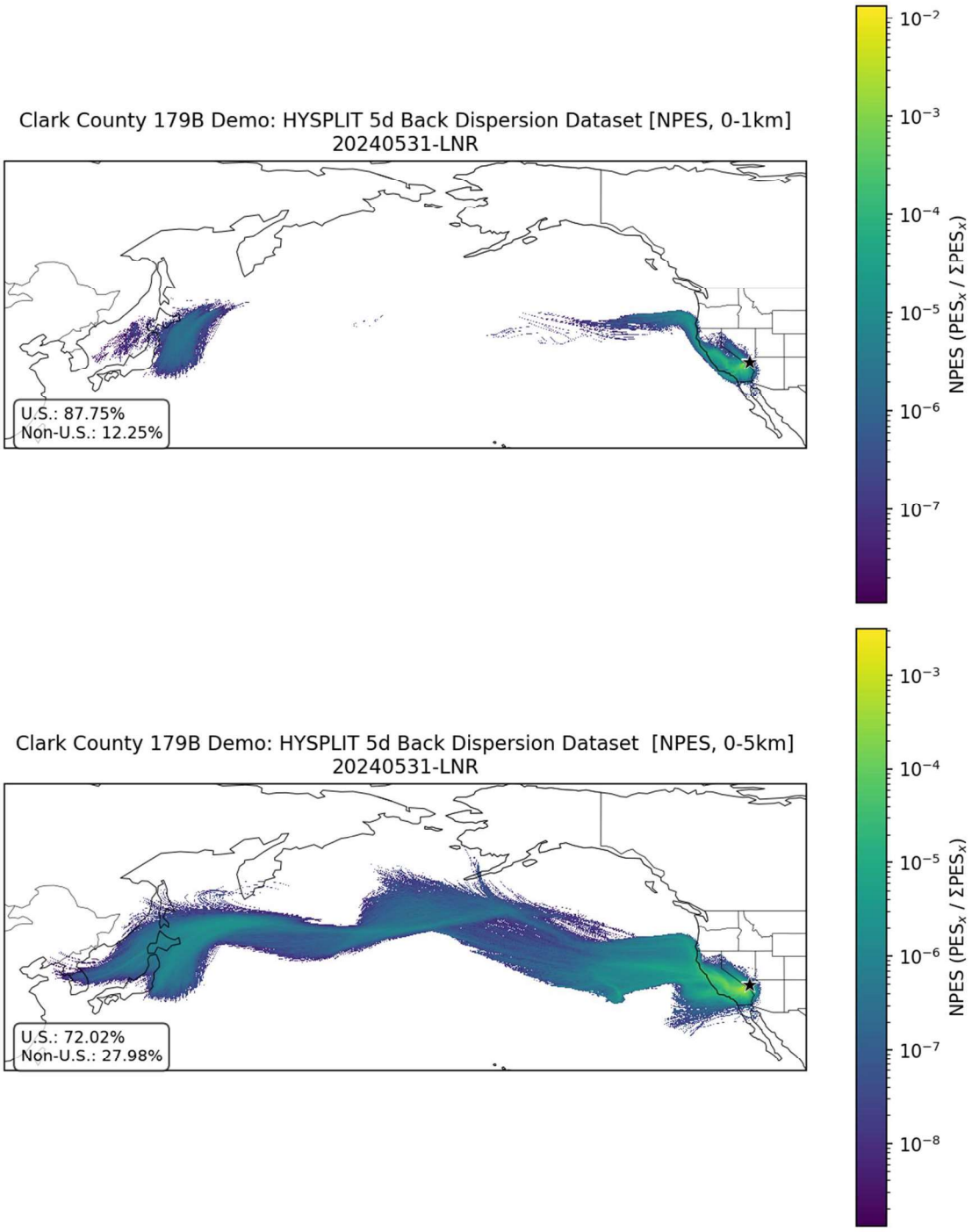

Figure B-29. Clark County 5-day back dispersion-based NPES. Results for May 31, 2024, with the long-range international transport (LNR) air transport regime. NPES is based on the average concentration of a generic, inert tracer gas between 0 and 1 km (top panel) and 0 and 5 km (bottom panel).

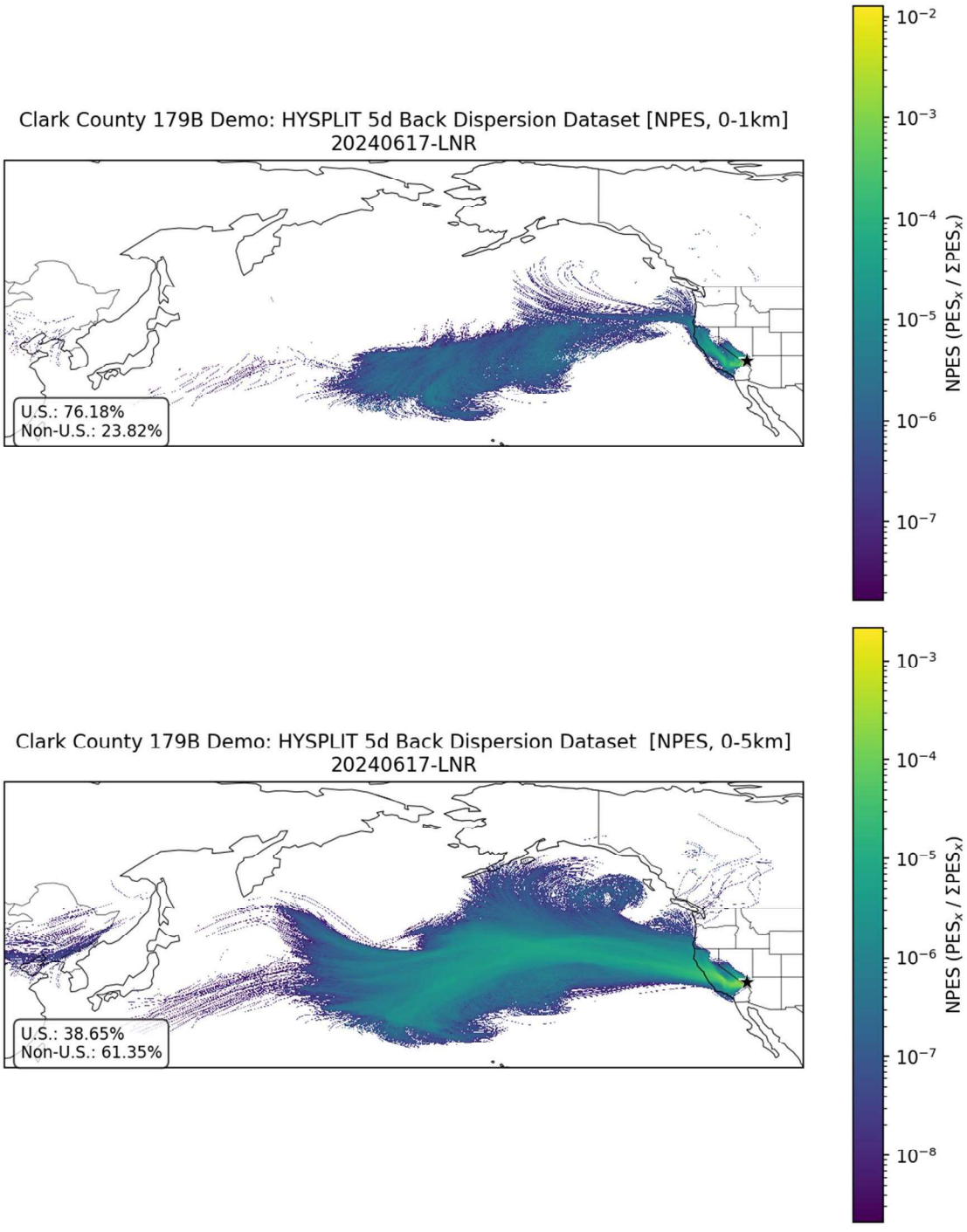

Figure B-30. Clark County 5-day back dispersion-based NPES. Results for June 17, 2024, with the long-range international transport (LNR) air transport regime. NPES is based on the average concentration of a generic, inert tracer gas between 0 and 1 km (top panel) and 0 and 5 km (bottom panel).

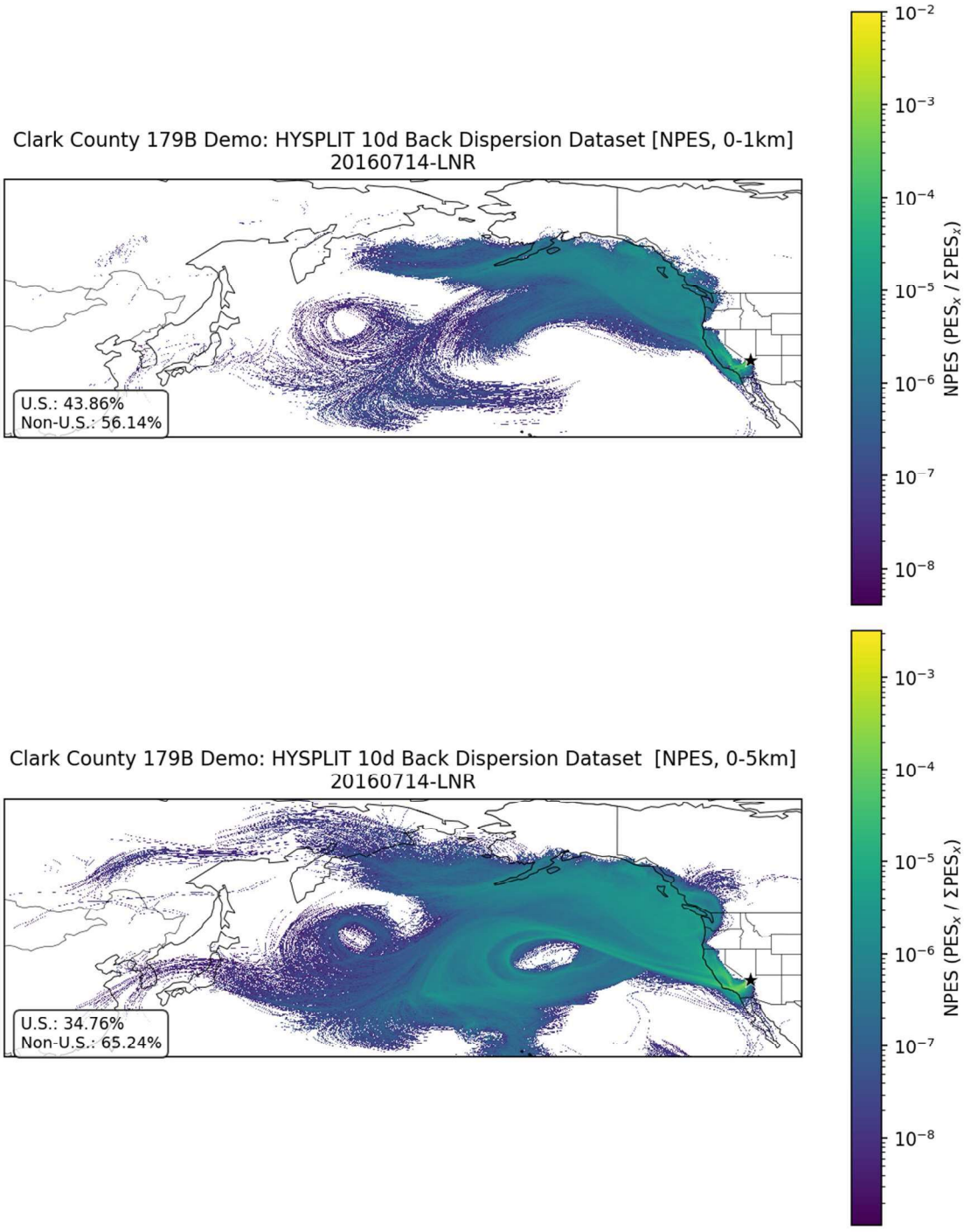

Figure B-31. Clark County 10-day back dispersion-based NPES. Results for July 14, 2016, with the long-range international transport (LNR) air transport regime. NPES is based on the average concentration of a generic, inert tracer gas between 0 and 1 km (top panel) and 0 and 5 km (bottom panel).

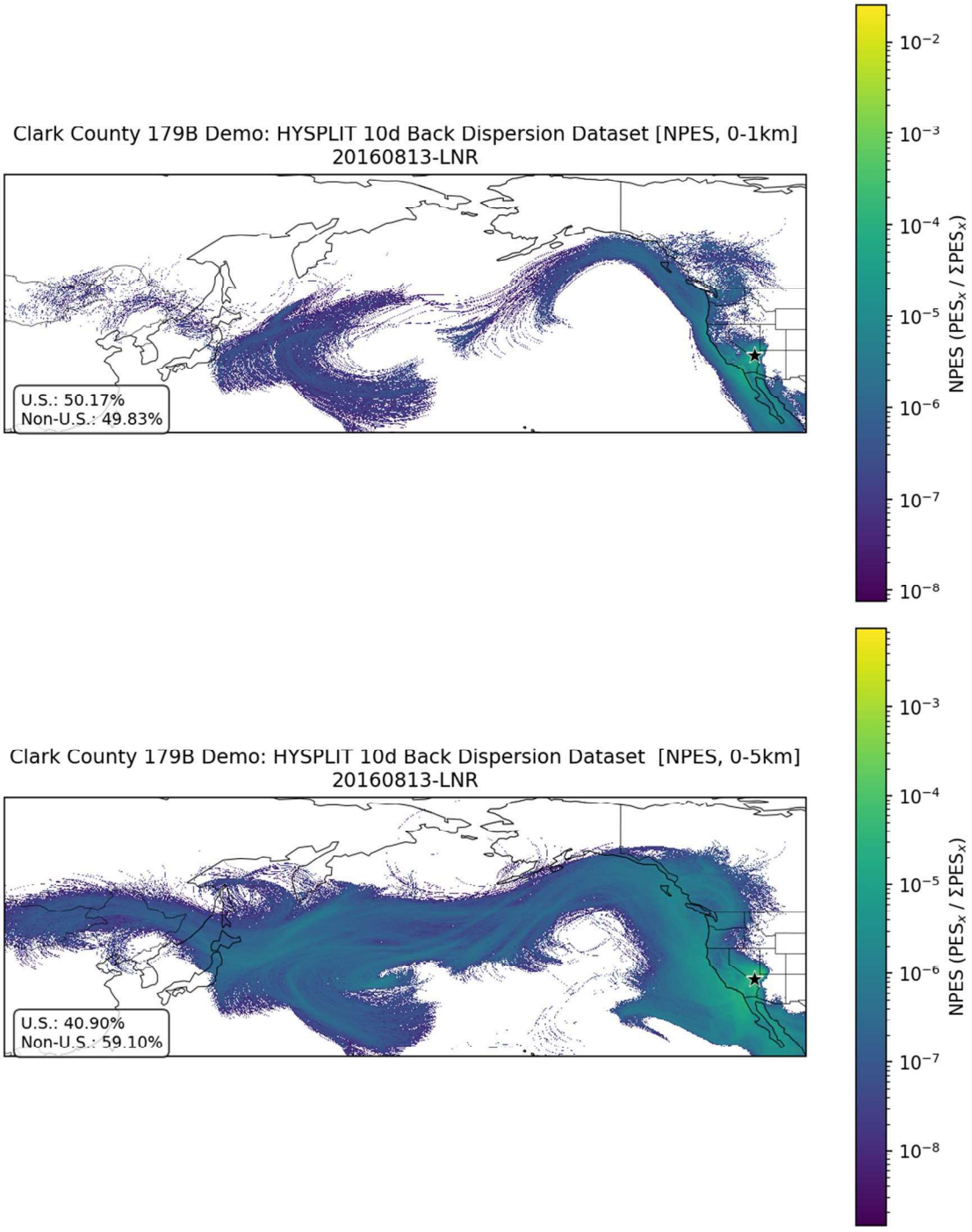

Figure B-32. Clark County 10-day back dispersion-based NPES. Results for August 13, 2016, with the long-range international transport (LNR) air transport regime. NPES is based on the average concentration of a generic, inert tracer gas between 0 and 1 km (top panel) and 0 and 5 km (bottom panel).

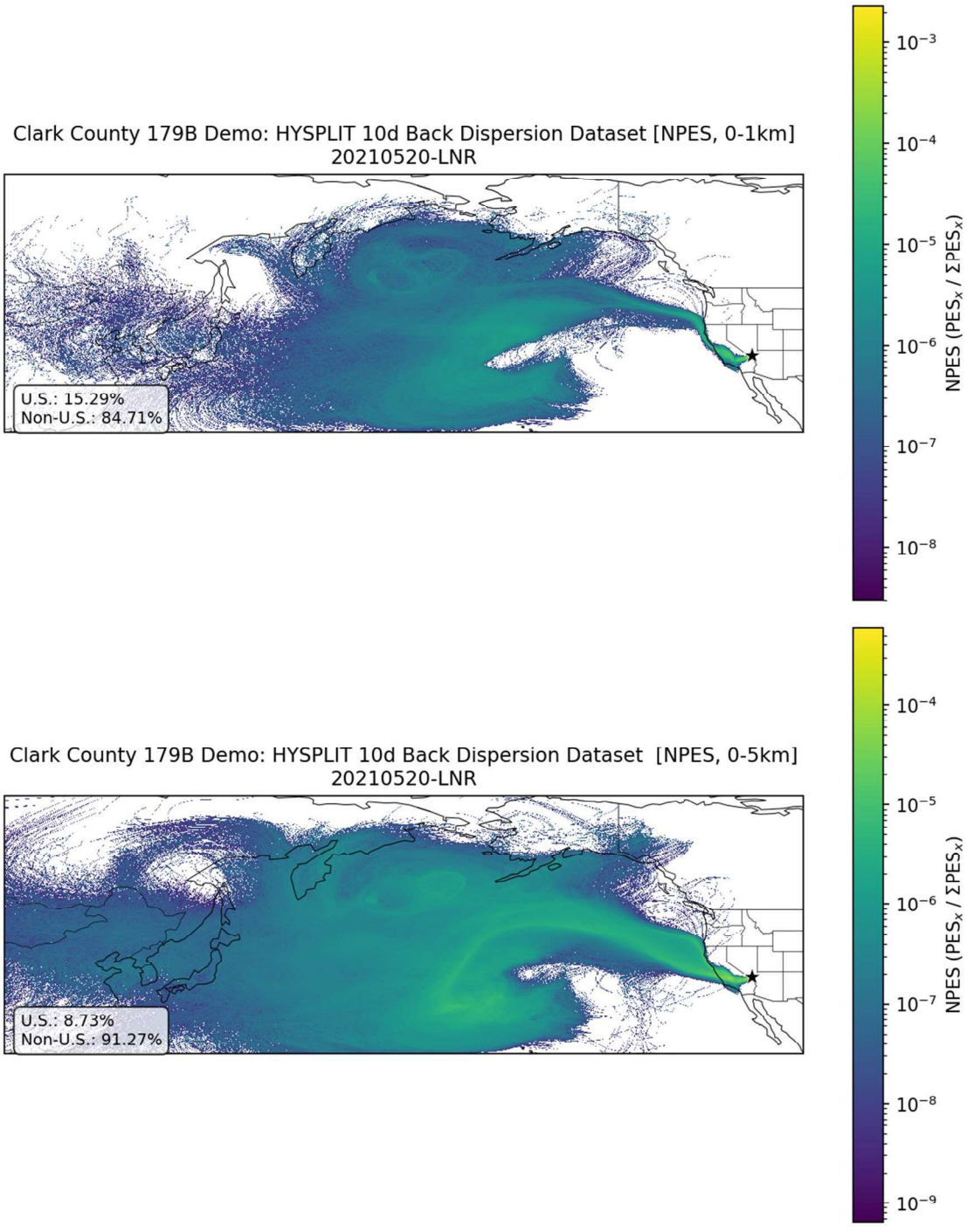

Figure B-33. Clark County 10-day back dispersion-based NPES. Results for May 20, 2021, with the long-range international transport (LNR) air transport regime. NPES is based on the average concentration of a generic, inert tracer gas between 0 and 1 km (top panel) and 0 and 5 km (bottom panel).

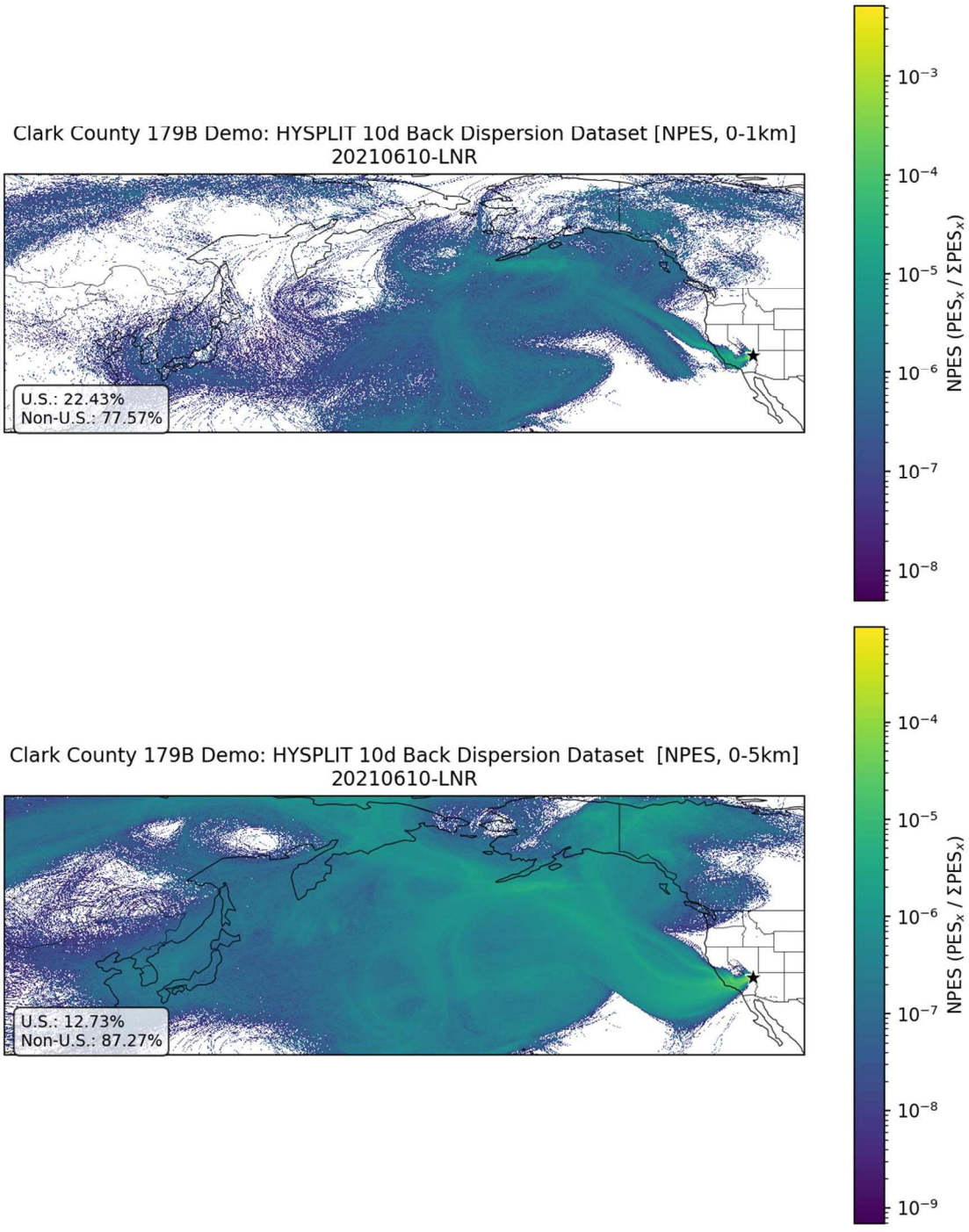

Figure B-34. Clark County 10-day back dispersion-based NPES. Results for June 10, 2021, with the long-range international transport (LNR) air transport regime. NPES is based on the average concentration of a generic, inert tracer gas between 0 and 1 km (top panel) and 0 and 5 km (bottom panel).

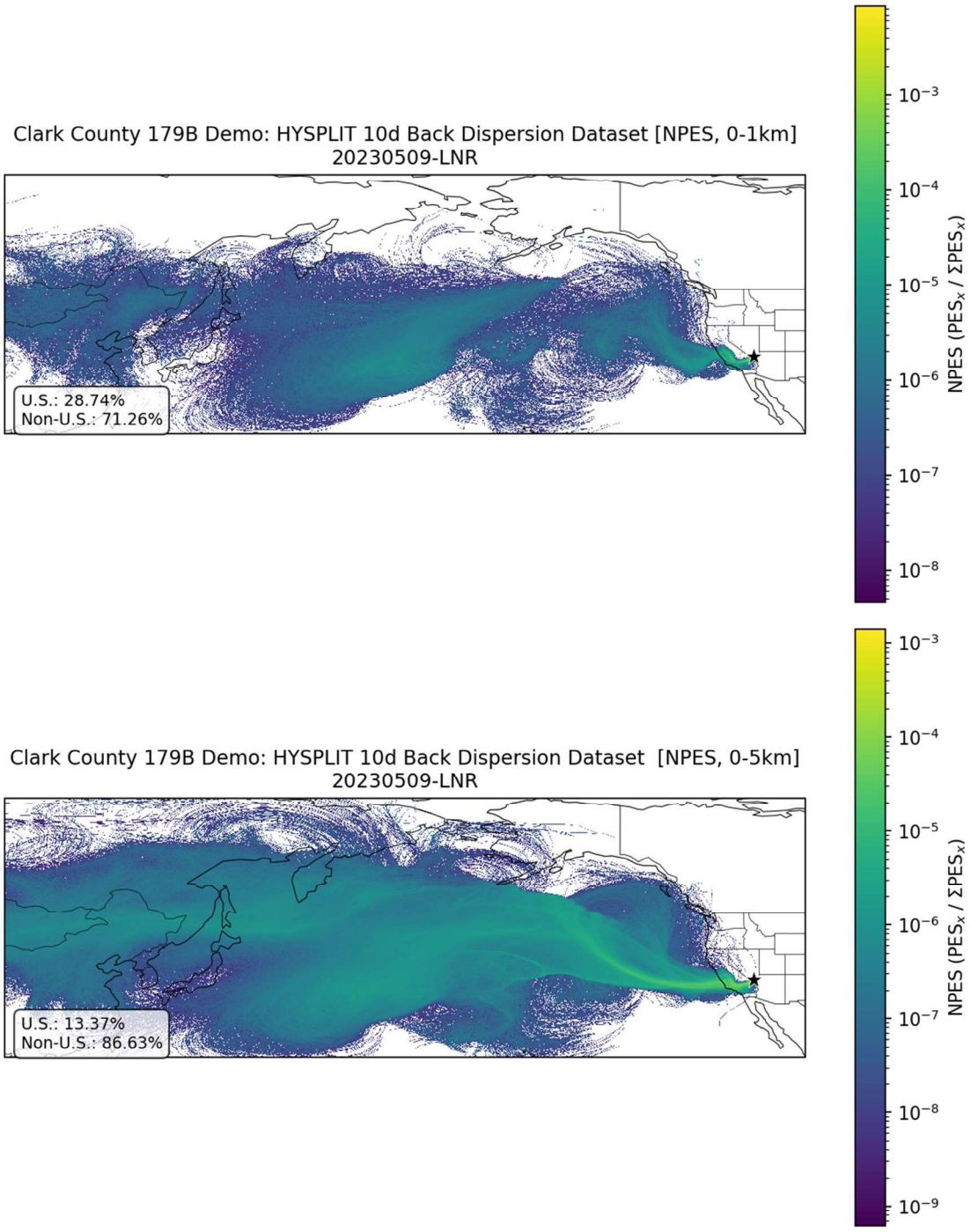

Figure B-35. Clark County 10-day back dispersion-based NPES. Results for May 9, 2023, with the long-range international transport (LNR) air transport regime. NPES is based on the average concentration of a generic, inert tracer gas between 0 and 1 km (top panel) and 0 and 5 km (bottom panel).

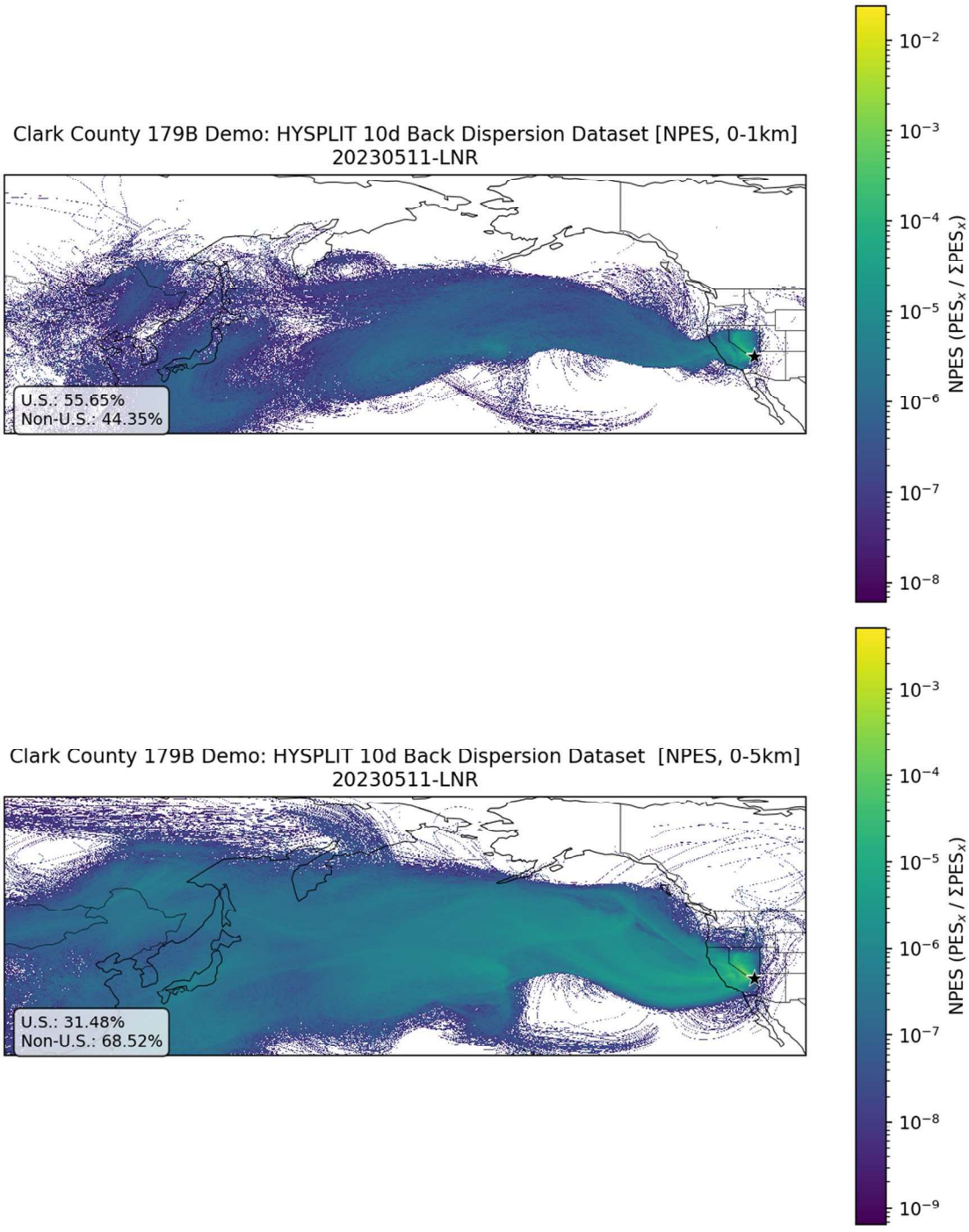

Figure B-36. Clark County 10-day back dispersion-based NPES. Results for May 11, 2023, with the long-range international transport (LNR) air transport regime. NPES is based on the average concentration of a generic, inert tracer gas between 0 and 1 km (top panel) and 0 and 5 km (bottom panel).

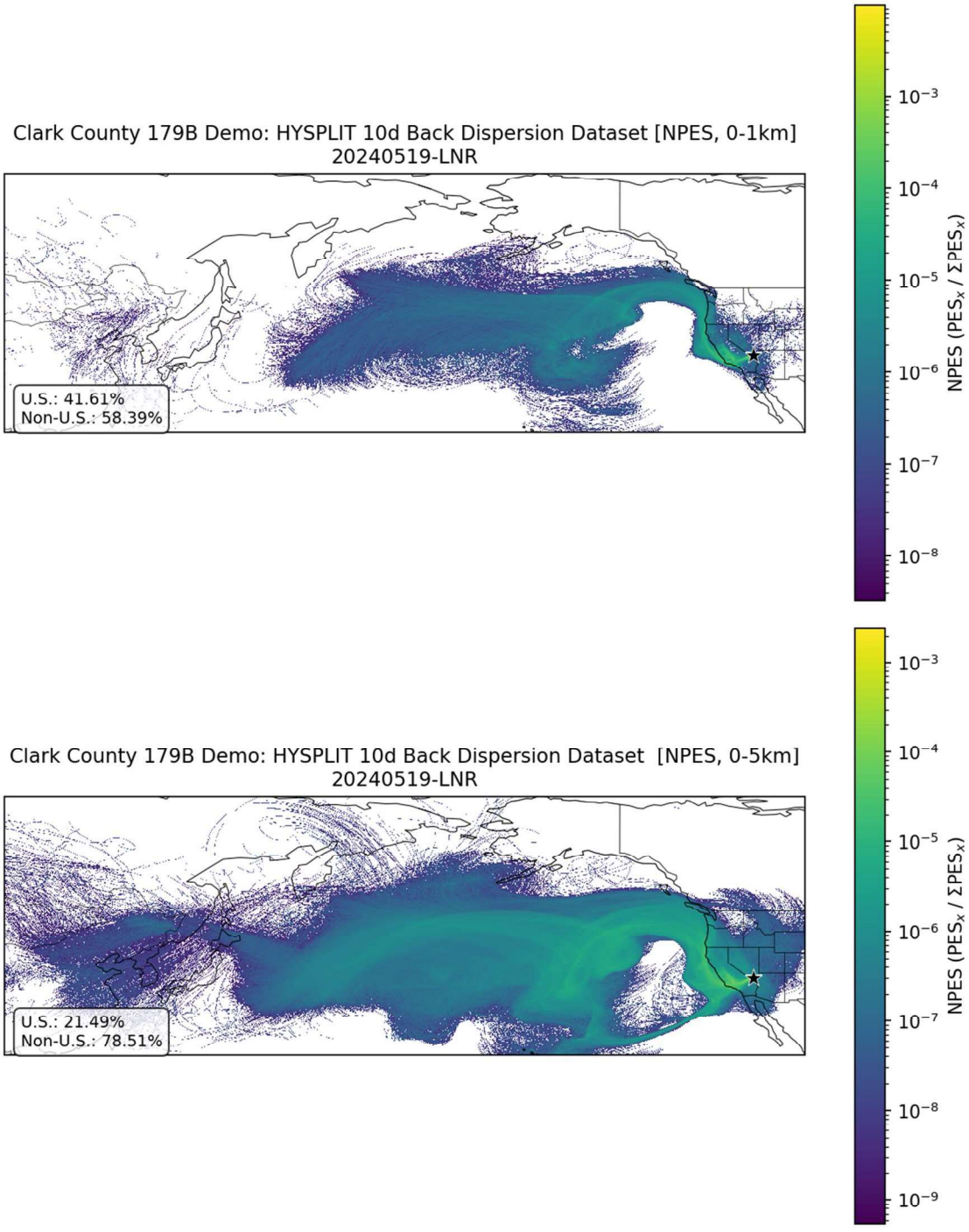

Figure B-37. Clark County 10-day back dispersion-based NPES. Results for May 19, 2024, with the long-range international transport (LNR) air transport regime. NPES is based on the average concentration of a generic, inert tracer gas between 0 and 1 km (top panel) and 0 and 5 km (bottom panel).

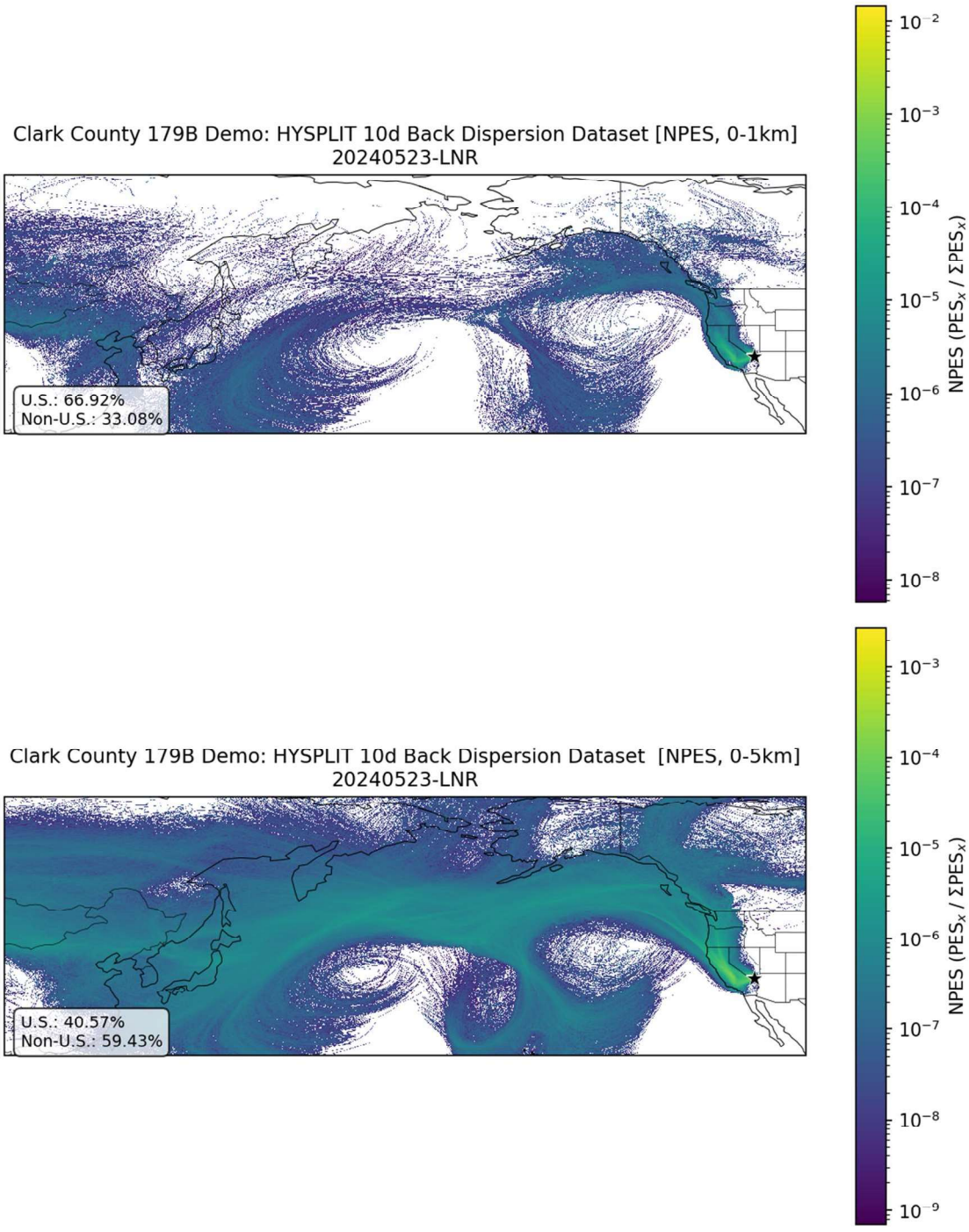

Figure B-38. Clark County 10-day back dispersion-based NPES. Results for May 23, 2024, with the long-range international transport (LNR) air transport regime. NPES is based on the average concentration of a generic, inert tracer gas between 0 and 1 km (top panel) and 0 and 5 km (bottom panel).

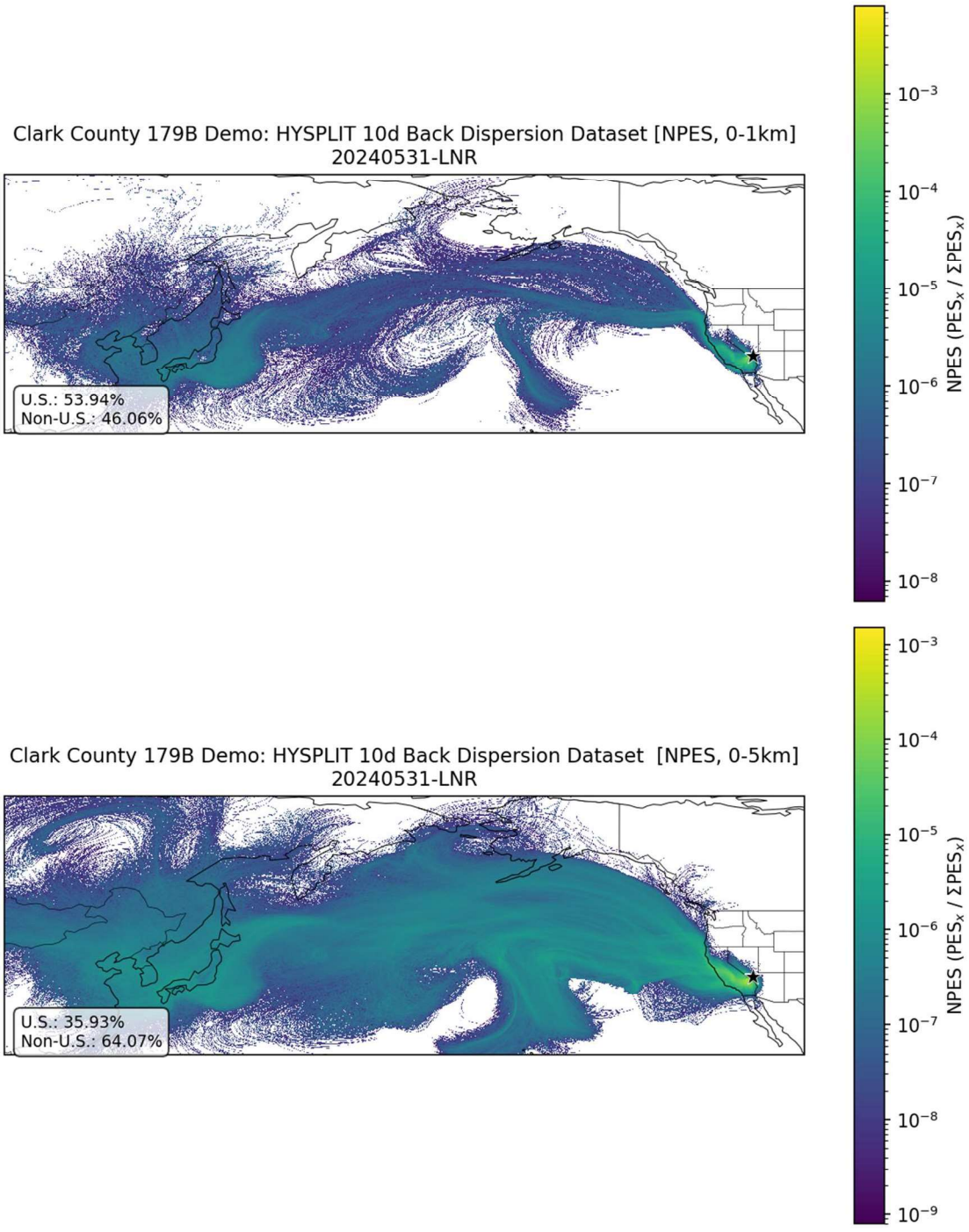

Figure B-39. Clark County 10-day back dispersion-based NPES. Results for May 31, 2024, with the long-range international transport (LNR) air transport regime. NPES is based on the average concentration of a generic, inert tracer gas between 0 and 1 km (top panel) and 0 and 5 km (bottom panel).

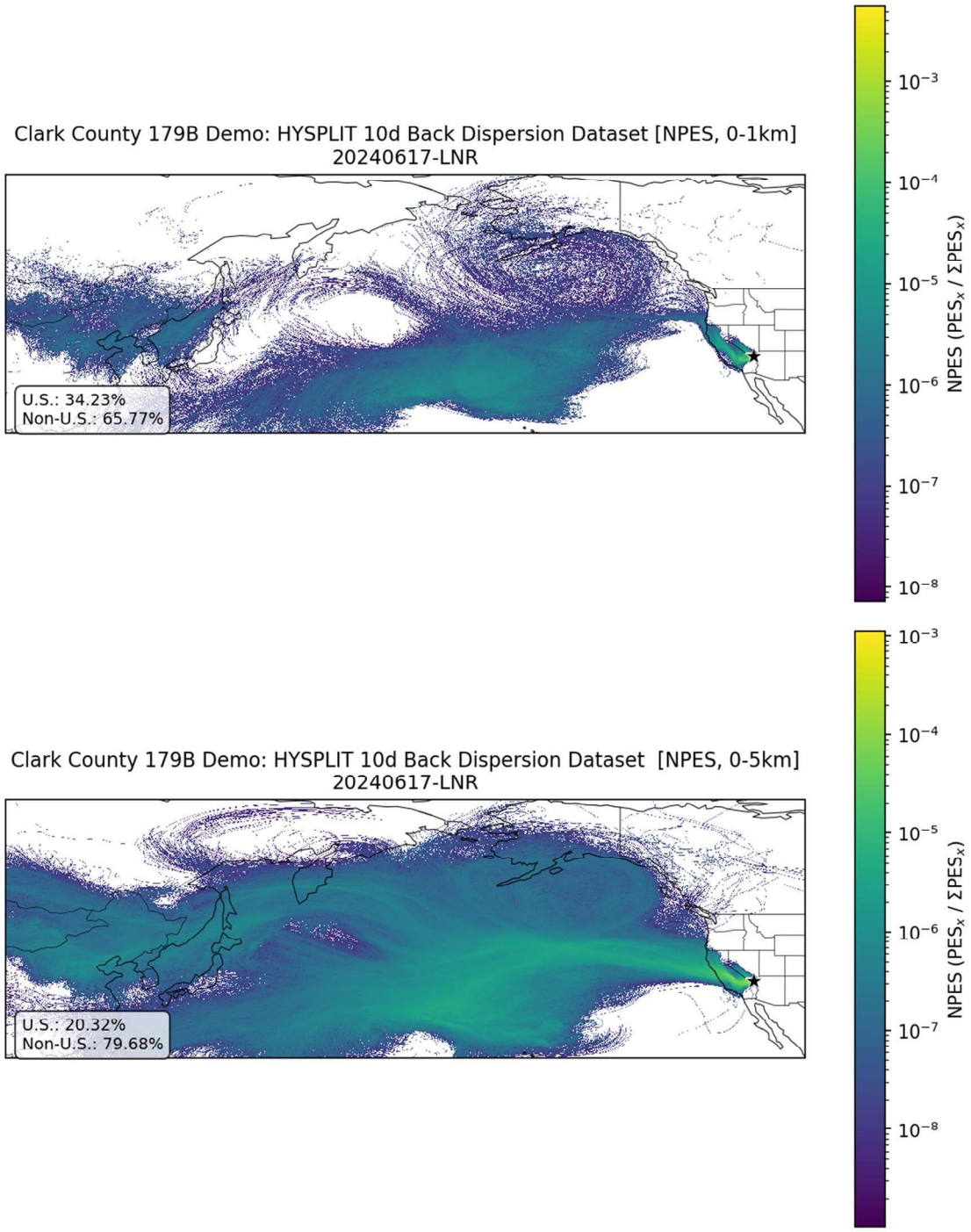

Figure B-40. Clark County 10-day back dispersion-based NPES. Results for June 17, 2024, for the long-range international transport (LNR) air transport regime. NPES is based on the average concentration of a generic, inert tracer gas between 0 and 1 km (top panel) and 0 and 5 km (bottom panel).

Attachment 3. LOC Transport Back-Trajectories

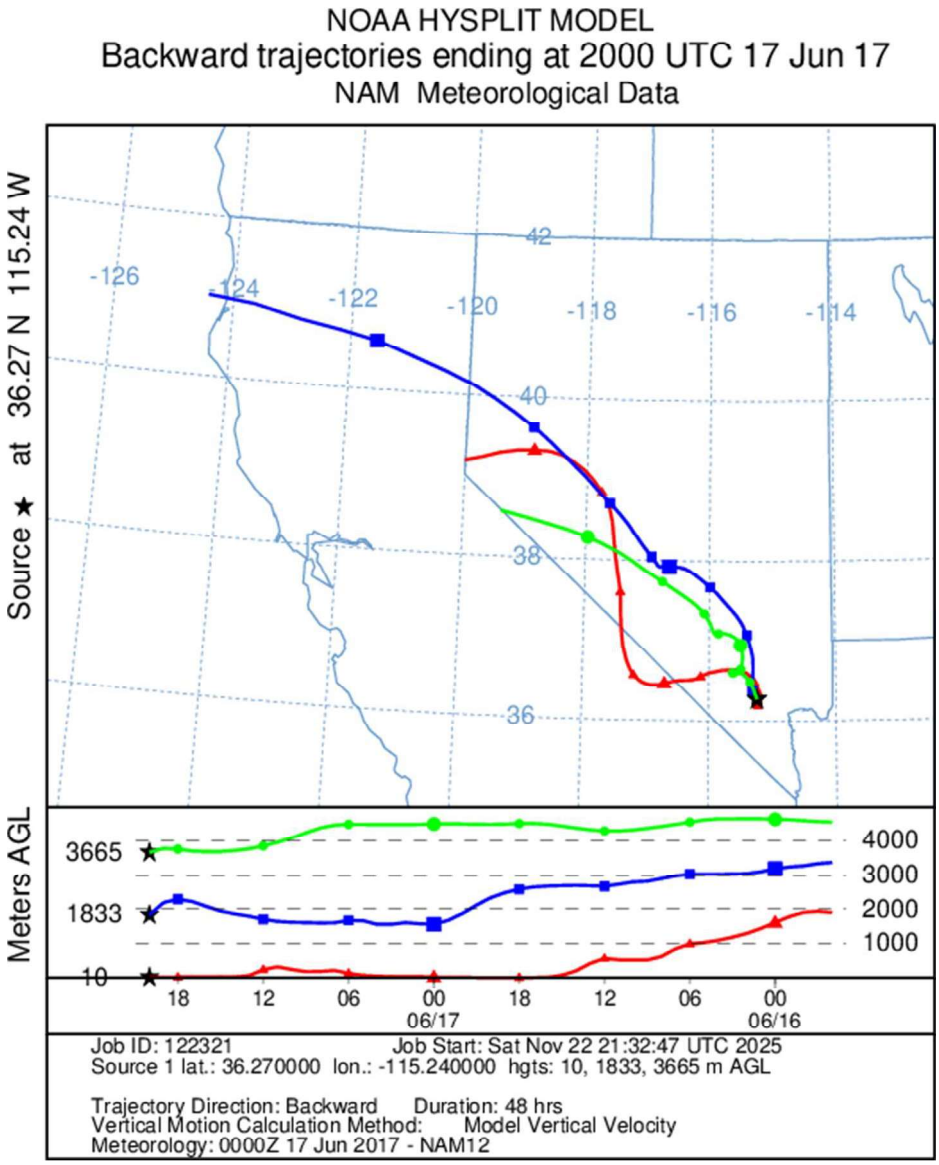

Figure C-1. Back-trajectories initiated on June 17, 2017, at 20:00 UTC (12:00 PST).

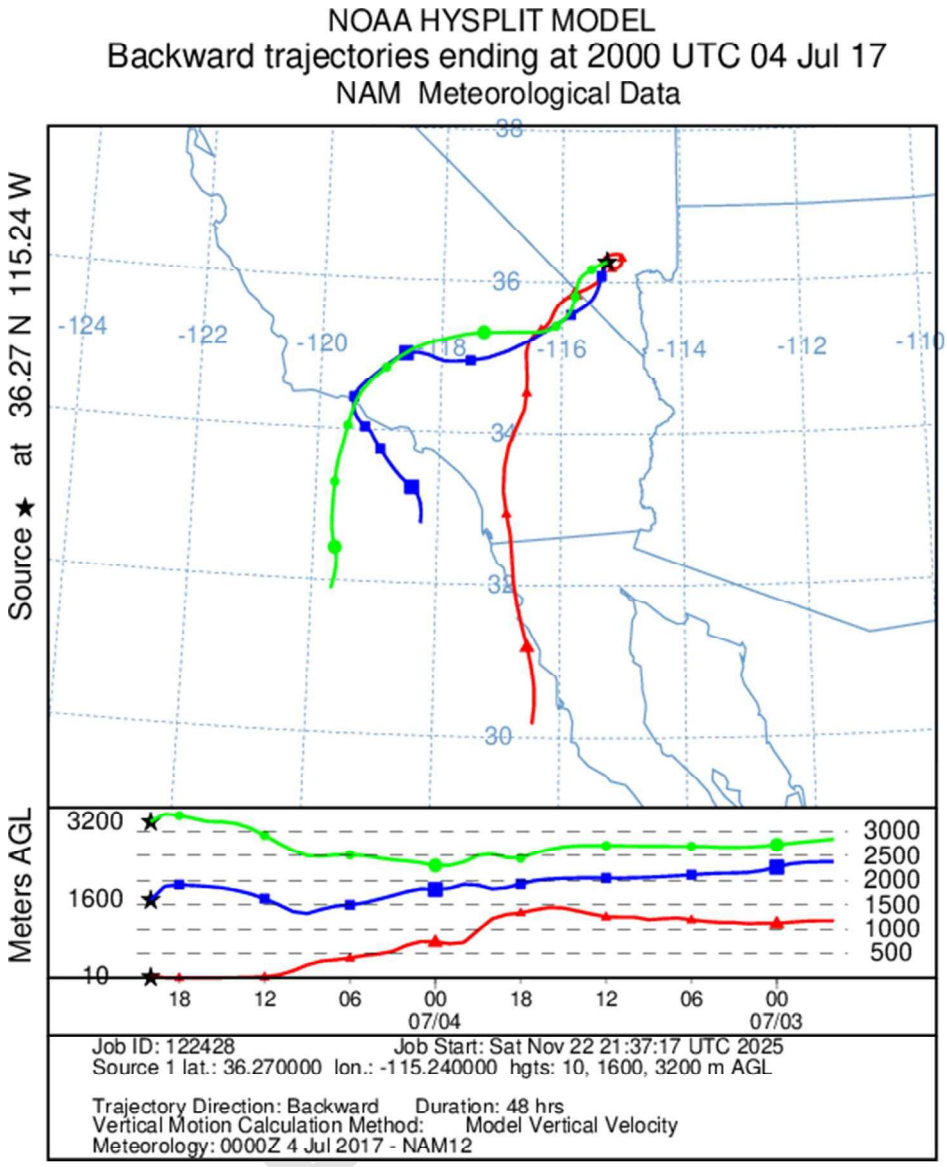

Figure C-2. Back-trajectories initiated on July 4, 2017, at 20:00 UTC (12:00 PST).

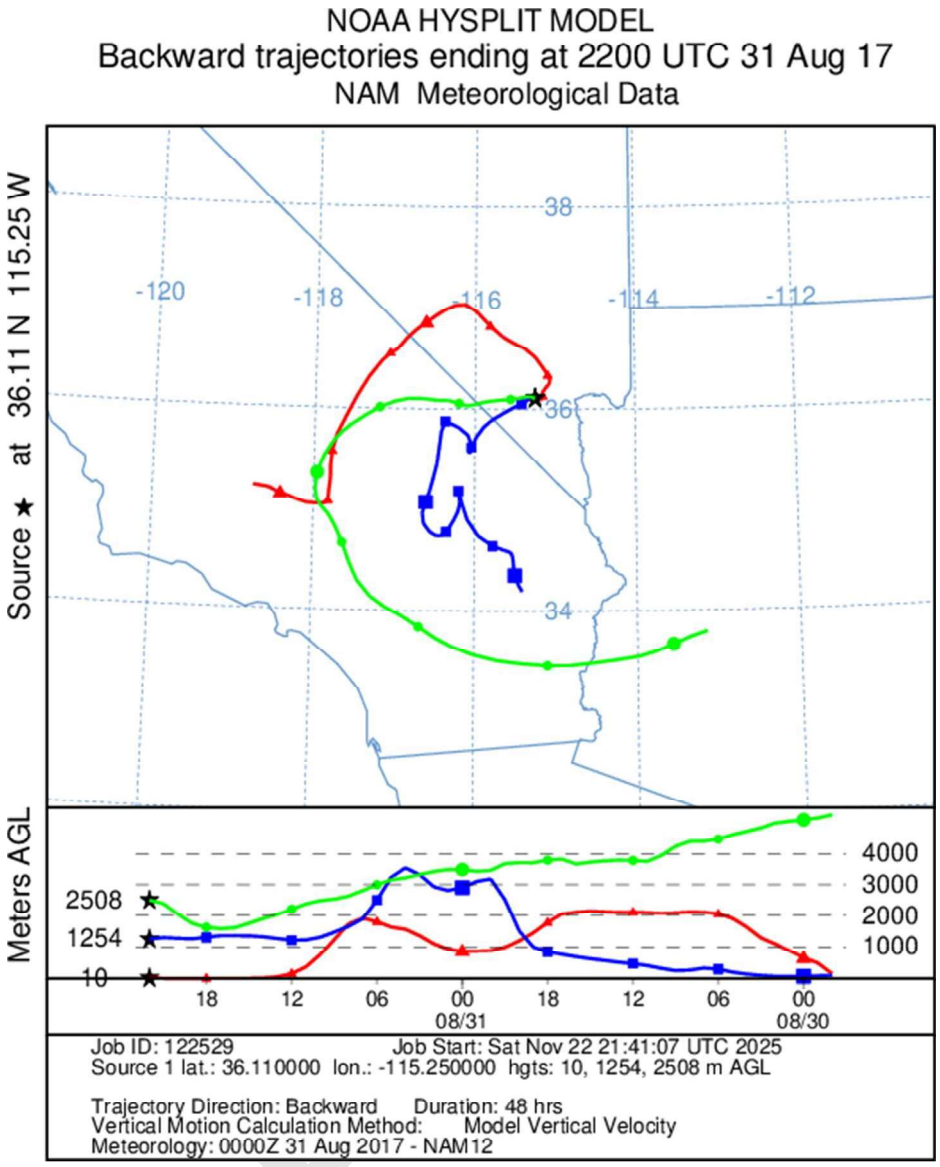

Figure C-3. Back-trajectories initiated on August 31, 2017, at 22:00 UTC (14:00 PST).

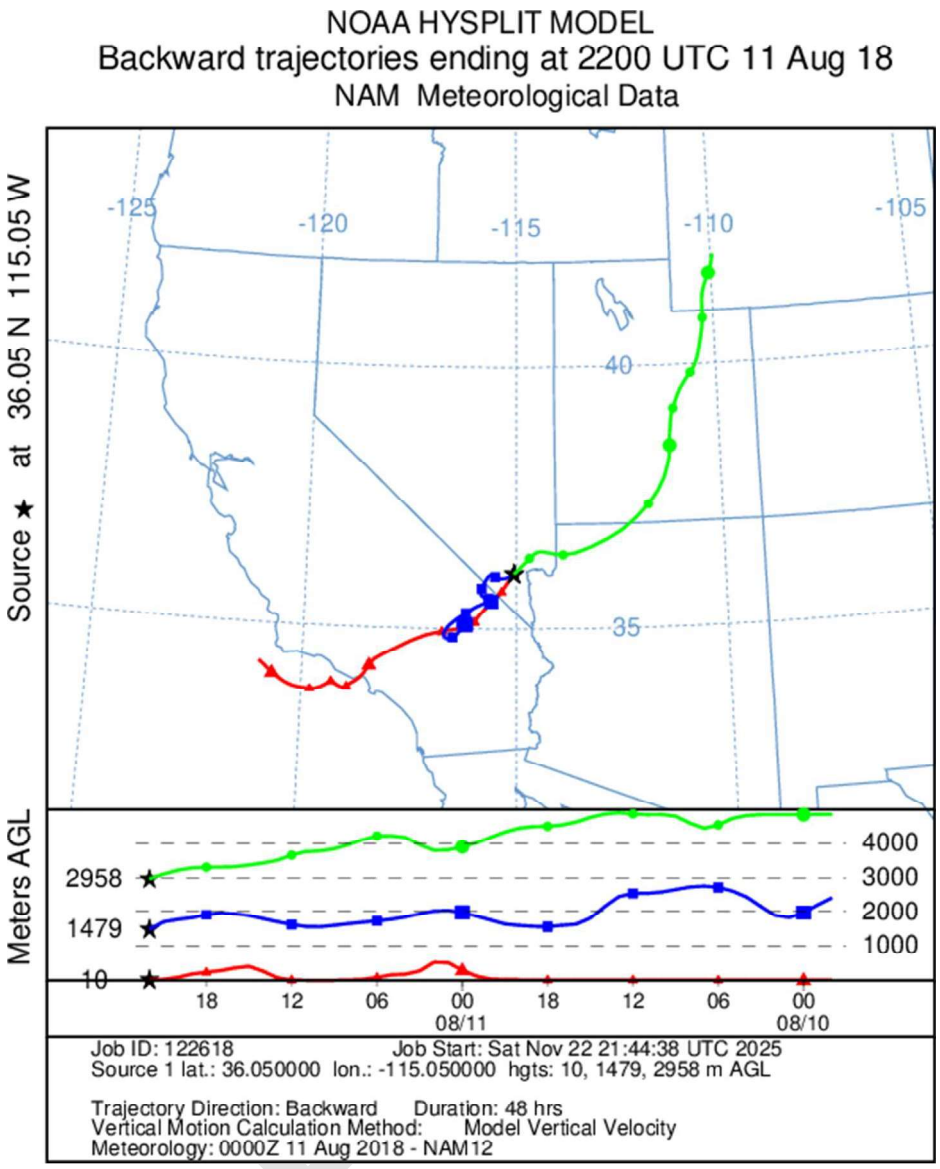

Figure C-4. Back-trajectories initiated on August 11, 2018, at 22:00 UTC (14:00 PST).

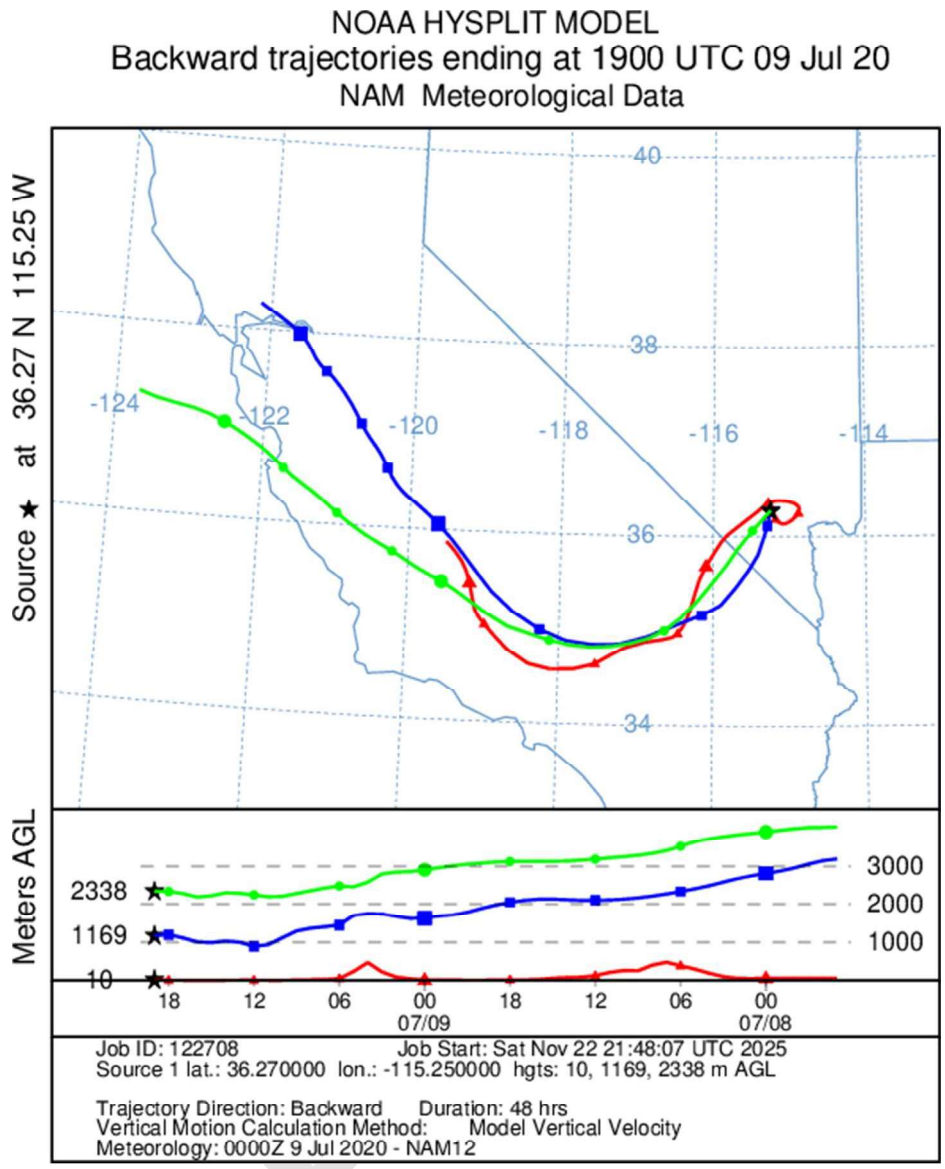

Figure C-5. Back-trajectories initiated on July 9, 2020, at 19:00 UTC (11:00 PST).

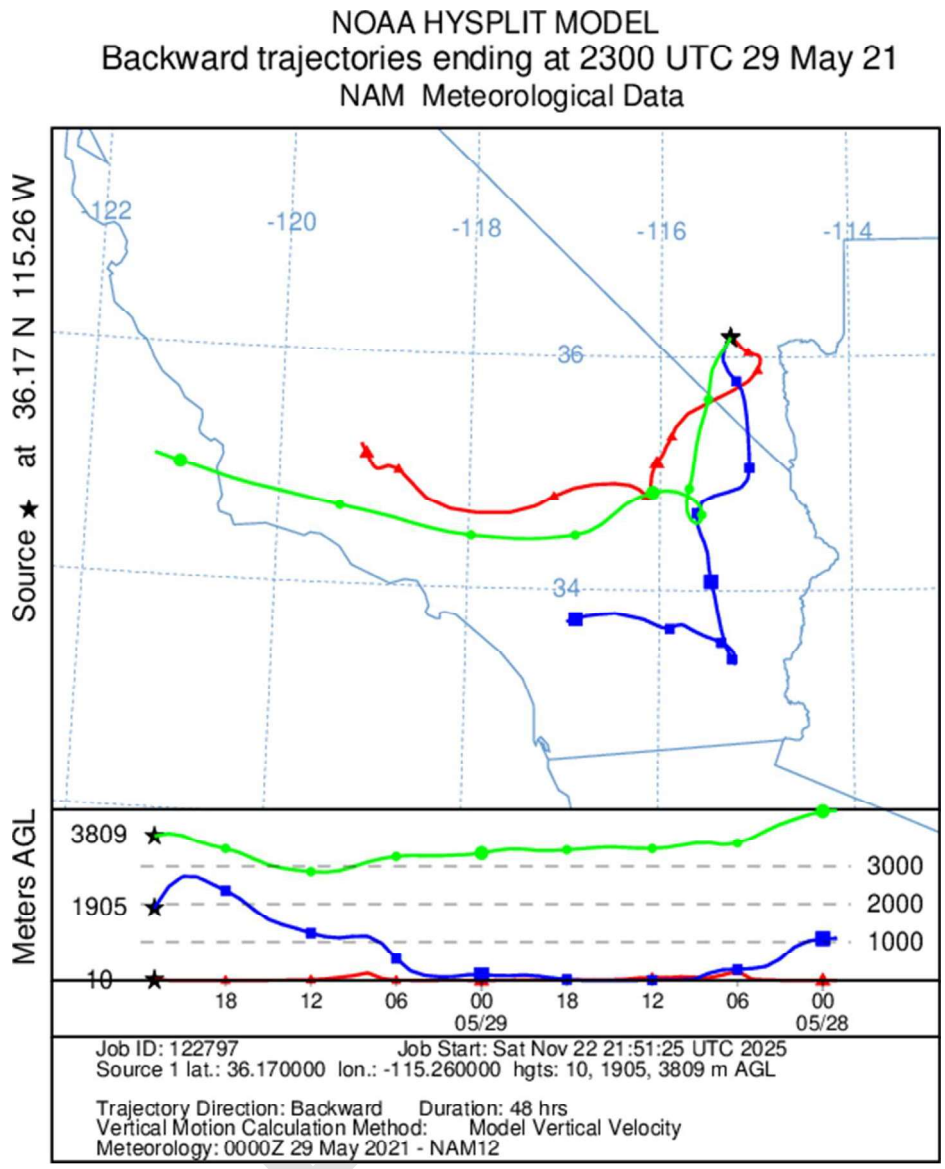

Figure C-6. Back-trajectories initiated on May 29, 2021, at 23:00 UTC (15:00 PST).

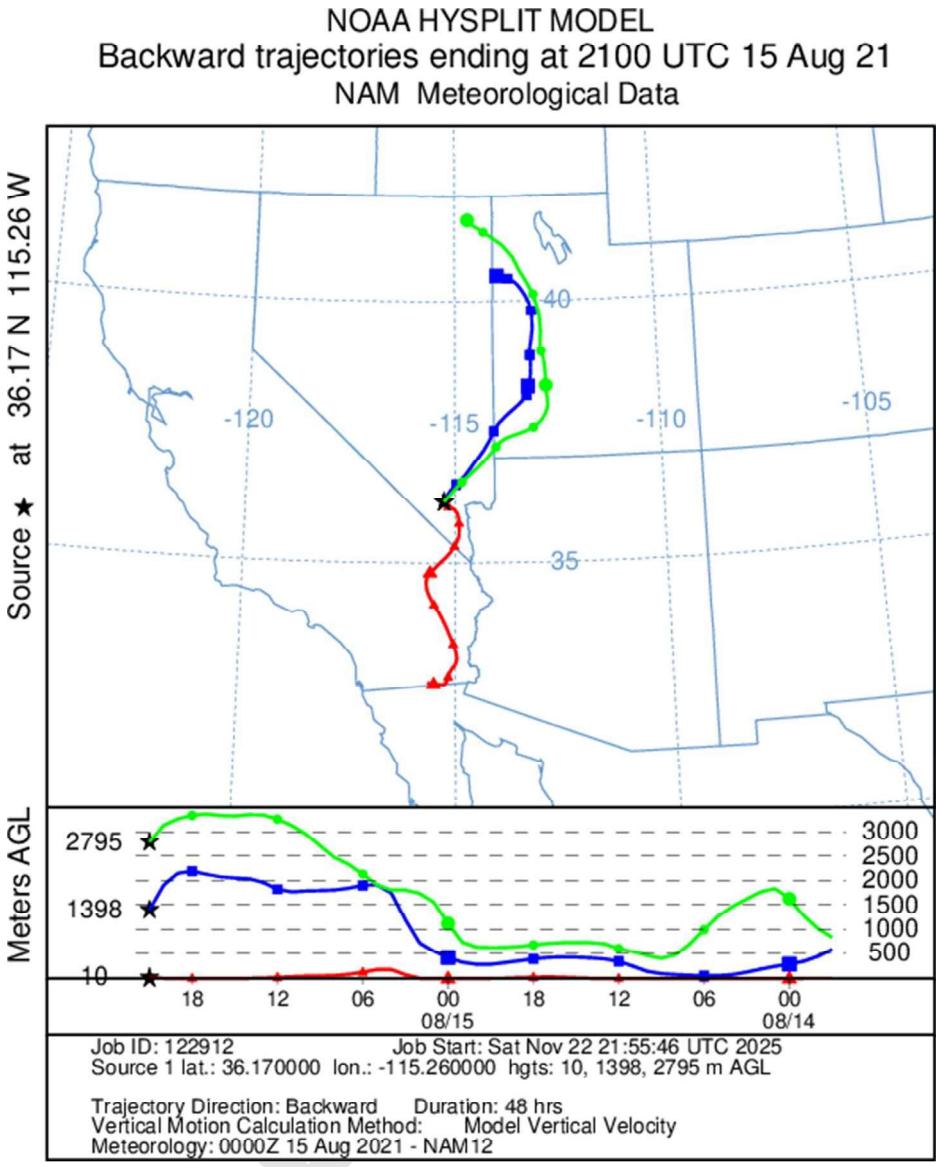

Figure C-7. Back-trajectories initiated on August 15, 2021, at 21:00 UTC (13:00 PST).

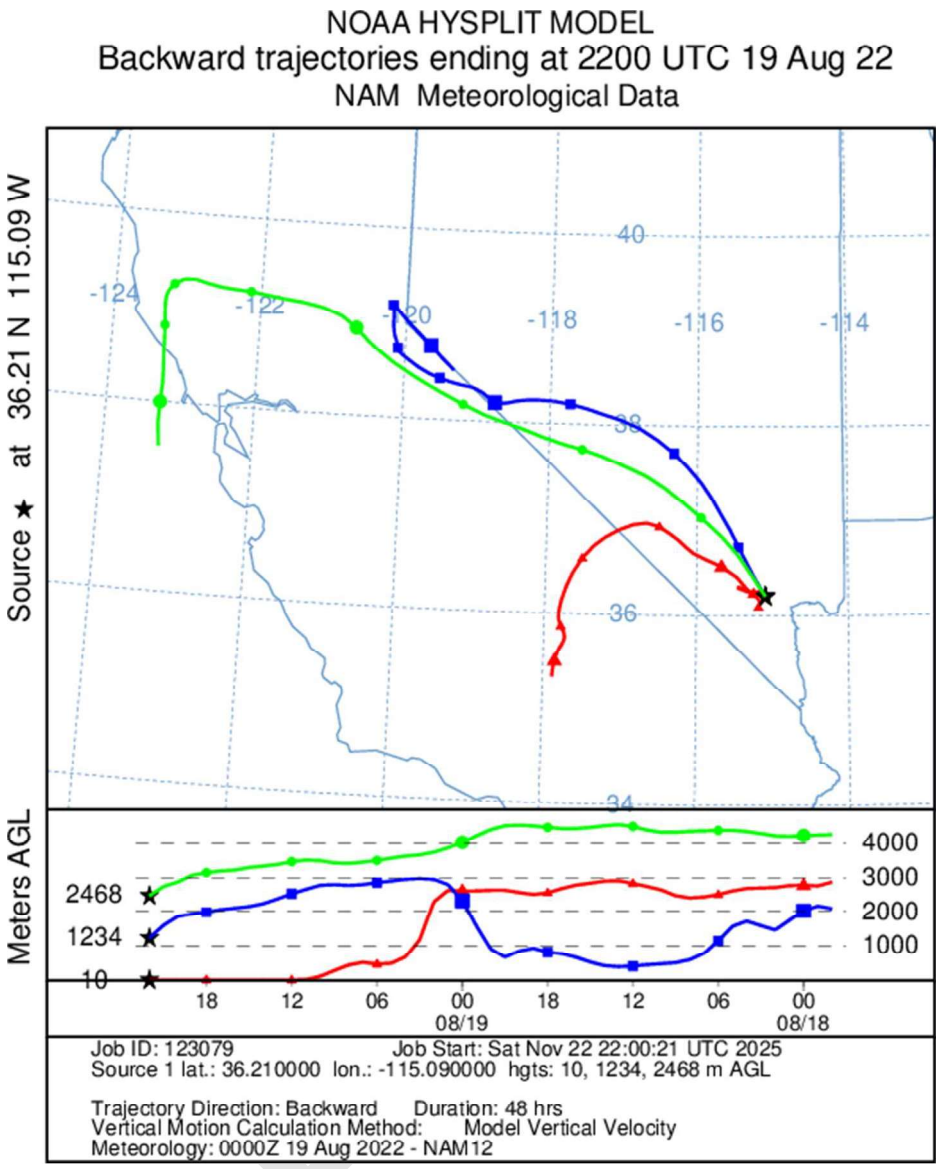

Figure C-8. Back-trajectories initiated on August 19, 2022, at 22:00 UTC (14:00 PST).

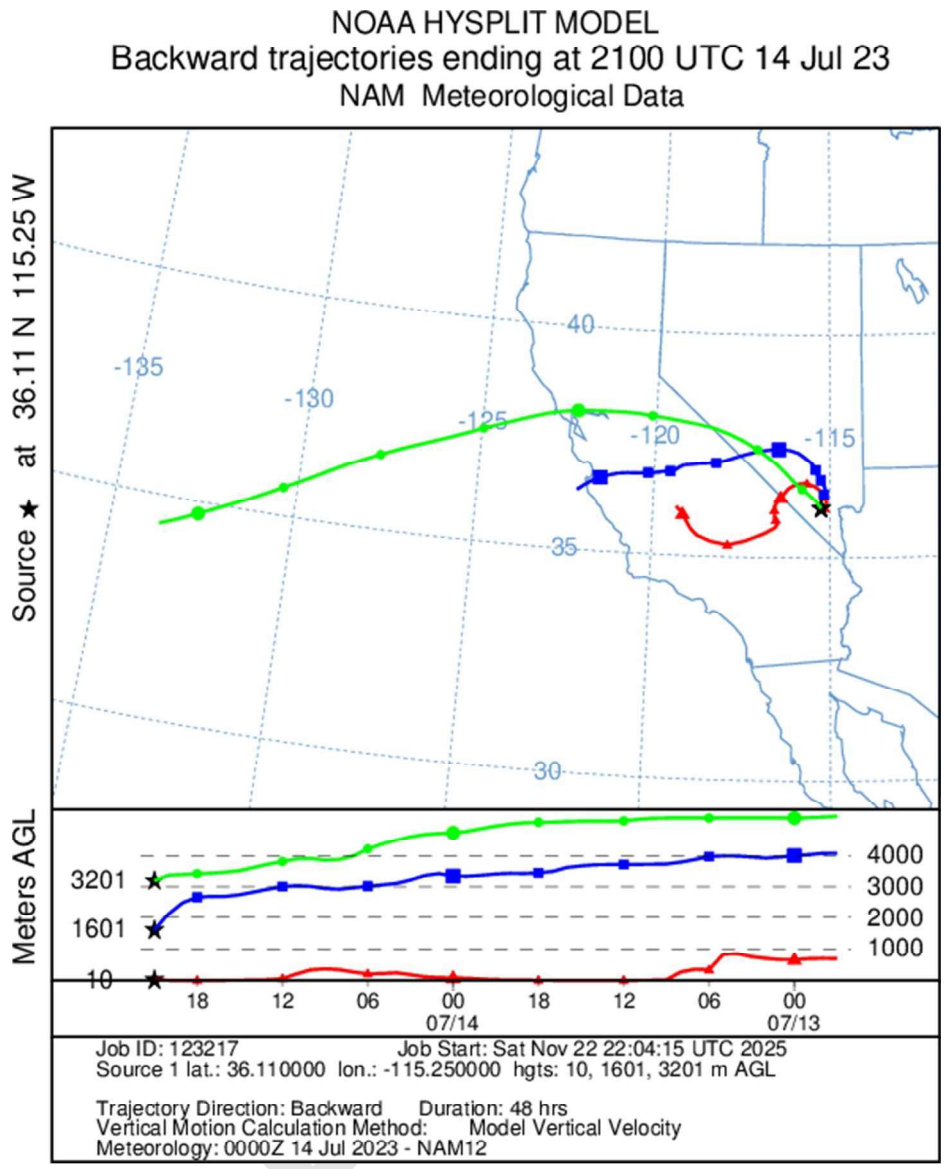

Figure C-9. Back-trajectories initiated on July 14, 2023, at 21:00 UTC (13:00 PST).

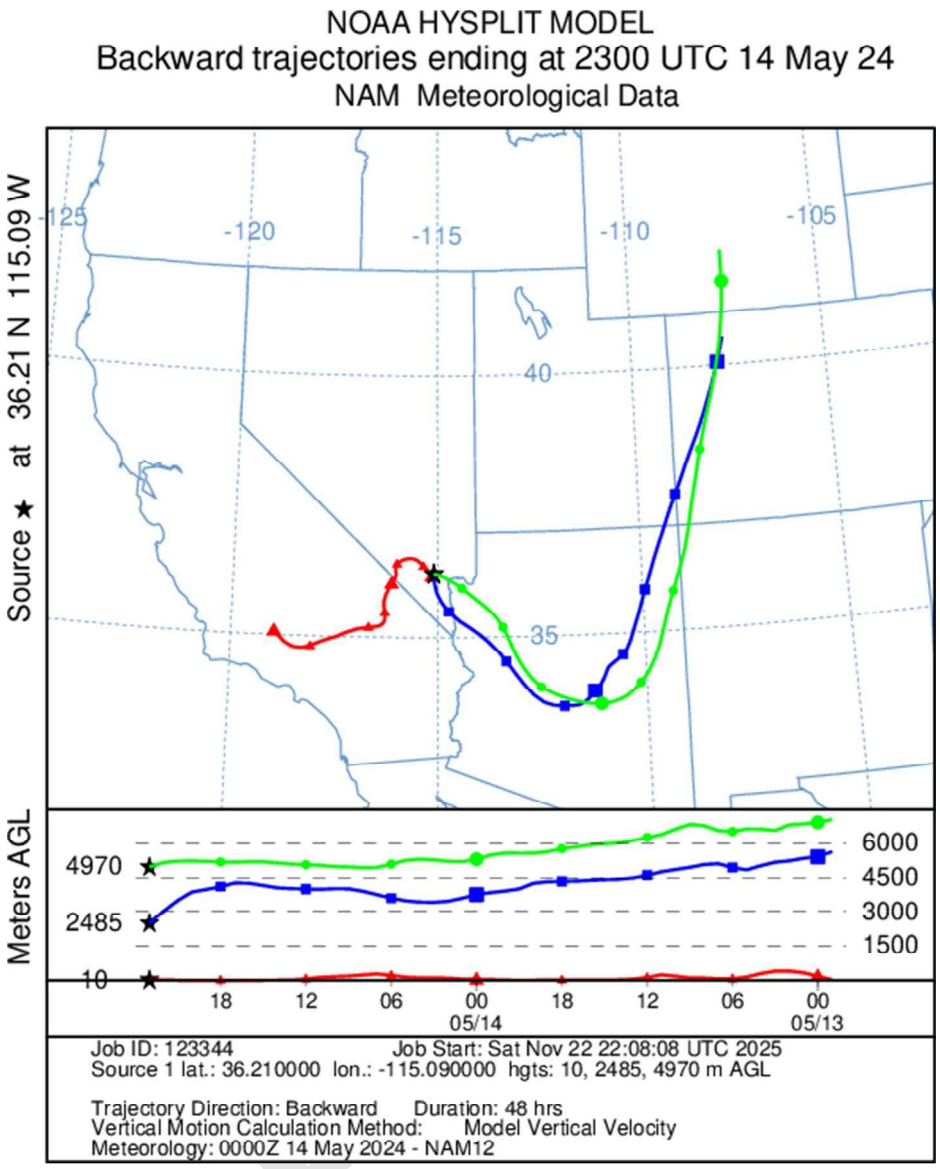

Figure C-10. Back-trajectories initiated on May 14, 2024, at 23:00 UTC (15:00 PST).